

Distribution Agreement In presenting this thesis or dissertation as a partial fulfillment of the requirements for an advanced degree from Emory University, I hereby grant to Emory University and its agents the nonexclusive license to archive, make accessible, and display my thesis or dissertation in whole or in part in all forms of media, now or hereafter known, including display on the world wide web. I understand that I may select some access restrictions as part of the online submission of this thesis or dissertation. I retain all ownership rights to the copyright of the thesis or dissertation. I also retain the right to use in future works (such as articles or books) all or part of this thesis or dissertation.

Signature: ____Sydney Sunna_____ Date 07-10-2023

Proteomic profiling of neuronal and microglial cells using TurboID in inflammatory and homeostatic states for extension into in vivo systems.

By

Sydney Nicole Sunna

Doctor of Philosophy

Graduate Division of Biological and Biomedical Science, Neuroscience

Srikant Rangaraju MBBS MS

Advisor

Nicholas Seyfried, Ph.D.

Advisor

Ranjita Betarbet, Ph.D.

Committee Member

Steven Sloan, Ph.D.

Committee Member

Allan I. Levey, M.D., Ph.D.,

Committee Member

Accepted:

Kimberly J. Arriola, Ph.D.

Dean of the James T. Laney School of Graduate Studies

Date

Proteomic profiling of neuronal and microglial cells using TurboID in inflammatory and homeostatic states for extension into in vivo systems.

By

Sydney Nicole Sunna

B.Sc., University of Arizona

Advisors: Srikant Rangaraju, MBBS, M.Sc. & Nicholas T. Seyfried, Ph.D.

An abstract of

a dissertation submitted to the Faculty of the

James T. Laney School of Graduate Studies of Emory University

in partial fulfillment of the requirements for the degree of

Doctor of Philosophy

in the Graduate Division of Biological and Biomedical Science (GDBBS)

Neuroscience (NS)

2023

Abstract

Proteomic profiling of neuronal and microglial cells using TurboID in inflammatory and homeostatic states for extension into in vivo systems.

By Sydney Sunna

The brain is a cellularly complex organ possessing glia, neurons, and vascular cells. Each cell type supports distinct physiological roles in homeostatic states to orchestrate higher-order cognitive processes. Likewise, each cell type expresses unique proteomic profiles capable of emerging physiological phenotypes with distinct vulnerabilities in neurodegenerative disease. Alzheimer's disease (AD) is the most common neurodegenerative disease, and ongoing systems-level analyses continue to highlight the importance of cellular complexity with disease progression. Bulk brain analyses provide a broad picture of global molecular transformations occurring in the brain that correlate with disease pathology and other traits. However, these bulk methods cannot directly resolve molecular changes occurring in distinct brain cell types. Cellular isolation upstream of mass-spectrometry poses important challenges ranging from contamination from other cell types, reliance on well-validated surface markers which can alter in disease states, and the inability to purify adult neurons. The recent development of proximity-based biotin ligases including TurboID, have made it possible to label and purify cellular proteomes in living cells and animals without the need for cellular isolation. This thesis includes the foundational in vitro studies validating the use of TurboID-based proximity labeling to resolve proteomic differences between two brain cell types (neurons and microglia) under both homeostatic and neuroinflammatory contexts. Additionally, these studies interrogated the proteomic breadth captured by cytosolic TurboID-mediated biotinylation, the impact of TurboID expression on homeostatic phenotypes, the cellular-distinction of proteins labeled by cytosolic TurboID, and the propensity of agnostically-directed cytosolic TurboID to label proteins of disease relevance in homeostatic and neuroinflammatory conditions. Our proteomic analyses demonstrate that cytosolic TurboID and streptavidin-based affinity purification capture >50% of microglial and neuroblastoma proteomes. Cytosolic expression of TurboID minimally impacted cellular proteome abundances, and did not significantly impact cellular respiration or microglial cytokine release profiles with inflammatory challenge. TurboID-NES captured proteins of relevance to neurodegeneration in both microglia and neuroblastoma cell lines, and successfully captured a portion of microglial proteomic changes in response to inflammatory challenge. These in vitro experiments laid the foundation for the generation of novel *Rosa26^{TurboID/wt}/Camk2a-Cre* mice capable of labeling excitatory neuronal proteomes in living mice. This thesis includes foundational experiments validating the genetic strategy underlying the *Rosa26^{TurboID/wt}/Camk2a-*

Cre mice, as well as experiments assessing the impact of inflammation specifically on the proteomes of excitatory neurons, which are not apparent at the bulk proteome level. Using TurboID as a discovery tool, our findings show that neuroinflammation is associated with an increase in glutamatergic post-synaptic proteins in Camk2a neurons which may be indicative of neuronal hyper-excitability.

Proteomic profiling of neuronal and microglial cells using TurboID in inflammatory and homeostatic states for extension into in vivo systems.

By

Sydney Sunna

B.Sc. University of Arizona, 2017

Advisors: Srikant Rangaraju, MBBS and Nicholas Seyfried, Ph.D.

A dissertation submitted to the Faculty of the Graduate School of Emory University in partial fulfillment of the requirements for the degree of Doctor of Philosophy.

Program in Neuroscience

Graduate Division of Biological and Biomedical Sciences

2023

Acknowledgements

Thank you to my mentors, Dr. Rangaraju and Dr. Seyfried. Humbly, I am among the most privileged scientists in the world to have had the once-in-a-lifetime opportunity to be mentored by Dr. Rangaraju & Dr. Seyfried. Dr. Rangaraju empowered me to grow as a humanitarian, as a scientist, and as a leader. Dr. Rangaraju taught me compassion, ethics, honesty, determination, and an apex work-ethic are possible and necessary for a significant positive impact on the world. Thank you to Dr. Seyfried, who welcomed me warmly into the lab and showed me how to strategically craft stories from my scientific work. Thank you to both mentors for your kindness, abundant patience, humor, project development strategy, and great care. Thank you to my committee for your support and guidance. Thank you to Dr. Rayaprolu, for warmly and aptly teaching me everything from grant writing to wet-lab science. Thank you to Hailian and Lihong, for your warm welcome into the lab, and your scientific talent. Thank you to Dr. Hurst, my best friend, who was always there for me from day one. Thank you to Duc Duong, Dr. Ping, Dr. Dammer, Dr. Bagchi, and Dr. Watson for your training and insight. Thank you to Christine Bowen, for our discussions over the lab bench on world politics, civil rights, and, of course, microglia. Thank you to Juliet Santiago, who's quick wit always makes me laugh. Thank you to Christina Ramelow, for staying up late at the bench with me, soul-searching, and passionate plans for our futures which never failed to energize me and renew my love of science. Thank you to Dr. Kumar, for helping improve my imaging skills. Thank you to Dr. Espinosa-Garcia, for sharing your contagious scientific enthusiasm, vast knowledge and thoughtful insights, mornings, and coffee with conmigo. Thank you, Ali Tfaily, for your laughter, kindness, friendship, and shared level of high enthusiasm. Thank you, Aditya Natu, for your good-humor, your finance-savvy, and your alacrity in teaching us how to code. Thank you to Ananth Shantaraman for being a kindred spirit. Thank you to my previous mentors, Dr. Hrubby, and Dr. Gronenberg, for believing in me, and corresponding with me all these years. Thank you to Dr. Cowell, for your humor and mentorship. Thank you to Dr. Nighorn for teaching me nearly everything I remembered from undergraduate neuroscience coursework. Thank you to Dr. Deekonda, my first mentor, for patiently and warmly training me in organic synthesis. Thank you to my beloved husband, Adam Cunningham, who believes in me, supports me, and preserves within me the pure childlike wonder of the natural world, of science, and of mathematics. Thank you to Conor and Ava Chard, for your friendship. Thank you to my mom for being my best cheerleader, and thank you to my father for imparting upon me a strong work ethic always mindful of humanitarian impacts. Thank you to my beloved brothers, for teaching me how to read, an encouraging me to educate myself from a young age. Thank you to Kaylee Fitch, for sharing your love of science with me, your friendship. Thank you to Noura Abbassi for your differential abundance analyses on microglial proteomes we performed this summer, and your thoughtful discussion. Thank you to Rahaf Abbassi for always making me laugh and reminding me that home is not a place but a family.

Table of Contents

I.	Introduction.....	11
i.	Historical Background.....	13
a.	The neuron doctrine and dawn of microglial research.....	13
b.	The discovery of Alzheimer’s disease	14
ii.	Pathological Characterization of Alzheimer’s disease	15
a.	Histological characterizations of Alzheimer’s disease in post mortem human brain.....	15
b.	Clinically-staging Alzheimer’s disease.....	16
c.	Genetic Landscape of Alzheimer’s disease	18
d.	Limitations to the Amyloid Cascade Hypothesis and amyloidogenic transgenic mouse models.....	20
iii.	Inflammation in prodromal AD	21
a.	The central nervous system presents unique challenges to canonical understandings of immunity	21
b.	Inflammation in aging contributes to vulnerability in prodromal Alzheimer’s disease	22
c.	The evolutionarily-conserved role of Toll Like Receptors as mediators of innate immunity.....	23
d.	The relevance of lipopolysaccharide-induced inflammation in neurodegeneration	24
e.	LPS as a model of neuroinflammation in neurodegenerative disease; strengths and limitations.....	26
f.	Introduction to microglia in Alzheimer’s disease.....	29
	Figures	30
II.	Advances in proteomic phenotyping of microglia in neurodegeneration.....	31
i.	Microglia are the resident macrophage of the central nervous system	32

ii.	Genome Wide Association Studies implicate microglia in late onset Alzheimer's disease.....	33
iii.	Transcriptomic diversity of microglia in murine models of Alzheimer's disease and human Alzheimer's disease	34
iv.	The impact of microglia signaling on Alzheimer's disease pathogenesis	37
v.	Bulk-brain proteomic studies	41
	a. Bulk brain proteomics studies reveal metabolic re-programming in glial cells in AD brain	42
	b. Bulk brain studies provide evidence for increased inflammasome activation in AD brain.....	44
	c. Complement signaling in transition from mild cognitive impairment to AD dementia.....	46
vi.	Isolation-based proteomic interrogations of microglia.....	49
	a. What have we learned from isolation-based microglial proteomics in AD pathology?.....	52
vii.	Emerging proteomic labeling approaches circumvent the need for isolation	56
	a. Nascent proteomic in vivo labeling using bio-orthogonal chemistry (BONCAT).....	57
	b. Proximity labeling methods for in vivo proteomic labeling	58
viii.	Figures	60
III.	Cellular proteomic profiling using proximity labeling by TurboID-NES in microglial and neuronal cell lines	66
i.	Abstract.....	67
ii.	Introduction	68
iii.	Results	72
	a. Generation and validation of stably-transduced microglial and neuronal TurboID-NES cell lines.....	72

b.	TurboID-NES-based MS captures representative proteomes in mammalian microglial and neuronal cell lines.....	73
c.	TurboID-NES over-expression has minimal impact on cellular proteomic and functional profiles of BV2 and N2A cells.....	78
d.	TurboID-NES biotinylates a variety of subcellular compartments within BV2 and N2A cells including several neurodegenerative disease-relevant proteins.....	82
e.	BV2 proteomes biotinylated by TurboID-NES capture Lipopolysaccharide driven changes, partially reflected in the whole-cell BV2 proteomes	85
iv.	Discussion	89
v.	Conclusion.....	97
vi.	Materials and Methodology	98
vii.	Figures	119
IV.	Extension of TurboID into murine Camk2a neurons.....	129
i.	Introduction	129
ii.	Paving the way to in vivo extension of TurboID.....	131
a.	In vitro validation studies confirm the Cre-lox genetic strategy	131
iii.	In vivo biotinylation of murine neuronal proteomes mediated by Adeno Associated viral delivery.....	133
a.	AAV9-TurboID-dsRES into to Camk2a-Cre ^{ERT2} cortex and striatum	134
b.	AAV9-hSyn-Cre into hippocampi of TurboID floxed mice.....	134
iv.	Creation and validation of the novel Rosa26 ^{TurboID/wt} mice	135
v.	Methodology	137
vi.	Figures	143
V.	Impact of LPS on Rosa26^{TurboID}/Camk2a-Cre^{ERT2} proteomes	149
i.	Introduction	149
ii.	Experimental design	150
a.	Resolving the impact of LPS on excitatory neurons in vivo	150

iii.	Methodology	154
iv.	Preliminary conclusions	158
v.	Figures	162
VI.	Discussion.....	172
i.	Integrated summary of findings & field implications	172
a.	Establishing the proteomic breadth captured by TurboID-NES	174
b.	TurboID-NES efficiently labels trafficking proteins and can be applied to capturing stress-induced changes in trafficking	175
c.	TurboID-NES has minimal impacts on cellular physiology	177
d.	TurboID-NES captures cellularly distinct proteins of disease relevance	179
e.	Aspects of LPS-mediated inflammation captured by TurboID-NES labeling	179
f.	Capturing LPS impacts on glutamatergic neuronal proteomes	184
g.	Conclusion	185
ii.	Future applications of TurboID	186
a.	Resolving cell-autonomous and non-cell autonomous mechanisms of neuroinflammation	186
b.	Applications of TurboID-NES to systems level analyses in diverse brain cell types	188
iii.	Figures	189
VII.	Bibliography	193

I. Chapter 1. Introduction

Alzheimer's disease (AD) is the most common neurodegenerative disease and 6th leading cause of death in the United States¹. AD is characterized by sequential aggregation of amyloid-beta (A β) and tau proteins in the brain, resulting in neurofibrillary tangles, plaques, neuronal and synaptic loss, and neuroinflammation^{2,3}. The greatest risk factors for AD include age, genetics, and family history⁴⁻⁹. The global dementia prevalence in 2050 is projected to increase to 131.45 M people². In 2019, the United States spent \$1313.4B to care for 55.2M people with dementia¹⁰. Advanced age is among the strongest risk factors for AD¹¹. Our global ageing population, in combination with a lack of effective preventative methods, early clinical diagnostic biomarkers, and safe and efficacious treatment methods for AD dementia have already exacted an enormous burden on our healthcare systems, requiring policy reform and structural changes to care for ageing populations¹².

Alzheimer's disease progresses in irreversible stages. In clinical populations with Late-Onset AD (LOAD), there is a 19-year prodromal period defined by A β accumulation before the clinical manifestation of cognitive impairment¹³⁻¹⁶. This prodromal period is called the asymptomatic stage (AsymAD), and represents a critical window of potential therapeutic intervention before the onset of irreversible neurodegeneration. As AD progresses, extracellular amyloid deposition and intracellular tau accumulation, and chronic inflammation accompany the

death of neurons and synaptic loss; the strongest pathological correlate of cognitive decline^{10,17}. Over time, continued synaptic loss and neural atrophy results in progressive cognitive impairment and psychiatric symptoms, including apathy and depression. Patients initially present with impairments to short-term memory and olfaction memory¹⁸ in early stages, then further clinical advancements include impairments to communication, problem solving, and judgement¹⁰. In its final stages, AD patients have difficulty walking, speaking, eating, and swallowing and suffer a general decline in their quality of life and physical health¹⁰. AD patients lose their capacity to live independently and require constant care from family members or healthcare professionals. AD is an insidious and utterly devastating disease; presenting an enormous economic and emotional burden to already grieving families and care-takers.

AD represents a dire epidemic crisis with an urgent need for therapeutic intervention strategies which prevent synaptic loss and cognitive decline before the onset of neurodegeneration. Traditional therapeutic tools, including cholinesterase inhibitors, psychiatric medications (antidepressants & antipsychotics), and the NMDA antagonist memantine, only manage symptoms and quality of life of patients without treating the underlying physiology¹⁹⁻²¹.

Recently, a new wave of amyloid-targeting monoclonal antibodies entered clinical trials with Aducanumab and Lecanemab gaining FDA approval via the accelerated approval pathway^{22,23}. Prescription of amyloid-targeting monoclonal antibodies remains restricted across healthcare centers because of their dangerous side effects, including brain edema and

hemorrhage and 1 lethality linked to aducanumab, and overall uncertain therapeutic benefit²⁴. Therefore, there remains an outstanding dire need to develop therapeutic strategies that can take place before irreversible synaptic loss and cognitive decline; requiring a refined understanding of the molecular transformations taking place in distinct cell-types with disease progression.

i. Historical background

The neuron doctrine and dawn of microglial research.

After Camillo Golgi's landmark development of the silver staining technique in 1873, the late nineteenth and turn of the twentieth century saw significant histological breakthroughs which allowed scientists to observe and manually illustrate brain cells with unprecedented detail²⁵. The Spanish neuroscientist, pathologist, and artist Santiago Ramón y Cajal used the Golgi staining method to meticulously stain and illustrate brain cells²⁵. This diligent work precipitated the momentous discovery that discrete nerve cells, rather than a continuous network, comprise nervous tissue. Camillo Golgi and Santiago Ramón y Cajal jointly earned the Nobel prize in 1906 for their contributions to *The Neuron Doctrine*²⁶. Around this time, the physician and public health activist, Rudolf Virchow discovered "Nervenkitt" or 'Neuroglia' in the mid nineteenth century and was among the first to identify phagocytes filled with "fatty substances" in the central nervous system (CNS) under pathological conditions, in agreement with prior findings of phagocytic cells within injured brains²⁷⁻³⁰. In 1899, a Scottish pathologist, William Ford Robertson modified the Golgi staining method using platinous oxide, capable of staining myelinating CNS

cells. His detailed illustrations demonstrated that ‘Neuroglia’ are made of discrete ‘elements’ Robertson termed these cells ‘mesoglia’ hypothesized to be of mesodermal origin due to their staining properties. This discovery sparked interest the interest of Cajal, who began to intensely study neuroglia from 1911-1913²⁵. Cajal’s student, Nicolás Achúcarro, developed staining methods capable of identifying brain cells of phagocytic capabilities ³¹. Cajal incorrectly described these phagocytic mesoglia as a new class of cells, ‘a third element’; as corpuscles which lack processes ³¹. A prominent pupil of Nicolás Achúcarro, a Spanish neuroscientist known as Pío del Río-Hortega developed silver carbonate stain capable of resolving the fine processes of this new class of cells of mesodermal origin; eventually termed Microglia³¹. The innovative staining methodologies of the turn of the twentieth century provided physicians and histologists unprecedented tools to discover, refine, and classify different brain cell types under both homeostatic and disease conditions. These breakthroughs, controversies and methodologies continue to shape our modern understanding of neurons and microglia.

The discovery of Alzheimer’s disease.

During this same time period, the German psychiatrist Alois Alzheimer, who studied with Nicolás Achúcarro in Munich, was the first to describe Alzheimer’s disease in a clinical patient, Auguste Deter³². In 1901, Auguste Deter rapidly developed a host of psychiatric symptoms ranging from sleep disorder, memory loss, aggression, crying spells, memory disturbances and persecutory delusions ³³. At just 50 years of age, Auguste’s husband noticed her rapid change in

personality and condition and committed her to the Community Psychiatric Hospital at Frankfurt where she remained inpatient until her death 5 years later in 1906³³. Alzheimer studied Auguste's symptomatic progression during her long-term inpatient residency, and after the autopsy, described the histological and morphological alterations in her postmortem human brain tissue³³. These alterations; plaques, and tangles in the brain, later became known as the key 'pathological hallmarks' of Alzheimer's disease.

ii. Pathological Characterization of Alzheimer's disease

Histological characterizations of Alzheimer's disease in post mortem human brain

Alois Alzheimer first described the key pathological lesions of Alzheimer's disease (AD) in 1907. Extracellular amyloid plaques, intracellular neurofibrillary tangles, and glial inflammation became the hallmark pathological features of AD, and remain central to the post-mortem diagnosis of AD today^{34,35}. The amyloid cascade hypothesis posited by John A. Hardy and Gerald A. Higgins in 1992 is that deposition of A β protein is the causative agent of AD, as tau tangles, cell loss, vascular damage follow the initial deposition of A β protein³⁶. The amyloid cascade hypothesis provided the field a framework to conceptualizing the pathological progression of AD in stages; defined by histological characterization of amyloid and tau burden and how these depositions correlate with cognitive impairment.

Clinically-staging Alzheimer's disease.

Even though A β accumulation begins earlier than tau, both pathologies progress in a predictable and rigorously defined pattern through the brain with progressive advancement of AD etiology. A β deposits begin in the neocortex (Thal phase 1) and spread along anterograde connections to the limbic regions (Thal phase 2), including the entorhinal cortex, subiculum, and cingulate gyrus, and then A β spreads to the basal ganglia and thalamus (Thal phase 3) before advancing towards brainstem structures (Thal phase 4) and finally the cerebellar cortex (Thal phase 5)³⁷. In 1986 the National Institute on Aging (NIA) funded the Consortium to Establish a Registry for Alzheimer's Disease (CERAD) to develop standardized and clinically-validated, neuropsychological and neuropathological assessments for staging AD³⁸. The neuropathological assessment is a semiquantitative test in post mortem human brain sections including hippocampus, amygdala, and neocortical regions for the frequency of senile plaques and neurofibrillary tangles, related to the age of the patient³⁸. Then in 1991, the German anatomist, Heiko Braak, published a landmark publication which fundamentally impacted the collective understanding of neuropathological AD staging. Braak obtained 83 autopsied human brains, including 21 from 'demented old-aged individuals', and sectioned fixed brains into 100 μ m and stained for the presence of amyloid, neurofibrillary tangles (NFT)³⁹. Braak defined VI stages of progressive NFT pathology. Stages I-II feature mild to severe NFT alterations in the transentorhinal layer, stages III-IV progress to both the transentorhinal region and proper

entorhinal cortex, with a 'mild involvement' of the first Ammon's horn sector³⁹. Stages V-VI features destruction of isocortical sensory association areas. In contemporary clinical neuroscience, CERAD scoring of neuritic plaques and Braak scoring of the distribution of NFTs are both histological tools used to stage and diagnose AD⁴⁰. In 1958, the Baltimore Longitudinal Study in Aging (BLSA) initiated and represents one of the longest-ongoing studies of aging in the world⁴⁰. Accruing more than 200 autopsied subjects, this study correlates AD neuropathological metrics to cognitive clinical outcomes. A combination of clinical, pathologic, morphometric, and biochemical assays defined a subpopulation of people with hallmarks of AD (amyloid and tau) without cognitive decline⁴⁰. The discovery of this subpopulation of people with amyloid and tau deposition without cognitive impairment shifted the conceptual framework of AD staging towards a continuum. The Jack model projects dynamic accumulation of AD biomarkers against clinical disease stage, illustrating this continuous framework (**Figure 1.1**)^{14,41}. A newly-defined stage, known as asymptomatic Alzheimer's disease (AsymAD), characterizes a protracted prodrome of AD pathology prior to mild cognitive impairment (MCI) and cognitive decline. One landmark longitudinal study conducted by Victor Villemagne et al., 2013 calculated the rates of A β deposition, cerebral atrophy, and cognitive decline in 145 healthy participants, 36 MCI and 19 AD patients¹³. Their results showed that 82% of the 200 patients showed a positive and linear increase in A β accumulation, estimated to take 19.2 years to go from threshold (11)C-PiB positivity to the A β levels observed in AD patients. Furthermore, their projections showed

hippocampal atrophy begins 4.2 years before the onset of dementia¹³. This study impacted the conceptual framework of AD by showing that amyloid deposition begins nearly 2 decades prior to the onset of dementia. In conclusion, contemporary frameworks provides clinically-stage AD on a continuum characterized by a protracted prodromal period of A β accumulation prior to synaptic loss, atrophy, cognitive decline, and dementia.

Genetic Landscape of Alzheimer's disease

AD is a complex, multigenic, and genetically heterogenous disease. AD can be broadly classified into two categories; familial AD and sporadic AD. Patients with familial early onset AD (EOAD), account for approximately 1-5% of all cases, and the onset of cognitive decline begins before individuals reach the age of 65 years old. Sporadic late onset AD (LOAD) is more prevalent, representing approximately 95% of all cases, occurring in patients over the age of 65 (*see chapter 2.2 for Genome Wide Association Studies on LOAD patients*)⁴². An estimated 1-2% of AD patients inherit an autosomal dominant (ADAD) form of the disease, inheriting mutations with near certainty of developing AD with clinical symptoms beginning from 30-50 years of age⁴³. ADAD is associated with three mutations; Amyloid Precursor Protein (*APP*) on chromosome 21q21, Presenilin 1 (*PSEN1*) on chromosome 14q24.2, and Presenilin 2 (*PSEN2*) on chromosome 1q42.13⁴⁴. Mutations within *APP* represent 10-15% of EOAD cases⁴⁵⁻⁴⁸. In the late 1980's Jie Kang and colleagues hypothesized correctly that the A β peptide, termed in their publication the "A4 protein", is the same polypeptide protein found in aged individuals with trisomy 21, and is of

neuronal origin and a cleavage product of a larger precursor protein⁴⁹. They isolated the 40-residue A β peptide from purified plaque cores, and identified its sequence⁴⁹. Missense mutations of APP, including the “Swedish” mutations, described by Mike Mullan in 1992, (*APPSW*, *APP670N* and *M671L*) and “London” mutations, described by Alison Goate and John Hardy in 1991, (*APPLON* and *APPV717I*) lead to increased A β production^{50,51}. PSEN1 and PSEN2 are integral membrane proteins which comprise catalytic components of γ -secretase, an intramembrane protease that cleaves transmembrane proteins to variable lengths, including APP (39-42 amino acids)⁵². In 1995 R. Sherrington and colleagues identified a mutation within *PSEN1*⁴⁸. *PSEN1* mutations are fully penetrant, cause the most severe forms of AD account for 18-50% of EOAD cases^{48,53}. In 1995, Levy-Lahad and colleagues described a point mutation substituting an isoleucine for an Asparagine (N141I) in *PSEN2* affecting people in Volga German AD kindreds⁵⁴. Taken together, the common molecular phenotype across a majority of the >200 EOAD mutations in *APP*, *PSEN1*, and *PSEN2* increase the ratio of A β ₄₂: A β ₄₀^{55,56}. Despite the relatively low prevalence of EOAD compared with LOAD, ADAD families provided historical insights into AD etiology and the high genetic penetrance of these mutations provide strong evidence for the amyloid cascade hypothesis which has long guided the field of AD research. Discovery of human genetic mutations in ADAD families facilitated the development of transgenic animal models which in turn support the attempted development of disease-modifying therapeutics.

Limitations to the Amyloid Cascade hypothesis and amyloidogenic transgenic mouse models

The amyloid cascade hypothesis places A β as the initial causative agent in AD pathology, upstream of neurodegeneration and clinical symptoms³⁶. The contributions of research on ADAD families profoundly shaped the course of AD research to focus on amyloid pathogenesis, though repeated failures of amyloid-targeting drugs and presenilin inhibitors warrants criticism on the pathogenic sufficiency of A β ⁵⁷. Furthermore, repeated independent studies consistently show A β plaque deposition within the brains of cognitively normal individuals^{15,40,58-60}. Murine models likewise engineered based on familial AD mutations are also limited and there is currently no mouse model which displays the full spectrum of human AD etiology⁶¹. Amyloidogenic murine models of AD based on familial AD mutations only recapitulate amyloid-related disease mechanisms and suffer from artifacts inherent to driving the overexpression of toxic amyloid species. For example the 5xFAD mouse model, receives its namesake from the expression of 3 familial human *APP* (Swedish, London and Florida mutations) and 2 *PSEN1* (M146L and L286V) transgenes⁶². The 5xFAD mouse model specifically drives the over-expression of high levels of mutant APP under the Thy1 promoter⁶³. The rapid and aggressive A β pathology exhibited by the 5xFAD mouse models is limited by its production of A β and artefacts inherent to the overproduction of A β . Furthermore, the complex relationship between amyloid deposition, inflammatory changes, synaptic loss, and cognitive decline is incompletely understood.

iii. Inflammation in prodromal AD

Inflammatory activation is a central mechanism in neurodegeneration as the immune system responds to pathologic lesions and neuronal injury⁶⁴⁻⁶⁶. Prolonged activation of inflammatory pathways is a risk factor for the progression of AD, and epidemiological studies in humans demonstrates the neuroprotective efficacy of long-term anti-inflammatory drug use in delaying the onset of cognitive decline⁶⁷⁻⁷⁰. Repeated clinical failures of anti-inflammatory drugs to treat AD after clinical cognitive impairment suggests that early attenuation of chronic inflammation may be key⁷¹.

The central nervous system presents unique challenges to canonical understandings of immunity.

The brain was historically regarded as an immune privileged organ; guarded from peripheral immune cells by the blood brain barrier (BBB)⁷². In the periphery, inflammation supports tissue homeostasis⁷³, mounts defenses against pathogens by producing cytotoxic substances⁶⁵, clears damaged cells by phagocytosis⁷⁴, recruits other immune cells to sites of damage by chemokine signaling⁷⁵, and promotes wound-healing. The central nervous system presents unique challenges to nearly each one of these critical inflammatory processes. Macrophages are critically important to removing pathogens or irreparably damaged cells from the body. To this end, macrophages have a wide arsenal of inflammatory mediators which contribute to neurodegeneration in disease. Proinflammatory cytokines such as Tumor Necrosis

Factor alpha (TNF- α), Interleukin-1 (IL-1) and Interleukin-6 (IL-6) increase axonal vulnerability and have been shown to be neurotoxic in neuron-glia cocultures⁷⁶⁻⁸¹. Activated immune cells secrete neurotoxic inflammatory molecules to uniquely vulnerable post-mitotic neurons⁸². Removal of neurons which cannot replace themselves through mitosis presents risk to the functionality of higher-order brain circuitry. Both the rigidity of the skull encasing the brain and the BBB cannot tolerate swelling nor the recruitment of peripheral immune cells, respectively. The unique vulnerability of nervous tissue and its physical separation from the periphery challenged canonical understandings of immunology and stimulated ongoing controversy regarding the dual detrimental and beneficial roles of the immune system in the brain; a controversy which persists today.

Inflammation in aging contributes to vulnerability in prodromal Alzheimer's disease

Neuroinflammation with respect to AD must be contextualized with respect to age, a strong risk factor for AD¹¹. Transcriptomic analysis of human hippocampal and cortical tissue of cognitively-normal aged brains (60 – 99 years old) show major changes in immune-related gene expression compared to younger brains (20 - 59 years old)⁸³. Notably, from a probe set size of 759 immune-related genes, 40% were significantly altered in aged hippocampi⁸³. In all brain regions assessed, a majority of inflammatory genes (64-84%; regional variation) were upregulated with age. In age matched AD brains, only 6% of the 759 immune-related gene probes were significantly changed. Innate immune system response genes, including complement signaling, toll like

receptor (TLR) signaling, and inflammasome activation were significantly upregulated in both age and AD, though the extent of gene response is far greater in cognitively normal aging compared with AD⁸³. One interpretation of these results could be that increased activity of innate immunity with age, long before earliest signs of clinical dementia, could be an important facet of prodromal AD contributing to vulnerability in neurodegeneration.

The evolutionarily-conserved role of Toll-Like Receptors as a mediator of innate immunity

One central mechanism regulating immunity lies within toll-like receptor signaling (TLR). TLRs and downstream nuclear factor kappa b (NF- κ B) signaling likely originated near the conception of animal evolution, and are found broadly throughout the animal kingdom with few exceptions⁸⁴. Broad roles across the animal kingdom of TLRs include regulating host-immune responses through NF- κ B signaling in insects and vertebrates, and contribute to organ development and embryonic development through cell-adhesion in insects and vertebrates, respectively⁸⁴. TLR's are widely expressed in the central nervous system, including in neurons⁸⁵, microglia⁸⁶, cultured astrocytes⁸⁷, and are broadly classified based on the ligands which bind to them, as well as their associated loss of function phenotypes⁸⁴. Humans express 10 functional TLRs (1-10) and mice express 12 (1-9, 11-13). Various combinations of TLR subtypes are expressed across immune and non-immune cells⁸⁸. TLRs are expressed both at the cell surface membrane to recognize disease/pathogen associated molecular patterns (DAMP or PAMP, respectively)

including lipids, proteins and lipoproteins comprising microbial cell walls, as well as in endolysosomal compartments to recognize nucleic acids^{88,89}. Following ligand-binding to TLR's, complex signaling cascades lead to downstream transcriptional control of interferon-inducible genes and pro-inflammatory cytokines⁸⁹.

The relevance of lipopolysaccharide-induced inflammation in neurodegeneration

The endotoxin hypothesis of neurodegeneration posits that lipopolysaccharides (LPS) produced peripherally by gram-negative bacteria contribute to neurodegeneration⁹⁰. Mechanistically, gram negative bacteria present in the gums, skin, gut, and other tissues contribute to high blood plasma levels of LPS during bacterial infection. LPS antigenicity is best understood through its interaction with TLR-4, a receptor expressed predominantly on the surface of microglia. Gram negative bacteria, including *B. fragilis* and *E. coli* in the human gastrointestinal (GI) tract produce pro-inflammatory lipopolysaccharides capable of impacting human neurons⁹¹⁻¹⁰⁰, whereas commensal species like *B. dorei* can produce antagonistic forms of lipopolysaccharides which inhibit TLR-4 and attenuate immune responses¹⁰¹. The impacts of age and environmental pesticide exposure on the composition of GI microbiota, and potential impacts on the gut-brain axis are emerging areas of investigation, especially in the context of Parkinson's disease (PD), as pesticide exposure incurs a two-fold increased risk for PD¹⁰². Fascinatingly, human postmortem AD neocortical and hippocampal brain lysates show a significant increase in GI-derived lipopolysaccharide compared with non-AD controls¹⁰³, and

elevated plasma LPS in sporadic Amyotrophic Lateral Sclerosis and sporadic AD patients¹⁰⁴. Likely derived from the peripheral GI tract, it is possible that the dysregulation of both the blood brain barrier and gut microbiome in contexts of age and neurodegenerative disease may allow GI-derived LPS to directly impact both microglia and neuronal phenotypes.

Overall, LPS itself has been found to be elevated in brain and plasma in neurodegenerative cases. Peripheral sources of LPS are complex, and likewise have complex impacts on microglia and their role in neurodegeneration. LPS binds to CD14 and agonizes TLR-4; activating NF- κ B and the transcriptional activation of hundreds of inflammatory genes¹⁰⁵⁻¹⁰⁷. Additionally, downstream signal transduction cascades lead to the rapid transcription and release of pro-inflammatory cytokines including interleukins (IL-1, IL-6, IL-12, IL-17A, IL-18), p40, nitric oxide synthase (NOS), Tumor Necrosis Factor alpha (TNF α), chemokines (CCL2, CCL5, and CXCL8) and complement receptors C3, C3a, and C5a¹⁰⁸⁻¹¹⁰. LPS also activates caspases which proteolytically cleaves the proforms of interleukin cytokines and gasdermin-D to permeabilize the cell membranes and excrete mature interleukins into the extracellular environment, and induce pyroptosis and NLRP inflammasome activation^{90,111} (*for inflammasome activation in AD contexts, see Chapter 2.5*). LPS also activates pattern recognition receptors; RAGE, TREM2, scavenger receptors, β_2 integrins¹¹¹⁻¹¹⁶. These pattern recognition receptors play roles in both clearing LPS and promoting inflammatory toxicity. An important member of β_2 integrins includes complement receptor 3 (CR3), which contribute to the generation of reactive oxygen species

(ROS), neurotoxicity and phagocytosis of neurons (*for complement in AD contexts, see chapters 2.4-2.5*). LPS, as a main constituent of gram-negative bacterial cell walls, drives a strong inflammatory response from the innate immune system; as evolution selected for these robust immune responses capable of surmounting bacterial infection. However, these strong inflammatory responses can contribute to neuronal damage via comparable mechanisms of AD etiology⁹⁰.

LPS as a model of neuroinflammation in neurodegenerative disease; strengths and limitations.

There is no model of neurodegenerative disease which captures all aspects of the etiology. Genetic models of AD in mice (e.g., 5xFAD, 3xTg, APOE risk) significantly contribute to the collective understanding of AD etiology, though each model suffers distinct limitations. Briefly, some limitations include over-expression of amyloid and absence of pathological tau with 5xFAD^{61,117,118} and undocumented neuronal loss has in 3xTg¹¹⁹. Given the genetic heterogeneity of AD and other neurodegenerative diseases in humans, it is important to supplement genetic models of neurodegeneration with models of neuroinflammation, a common pathological hallmark of neuronal injury across several neurodegenerative diseases. It is important to note that inflammatory challenge is not interchangeable with neurodegeneration, rather inflammation itself is a complex biological process which merits independent study. Briefly, this thesis discusses the strengths and limitations of using LPS to model neuroinflammation in neurodegenerative contexts.

LPS-challenge recapitulates key aspects of neurodegeneration relevant to Alzheimer's disease etiology, including cognitive impairment^{120,121}, synaptic loss¹²², the production of pro-inflammatory cytokines such as IL-1, IL-6 and TNF α ¹²³⁻¹²⁵. LPS can also drive amyloidosis and tau hyperphosphorylation¹²⁶⁻¹²⁹. For example, a few studies show that IL-1 β , IL-6, and TNF α can augment APP expression and upregulate transcription of messenger RNA (mRNA) encoding β -secretase¹³⁰⁻¹³³. Neuronal damage, A β deposition and LPS activate toll-like-receptors on microglia, including TLR-4, which in turn lead to neuronal loss, memory impairment and behavioral changes¹³⁴⁻¹³⁶. Genetic susceptibility to AD may also play a role in LPS sensitivity in mice and humans. For example, an ex vivo whole blood assay of TLR-induced cytokines gave an intravenous injection of 2 ng/kg of LPS to healthy volunteers with differing APOE genotypes. Blood derived from APOE4 positive subjects had significantly higher TNF α , IL-1 β , IL-17, INF γ , C-CSF, IL-8, and IP-10¹³⁷. These findings suggest that there may be an overlap between genetic risk for AD and robust innate inflammatory responses which may drive chronic neuroinflammation. The complex interaction between genetic risk and response to inflammatory challenge warrants caution when extrapolating studies using LPS to clinical interpretations.

Though LPS administration and its associated memory impairment has been proposed as a non-genetically manipulated neuroinflammation model of AD¹³⁸, the rationale expressed in *this thesis* contends that while LPS-administration replicates a number of important components of AD etiology: neuroinflammation, amyloidosis, and memory impairment, it is not explicitly a

model of AD. Instead, LPS administration can be useful in isolating the role of neuroinflammation in cognitive decline. Several important factors to consider when modelling neuroinflammation with LPS are the dose, duration, route of administration, and higher sensitivity humans have to LPS when compared with mice^{90,139}. For example, murine studies show that 7 days of intraperitoneal LPS administration (250 µg/kg) significantly impaired mouse performance in the Morris water maze test and corresponded with hippocampal A β deposition, whereas 3 days of LPS administration had more modest cognitive impairments and no significant change in hippocampal A β deposition¹⁴⁰. In rodents, multiple doses of 1 mg /kg of LPS over several days cause rapid neurodegeneration capable of modelling PD and AD; whereas a single acute intraperitoneal injection of 5 mg /kg can cause microglial activation which lasts for longer than 1 year and loss of dopaminergic neurons in the substantia nigra 10 months after dose, and direct injection into the brain is sufficient to induce neuronal loss¹⁴¹⁻¹⁴⁵. Therefore, there is a wide variation in pathological outcomes which depend on the species, dose, duration, and route of administration of LPS. Chronic, repeated, peripheral and lower-doses of LPS in rodent models can elicit neuroinflammatory changes in the brain that are also observed in human AD^{146,147}.

Introduction to Microglia in Alzheimer's Disease

A seminal histological study in 1988 conducted by McGreer et al., demonstrated an intimate association of microglia, the brain's resident macrophage, with senile plaques in AD¹⁴⁸. Other studies in the 1980's report immune-related proteins within proximity to A β plaques^{123,149}. On a temporal scale, microgliosis closely follows initial amyloid deposition, and phagocytosis of amyloid plaques by microglia can lead to activation⁴¹. Briefly, activated microglia can secrete toxic proinflammatory cytokines, and through complement signaling, can lead to early synaptic loss in A β mouse models^{64,150}. Despite histological and epidemiological evidence implicating innate immunity as central drivers of aging, neurodegeneration, and AD microglia have been historically difficult to study given their minority status in the brain, resistance to viral genetic delivery. Furthermore, unlike neurons, microglia do not communicate via action potentials, eluding interrogation by electrical physiology means. Furthermore, intense controversy regarding the role of the brain's immune system impacted the scientific discourse surrounding neuroinflammation. Technical advancements in the last two decades in genomic, transcriptomic, and proteomic methodologies have made possible refined understandings of microglia's central role in neurodegeneration (*See Chapter 2*).

iv. Chapter I. Figures

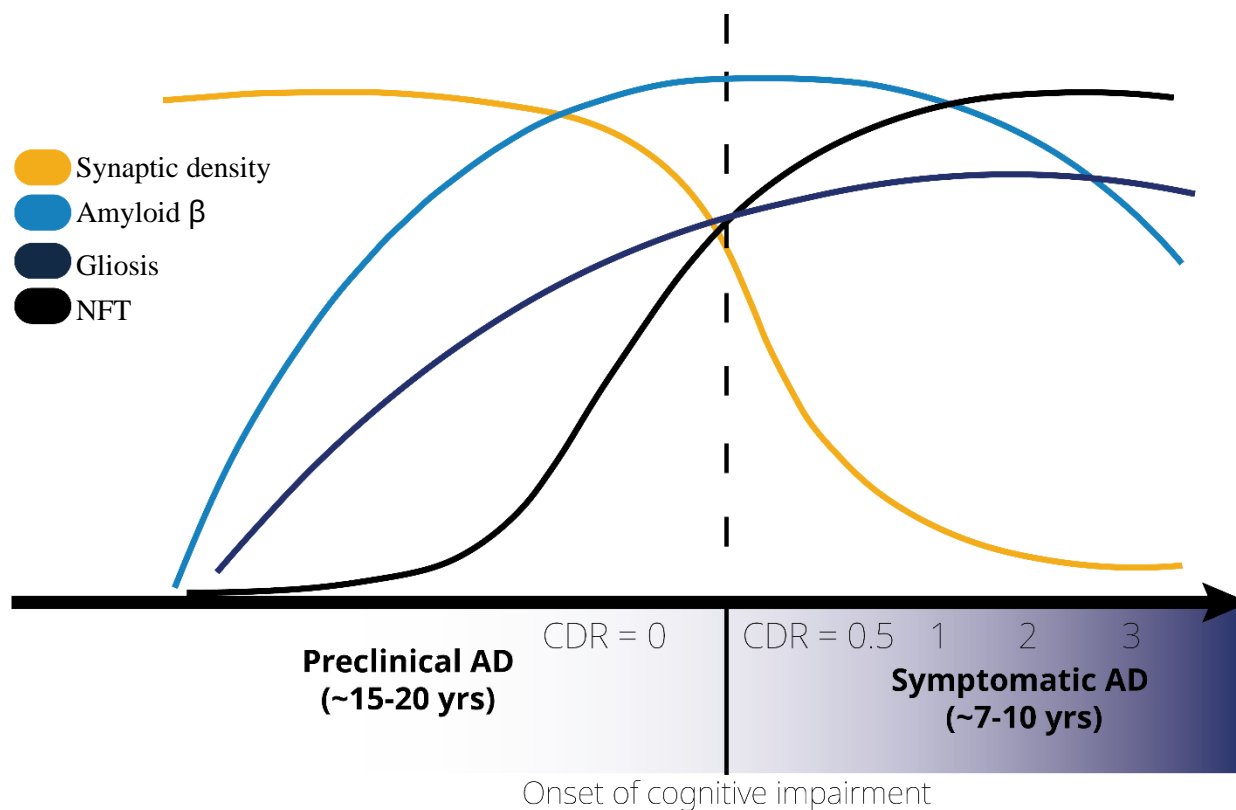


Figure 1.1. Pathological correlates to cognitive decline in Alzheimer's disease. Pathological hallmarks of AD, including synaptic loss, amyloid deposition, gliosis and pathological tau tangles provide biomarkers capable of correlating to clinical outcomes as assessed by the clinical dementia rating scale. Amyloid deposition begins decades prior to the onset of clinical decline, followed by chronically activated astrocytes and microglia which localize to neuronal injury and amyloid plaques. Neurofibrillary Tau Tangles (NFT) accumulation precedes synaptic loss. Synaptic loss is the strongest pathological correlate of cognitive decline (figure modified from Long & Holtzman, 2020⁴¹).

Chapter II. Advances in proteomic phenotyping of microglia in neurodegeneration.

Abstract:

Microglia are dynamic resident immune cells of the central nervous system (CNS) that sense, survey, and respond to changes in their environment. In disease states, microglia transform from homeostatic to diverse molecular phenotypic states that play complex and causal roles in neurologic disease pathogenesis, as evidenced by the identification of microglial genes as genetic risk factors for neurodegenerative disease. While advances in transcriptomic profiling of microglia from the CNS of humans and animal models have provided transformative insights, the transcriptome is only modestly reflective of the proteome. Proteomic profiling of microglia is therefore more likely to provide functionally and therapeutically relevant targets. In this review, we discuss molecular insights gained from transcriptomic studies of microglia in the context of Alzheimer's disease as a prototypic neurodegenerative disease, and highlight existing and emerging approaches for proteomic profiling of microglia derived from in vivo model systems and human brain.

*Chapter II includes modified excerpts from the review publication published in the journal *Proteomics* on April 15th, 2023 [2200183] DOI <https://doi.org/10.1002/pmic.202200183>

i. Microglia are the resident macrophage of the central nervous system

Microglia are the predominant resident myeloid cells of the central nervous system (CNS). Under homeostatic conditions, they survey microenvironments in the brain to phagocytose pathogens, dead cells, and cellular debris^{151,152}. During development, they are critical to refining synaptic architecture by pruning supernumerary synapses. When microglia respond to activating signals or triggers, they dramatically change their morphology from highly ramified to amoeboid states, proliferate, produce cytokines, and upregulate phagosome machinery¹⁵³⁻¹⁵⁷. Microglia can also contribute to CNS injury by producing neurotoxic factors, and potentially engulfing healthy synapses. Despite their critical roles in homeostasis, development, and disease, they have been historically difficult to study. Microglia comprise 10 -12% of total brain cells with regional variation^{158,159}. They do not communicate with action potentials as neurons do, and unlike other brain cell types, they derive from myeloid lineage¹⁶⁰. Historically, microglia's minority status in the brain along with the lack of surface markers suitable to distinguish microglia from other myeloid and brain cells have posed technical obstacles in isolation and molecular characterization. Additionally, microglia evade viral infection, thus making viral direction of genetic vectors exceedingly challenging. Despite these traditional technical barriers to genetically manipulating and isolating microglia from brain, there have been clues that microglia are causal mediators of autoimmune, aged, inflammatory, and neurodegenerative conditions^{161,162}.

ii. *Genome wide association studies implicate microglia in late onset*

Alzheimer's disease

A series of GWAS in late-onset Alzheimer's disease (LOAD) patient populations showed that microglia are important mediators of AD¹⁶³⁻¹⁶⁹. While only comprising 10-12% of the total brain cell population, microglia express several risk genes (e.g., *TREM2*, *CD33*, *APOE*) associated with LOAD^{158,170,171}. Apolipoprotein E (*APOE*) is one of the strongest and common genetic risk factors for LOAD, and is highly expressed at the transcript level in both astrocytes and microglia, and several studies have identified immune regulatory roles for *APOE* in animal models of AD pathology^{172,173}. The *APOE4* allele¹⁷⁴, as compared to *APOE3*, increases the risk for LOAD by threefold in heterozygous E3/E4 carriers and 15-fold in homozygous (E4/E4) carriers¹⁷⁵⁻¹⁷⁷. Additionally, microglia highly express triggering receptor expressed on myeloid cells 2 (*TREM2*), a gene which encodes a protein critical for microglial survival and proliferation, immune signaling, phagocytosis and recruitment to A β plaques¹⁷⁸⁻¹⁸⁰. GWAS revealed that partial loss-of-function mutations in *TREM2* significantly increased the risk of late onset AD by 3-5-fold^{179,181,182}. Stemming from these seminal human genetic studies, selective genetic modulation of these AD risk-genes specifically in microglia using conditional genetic approaches in animal models have advanced our understanding of how these microglial genes contribute to AD pathogenesis^{178,183-}

iii. Transcriptomic diversity of microglia in murine models of Alzheimer's disease and human Alzheimer's disease.

Advancements in single-cell RNA sequencing (scRNA-seq) of brain myeloid cells from animal models of AD pathology and post-mortem human brain from AD subjects have refined our understanding of the complex and diverse molecular transformations of microglia. A landmark study conducted in 2017 used scRNA-seq to isolate transcriptomes of microglia from differentially aged wild-type and transgenic 5xFAD mice, a model of A β pathology, and identified a unique population of DAM¹⁸⁷. Within 5xFAD mice, microglia transition from a homeostatic state to a DAM state between the ages of 3-8 months¹⁸⁷. DAM transcriptomic signatures included high expression of previously identified human AD risk genes (APOE and TREM2) and included a repression of homeostatic genes (Cd33, Csf1r, Cst3, Cx3cr1, P2ry12, P2ry13, Tmem119). DAM also exhibited signatures of increased lipid metabolism, phagocytosis, and lysosomal activity. Genetic loss of Trem2 in 5xFAD mice further resolved two sequential phases within the DAM activation cascade. The first Trem2-independent phase represses homeostatic factors, whereas the second Trem2-dependent phase prepares microglia for increased phagocytic activity¹⁸⁷. Since this study was published, a multitude of microglial scRNA-seq investigations have been conducted in a wide variety of mouse models of neurodegeneration in and beyond amyloid-based models¹⁸⁸. Converging evidence now supports wide prevalence of DAM across various models of

CNS injury, inflammation, and aging ¹⁸⁹⁻¹⁹¹, although A β pathology appears to be one of the strongest inducers of the DAM phenotype. Taken together, it is possible that DAM phenotypes may be a universal microglial response to injury ¹⁸⁹⁻¹⁹¹. The immense complexity of microglial transcriptomic phenotypes in the brain have also necessitated standardization in definitions of microglial states and nomenclature ¹⁸⁸.

Transcriptomic signatures of human microglia are also known to diverge significantly from those of rodent microglia in homeostatic and neurodegenerative conditions ^{170,192-196}. ScRNA-seq studies on microglia isolated from postmortem human brain regions (prefrontal cortices, frontal cortices, and parietal lobes) demonstrate divergence in human AD gene-signatures distinct from mouse models though APOE emerges as a common differentially enriched gene in mice and humans ^{192,194,197}. Consistent with mouse models, TREM2 loss-of-function mutations in humans weakens microglial activation in humans ¹⁹³. In a large human microglia single-cell analysis of over 16,000 microglia from human AD and nonpathological control cases ¹⁹⁶, Olah et al., 2020 identified nine transcriptional clusters with 80% of the microglia clustering into 2 homeostatic clusters ¹⁹⁶. The only cluster containing genes significantly altered with pathologic diagnosis of AD in the human dorsolateral prefrontal cortex overlapped considerably (>85%) with the murine DAM expression profile, with enrichment in genes involved with inflammatory demyelination, ischemia, and AD ¹⁹⁶. However, this cluster significantly decreased its expression

in AD with histological validation of reduced frequency of microglia associated with this cluster in AD human brain.

The reported transcriptomic discord between human and rodent microglia are likely driven by a combination of biological and experimental parameters. Importantly, rodent models are maintained in well-controlled environments with sterilized food, water, bedding, and cages¹⁹⁸. These environments are designed to reduce incidence of pathogen and contaminant exposure over the animal's lifetime and therefore may impact immune activation, which could confound interpretations comparing human and rodent studies. ScRNA-seq studies on fresh rodent brain are more amenable to intact-isolation of microglia as compared to human tissues which are typically frozen¹⁹⁹. Studies using archived (frozen) postmortem human brain samples are also confounded by on post-mortem interval, comorbidities, and independent effects of aging. Furthermore, human brain samples of advanced neurodegeneration introduce a sampling bias towards terminal disease stage¹⁹⁹. Alternatively, animal models lend experimental control over selecting final age end-points which can reflect initial, moderate, and advanced disease states. Given these caveats, the level of discordance in transcriptomic characteristics and immune responses between mouse and human microglia still remains to be clarified. Given these apparent discordances, it is critical to assess microglial transcriptomic signatures directly from human brain samples to verify observations made in mouse models²⁰⁰.

iv. The impact of Microglia signaling on Alzheimer's disease pathogenesis

Despite advancements in our understanding of the transcriptomic diversity across subpopulations of microglia in disease, proteomic studies are critical to reveal cell signaling mechanisms. Proteins, not transcripts, are the effector molecules of signaling cascades that give rise to microglial phenotypes and coordinate specific biological functions ²⁰¹. Microglia depend on intra and inter cellular signaling to sense injury, transition to activated states, mobilize to the sites of pathological insults, phagocytose debris, and prune synapses ²⁰². These functions are carried out by complex signaling cascades, some of which are highlighted in **Figure 2.1**. Microglia use the fractalkine receptor (CX3CR1) to bind and promote phagocytosis of microtubule-associated protein tau (MAPT) ^{203,204}. TAU can interact and promote the seeding of A β plaques and are more readily phosphorylated in the presence of A β ²⁰⁵. Microglia rely on TREM2 signaling to detect environmental cues (e.g., APOE, A β , phospholipids, and apoptotic cells), direct motility to injury sites, stimulate proliferation, and induce the DAM program ²⁰⁶⁻²⁰⁹. TREM2 decrease reduces microglia activation observed by impaired phagocytic capacity of injured neurons and decreased inflammatory responses ²¹⁰. Cell surface presence of TREM2 requires adaptor protein DNAX-activation protein 12 (DAP12) to initiate intracellular signaling via the recruitment of the tyrosine protein kinase SYK ^{211,212}. Mice lacking SYK showed exacerbated A β neuropathology and worse behavioral deficits ²¹³. TREM2 also associates with DAP10 to promote the recruitment of phosphatidylinositol 3-kinase (PI3K) ²¹⁴. TREM2-DAP12-DAP10 signaling primes downstream

protein and lipid phosphorylation events which initiate a myriad of signaling cascades supporting diverse cellular responses. These responses include cytoskeletal reorganization and Ca²⁺ signaling which both in turn influence microglial motility and process extension, mechanistic target of rapamycin (mTOR) signaling which promotes proliferation and differentiation of immune cells, autophagy, and apoptosis, and mitogen-activated protein kinase (MAPK) activation^{179,215}. In turn, MAPK cascades, including the extracellular signal-regulated kinases 1 and 2 pathway (ERK1/2) regulates gene transcription to promote cell proliferation, migration and immune function²¹⁶. Studies found that the MAPK/ERK pathway is a central mechanism of AD and is strongly correlated with AD pathology and cognitive decline²¹⁷⁻²²⁰. Notably, the strong association between MAPKs (ERK1 and 2) and human AD pathology was identified at the proteomic, but not at the transcriptomic level²²⁰. Because post-transcriptional and post-translational regulation is important for some proteins, jointly measuring both RNA and protein can reveal disease-relevant regulatory mechanisms²²¹⁻²²⁴. Joint measurement of RNA and protein can also reveal changes at the RNA-level not reflected at the protein-level and vice-versa. In mouse models of AD pathology, microglia are characterized by elevated ERK signaling, and ERK inhibition reduces microglial activation and proinflammatory immune responses²¹⁷. Taken together, TREM2 is a critical surveillance sensor that enables microglia to detect pathological cues in the environment, induce activation programs via an orchestration of signaling cascades

(e.g., Ca²⁺, mTOR, MAPK/ERK) that enable microglia to proliferate, mobilize to damage-sites, and clear cellular debris and pathological proteins.

In addition to the signaling cascades which enable microglia to sense and respond to the extracellular environment, activated microglia produce cytokines which in turn change the phenotypes other brain cells, such as astrocytes (**Figure 2.1**). For in-depth reviews on astrocyte-microglial crosstalk, see Matejuk & Ransohoff., 2020; and Vainchtein & Molofsky., 2020 ^{225,226}. Briefly, media derived from LPS-activated microglia containing elevated levels of IL-1 α , TNF α , and C1Q induce an activated neurotoxic phenotype in astrocytes which contribute to neuronal death ²²⁷. Furthermore, studies show that microglia-astrocyte crosstalk is necessary for the astrocytic Toll-like receptor (TLR) induced inflammatory response ^{228,229}. Although studies have shed light on the molecular cross-talk between microglia and astrocytes, future work that integrates proteomic approaches will uncover novel mechanisms of microglial-astrocytic crosstalk and contributions to neurodegeneration.

Another class of key microglial signaling effectors in development and pathology includes complement proteins. The complement cascade is a critical effector mechanism of the CNS and peripheral immune response that comprises of over 40 proteins ²³⁰. Neurons and their synapses express complement activators “eat me signals” as well as complement inhibitors “don’t eat me signals,” which evolved in the mammalian CNS to support the refinement of synaptic architecture by microglia during critical developmental periods ^{151,231,232}. In neurodegenerative

contexts, injurious stimuli (e.g., apoptotic cells, pathological proteins such as A β and TAU) activate the C1 complex (C1Q, C1R2, and C1S2)²³⁰. Following C1 complex activation, complement proteins C2 and C4 combine to create the C3 convertase, C4B2B. C4B2B cleaves C3 to form C3A, which promotes chemotaxis and microglial activation via the C3A receptor, C3AR. When C1 binding initiates complement activation on synapses, C3 tags them for elimination via microglial phagocytosis^{151,233}. In AD, the complement pathway contributes to synaptic loss and neuronal damage²³⁴⁻²³⁶. One recent large scale proteomics study conducted by Bai et al., 2020 used differentially staged post-mortem human AD brain to identify complement proteins as a key hallmark denoting pathological transition from mild cognitive impairment to AD²³⁷. While we discussed TREM2 and complement mediated signaling as key AD-related pathways in microglia, several other receptor-mediated signaling pathways exist in microglia based on the diverse array of surface receptors expressed by these cells^{202,238,239}. Taken together, microglia employ complex signaling cascades to support a wide variety of phenotypic changes in neurodegeneration. Signaling cascades and disease mechanisms rely in large part on the tight regulation of post-transcriptional and post-translational changes which transcriptomics cannot resolve, proteomic investigations are needed. Additionally, since proteomic changes are modestly reflected by transcriptomic-level changes, studies focused on proteomic profiling of microglia are critical to expand our understanding of microglial contributions to disease^{240,241}.

v. *Bulk-brain proteomics studies*

As compared to the transcriptome, the proteome of microglia is orders of magnitude more complex and is more proximate to biological functions. Poor concordance between the transcriptome and proteome particularly in the CNS, has been observed^{242,243}. Transcriptomic analyses are unable to capture post-translational modifications (PTMs), many of which regulate protein function and localization within the cell. PTMs are more likely to represent druggable targets for disease-modification as well as potential biomarkers in neurodegeneration. Therefore, complimentary assessments of the transcriptome and proteome of bulk tissue and of individual CNS cell types can provide a comprehensive understanding of cellular functions and disease processes. Quantitative mass spectrometry (MS) has been successfully applied to analyze postmortem human and mouse brain. These MS-based studies of bulk tissue are coupled with bioinformatic approaches to resolve several groups (or modules) of co-expressed proteins, which may represent shared biological functions, cellular endophenotypes, subcellular compartments, or shared upstream regulation^{220,244}. These network-based approaches shaped the current understanding of the proteomic transformations that occur in the brain in neurodegeneration. While bulk tissue proteomics do not directly resolve cell type-specific biology, it is possible to indirectly infer cellular mechanisms by deconvoluting the bulk proteome using reference gene/protein markers of individual brain cell types. In this manner, postmortem human bulk tissue proteomics provide excellent opportunities to study immune and glial mechanisms of AD,

with potential inferences related to microglia. We next highlight insights into metabolic, inflammasome and complement related immune protein alterations that occur in AD brain, as revealed by recent bulk tissue MS studies.

Bulk brain proteomics studies reveal metabolic re-programing in glial cells in AD brain

In a large-scale label-free quantification (LFQ)-MS analysis of over 2000 post-mortem brain samples, 453 of which were derived from asymptomatic/prodromal AD (AsymAD) or AD cases, a module of proteins (M4) enriched with microglial markers and sugar metabolism proteins, emerged as the module with the strongest correlation to AD traits including cognition, A β deposition, neurofibrillary tangles, and overall functional status ²⁴⁵. M4 proteins increased significantly in AD cases compared to controls. In addition to containing several AD genetic risk factors, the hub proteins associated with the M4 module include MSN, PLEC, ITGB1, PRDX1, and CD44. Specifically, glycolytic proteins including LDHB, PKM, and GAPDH and proteins associated with glycolytic flux including PRDX1, DDAH and PARK7 were also representative of the M4 module, along with glial proteins CASP1, SPP1, and MAPK1 ²⁴⁵. Conversely, another module (M3) enriched in mitochondrial proteins, including electron transport activity (ATP1A3) and NADH dehydrogenase activity (NDUFA9 and NDUFA10), was decreased in AD, independent of aging ²⁴⁵. The simultaneous decrease in mitochondrial proteins and increase in glycolysis proteins in the brain exhibits the metabolic reprogramming known as the Warburg effect ²⁴⁶⁻²⁴⁸.

Since M4 was disproportionately enriched in microglial and astrocyte protein markers, it is likely that glial metabolic reprogramming towards glycolysis is a major pathogenic phenotype of AD pathology. As homeostatic microglia transform to DAM, they shift from aerobic respiration with oxidative phosphorylation produced ATP, to utilize glycolysis for ATP production. These proteomic findings are also consistent with literature describing a state of insulin resistance in AD brain ²⁴⁹. Lipid peroxidation, resulting in lipid degradation via 4-hydroxynonenal also increases with the severity of AD ²⁵⁰. Increases in glycogen-synthase kinase 3 β in AD patients further promotes oxidative stress within the brain ²⁵⁰. In a following deeper proteomic study of control and AD post-mortem brains, the parent M4 module was further sub-divided into two modules: M7 (enriched in MAPK signaling proteins) and M11 (Cell-Extracellular-Matrix [ECM] interactions) ²²⁰, both of which were strongly associated with cognitive decline, even after adjusting for neuropathological AD hallmarks ²²⁰. Taken together, these studies demonstrate that microglial metabolic shifts (metabolic reprogramming) associate with cognitive decline independent of AD neuropathology. Bulk brain proteomes suggest that microglial metabolic reprogramming is a key driver of AD etiology, thus the relationship between metabolism and neuroinflammation warrants further investigation. Whether the glial, metabolic, and immune protein changes captured in M4 in AD are protective or detrimental, is unclear and requires direct investigation in appropriate model systems.

Bulk brain studies provide evidence for increased inflammasome activation in AD brain.

Inflammasomes are critical mechanistic components of the innate immune system's ability to detect pathogens and mount a concerted cellular response against them ²⁵¹. Inflammasomes are made up of multi-protein complex with specialized sensory, adaptor and effector caspase components ^{251,252}. The activation of the NOD-, LRR-, and pyrin domain containing 3 (NLRP3) inflammasome, specifically, is associated both with human post-mortem AD brain and transgenic mouse models of AD ²⁵³⁻²⁵⁷. Caspase-1 (CASP1), a key component of the NLRP3 inflammasome, is also upregulated in AD brain and is a member of module M4, that contains proteins upregulated in AD several of which are enriched in microglia and involved sugar/carbohydrate metabolism ²⁵⁸. The NLRP3 inflammasome is a multiprotein complex heavily involved in inflammation, particularly in the cleavage and release of the interleukin (IL) -1 β and IL-18 proinflammatory cytokines ²⁵⁹. Proinflammatory responses in microglia depend heavily on bioenergetic shifts. A strong component of the proinflammatory response and bioenergetic shifts, the NLRP3 inflammasome is also activated in frontotemporal dementia (FTD) patients ²⁵⁴. Ising et al found an increase in cleavage of caspase 1, mature IL-1 β , and apoptosis associated speck like proteins (ASC) in AD and FTD patients ²⁵⁴. This was also highlighted in Tau22 mice, which overexpress Tau through IHC and western blots ²⁵⁴. These Tau 22 mice also show higher Casp1 and Il1b gene expression ²⁵⁴. When crossing Tau22 mice with Pycard or Cias1 deficient mice

(Tau22/Asc^{-/-} or Tau22/Nlrp3^{-/-}), there was a reduction in cleaved CASP1 and IL-1 β as well as a reduction in spatial memory showed through a Morris water maze ²⁵⁴. Westerns of Tau22/Asc^{-/-} and Tau22/Nlrp3^{-/-} mice show a decrease in PP2A phosphatase activity and 18 genes, including Ccl3 ²⁵⁴. Injection of APP/PS1 into inflammasome KO mice shows an increase in IL-1 β and phosphorylated TAU ²⁵⁴. Meissner et al highlights the strong connection between metabolism and the NLRP3 inflammasome through evaluating changes in superoxide dismutase 1 (SOD1) influence on the NLRP3 inflammasome ²⁶⁰. In vitro, SOD-1 deficient macrophages show a reduction in cleaved IL-1 β and IL-18, while inflammasome independent cytokines such as TNF- α and KC remain unaffected ²⁶⁰. SOD-1 deficient macrophages have increased reactive oxygen species (ROS) due to the lack of superoxide presence²⁶⁰. In vivo in SOD-1 KO mice that received LPS and ATP stimulation to induce inflammasome formation, reduced glutathionylation was observed, further inhibiting CASP1 activity as shown by a reduction NLRP3 inflammasome cleavage of IL-1 β ²⁶⁰. Recently, therapeutic targets for the inflammasome are being developed for treatment of AD. One such therapeutic agent is JC124, a sulfonamide-based selective inhibitor of the NLRP3 inflammasome. APP/PS1 mice treated with JC124 showed improvements in behavioral contexts such as fear conditioning ²⁶¹. JC124 treatment also reduced microglial and astrocyte activation as measured by a reduction in IBA1 and GFAP positivity, while potentially increasing synaptic plasticity through measurable increases in synapsin 1, synaptophysin, and PSD-95 ²⁶¹. JC124 also reduced the A β plaque load and IL-1 β and CASP1 ²⁶¹. This positions the

NLRP3 inflammasome as a potential target for regulating microglial activity and attenuating the detrimental effects of AD pathology.

Complement signaling in transition from mild cognitive impairment to AD dementia.

Several proteomic studies on differentially-staged AD postmortem human brain implicate complement signaling in the transition from mild cognitive impairment to AD. Under homeostatic conditions, neurons express complement activators and inhibitors to mark their synapses for pruning by microglia (see Section 3 for comprehensive review of complement signaling). This role is critical to the refinement of synaptic architecture ^{151,231,262,263}.

In the context of AD etiology, complement signaling is necessary for synaptic toxicity of amyloid in mouse models ²³⁵ and expression of complement components C3 and C3A receptor (C4AR1) correlate positively with cognitive decline and Braak staging in human AD ²⁶⁴. Additionally, C3AR-deficiency in PS19 mice rescues tau pathology and attenuates neuroinflammation, synaptic deficits, and neurodegeneration ²⁶⁴, C3-deficient C57BL/6 mice exhibit resilience against age-dependent CA3 neuronal loss and enhanced synaptic plasticity at 12 months ²⁶⁵, and aged C3-deficient APP/PS1 mice perform significantly better on learning and memory tests than APP/PS1 mice ²³³. In human bulk-brain proteomic studies, complement proteins significantly increase with disease stage ^{237,258,266}. In one human brain proteomic study, Bai et. al., 2020 used TMT-MS to analyze the proteomes of 90 human frontal cortical samples from

varying disease stages including mild cognitive impairment (MCI) and later-stage AD ²⁶⁷. The protein cluster associated with the transition from MCI to AD included complement proteins (CR1, C1S, C3, C4A and C4B), which were consistent with high abundance of complement proteins C4A and C4B also contained in the M4 module in the independent analysis discussed above ²⁴⁵. It is possible that chronic activation of microglia by sustained A β and TAU deposition up-regulates microglial complement signaling; increasing microglial-mediated synaptic pruning. Given that synaptic loss, not A β nor TAU accumulation, is the strongest pathological correlate to cognitive decline, ^{268,269} it is possible that chronically activated microglia are aberrantly pruning synapses, advancing the transition from MCI to AD in human patients. Furthermore, in addition to generating human MCI and AD bulk brain proteomes, Bai et al., 2020 also generated bulk cortical proteomes deriving from differentially aged wildtype and 5xFAD mice (3, 6, and 12 months) ²³⁷. The analysis compared differentially abundant proteins (DAPs) from 5xFAD mice with human MCI and AD patients and found that the proteomes from older 5xFAD mice (12 months) were most reflective of human AD pathology, sharing 89 and 169 protein alterations with human MCI and AD brain, respectively. The analysis identified 37 human-specific and 69 5xFAD mouse specific DAPs. Uniquely in humans, AD pathology significantly reduces the abundance of specific synaptic proteins (CAMK2 and NPTX2) and neurotrophic factors (BDNF and VGF) ²³⁷, a trend which deviates from 5xFAD mouse models in this study. While synaptic loss in 5xFAD mice is well documented; several studies converge to show significant synaptic loss only beyond 4

months of age, none of these studies herein referenced note a decrease in the proteins CAMK2 or NPTX2 specifically^{118,235,270-273}. Due to the limitations of bulk-brain proteomics, the microglial-specific proteomic changes taking place during the transition from MCI to AD in humans or in mouse models of neurodegeneration are currently not known, despite many studies linking complement signaling with synaptic loss and cognitive decline in both mouse and human studies.

The divergence of vulnerability of sub-classes of neuronal and synaptic loss between human AD brain and brains derived from mouse models of neurodegeneration highlight the importance of caution when interpreting the physiological significance of neurodegenerative pathology exhibited by mouse models of AD. There is currently no mouse model which displays the full spectrum of human AD etiology⁶¹. The 5xFAD mouse model specifically drives the over-expression of high levels of mutant APP under the Thy1 promoter⁶³. The rapid and aggressive A β pathology exhibited by the 5xFAD mouse models must be taken into consideration. Whether or not proteomic differences between human AD and murine 5xFAD mouse models are due to differences in microglial cells specifically are difficult to assess in analyses deriving from bulk brain tissue. The inability to resolve cell-type specific changes from bulk tissue lends necessity for isolation-based approaches.

vi. Isolation-based proteomic interrogations of microglia

With the advent of fluorescence-activated cell sorting (FACS), magnetic activated cell sorting (MACS) and immunopanning approaches, it is possible to distinguish microglia from other brain myeloid populations (infiltrating, perivascular and border-associated macrophages) with high confidence, and subsequently isolate relatively pure microglia from adult mammalian brain for down-stream proteomics studies (**Figure 2.2**)^{202,244,274-278}. These methods utilize antibodies against microglial surface proteins to positively identify and then purify these cells. FACS, MACS and immunopanning result in high microglial yields from both rodent and human brain tissue prepared using either enzymatic or mechanical dissociation methods. In our hands, CD11B+ bead-based MACS isolation typically yields 100,000-200,000 live microglia from one adult mouse brain while FACS-based purification yields 50,000-100,000 CD11B+ CD45 intermediate microglia from one mouse brain^{244,274,276}. Additional purity of microglia can be obtained by using additional microglial markers such as TMEM119. These numbers are compatible with bulk proteomics studies which can investigate molecular characteristics of microglia as a whole population. The ability to use cell sorting methods (FACS or MACS) and immunopanning to isolate microglia from both human brain and rodents enables us to directly compare molecular transformations in postmortem human brain tissue with mouse models of aging and neurodegeneration. FACS-based microglial isolation from post-mortem human brain tissue is possible, and can be accomplished using a combination of markers such as CD11B CD45, along with other

lymphocytes, monocyte, and neutrophil markers. However, unlike mouse tissue where adequate cardiac perfusion can remove unwanted blood-derived monocytes, human post-mortem tissues typically contain non-microglial myeloid cells in variable proportions which are more difficult to exclude during purification ²⁷⁹.

One long-standing challenge inherent to cell-sorting based isolation methods of microglia relies on the detection and validation of microglial markers. Because microglia derive from myeloid lineage, and must undergo developmental transformation as microglial progenitor cells, it is exceedingly challenging to distinguish microglia from other macrophages residing in the choroid plexus, meninges, and perivascular spaces, especially in the setting of brain injury or established neuropathology ¹⁶⁰. This is because some monocyte markers are upregulated (e.g., CD45-high) while canonical microglial markers (e.g. Tmem119) are decreased with progressive pathology ²⁸⁰. Under homeostatic conditions, mouse microglia typically express high CD11B-positive (+), low to intermediate levels of CD45 and low Ly6c on the cell surface, whereas non-microglial macrophages express high levels of CD45 and Ly6c under homeostatic conditions ²⁸¹⁻²⁸³. In mouse models of AD, mononuclear phagocytes (MP) in the central nervous system have a higher proportion of CD45high cells, and CD45high surround and phagocytose A β , and demonstrate persistently elevated phagocytic capacity for fibrillar A β 42 with age ²⁸⁴. While FACS can purify microglia using both positive and negative selection using a combination of markers, MACS typically relies only on CD11B as a positive selection marker. Therefore, MACS and FACS

purified microglia result in different levels of contamination by non-microglial myeloid cells, a factor that must be considered in experimental design.

There are notable assay-level differences in microglial proteomes prepared between FACS and MACS. MACS has been shown to have a comparatively higher yield than FACS, with a cell viability exceeding 85% for both ²⁸⁵. Additional considerations include the longer processing time for FACS, and molecular alterations associated with FACS protocol and the difficulty of using multiple marker profiles, and inability to perform live/dead gating with MACS ^{285,286}. Additionally, one study compared the proteomic differences between microglia isolated via FACS or MACS from 4-month-old C57/Bl6J wildtype mice ²⁷⁶. MACS-isolated microglial proteomes showed high abundance of non-microglial synaptic and neuron-projection proteins despite >90% microglial purity, whereas FACS-isolated microglial proteomes showed enrichment of immune function proteins. Another advantage of FACS is the ability to isolate other brain cell types in parallel (e.g., macrophages, endothelial cells, astrocytes, and oligodendrocytes while MACS only allows one cell type at a time ²⁸⁷. On the other hand, MACS is much faster than FACS, while FACS is generally associated with higher cell loss ^{285,288}. Despite the differences in proteomic purity, both methods yielded a consensus set of 203 core microglial proteins, including IBA1, COTL1, and AD-relevant proteins such as potassium channel tetramerization domain-containing protein 2 (KCTD2), bridging integrator 1 (BIN1), and Moesin (MSN) ^{275,276}.

What have we learned from isolation-based microglial proteomics in AD pathology?

Advanced age is the strongest risk factor for AD ²⁸⁹. It is important to isolate the impact of advanced aging on microglial phenotype to contextualize studies of microglial changes with age and AD etiology. The first study to isolate the impact of age on microglial proteomes, without the context of disease, compared primary microglia of 3-5-month-old mice to those of 20-24 months ²⁹⁰. They identified 156 DAPs involved with inflammatory signaling, mitochondrial function, and cellular metabolism with age. Notably, this study identifies an age-dependent decrease in mTORC2; contributing to a pro-inflammatory phenotype. mTORC2 promotes protein synthesis in response to growth factors and in-turn regulates cellular metabolism and macrophage polarization ^{291,292}. With age, microglia lose their ability to sense and respond to growth factors in the environment, via the reduction of mTORC2. Microglia in turn lose their plasticity, or their ability to polarize between inflammatory and homeostatic states²⁹¹. These results are consistent with a human AD proteomic study identifying showing a decrease in both the transcriptional regulation of inflammatory signaling and a decrease in polarization with age, and an increase in mitochondrial proteins using fatty acids and ketone bodies as energy substrates ²⁴⁵. Both human and mouse proteomic studies converge to show a unique aged microglial phenotype characterized by shifts in transcriptional regulation of inflammatory signaling, a metabolic re-programming shifting from glucose to fatty acids and ketones to generate energy, and a loss of plasticity. These proteomic studies on aged microglia are consistent with other

studies showing that aged microglia mount a larger inflammatory response to acute inflammatory stimuli compared with younger mice ^{293,294}, and morphologically shift to amoeboid, less ramified states characterized by cytoplasmic hypertrophy ²⁹⁵⁻²⁹⁷. The age-driven changes in microglial metabolism and plasticity are important to take in consideration with studies assessing the impact of inflammation or AD etiology on the isolated microglial proteome.

Neuroinflammation, as characterized by activation of microglia and astrocytes and an increased expression of pro-inflammatory cytokines, is a central component of age and a hallmark of post-mortem human AD brain ^{83,298-302}. To distinguish the relative impact of inflammation and A β pathology on the microglial proteome in aged mice (6-7 months), Rangaraju et al., 2018 performed a quantitative MS study on purified CD11B+ microglia from wildtype mice, wildtype mice treated with Lipopolysaccharide (LPS), and 5xFAD mice ²⁷⁵. LPS suppressed mitochondrial oxidative phosphorylation with concurrent increases in stress-response and glycolytic proteins ²⁷⁵. When comparing DAPs enriched in 5xFAD brain or LPS-treated mice, this study identified several common proinflammatory proteins (top 5 including CLU, NUDT2, GLIPR2, DIABLO, and CSTF) and 30 proteins which were decreased both in 5xFAD and LPS treated mice (top 5 including BCORL1, PLEKHG1, RASGEF1A, IPO4, and BICD1). The direction of change of common proteins between 5xFAD and LPS were largely concordant ($r=0.47$), suggesting that A β pathology induces a pro-inflammatory state in microglia. Pleckstrin homology and RhoGEF domain containing G1 (PLEKHG1) was decreased in microglia derived from both LPS-treated

mice and 5xFAD mice has been associated with human AD as well. For example, a recent study integrated single-nuclei RNA-seq (snRNA-seq) and proteomic datasets from human AD cortical and serum samples, and identified PLEKHG1 as a novel candidate biomarker. PLEKHG1 shows a decreased gene expression in human AD, though no studies have yet reported the role of PLEKHG1 in the nervous system ³⁰³.

Rangaraju et al., 2018 then identified specific proteomic changes in murine 5xFAD microglia consistent with proteomic datasets derived from frontal cortices of human post-mortem AD tissue. They identified 11 proteins similarly increased with Alzheimer's disease and 5xFAD microglia (CLU, COTL1, HTRA1, APOE, APP) and 23 proteins decreased with AD and 5xFAD (including VGF, RTN, ALPL, SCN3A, and CAMK4). Notably, Clusterin (CLU) is a common protein which is significantly increased in microglia in response to acute inflammation (LPS), in microglia in murine models of amyloid pathology (5xFAD), and in human AD brain. CLU is an apolipoprotein that binds to TREM2 and facilitates microglial uptake of amyloid-beta (A β), and has long been associated with AD genetic risk ^{166,207,304}. Neuroinflammation induced by repeated LPS has been shown to induce memory impairment, increased activity of β and γ secretases, and increase generation of toxic species of A β 1-42^{126,305-307}. The generation of toxic A β is a common etiology across LPS administration, 5xFAD pathology, and human AD, and the resulting increase in microglial-derived CLU emerges as a conserved response to facilitate microglial engulfment of these toxic amyloid species.

To understand microglial proteomic changes preceding A β plaques, Boza-Serrano et al., 2018 used MACS to isolate CD11B⁺ primary microglia from WT and 5xFAD aged to time points before plaque deposition (2 weeks and 6 weeks), and after plaque deposition (10 weeks), for downstream MS analysis³⁰⁸. Their results showed a significant increase in inflammatory pathways in 5xFAD mice before the onset of plaque deposition. One hypothesis posits that neuronal release of soluble A β at 6 weeks could be activating microglia prior to the presence of insoluble plaque deposition. A comprehensive proteomic study of acutely isolated microglia from later stages of 5xFAD mice showed that APOE expression is enriched in 5xFAD mice and increases with age in both wildtype and 5xFAD mice¹⁴⁷. The histological characterizations of this study did not detect APOE in ramified microglia whereas plaque-associated microglia contained APOE and A β , suggesting that both may be phagocytosed by plaque-associated microglia.

A recent investigation used high resolution MS to generate ex vivo human microglial maps isolated from 5 amygdalohippocampectomy samples to compare with proteomes generated from primary mouse microglia and BV2 cell lines³⁰⁹. This comprehensive study identified 9,456 human microglial proteins and 9,629 mouse microglial proteins. Comparing proteomes generated from ex vivo mouse and human microglia showed a significant enrichment in FC receptor activation, phagocytosis and inflammatory responses in human microglia³⁰⁹. Human microglia also showed a significant enrichment in proteins associated with key AD risk loci (APOE, CLU, and SORL1) and inflammatory cytokines IL-18 and immune cell marker CD45. Comparisons between in vitro

and ex vivo microglia altogether revealed a higher prevalence of homeostatic markers in ex vivo microglia; with notable absence of homeostatic microglial markers P2RY12, TMEM119 and CX3CR1 in mouse BV2 microglial cell lines ³⁰⁹. These findings have critical implications on the divergent identities of homeostatic and activated microglia between human and murine microglia, and between in vivo and in vitro culture models.

vii. Emerging proteomic labeling approaches circumvent the need for isolation.

Traditional methods to isolate microglia from adult brain rely on harsh reagents or mechanical dissociation and require fresh unfrozen brain tissue. The isolation process alters the microglia transcriptome and likely the proteome, introducing artifacts into datasets, likely confounding the ability to confidently determine the microglial proteome in their native state ³¹⁰. Furthermore, the harsh conditions of the isolation process introduce a sampling bias to isolating healthy microglia; limiting our ability to effectively capture disease-associated proteomic changes. The unmet need to capture the native proteomic signatures of microglia and other neural- and glial- cell types, in homeostatic and disease-associated states, has motivated the development of in vivo protein-labeling methodologies, which can be combined with affinity purification and MS (**Figure 2.3**). Broadly, in vivo proteomic labeling can be achieved via metabolic labeling of nascent proteins using bio-orthogonal non-canonical amino acid tagging

(BONCAT) as well as by proximity-dependent biotinylation methods, including cell type-specific in vivo biotinylation of proteins (CIBOP).

Nascent proteomic in vivo labeling using bio-orthogonal chemistry (BONCAT)

The BONCAT strategy is a method of labeling newly synthesized proteins with a methionine (Met) analogue using a mutated Met tRNA synthetase (MetRS, mutation L274G) ³¹¹. In the presence of the mutant MetRS, newly-synthesized or nascent proteins incorporate azidonorleucine (ANL), a methionine analogue with a “Click”-able azide moiety, in place of Met. Using the conditional MetRS-L274G mouse model (Strain Jackson Labs mouse strain #028071) combined with a Cre driver line (CamK2a promoter for excitatory neurons and Gad2 promoter for inhibitor neurons), the proteome of excitatory and inhibitory neurons in vivo were labeled and characterized by MS ³¹². After supplying ANL into the drinking water for 3 weeks, the mice labeled newly synthesized proteins with the clickable methionine analogue. After conjugating ANL-tagged proteins to biotin alkyne, the labeled peptides can be purified by means of streptavidin-based affinity capture. Because the BONCAT method only labels newly synthesized proteins, there may be challenges with achieving a desired depth of proteome, however, this feature may be an asset for studying event-related or stimuli-related changes to the proteome. Recently, BONCAT has been successfully applied to astrocytes as well ³¹³. The extension of the BONCAT

method to label and profile microglia, other brain immune cells and glial subtypes has not been reported thus far.

Proximity labeling methods for in vivo proteomic labeling.

As a complimentary approach to BONCAT, which labels the nascent proteome, more global cellular proteomic labeling can be achieved using proximity labeling methods. One proximity labeling method for native-state proteomics of neurons and glia in the brain utilizes ascorbate peroxidase (APEX). APEX rapidly biotinylates proteins within <20 nm radius of the peroxidase enzyme³¹⁴⁻³¹⁶. In the presence of hydrogen peroxide, APEX oxidizes biotin-phenols to phenoxy radicals which in turn biotinylate nucleophilic sites on amino acids³¹⁶. Since its inception, APEX has been used for several applications, ranging from mapping protein-protein interactomes³¹⁷, purifying proteomes of subcellular organelles by means of fusing APEX to specific site of interest³¹⁸, to transcriptomic profiling^{319,320}. Unlike TurboID-based CIBOP where biotinylation can occur in vivo, APEX-based labeling requires hydrogen peroxide for biotinylation, which can only be performed ex vivo after tissue isolation or dissection. Chen et al., in 2015 successfully applied the technology to live *Drosophila* tissue³²¹ and recently APEX has been successfully used for cell type-specific ex vivo labeling of mouse brain tissues to resolve subcellular proteomics of neuronal subtypes^{322,323}.

Several biotin ligases with varying degrees of promiscuity, labeling-radius, and efficiency have been developed (including BioID and TurboID)³²⁴⁻³²⁶. Among these, TurboID is a proximity-labeling biotin ligase engineered to promiscuously biotinylate proteins within minutes and within a 10 nm radius^{327,328}. Cytosolic proteomic labeling of several thousand proteins in mammalian cells can be achieved if TurboID is fused to a nuclear export sequence (TurboID-NES). TurboID-NES was recently engineered into the safe-harbor chromosomal Rosa26 locus of mice, for conditional TurboID expression in cell type or tissues of interest in vivo³²⁹. By expressing Cre-recombinase under astrocyte-specific and neuron-specific promoters (Aldh1 and Camk2a, respectively), using a combination of AAV-based or transgenic Cre recombinase expression, TurboID-NES was expressed in CAMK2A excitatory neurons and ALDH111 positive astrocytes in the adult mouse brain. This study then used streptavidin enrichment of biotinylated proteins and MS, and quantified 1,380 proteins labeled and enriched in both neurons and astrocytes, each with distinct cell type proteomic signatures, and furthermore, unique regional proteomic differences in the mouse brain³²⁹. To date, the CIBOP approach has been applied to neurons and astrocytes, and within in vitro BV2 and N2A cell lines, although extensions to other glial cell types in vivo including microglia are anticipated^{330,331}. The CIBOP approach paired with MS-based proteomics may provide much needed proteomic insights into glial contributions to neurological disease pathogenesis.

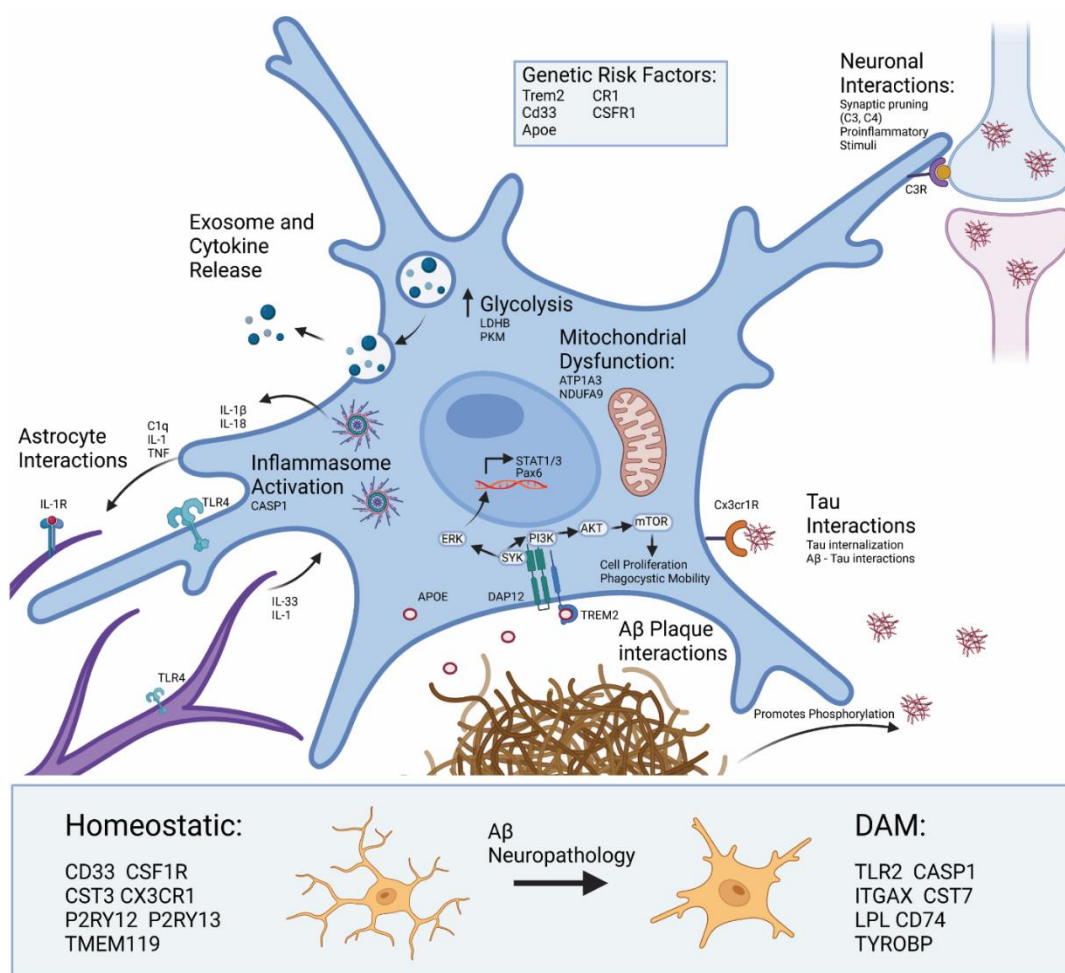
v. **Chapter II Figures**

Figure 2.1 Microglial responses in Alzheimer's disease. Several genetic risk loci for AD (TREM2, CD33, CSF1R, CR1, APOE) encode proteins involved in signaling cascades that support broad phenotypic shifts in motility, metabolism, phagocytosis, proliferation, cytokine production, exosome production and release, and apoptosis. Microglia use complement signaling to identify both healthy and dead neurons for degradation. Microglia can use signaling cascades to detect and recruit to pathological proteins including TAU and A β . For example, fractalkine signaling (via fractalkine receptor CX3CR1) allows microglia to detect and phagocytose Tau^{203,332,333}. Microglial interactions with A β plaques are distinct, where microglia actively surround A β plaques and interact with them via mechanisms involving APOE, TREM2 and its receptor. This receptor is responsible for the TREM2-dependent signaling pathway which results in activation of SYK and ERK^{334,335}. ERK then crosses the nucleus to allow for transcription of key inflammatory signaling molecules such as STAT1. Whereas activation of the mTOR pathway leads to further

phagocytosis and cell proliferation. TAU and A β can also directly interact with each other, where tau tangles can act as a seed for A β plaque accumulation and A β can promote the phosphorylation of tau necessary for tau fibrillization. Cross-talk between microglia and astrocytes is largely responsible for activation of the TLR4 and IL1R on both cell types which can shift astrocytes and microglia toward more proinflammatory cytokine release ²²⁶. Proteomic studies evidence an increase in CASP1 as well as IL-1 β indicating formation and activation of the NLRP3 inflammasome which cleaves proIL-1 β and proIL-18 prior to release from microglia. These signaling events also result in increased production and release of exosomes that contain key signaling proteins like TNF, and other cargo. This corresponds with metabolic reprogramming in microglia, where there is an increased movement of glucose to glycolysis but a reduction in mitochondrial activity, which in turn sustains ATP production and calcium-dependent mechanisms necessary for DAM function. A β and other neuropathologies also transform microglia from homeostatic and disease-associated microglia (DAM) states, and key markers of these states also shown below. ^{190,336}

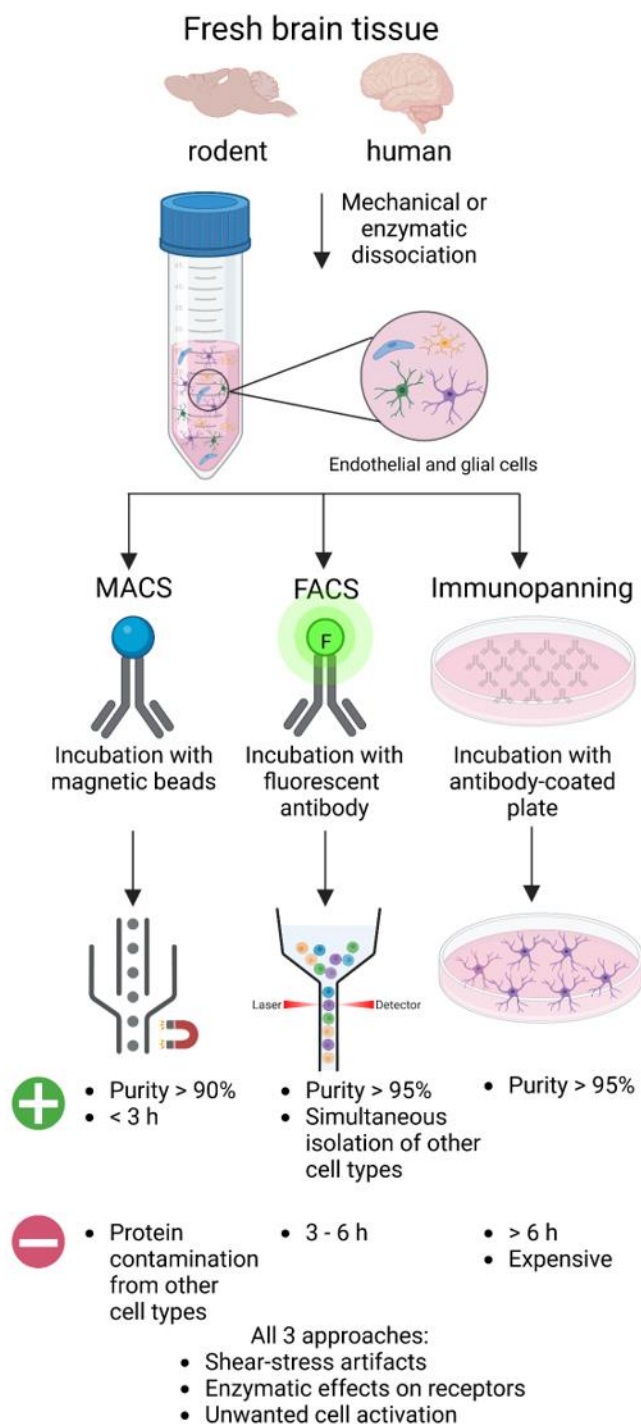


Figure 2.2 Isolation-dependent approaches for microglial proteomics. Acute isolation of microglia and other brain cell types requires fresh brain tissue that undergoes mechanical or enzymatic dissociation to generate a heterogenous single-cell suspension that can be prepared for MACS, FACS, or immunopanning methods. For MACS, the single-cell suspension is

incubated with a magnetic microbead conjugated to an antibody that binds a cell surface receptor. Then, a magnet is used to select for the desired cell type and the unbound cells are washed away. The magnetically bound cells are released and collected for downstream analysis. For FACS, the single-cell suspension is incubated with a fluorophore-conjugated antibody specific to a cell surface receptor. Following, the desired cell type is sorted based on size and fluorescent signal. The sorted cells are collected for downstream analysis. For immunopanning, single-cell suspensions are plated on a cell culture dish coated with an antibody specific to a cell surface receptor. The unbound cells are washed away, and the bound cells are collected for downstream analysis.

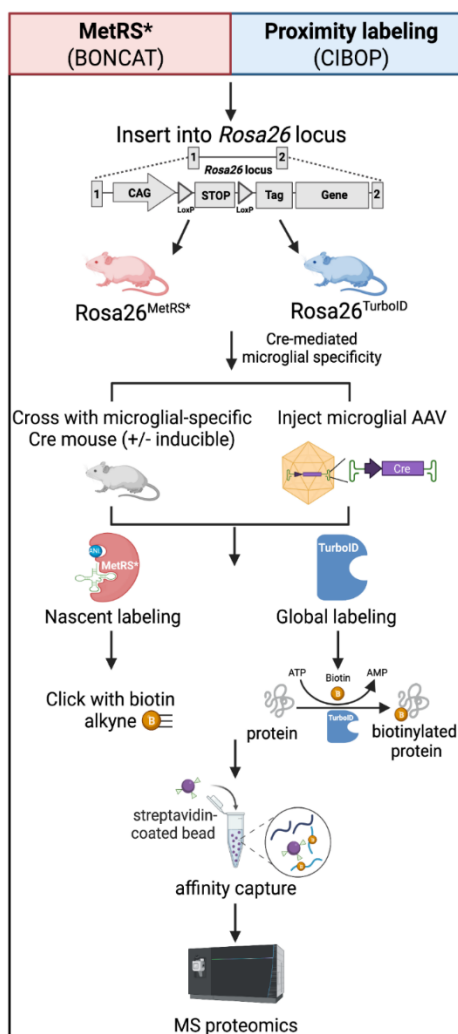


Figure 2.3 Isolation-independent methods for in vivo proteomic labeling of microglia. In vivo biorthogonal amino acid tagging (BONCAT) of proteins (red panel) and cell type-specific in vivo biotinylation of proteins (CIBOP) (blue panel) is achieved by inserting mutant MetRS (L274G) or MetRS*, or TurboID, into the *Rosa26* locus to generate in vivo proteomic labeling in mouse models. Following, microglia specificity can be achieved by either breeding the MetRS* or TurboID models with a microglia-specific Cre mouse, with or without inducibility, or by injecting a microglial-specific adeno-associated virus (AAV) to deliver Cre. MetRS* contains a mutation (L247G) in the amino acid binding site which tags nascent proteins with an azide tagged methionine analog, azidonorleucine (ANL). The azide residue of ANL can undergo “click” chemistry in which ANL-tagged proteins residues are “clicked” with a PEG-biotin-alkyne. Proximity labeling using CIBOP is achieved by the biotin ligase, TurboID, that biotinylates endogenous proteins in close proximity. After, MetRS* or TurboID tagged proteins can undergo

biotin affinity capture using streptavidin-coated beads and processed for downstream mass MS-based proteomics.

Chapter III. Cellular proteomic profiling using proximity labeling by TurboID-NES in microglial and neuronal cell lines.

Briefs:

TurboID-based proximity labeling of cytosolic proteins coupled with mass spectrometry represents a promising approach for proteomic profiling of specific cell types in vitro and in vivo, although the breadth of proteomic coverage, the ability to distinguish cell types and to capture pathological responses, and potential impacts of TurboID-mediated proteomic labeling on cellular physiology, are unknown. To inform in vivo applications of TurboID-NES, we interrogated the proteomic coverage achieved by TurboID-NES in neuronal and microglial cell lines under homeostatic and inflammatory conditions.

*Original findings published in the journal of *Molecular & Cellular Proteomics* on April 14th, 2023 [100546] <https://doi.org/10.1016/j.mcpro.2023.100546>. Supplemental Data and Datasheets can be found online at: <https://pubmed.ncbi.nlm.nih.gov/37061046/>

i. Abstract

Different brain cell types play distinct roles in brain development and disease. Molecular characterization of cell-specific mechanisms using cell type-specific approaches at the protein (proteomic) level, can provide biological and therapeutic insights. To overcome the barriers of conventional isolation-based methods for cell type-specific proteomics, in vivo proteomic labeling with proximity dependent biotinylation of cytosolic proteins using biotin ligase TurboID, coupled with mass spectrometry (MS) of labeled proteins, emerged as a powerful strategy for cell type-specific proteomics in the native state of cells without the need for cellular isolation. To complement in vivo proximity labeling approaches, in vitro studies are needed to ensure that cellular proteomes using the TurboID approach are representative of the whole cell proteome, and capture cellular responses to stimuli without disruption of cellular processes. To address this, we generated murine neuroblastoma (N2A) and microglial (BV2) lines stably expressing cytosolic TurboID to biotinylate the cellular proteome for downstream purification and analysis using MS. TurboID-mediated biotinylation captured 59% of BV2 and 65% of N2A proteomes under homeostatic conditions. TurboID labeled endo-lysosome, translation, vesicle and signaling proteins in BV2 microglia, and synaptic, neuron projection and microtubule proteins in N2A neurons. TurboID expression and biotinylation minimally impacted homeostatic cellular proteomes of BV2 and N2A cells, and did not affect LPS-mediated cytokine production or resting cellular respiration in BV2 cells. MS analysis of the microglial biotin-labeled proteins

captured the impact of LPS treatment (>500 differentially-abundant proteins) including increased canonical pro-inflammatory proteins (Il1a, Irg1, Oas1) and decreased anti-inflammatory proteins (Arg1, Mgl2).

ii. Introduction

The brain is a complex organ possessing heterogeneous populations of neurons, glia, and vascular cells. The orchestration of interactions within cell types (cell autonomous) and between cell types (non-cell autonomous) support higher-level processes critical to development, aging, and neurodegeneration. Protein-level analyses using mass spectrometry (MS) expands upon other systems-level analyses, including genomics and transcriptomics. Specifically, proteomics can profile total protein abundances, identify post-translational modifications, and resolve protein-level changes occurring in subcellular compartments. A central challenge to neuroproteomics is the difficulty in obtaining cell-type specific proteomes from brain tissue.

Traditional approaches to isolating cell-type specific proteomes for MS including fluorescence activated cell sorting (FACS) and magnetic activated cell sorting (MACS) require fresh brain tissue, and the harsh and laborious processing itself poses challenges.^{337,338} A majority of adult neurons do not survive the isolation process, and sampling bias for healthier non-neuronal brain cells able to withstand the isolation process limits proteomic profiling in disease states. Additionally, contamination from proteins derived from non-target cell types persists. The

challenges to maintaining cellular integrity with isolation methods motivated the field to innovate novel methods of applying cell-type specific labeling to *in vitro* and *in vivo* systems.

One approach to achieve cell type-specific proteomic labeling uses BioOrthogonal Non-Canonical Amino Acid Tagging (BONCAT) in which a mutated methionyl-tRNA synthetase (MetRS) incorporates azidonorleucine (ANL), a methionine analogue, into newly synthesized peptides.^{311,339,340} Subsequently, cell lysates or brain homogenates undergo click chemistry with biotin-alkyne to biotinylate the ANL-containing peptides. By driving MetRS expression under a cell-type-specific promoter and enriching biotinylated peptides by streptavidin affinity-purification, BONCAT can purify cell-type specific newly-translated proteins.^{341,342} One advantage of this strategy lies in its ability to label and purify low-abundant and newly-synthesized proteins. A limitation may be low proteomic depth and biases towards proteins with high turnover. The BONCAT approach has thus far been applied to characterize excitatory and inhibitory neurons of mice and rats in both *in vivo*, *ex-vivo*, and *in vitro* contexts.³⁴¹⁻³⁴⁴ To date, extension to other neuronal and glial cell types has not yet been published.

In contrast to the BONCAT approach which labels only newly synthesized proteins, proximity-labeling techniques rely on biotin ligases which biotinylate nearby interactors. BioID is a promiscuous biotin-ligase engineered from the site-specific biotin ligase, BirA, endogenously produced by *Escherichia coli*.³⁴⁵ Because BioID is non-toxic, this technology opened up opportunities for *in vivo* applications, though the reaction kinetics of biotin-labeling takes place

over 18-24 hours.³⁴⁶ Alice Ting's group used yeast surface display mediated directed evolution to improve the reaction kinetics of BioID by introducing 15 mutations in the catalytic domain relative to wild-type BirA.³⁴⁷ This biotin ligase, termed TurboID, can robustly and promiscuously biotinylate proteomes in living cells and animal models without cellular toxicity, in as little as 10 minutes in cell culture systems.^{347,348} Versatile in its applications, TurboID has been fused to proteins of interest to map protein interactomes, targeted to a subcellular compartments of interest, and has been exported out of the nucleus to label cytosolic proteins.³⁴⁹⁻³⁵⁴ Additionally, to biotin-label proteins proximal to intermembrane contact sites, split-TurboID was recently developed in which two inactive fragments of TurboID reconstitute in the presence of rapamycin.^{348,355} When driven under a cell-type specific promoter, both TurboID and split-TurboID can label cellularly distinct proteomes in their native state for downstream affinity capture and MS. These advancements, which enable robust, targeted, and non-toxic biotinylation of cell-type specific proteomes has yielded promising applications to neuroproteomics. Recently, split-TurboID has been applied to perisynaptic-cleft proteome discovery between astrocyte and neurons *in vivo*.^{353,356} A novel transgenic mouse model for conditional expression of TurboID with a nuclear export sequence (TurboID-NES) was also recently developed to resolve region-specific proteomic signatures of CamK2a neurons and Aldh1l1 astrocytes in adult mouse brain.^{331,356} These recent advances position cell type-specific *in vivo* biotinylation of proteins (CIBOP) as a

promising approach to resolve distinct cellular proteomes in different *in vivo* homeostatic and pathological contexts.

In anticipation of *in vivo* proximity labeling applications of TurboID-NES for cell type-specific proteomics, it is important to establish the effects of global cytosolic biotinylation on molecular and cellular processes in mammalian cells. It is also critical to characterize the breadth of cytosolic proteins labeled by TurboID-NES, determine how reflective these proteins are of untransduced whole cell proteomes and identify any inherent biases of the TurboID-NES approach. In order to support the use of TurboID-NES to label cytosolic proteins which are also relevant to cellular identity, it is important to test if TurboID-mediated proteomics can differentiate two distinct cell types, such as neurons and microglia. Finally, we need to ascertain whether proteomic changes induced by inflammatory stimuli can be efficiently and reliably captured by the TurboID-NES biotinylation of cytosolic proteins. These data are critical for interpreting proteomic results from TurboID-NES proximity labeling studies that aim to label the cellular proteome in mammalian systems *in vitro* and *in vivo*. To answer these questions under controlled experimental conditions, we generated neuroblastoma (N2A) and immortalized microglial (BV2) cell lines that stably express V5-TurboID-NES to label the cellular proteome excluding the nucleus. We examined the extent and coverage of cytosolic proteomic labeling by TurboID-NES in N2A and BV2 cells, under resting and lipopolysaccharide (LPS)-stimulated inflammatory conditions, using label-free quantitation (LFQ) mass spectrometry. We found that TurboID-NES expression

preserves the ability to resolve distinct cellular proteomes at the MS level under homeostatic states and inflammatory challenge.

iii. Results

Generation and validation of stably-transduced microglial and neuronal TurboID-NES cell lines.

We created a lentiviral vector incorporating the V5-TurboID-NES sequence (Addgene plasmid #107169) including a Green Fluorescence Protein (GFP) separated by a T2A linker, and a puromycin resistance gene (**Figure 3.1A**). The NES sequence was incorporated to limit biotinylation to the extra-nuclear compartment. We then generated lentiviruses carrying this vector and transduced BV2 mouse microglia and N2A mouse neuroblastoma cells (MOI 5:1) followed by positive selection with puromycin for at least 2 passages and then fluorescent activated cell sorting (FACS) of GFP-positive cells. These sorted cells were then maintained in puromycin for passages to maintain stably-transduced BV2-Turbo and N2A-Turbo lines (**Figure 3.1B**) but cultured in puromycin-free medium prior to experimentation. After genetically screening successfully transduced cell lines with puromycin, we used western blotting (WB) and immunofluorescence (IF) to confirm robust biotinylation of proteins in cell lysates (**Figure 3.1C**) and confirm cytosolic localization of V5-TurboID-NES and biotinylated proteins (**Figure 3.1D, 3.1E**). WB probing for biotinylated proteins consistently identified bands in untransduced

controls which likely represent endogenously biotinylated carboxylases such as pyruvate carboxylase (~130 kDa), 3-methylcrotonyl coA carboxylase (~75 kDa) and propionyl coA carboxylase (72 kDa) (**Figure 3.1C**).³⁵⁷ The IF data in **Figure 3.1D** and **3.1E** confirmed the functionality of the NES, and the predominant biotinylation of cytosolic proteins in both BV2-TurboID-NES and N2A-TurboID-NES cells.

TurboID-NES-based MS captures representative proteomes in mammalian microglial and neuronal cell lines.

After confirming stable expression, cytosolic localization, and functionality of V5-TurboID-NES in BV2 and N2A cell lines, we prepared cell lysates for LFQ-MS studies. Transduced and untransduced BV2 and N2A cells received 1 µg/mL of LPS or equal volume of phosphate-buffered saline (PBS) in addition to 200 µM biotin supplementation for 48 hours. LPS was used as a general immune stimulus to activate BV2 cells while anticipating marginal or no effects of LPS on N2A. Whole-cell (WC) lysates were prepared in parallel with lysates undergoing streptavidin affinity-purification (AP) to enrich for biotinylated proteins (n = 4 / experimental condition) (**Figure 3.2A**). WC lysates underwent Coomassie staining and were probed with Streptavidin-680 to confirm robust biotinylation of proteins in transduced cell-lines (**Figure 3.2B, 3.2C**). Proteins bound to streptavidin beads were boiled and resolved with gel electrophoresis (**Figure 3.2D, 3.2E**). Proteins released from streptavidin-beads were probed for biotinylation using streptavidin 680, and silver-stained gels were run to confirm minimal binding of non-biotinylated proteins in untransduced

lysates. In BV2 AP lysates, LPS treatment induced differential banding patterns visible in smaller molecular weight proteins (10-40 kDa) (**Figure 3.2D**). The silver stain and western blots provided evidence for not only the capacity of TurboID-NES to biotinylate proteins altered by LPS treatment, but also the ability to affinity-purify LPS-altered proteins biotinylated by TurboID-NES. Notably, LPS did not alter protein banding patterns in either the silver stain or western blots of N2A samples. After confirming the enrichment of biotinylated proteins in TurboID-NES-transduced BV2 and N2A cell lines, we submitted these same samples for LFQ-MS. Raw LFQ and intensity values are found in **Supplemental Datasheet 1A (SD 1A)**.

First, we used PCA for dimension reduction of LFQ proteomic data obtained from all whole cell samples and transduced AP samples (**SF 3.1A, 3.1B**). LFQ-MS data used for WC-level comparisons are available in (**SD 2A**) and TurboID-normalized intensity values used for AP-level comparisons are available (**SD 2B**). WC samples included BV2 (n = 4), BV2+LPS (n = 3), BV2+TurboID-NES (n = 4), BV2+TurboID-NES+LPS (n = 4) N2A (n = 4), N2A+LPS (n = 4), N2A+TurboID-NES (n = 4), and N2A+LPS+TurboID-NES (n = 4) (**SF 3.1A**). Due to the high number of missingness in the non-transduced +AP samples that only captures endogenously biotinylated proteins, we performed PCA on +TurboID-NES or +LPS+TurboID-NES BV2 and N2A AP samples (n = 4/group) (**SF 3.1B**). In the PCA of WC samples, PC1 described ~32% of variance across WC proteomes and captured cell type differences between BV2 and N2A cells without contribution from TurboID-NES status or LPS treatment (**SF 3.1A**). The full WC principal component matrix

can be found in (SD 1B). In PCA of AP samples, PC1 accounted for 48% of the variance and also captured BV2 N2A cell type differences. PC2 accounted for 10% variance and captured the effect of LPS only in BV2 cells and not in N2A cells (SF 3.1B). The AP principal component matrix can be found in (SD 1C). These PCA analyses of WC as well as AP proteomes confirmed that the cell type differences between BV2 and N2A proteomes, rather than TurboID-NES expression or proteomic biotinylation, explained the majority of variance in our data. Importantly, biotin-enriched proteomes from AP samples successfully resolved cell type differences as well as LPS-treatment effects within the BV2 cells.

To assess the global proteomic differences and similarities between untransduced WC proteomes (BV2 or N2A whole cell, $n=4$ / group) and their TurboID-NES-transduced and biotin-enriched counterparts (BV2+TurboID-NES_{AP} or N2A+TurboID-NES_{AP}, $n = 4$ / group), we performed k-means clustering analysis (Figure 3.3A). We identified 6 distinct clusters using the elbow method for cluster number optimization (SF 3.2). We identified clusters of proteins preferentially abundant in WC proteomes (Cluster 1), and clusters of proteins shared in abundance between TurboID-NES AP samples and their WC counterparts (Clusters 3 and 6). Interestingly, we also identified clusters of proteins distinct to TurboID-NES AP samples which TurboID-NES-mediated biotinylation showed preferential abundance for (Clusters 2 and 4). Finally, we identified a cluster of proteins which are shared in enrichment between TurboID-NES AP cells (Cluster 5). LFQ-MS identified 3,064 proteins in BV2 proteomes, of which TurboID-NES

biotinylated 1,815 or ~59% LFQ MS identified 3,173 proteins in N2A proteomes, of which TurboID-NES biotinylated a total of 2,056 proteins or ~65% (**Figure 3.3B**).

We performed gene set enrichment analyses (GSEA) using each of the 6 cluster-sets compared with the background proteome of all proteins identified in the LFQ-MS dataset (~2187 proteins; **SD 2A**), using KEGG and Gene-Ontology (GO) reference databases.³⁵⁸⁻³⁶² GSEA of the WC Cluster 1 (630 proteins) showed enrichment of nuclear, mitochondrial, cell surface and RNA metabolic proteins (**Figure 3.3C, 3.3D**). Cluster 1 represented proteins derived from compartments less accessible to biotinylation by TurboID-NES in both cell types. In contrast, Cluster 5 (425 proteins) contained proteins selectively abundant in both BV2 and N2A transduced AP samples. Cluster 5 represented a group of proteins preferentially labeled by TurboID-NES in both cell types. GSEA of Cluster 5 showed enrichment of Golgi apparatus, vesicle-mediated transport, and endocytosis related proteins, indicating that TurboID-NES preferentially biotinylated Golgi, endocytic, secretory compartments in both cell types. As TurboID-NES trafficked throughout the cytosol, it came in contact with vesicular compartments and labeled proteins involved in vesicular transport. Because vesicle-mediated transport is a biologically conserved function inherent to both microglial and neuronal cells, we expected that the abundance of vesicular-trafficking proteins labeled by TurboID-NES would not differ by cell-type.

In contrast to Clusters 1 and 5 which primarily differentiated WC from AP samples, we identified cell type-specific clusters (Clusters 3 and 6) that were highly abundant in either N2A or BV2 cells, regardless of WC or AP status. Cluster 3 (323 proteins), the 'N2A shared' cluster showed a high abundance of proteins shared between WC and transduced AP N2A cells. The 'N2A shared' cluster contained proteins enriched in endoplasmic reticulum, cell body and viral transcription proteins, potentially explained by the rapidly-dividing stem-cell-like origin of N2A cells. Cluster 6 (226 proteins), the 'BV2 shared' cluster, was highly abundant in WC and AP samples from BV2 cells. The 'BV2 shared cluster' was enriched in proteins associated with immune cell (leukocyte activation and trafficking), hematopoietic lineage, lysosomal, plasma membrane, translation, vacuole, metabolism and phagosome functions as would be expected for BV2 microglial cells.

Clusters 2 and 4 showed cell type-specific proteomic differences apparent only in the AP samples but not in the WC lysates. These may be proteins which are expressed at low-levels in the whole cell, and are enriched by TurboID-NES labeling and AP. These clusters therefore represented proteomic features of N2A and BV2 cell types that were readily revealed by the TurboID-NES approach and are less apparent at the level of WC proteomes, potentially via preferential access of TurboID-NES to specific cellular compartments. Cluster 2 (350 proteins) was highly abundant in N2A AP samples compared to BV2 AP samples, and were enriched in proteins involved in long-term potentiation, calcium signaling, Hedgehog signaling, consistent with ontologies expected in neuronal-origin N2A cells. Cluster 4 (233 proteins), on the other hand,

was highly abundant in BV2 AP samples and were enriched in endocytosis, ribosomal subunits, phagocytosis, Rho GTPase activity, rRNA processing and translation terms, consistent with a phenotype expected in immune and phagocytic cells such as BV2 microglia. The GSEA of clusters 2 and 4 show that TurboID-NES mediated biotinylation can enrich proteins in N2A and BV2 proteomes, respectively, which are not readily distinguished at the WC level.

Taken together, these proteomic analyses of N2A and BV2 TurboID-NES AP proteomes along with respective WC proteomes, showed that TurboID-NES proteome was representative of the whole cell proteome. In addition, TurboID-NES preferentially biotinylated several classes of proteins shared across mammalian cell types, as well as proteins unique to microglial or neuronal cell type origin. While many of these biotinylated proteins captured changes apparent at the WC level, several cell type-specific proteomic differences were more apparent in the TurboID-NES AP proteomes as compared to the WC proteomes.

TurboID-NES over-expression has minimal impact on cellular proteomic and functional profiles of BV2 and N2A cells.

Lentiviral transduction and over-expression of TurboID-NES in mammalian cells could potentially impact basic cellular functions and phenotypes, and therefore could have confounding implications for *in vivo* applications of TurboID-NES. To test whether TurboID-NES expression impacts cellular phenotypes under both homeostatic and inflammatory conditions, we compared

whole cell transduced and untransduced proteomes, collected culture supernatants for cytokine profiling in response to LPS challenge, and we assessed the respiratory activity of living BV2 cells. To test the hypothesis that TurboID-NES expression itself impacts the WC proteome, we performed differential expression analysis (DEA) comparing BV2+TurboID-NES_{WC} - BV2_{WC} (**Figure 3.4A**) and N2A+TurboID-NES_{WC} - N2A_{WC} (**Figure 3.4B**). Only 53 BV2 proteins and 74 N2A proteins, including TurboID-NES, were significantly changed with TurboID-NES expression out of 2,187 total proteins. The DEA comparing transduced and untransduced BV2 or N2A proteomes can be found in (**SD 2C, SD 2D**). This proteomic result provided evidence that TurboID-NES expression minimally impacted WC proteomes of BV2 and N2A cells under resting conditions. The small sizes of the whole cell TurboID-DEP input lists did not yield gene ontology terms in the over-representation analysis. However, the top 5 increased terms from the DEA comparing BV2+TurboID-NES_{WC} - BV2_{WC} included Histone H1.0; H1f0, phosphoserine phosphatase Psph, and kinases; Adrbk1, and Prkab1 and TurboID itself. The 5 most decreased proteins with TurboID transduction in BV2 include vesicle membrane protein, Vat1l, Rho-related GTP binding protein, Rhoc, mitochondrial tRNA ligase Tars2, U3 small nucleolar RNA-associated protein, Utp14a, and cell adhesion molecule 1, Cadm1. When assessing the impact of TurboID expression on N2A WC proteomes, N2A+TurboID-NES_{WC} - N2A_{WC}, the DEA revealed the top 5 increased proteins included TurboID, dehydrogenase / reductase family member 7, Dhfr7, Niban, Fam129a, Nuclear valosin, Nvl, and disabled homolog 2, Dab2. The 5 most decreased proteins with TurboID

transduction in N2A included putative methyltransferase Nsun7, COBW domain containing protein 1, Cbwd1, putative helicase MOV-10, Mov10, and AHNAK nucleoprotein 2, Ahnak2. Taken together, TurboID transduction in BV2 and N2A cells impacts the abundance of 2% and 3% of the proteins identified in the WC proteome, respectively. Although a minority of proteins are significantly impacted by TurboID, we did observe modest yet significant alterations in nuclear-associated proteins in both cell types, including Histone H1.0 ($-\text{Log}_{10}$ p value = 1.34, Log_2FC = 2.98) in BV2 and Nuclear valosin-containing protein, Nvl ($-\text{Log}_{10}$ p value = 1.33, Log_2FC = 1.10) in N2A.

In applying the CIBOP approach to immune cells and inflammatory disease models, it is important to confirm that TurboID expression has a minimal impact on both homeostatic and inflammatory cytokine release profiles. Then, we collected supernatants from TurboID-NES transduced and untransduced BV2 and N2A cells in response to 48 hours of LPS challenge or PBS ($n = 6/\text{group}$) for profiling of 31 cytokines using a Luminex multiplexed immune assay. The raw intensity values, proceeding the subtraction of average background intensity, are found in (**SD 1D**). PCA of secreted cytokines across all samples showed that the cellular identity of cytokines drives a majority of variance (captured by PC1; 94% variance) and that BV2-secreted cytokines robustly responded to LPS while N2A cells did respond to LPS based on secreted cytokine profiles (captured by PC2; 4% variance). The complete principal component matrix can be found in (**SD 1E**). Importantly, we also observed no separation of BV2 or N2A cells based on TurboID-NES

status (**Figure 3.4C**). To test if TurboID-NES expression impacts the magnitude of cytokine abundance in the presence of LPS, we compared the fold-induction of LPS-driven cytokine abundance changes between transduced and untransduced BV2 cytokines (**Figure 3.4D**). We observed strong concordance in LPS effects regardless of TurboID-NES status ($R^2=0.83$). The secretion of pro-inflammatory cytokines (e.g., macrophage inflammatory protein 2, interleukin 6, and tumor necrosis factor alpha) was increased to comparable extents in response to LPS while anti-inflammatory cytokine (Il-4) was suppressed by LPS to the same extent in BV2 control and BV2 +TurboID-NES cell lines (**Figure 3.4D**). This result confirmed that TurboID-NES expression did not significantly influence the cytokine release profiles of BV2 cells which received LPS.

To determine if either LPS or TurboID-NES expression impacted cellular respiration rates in transduced or untransduced BV2 cells, we used Seahorse assays of cellular respiration, oxygen consumption rate (OCR), and extracellular acidification rate (ECAR) as a measure of glycolytic activity (**Figure 3.4E-3.4G**). LPS significantly decreased the maximal respiration of untransduced BV2 cells ($p = 0.0004$), and we also observed a decrease in the maximal respiration in transduced BV2 cells, though the change was not significant ($p = 0.13$) (**Figure 3.4E**). Neither LPS challenge nor transduction status significantly impacted OCR or ECAR in BV2 cells. Taken together, TurboID-NES expression in BV2 and N2A cells had a minimal impact on WC proteomes and does not impact LPS-driven cytokine release. TurboID-NES expression had no significant impact on homeostatic cellular respiration nor glycolytic activity. These *in vitro* findings are of critical

importance in interpreting results derived from TurboID-NES-based proteomics by confirming absence of undesired effects of TurboID-NES over-expression in mammalian cells.

TurboID-NES biotinylates a variety of subcellular compartments within BV2 and N2A cells including several neurodegenerative disease-relevant proteins

The utility of expressing TurboID under cell-type specific promoters *in vivo* and the consequential purification of cellularly distinct proteins from total brain homogenate lies within the ability of TurboID-NES to label cellularly distinct proteins with disease relevance. Before comparing TurboID-NES-labeled proteomes of BV2 and N2A cells, we first assessed the enrichment of proteins biotinylated by TurboID-NES over endogenously biotinylated proteins. We used DEA to compare AP proteomes from untransduced BV2 lysates with TurboID-NES-transduced BV2 lysates (BV2+TurboID-NES_{AP} - BV2_{AP}), which showed that TurboID-NES biotinylated 1754 proteins, whereas 10 endogenously biotinylated proteins appear in the untransduced AP proteome (**Figure 3.5A; SD 2E**). DEA comparing AP proteomes from untransduced N2A lysates with TurboID-NES-transduced N2A lysates (N2A+TurboID-NES_{AP} - N2A_{AP}) showed that TurboID-NES biotinylated 2011 proteins, whereas 39 endogenously biotinylated proteins appeared in the untransduced AP proteome (**Figure 3.5B; SD 2F**). TurboID-NES expression in BV2 and N2A cell lines, and streptavidin-based affinity purification yielded a robustly biotinylated proteome sufficient to over-come the background of endogenously biotinylated proteins in untransduced AP samples.

To inform the application of CIBOP to future mouse models of disease, we tested the hypothesis that global cytosolic biotinylation of TurboID-NES can achieve a proteomic breadth sufficient for conclusive cellular distinction between glia and neurons. We performed DEA on AP proteomes from BV2 and N2A cell lines stably expressing TurboID-NES (N2A+TurboID-NES_{AP} – BV2+TurboID-NES_{AP}). We identified 936 proteins enriched in BV2+TurboID-NES AP samples and 404 proteins enriched in N2A+TurboID-NES AP (**Figure 3.5C**; **SD 2G**). Notably, TurboID-NES biotinylated proteins with relevance to Alzheimer’s disease (AD) in both microglial and neuronal cells. For example, Moesin (Msn), protein tyrosine phosphatase nonreceptor 6 (Ptpn6), C-terminal Src Kinase (Csk) and Plectin (Plec) were highly enriched in microglial proteomes labeled by TurboID-NES. Moesin has been identified as a hub protein for AD etiology in both human and 5xFAD mouse models^{240,258,363,364} and is necessary for P2X7R-dependent proteolytic processing of amyloid precursor protein.³⁶⁵ Both Csk and Ptpn6 have been identified as AD hub genes.³⁶⁶ Ptpn6 is associated via signaling pathways with CD33, a risk locus identified in human AD genome wide association studies.³⁶⁶⁻³⁶⁹ In N2A cells, TurboID-NES biotinylated AD-relevant proteins including Microtubule-Associated Protein tau (Mapt), Microtubule-associated protein 1A/B (Map1a; Map1b), A β precursor protein binding family B (Apbb1), and Calmodulin 1 (Calm1).

Without being directed to a specific subcellular compartment, TurboID-NES biotinylated a variety of proteins in microglial and neuronal cell lines. In BV2 cells, TurboID-NES biotinylated lysosomal, ribosomal, endosomal, and vesicular proteins. Additionally, TurboID-NES biotinylates

proteins important to receptor tyrosine kinase signaling (RTK) (**Figure 3.5D**). Gene-Set-enrichment analysis (GSEA) of microglial-enriched proteins biotinylated by TurboID-NES highlighted significant enrichment for translational machinery, endosomal proteins as well as intracellular trafficking of vesicles (**Figure 3.5E**). In N2A cells, TurboID-NES labeled proteins involved with trans-Golgi network trafficking, microtubule and neurofilament elements, endosomal and exosomal machinery, vesicular trafficking, and over 75 synaptic terms out of 404 terms identified in the enriched N2A biotinylated proteome (**Figure 3.5F**). GSEA of the N2A biotinylated proteome identified top terms associated with neuron projection, microtubule processes, and synaptic parts, supporting the ability of TurboID-NES to label synaptic proteins which could contribute to cell-type distinction (**Figure 3.5G**). Using the proteome of cellularly distinct proteins labeled by TurboID-NES identified in the DEA in **Figure 3.4A**, we mapped proteins to risk-loci associated with neurodegenerative diseases (**SF 3.3**). Using risk loci published in the Alzheimer's disease (AD) MAGMA³⁴¹, Parkinson's disease (PD) MAGMA³⁷⁰, and Amyotrophic lateral sclerosis / Frontotemporal dementia (ALS/FTD) MAGMA³⁷¹ datasets, we identified 82 and 46 AD-relevant and cellularly distinct proteins labeled by TurboID-NES in BV2 and N2A proteomes, respectively (**SF 3.3A**). We identified 32 and 17 PD-relevant and 84 and 29 ALS/FTD-relevant proteins in BV2 and N2A proteomes labeled by TurboID-NES and enriched by streptavidin-based affinity purification (**SF 3.3B, 3.3C**). Taken together, TurboID-NES, when directed into the cytosol for global biotinylation of proteins, biotinylated a breadth of proteins

sufficient to distinguish between microglial and neuroblastoma cell lines. Additionally, TurboID-NES biotinylated proteins critical to neurodegenerative etiologies. These proof-of-principle analyses support the future direction of TurboID-NES into distinct brain cell types within living mouse models of neurodegeneration.

BV2 proteomes biotinylated by TurboID-NES capture Lipopolysaccharide driven changes, partially reflected in the whole-cell BV2 proteomes.

After confirming that TurboID-NES robustly labeled distinct cellular proteomes with minimal impact on homeostatic phenotype, we hypothesized that TurboID-NES could label proteins impacted by LPS treatment. Our dimension reduction analyses confirmed our ability to resolve proteomic differences in transduced AP cells based on cell type and LPS challenge (**SF 3.1B**). To understand global differences between WC and AP proteomes differentially expressed by LPS treatment, we created a heatmap representation of LFQ intensity values (2350 proteins; **SD 2H**). We identified 6 distinct proteomic clusters (**Figure 3.6A**), as determined by the elbow-method optimization of number of clusters (**SF 3.4**). Two large clusters (Cluster 1 and Cluster 2) showed specific abundance differenced based on affinity purification (AP) status. Cluster 1 (943 proteins) was highly abundant in whole cell lysates as compared to AP samples with minimal effect of LPS, and was enriched in nuclear, mitochondrial, RNA binding and metabolic proteins (**Figure 3.6B, 3.6C**); proteins not readily accessible by a cytosolic-directed TurboID-NES. Cluster 2 (608 proteins) was conversely more abundant in BV2 AP proteins compared to whole cell lysates

with minimal effect of LPS, and were enriched in cellular membrane organization, endocytic, cytoplasmic location, RNA transport, ER lumen, translation and vesicle-mediated transport functions, consistent with groups of proteins preferentially biotinylated by TurboID-NES. More importantly, we identified clusters of proteins that captured LPS effects in WC lysates, or AP samples. LPS significantly decreased protein abundances in BV2 AP in clusters 3 (191 proteins) and 4 (236 proteins) and significantly increased protein abundances 5 (131 proteins) and 6 (241 proteins) (**SF 3.5**). Cluster 3 was enriched in cytosolic, lysosomal (hydrolase activity), and ribosome proteins, suggesting that the TurboID-NES approach captured an effect of LPS on translation and lysosomal functions that cannot be resolved at the whole cell level. Cluster 5, the 'BV2+ LPS shared cluster', was increased by LPS treatment in both WC and AP samples, and showed enrichment in terms such as response to IFN- γ , oxidative stress (hydrogen peroxide related processes), and peroxisome and phagosome functions, indicative of expected LPS-driven proteomic changes in microglia. Several inflammatory terms in Cluster 5 were previously reported in BV2 cells specifically in response to 1 $\mu\text{g}/\text{mL}$ LPS for 48 hours³⁷², which included antigen processing and presentation, and glycolysis / gluconeogenesis, reflecting a shift in bioenergetics induced by inflammatory stimuli (**Figure 3.6B, 3.6C**). Cluster 6 showed LPS-induced increased levels that were only apparent in AP samples, and were enriched in RNA binding, nucleolus localization, ribosome, translational activity and spliceosome functions. Cluster 6 may represent altered localization of RNA-interacting splicing proteins, as well as potential nuclear speckle and

nucleolar proteins from the nucleus to the cytoplasm due to LPS-induced stress. Such altered localization events are more likely to be captured using the TurboID-NES approach, rather than at the whole cell level. To rule out the possibility that LPS impacts TurboID-NES localization in BV2 cells, we performed ICC and WB studies on cytoplasmic and nuclear fractions (**SF 3.6A, 3.6B, 3.6E**). We performed colocalization analyses comparing the DAPI signal as a nuclear marker with V5 for TurboID-NES or StrepDylight to determine the percent of cytosolic TurboID-NES signal or biotinylation signal, respectively. Interestingly, LPS significantly increased the percent of cytosolic TurboID-NES and cytosolic biotinylation (**SF 3.6C, 3.6D**). We observed predominantly cytosolic localization of TurboID-NES (via V5 localization) and biotinylation in both ICC studies, as well as in WB analyses (**SF 3.6**). Taken together, it is likely that cytosolic direction of TurboID-NES can identify aberrantly trafficked proteins in response to LPS, though further studies are necessary.

We then compared the impact of LPS treatment on WC and AP proteomes using DEA. DEA of proteomic differences induced by LPS treatment in BV2 WC samples (BV2+LPS+TurboID-NES_{WC} - BV2+TurboID-NES_{WC}) and AP samples (BV2+LPS+TurboID-NES_{AP} - BV2+TurboID-NES_{AP}) identified 438 proteins impacted by LPS in the WC proteome and 535 proteins impacted by LPS in AP samples (**Figure 3.6D; SD 2J, SD 2I**). The top proteins increased with LPS treatment in the WC BV2 proteome included Immune-responsive gene 1 (IRG1), oligoadenylate synthetase-like 1 (Oasl1), interleukin 1 a (Il1a), Ring Finger Protein 213 (Rnf213), long-chain acyl-CoA

synthetase family member 1 (Ascl1), and intracellular adhesion molecule 1(Icam1). The proteins most down-regulated by LPS treatment in BV2 WC samples included Macrophage Mannose Receptor 1-Like Protein (Mrc1) macrophage galactose N-acetyl-galactosamine specific lectin 2 (Mgl2), and Eukaryotic translation elongation factor 1 delta (Eef1d) (**Figure 3.6D**). The top terms increased with LPS in BV2 AP samples included proteins such as Oas1, Gbp2, Syne1, Cyb5a, and Acs11. Proteins in the BV2 AP proteome most down-regulated by LPS treatment included Mgl2, Smap2, and Mrc2. LPS-increased proteins shared between the WC and AP samples, including Il1a, Irg1, Oas1, corresponded with pro-inflammatory M1 phenotypic markers, as well as non-canonical inflammasome mediators such as Gbp2.³⁷³⁻³⁷⁸ Proteins similarly decreased with LPS treatment shared between WC and AP BV2 proteins including canonical M2 markers such as Arg1 and Mgl2.³⁷⁹⁻³⁸² When comparing the overlap of proteins differentially expressed by LPS treatment in the WC and transduced AP BV2 proteomes, we identified 115 shared proteins that were differentially expressed in both AP and WC BV2. 323 proteins were differentially expressed in response to LPS only in the WC proteome while 430 proteins were differentially expressed in response to LPS only in the AP proteome (**Figure 3.6E**). Of the 115 proteins with shared LPS-induced differential expression we observed a moderate concordance based on magnitude ($\text{Log}_2\text{FC LPS}_{\text{WC}}$ Vs. $\text{Log}_2\text{FC LPS}_{\text{AP}}$) and direction of LPS effect (Coefficient of determination, $R^2= 0.52$) (**Figure 3.6F**). We identified 28 proteins that showed incongruent changes (**yellow**

points, Figure 3.6F) with LPS-induced increase in AP proteomes but LPS-induced decrease in WC proteomes.

iv. Discussion

Proteomics based on proximity-labeling strategies using biotin ligases (e.g. BioID, TurboID-NES) are being increasingly used in *in vitro* and *in vivo* experimental contexts and in model systems ranging from plants^{352,383-385}, yeast³⁸⁶, zebrafish^{387,388}, *Drosophila*^{389,390}, *C. elegans*^{351,391}, to mouse models^{331,353,356,392}. TurboID is one of the most efficient biotin ligases that can effectively label several proteins within a 10nm labeling radius in mammalian cells. The high catalytic activity, non-toxicity, and promiscuity of TurboID uniquely position TurboID as a powerful tool to obtain global proteomic snapshots of specific cells in homeostatic and disease states, particularly in multi-cellular models. Many recent studies have incorporated TurboID and split-TurboID³⁵⁵ to characterize interactomes and secretomes via fusion with proteins, organelles, and inter-cellular contacts.^{349,351,356,389,392-396} While one application of TurboID-based proteomics is to identify protein-protein interactors of proteins of interest or within specific subcellular compartments, another application of TurboID is to broadly label the cellular proteome of a specific cell type, so that cell type-specific proteomics can be resolved from a complex mixture of proteins derived from multiple cell types. The viability of the latter application was recently tested *in vivo* using genetic Cre/lox strategies to resolve neuronal and astrocyte proteomes in the native

state of these cells in mouse brain, a method referred to as cell type-specific *in vivo* biotinylation of proteins (CIBOP).³³¹ Whether these neuronal or glial proteomes obtained using CIBOP reflect global cellular proteomes, remains to be clarified. As interest in TurboID-based global cellular proteomics continues to grow, it is important to determine what fraction of the whole cell proteome in mammalian cells can be faithfully captured by the TurboID-NES approach, under both homeostatic (resting) conditions and following cellular perturbations (e.g., immune stress by LPS to mimic neuroinflammatory disease conditions). It is also important to determine whether TurboID-NES over-expression or excessive biotinylation impacts molecular phenotypes and cellular functions, and whether TurboID-NES-biotinylated proteomes have inherent biases as compared to the whole cell proteome. These questions can be answered by performing well-controlled *in vitro* studies using distinct types of mammalian cells. The results from such studies can inform the interpretation of proteomic findings gained from *in vitro* and *in vivo* applications of TurboID-NES in mammalian model systems, while considering the relative biases of this strategy for cell type-specific proteomics. To address these questions, we directed TurboID-NES to the cytosol using a NES, rather than using protein-specific or cellular compartment-restricted localization of TurboID-NES. We hypothesized that TurboID-NES could globally biotinylate a breadth of the cellular proteome sufficient to distinguish two distinct brain cell types (neurons

and microglia) and capture the effect of an inflammatory challenge, without significantly impacting functional or molecular phenotypes of cells that over-express TurboID-NES.

We generated murine N2A neuroblastoma and BV2 microglial cell lines that stably express TurboID-NES, and validated the expression and functionality of TurboID-NES using flow cytometry, biochemical, and immunocytochemical analyses. After validation of these stably-transduced TurboID-NES cell lines, we analyzed the TurboID-NES-biotinylated as well as the WC reference proteomes of sham-treated or LPS-treated cells using MS-based quantitative proteomics. We confirmed that TurboID-NES biotinylates >50% of the whole cell proteome in both N2A and BV2 cells, including proteins in a variety of subcellular compartments in the cytosol (e.g., endocytic machinery, ribosomal proteins, mRNA binding proteins, membrane proteins, vesicle-related and transport proteins, and cytoskeletal proteins). While a large proportion of biotinylated proteins were common to both cell types, several neuron-enriched and microglia-enriched proteins were indeed identified in the respective biotinylated proteomes. For example, BV2 microglial biotinylated proteomes captured endo-lysosomal and phagocytic proteins while neuron-projection and axonal transport proteins were labeled in N2A neurons, further verifying the validity of this approach to study cell type-specific mechanisms of distinct cell types rather than just homeostatic cellular mechanisms that are shared across cell types. These neuron-enriched and microglia-enriched proteins captured by the TurboID-NES approach also included several neurodegenerative disease-related proteins with causal implications in AD, PD and ALS.

This suggests that the TurboID-NES approach can be used to investigate disease-relevant biology in neurons and glia in mammalian systems.

Using the TurboID-NES approach, we also captured immune effects of LPS on BV2 cells. Some of these were shared at the whole cell level (e.g., increased expression of pro-inflammatory proteins Gbp2, Oasl1, Rnf213 and Icam1 and decreased expression of anti-inflammatory proteins such as Mrc1, Arg1 and Mgl2), indicating that TurboID-NES biotinylation captures core pathological transformations induced by long-term LPS stimulation in BV2 cells. KEGG terms in this cluster include antigen processing and presentation, glycolysis and gluconeogenesis, and alanine, aspartate and glutamate metabolism.³⁷² Previous studies assessing the longitudinal impact of LPS stimulation on BV2 proteomes similarly identified these major KEGG terms reflecting a strong metabolic shift in later LPS activation. Our results confirm that TurboID-NES expression does not impair metabolic functioning, and we confirm that biotinylation by TurboID-NES is able to biotinylate metabolic and immune responsive protein pathways impacted by long-term LPS stimulation. Importantly, LPS DEPs identified in transduced and affinity-purified BV2 cells correlate moderately with LPS DEPs at the WC level. Despite these consistent LPS-induced proteomic changes observed in WC and biotinylated BV2 proteomes, a relatively large group of protein changes due to LPS were identified only at the level of biotinylated proteins but not at the whole cell level. These LPS-induced proteomic changes preferentially captured by the TurboID-NES approach may be due to better access of TurboID-NES to specific cellular compartments,

such as the cytosol, which allow capture of post-translational effects of LPS, such as altered protein trafficking, nucleocytoplasmic transport of proteins from the nucleus to the cytosol or vice versa and altered localization of RNA binding, ribosomal and ribonucleoprotein-related proteins. Consistent with this, proteins involved in RNA binding, nucleolar proteins, ribosomal and translational machinery were selectively increased in the LPS-induced biotinylated proteome. We also observed a slight increase in trafficking of TurboID-NES to the cytosol with LPS stimulation, implying that the effects of LPS observed at the level of the biotinylated proteome are likely due to a combination of increased cytosolic localization of TurboID-NES and altered localization of biotinylated proteins. The LPS-induced changes in levels of ribonuclear proteins agree with reported ribosomal mechanisms involved in innate immune activation in microglia, that are responsible for translational repression and a divergence between mRNA and protein expression following LPS challenge.³⁹⁷ Furthermore, ribonuclear proteins within nuclear speckles may also be localized to the cytosol as a direct result of immune activation or a cell proliferative response to LPS stimulation, as has been reported previously.^{398,399} Finally, several nucleus-resident RNA binding and ribonucleoproteins can translocate to the cytosol to regulate mRNA translation by the ribosome. The ability to use TurboID-NES-based proteomics to investigate protein trafficking and mis-localization is of particular relevance to neurodegenerative disorders. Mis-localization of nuclear proteins to the cytosol occur in several neurodegenerative diseases, where RNA-binding proteins such as TDP-43, Tau and FUS can aberrantly localize to the cytosol

where they become more prone to aggregation.⁴⁰⁰ Therefore, the TurboID-NES approach when employed *in vivo* via CIBOP, could be specifically used to interrogate mechanisms of neurodegeneration that involve dysfunction of nucleocytoplasmic transport, changes in protein trafficking, and cytosolic aggregation.

Another important result of our study is that TurboID-NES over-expression had a minimal impact on the proteomes of both N2A and BV2 cells at the whole cell level and did not significantly impact cellular respiration or secreted cytokine profiles in response to LPS in BV2 cells. These findings suggest that cellular molecular composition and function are not meaningfully compromised using the TurboID-NES approach. This finding is consistent with the lack of electrophysiological alterations observed in *in vivo* TurboID-NES studies in Camk2a excitatory neurons.³³¹ These findings are indeed reassuring and support the use of TurboID-NES-based cellular proteomic profiling approaches to investigate mechanisms of disease with minimal effects on cellular functions due to TurboID-NES over-expression.

Despite the strengths of well-controlled *in vitro* studies, some limitations of our work need to be considered. Cell lines such as BV2 and N2A cells, despite their ability to recapitulate major cellular phenotypes of microglia and neuronal cells, display many well-known differences as compared to primary cells in the nervous system. Another limitation is that the LPS dose and duration used for (1 µg/mL for 48 hours) could have caused induced over-stimulation, cell-death, apoptosis or stress-induced changes in BV2 cells, leading to biased proteomic findings. However,

it is reassuring that our observed LPS effects on the BV2 whole cell proteome, generally agree with prior proteomics studies of BV2 cells using low dose (10-100ng/mL) and high concentrations (1 μ g/mL).^{401,402} Another limitation is related to the use of the NES in our TurboID studies. TurboID-NES was intentionally directed to the cytosol to increase the sampling of non-nuclear proteins, as well as to minimize undesired effects of excessive biotinylation of nuclear or mitochondrial proteins that are involved in key cellular functions, such as chromosomal stability and gene regulation and mitochondrial metabolic processes. To minimize the chance of relative biotin deficiency due to TurboID-NES over-expression, all experimental conditions included biotin supplementation in the medium. While this controlled for biotin deficiency, this may have induced some metabolic alterations due to excessive biotin in experimental conditions. However, in doing so, we also biased the biotinylated proteome away from nuclear, cell-surface, mitochondrial and intraluminal-directed proteins, which was evident when biotinylated AP proteomes were contrasted with WC lysate proteomes.

Beyond the scope of the methodologies in published in this study, alternative applications of TurboID and other proximity labeling methods can be used to recover proteins enriched in the WC proteomes over the AP proteomes, including cell surface and nuclear proteins. TurboID can be directed to the nucleus via inclusion of a Nuclear Localization Sequence (NLS) in lieu of a Nuclear Export Sequence (NES), wherein TurboID-NLS would remain localized within the nucleus to preferentially label nuclear proteins. Alternatively, TurboID without a localization

sequence can be used. By agnostically expressing TurboID throughout the cell, TurboID could label both nuclear and cytosolic proteins. Subsequent biochemical fractionations upstream of MS can purify for nuclear, cytosolic, and synaptic proteins. Direction of TurboID to the nucleus using an NLS could pose a challenge to cellular toxicity. When directed to the nucleus, TurboID could biotinylate key proteins involved with gene regulation and potentially alter the structure and functionality of those proteins. Therefore, it is necessary that future studies rigorously investigate the possibility of toxicity with a nuclear-direction of TurboID. Future studies may consider comparing proteomes using TurboID without NES to TurboID-NES to confirm whether cellular toxicity is indeed observed.

Furthermore, modifications to the proximity labeling approach may recover cell-surface proteins, otherwise not enriched in the AP samples within this study using the cytosolic TurboID-NES approach. Specifically, Split-TurboID and non-biotin-ligase proximity labeling methods can efficiently recover cell-surface proteins. A split-TurboID approach has been used to recover cell-type specific and cell-surface proteins interfacing at the tripartite synapse.³⁵³ The recent development of *In situ* cell-surface proteome extraction by extracellular labeling (iPEEL) is an alternative proximity-labeling method to biotin-ligase approaches which has been used to profile surface proteins of mature *murine* cerebellar Purkinje neurons with minute-temporal resolution.⁴⁰³ The Split-TurboID approach to enriching cell-surface proteins can be used *in vivo*, though its limitations include a low extracellular concentration of ATP needed for TurboID

catalytic activity.⁴⁰⁴ Whereas, iPEEL is currently limited in its applications in *ex vivo* environments. While both of these approaches have respective strengths and limitations, they can be used to efficiently recover cellularly distinct cell-surface proteins.

Our results demonstrate the ability of TurboID-NES-based cellular proteomics to capture a representative portion of disease-relevant and immune-relevant proteins in two distinct brain cell types, namely microglia and neurons, using immortalized cell lines. These results directly impact future directions of TurboID-NES using the CIBOP approach in transgenic mouse models of inflammation and neurodegeneration.

v. Conclusion

In conclusion, we generated transduced neuroblastoma and microglial cell lines expressing cytosolic TurboID-NES which yielded robustly labeled proteomes that covered a wide variety of subcellular compartments with no significant impact to cellular phenotypes. We identified a high representation of neurodegenerative disease-relevant protein pathways as well as a partial coverage of immune-relevant proteins in microglia. The breadth of the proteome labeled by TurboID-NES distinguished neuroblastoma cells from microglial cells, and TurboID-NES labeled over 50% of identified proteins within each cell type; supporting the *in vivo* application of TurboID-NES in its ability to purify cellularly-distinct proteomes. Our results also highlight inherent biases of TurboID-NES-based proteomics approaches which may be more suited to

investigate post-translational mechanisms such as protein trafficking which are not captured by whole cell proteomics.

vi. *Materials and Methodology*

A complete table of antibodies & reagents are provided (Tables 1 & 2).

Table 1. Antibodies used and their corresponding dilutions.

Antibody	Manufacturer	Catalogue #	Dilution
Rabbit anti V5	Abcam	ab206566	1:500
Rat anti α -tubulin	Millipore Sigma	MAB1864	1:1000
Goat anti β Actin	Santa Cruz Biotechnology	sc-1615	1:1000
Rabbit anti histone H3	Abcam	ab1791	1:5000
Donkey anti Rabbit 800	Invitrogen	A11374	1:10,000
Donkey anti Goat 680	LI-COR	A21084	1:10,000
Donkey anti Goat 800	LI-COR	A11370	1:10,000
Goat anti Rat 800	LI-COR	926-32219	1:10,000
Streptavidin DyLight 594	ThermoFisher	21842	1:1000
Streptavidin, Alexa-Fluor 680 Conjugate	Invitrogen	S32358	1:10,000
DAPI	Roche	10236276001	1 μ g/mL

Table 2. Reagents used and their manufacturer and catalogue numbers

Reagent	Manufacturer	Catalogue #
StartingBlockT20	Thermofisher	37543
HALT protease & phosphatase inhibitor cocktail	Thermofisher	78446
Dulbecco's Modified Eagle Medium (DMEM)	Gibco	11965-092
Penicillin-Streptomycin	Gibco	15140-122
Fetal Bovine Serum (FBS)	Gibco	26140-079
Biotin	Sigma Aldrich	B4639-100mg
LPS	Sigma-Aldrich	L4391-1mg
Puromycin	Sigma-Aldrich	P9620
4% Paraformaldehyde in PBS	Thermo Scientific	J19943-K2
0.05% Trypsin-EDTA	Gibco	253000054
Reagent A	Thermofisher	23222
Reagent B	Thermofisher	23224
Bovine Serum Albumin Standards	Thermofisher	23208
LB medium	Sigma Aldrich	28713-500G-F
Seahorse Flux Pack	Agilent	102601-100
Seahorse XF Media	Agilent	103575-100

Sodium Pyruvate	Sigma-Aldrich	S8636-100mL
L-Glutamine	Sigma-Aldrich	G7513-100ML
Glucose	Sigma-Aldrich	G8769-100mL
Oligomycin	Sigma-Aldrich	75351-5mg
FCCP	Sigma-Aldrich	C2920-10mg
Rotenone	Sigma-Aldrich	R8875-1G
Antimycin-A	Sigma-Aldrich	A8674-25mg

Cell Culture

N2A and BV2 cells were cultured in filtered Dulbecco's Modified Eagle Medium (DMEM) supplemented with high glucose and L-glutamine containing 1% penicillin-streptomycin, and 10% Fetal Bovine Serum (FBS). All media was vacuum-filtered with 0.2 μ m filters. The cells incubated at 37 degrees Celsius ($^{\circ}$ C) and 5% CO₂ until reaching 80% confluency. The splitting regimen took place twice weekly, plating one million cells onto a 100mm culture plate to a final volume of 10mL culture media. In preparation for Mass Spectrometry (MS) experiments, cells reached 95% confluency in 150 mm plates. Transduced cells expressing TurboID-NES were kept

in 2 µg/mL puromycin media until being plated for MS, wherein they forwent puromycin treatment.

Genetic Constructs & Gene Delivery

The V5-TurboID-NES_pCDNA3 and plasmid is a gift from Alice Ting (Addgene plasmid #107169). Plasmids were transformed using a competent *E. coli* strain DH5α according to manufacture protocols. Briefly, DH5 α cells were thawed on ice before aliquoting 50 µL into 1.5mL tubes. Constructs were diluted 1:1000 into autoclaved milli-Q water. LB medium was prepared and autoclaved by diluting 20 grams of LB Broth, Vegitone into 1000mL of H₂O. To the 50ul aliquots of DH5α competent cells, 5 µL of diluted constructs were mixed by turning the tubes upside down. The plasmids were incubated with the DH5α competent cells for 30 minutes on ice. Following incubation, the samples underwent heat-shock by for 42°C for 20 seconds and were placed on ice for 2 minutes. 500 µL of prewarmed LB medium were added to each sample before being placed on a rotor to shake at 225 rpm at 37°C for 1 hour. Plasmid DNAs were purified using QIAfilter Plasmid kits (Midi pre kit, Qiagen #12243) following manufacturer protocol. Restriction sites (underlined) were introduced via the following polymerase chain reaction (PCR) primers (V5.bstb.S; 5'-gcgctactctagagctagcgaattcgaagccaccatgggcaagcccatccccaa-3') (nes.Bam.A; 5'-agaaggcacagtcggcgccgcggatccttagtccagggtcaggcgtccagggg-3'). The V5-TurboID-NES sequence was subcloned into pCDH-EF1-MCS-BGH-PGK-GFP-T2A-Puro (CD550A-1) and

sequenced. N2A, and BV2 cells were transduced with a puromycin-resistant lentivirus construct of a V5-TurboID-NES containing a nuclear export sequence (V5-TurboID-NES) and a green fluorescence protein (GFP) connected via a T2A linker. Constructs were generated in Emory University's Viral Vector Core. Given a titer of 1.5×10^9 I.U./ml, we experimented with multiplicity of infection (MOIs) 5 and 10. In biological triplicates, 3 wells of each cell type received the lentivirus at either a MOI of 5 or 10, or received no virus (untransduced control). 48 hours following transduction, $\frac{1}{2}$ of the media was replaced with fresh media, and the cells were split 1:3 on 72 hours following transduction. Puromycin selection began 96 hours after transduction, $\frac{1}{2}$ of the media was replaced with 2 $\mu\text{g/ml}$ of puromycin for a final concentration of 1 $\mu\text{g/ml}$. For the following week, $\frac{1}{2}$ of the media was replaced every other day with fresh puromycin-containing media, to remove non-adhering cells. After this, the cells were split twice weekly and maintained with media containing 1 $\mu\text{g/ml}$ of puromycin. We validated the puromycin screening procedure by assessing the percentage of GFP positive cells with a fluorescent microscope and flow cytometry. A majority of cells were GFP positive three days after addition of puromycin selection. After >90% of the cells were GFP positive, the cells were maintained in 10 cm dishes in media

containing 1 $\mu\text{g}/\text{ml}$ of puromycin. Cells receiving the lentivirus at a MOI of 5 reached confluency sooner, and we did not observe a difference in transduction efficacy between MOI's 5 and 10.

Generation of whole cell lysates and supernatants, & confirmation of labeling.

BV2 and N2A cells transduced with V5-TurboID-NES or untransduced cells were seeded onto 10cm plates. 24 hours after plating, media was replaced either with biotin-supplemented media (200 μM) or media containing both LPS (1 $\mu\text{g}/\text{mL}$) and biotin supplementation (n = 6/group). 48 hours after media replacement, the media was taken off, centrifuged for 2 minutes at 800 rpm at room temperature (RT) to remove cellular debris, and preserved in a 15mL tube. Cells were dissociated using 2.5mL of 0.05% trypsin-EDTA. After trypsin dissociation, cells were rinsed and collected via manually pipetting with 7.5mL fresh media before being transferred to 15mL tubes. Supernatants and cell pellets were flash-frozen on dry-ice. Dissociated cells and supernatants were centrifuged at 800rpm for 2 minutes at RT. Supernatants were transferred to a fresh 15mL tube before being flash-frozen on dry ice. Cell pellets were washed twice with 10mL of ice-cold 1x phosphate buffer saline (PBS). Finally, cell pellets were resuspended in 1mL of ice-cold PBS and transferred to 2 mL LoBind Eppendorf tubes (Eppendorf #022431102). Cells were centrifuged for 2 minutes at 800rpm at RT before being flash-frozen on dry ice. Cell pellets were harvested in 500 μL Urea lysis buffer (8M Urea, 10mM Tris, 100mM NaH_2PO_4 , pH 8.5) with 1x HALT protease & phosphatase inhibitor cocktail without EDTA. Cell lysates were then sonicated at 30%

amplitude thrice in 5-second on-off pulses to disrupt nucleic acids and cell membrane. All cell lysates were centrifuged at 4 °C for 2 minutes at 12,700rpm. The supernatants were transferred to a fresh 1.5mL LoBind Eppendorf tube. The protein concentrations of the cell lysates were determined by Bicinchoninic acid (BCA) assay reagents using Bovine Serum Albumin Standards. Out of the 6 biological replicates prepared per experimental group, 4 samples per group were reserved for quality-control analyses performed prior and in addition to MS studies.

Immunoblotting

In each well, 10-20 µg of protein from cell lysates resolved in a 4-12% polyacrylamide gel and transferred onto iBlot 2 Transfer Stack containing nitrocellulose membrane using the BOLT transfer system. The membranes incubated for 1 hour at room temperature in StartingBlockT20 before receiving rabbit anti V5 primary antibody overnight at 4 °C or 1 hour at room temperature. After primary antibody incubation, the membranes underwent three rapid washes with 1x TBST followed by three 10-minute washes with 1xTBST. Membranes then underwent three rapid washes with 1x TBS and three 10-minute washes with 1xTBS. The membranes incubated for 1 hour at room temperature in a secondary antibody cocktail of streptavidin 680 to visualize biotinylated proteins and donkey anti rabbit 800 to visualize V5- tagged TurboID-NES. The membranes were then washed again as previously described before undergoing imaging via the Odyssey infrared Imaging System (LI-COR Biosciences).

Immunofluorescence

Immunofluorescent staining was performed as published previously with modifications for cultured cells.³³¹ Briefly, BV2 and N2A cells were seeded at ~50,000 cells onto autoclaved and HCl-ethanol-treated 25mm coverslips in a 6-well dish. All cells received supplemental biotin treatment (200 μ M) for the duration of maintenance. After reaching 50% confluency, cells were washed thrice with warm sterile PBS to remove media. Cells were fixed with 4% paraformaldehyde in PBS for 30 minutes and washed thrice in ice-cold PBS for 10 minutes, gently orbitally-rotating at 50 rpm (IKA, # KS 260). Fixed-cells were permeabilized and blocked simultaneously in a solution of 5% normal horse serum (NHS) in 0.25%TBST diluted in PBS for 1 hour at room temperature on the orbital-rotator. To each well, cells received 1mL of rabbit anti V5 (1:500) primary antibody solution in 1% NHS diluted in PBS overnight at 4 °C. All cells received a 5-minute incubation with DAPI for nuclear staining. All IF imaging was performed with a 60x oil-immersion objective taken using Keyence BZ-X810. Colocalization analysis was performed with slight modifications from previous methods.^{405,406} Briefly, we subtracted the target area (μm^2) of DAPI-signal overlap with V5 or biotinylation signal (nuclear-localizing TurboID-NES or biotinylated proteins, respectively) from the total area of V5 or Streptavidin signal using the Keyence BZ-X810 Analyzer hybrid-cell-count colocalization software. Only cells positive for both DAPI and V5 or Streptavidin DyLight were analyzed for colocalization analysis. Significance p values were assessed using the two-tailed Mann-Whitney test. The total target area counts (number of cells counted due to the presence of

a cell with overlapping of DAPI and V5 or Streptavidin DyLight signal) for transduced BV2 cells assessed for V5/DAPI colocalization was 1876 cells. The total target area counts for V5/DAPI colocalization for transduced BV2 cells receiving LPS challenge was 1945 cells. The total Streptavidin DyLight/DAPI colocalization target counts for transduced naïve BV2 cells was 2289 cells. The total target counts for Streptavidin DyLight/DAPI colocalization for transduced BV2 cells receiving LPS was 1638 cells.

Subcellular fractionation

Transduced and untransduced BV2 and N2A cells were plated in triplicates on 10cm plates and grown to 70% confluency. Cellular monolayers were rinsed with 10mL ice cold PBS, and PBS was aspirated. Cell monolayers were scraped with a sterile cell scraper in 2.97 mL PBS with 30 μ L of 100x HALT, added immediately prior to use. Cell slurries were transferred to 15mL tubes and centrifuged at 1,000 x g at 4°C for 5 minutes. The supernatants were removed and the pellet was washed once in 1 mL cold PBS. To obtain the WC fraction, 100 μ L of the cell slurry was transferred to a fresh 0.5 mL Eppendorf tube. The remaining 900 μ L of cell slurry was centrifuged at 1,000 x g at 4°C for 5 minutes. Supernatants were removed and 150 μ L of Hypotonic Lysis buffer (10 mM HEPES, pH 7.9, 20 mM KCl, 0.1 mM EDTA, 1 mM DTT, 5% Glycerol, 0.5 mM PMSF, 10 μ g/mL Aprotinin, 10 μ g/mL Leupeptin, 0.1% NP-40, 1x HALT) was added to cell pellets. Cell pellets incubated on ice for 5 minutes before being centrifuged at 15,600 x g at 4°C for 10 minutes. The supernatants were transferred to a fresh 0.5 mL tube as cytoplasmic fractions. The cell pellets

containing nuclei received 100 μ L of High Salt Buffer (20mM HEPES, pH 7.9, 0.4M NaCl, 1mM EDTA, 1mM EGTA, 1mM DTT, 0.5 mM PMSF, 10 μ g/mL Aprotinin, 10 μ g/mL Leupeptin, 1xHALT) and incubated for 30 minutes on ice. All fractions were sonicated for three 5-second on pulses followed by 5-second off pulses at 25% amplitude. Then, all samples were centrifuged for 10 minutes at 18,213 x g at 4°C. All supernatants were transferred to fresh 0.5 mL Eppendorf tubes and stored at -80°C until immunoblotting. To confirm the purity of subcellular fractionation, 20 μ g of protein resolved onto 4-12% acrylamide PAGE gels. After transferring, nitrocellulose membranes were probed with goat anti β -actin as a loading control, rat anti α -tubulin as a cytoplasmic marker, rabbit anti Histone H3, rabbit anti V5 to visualize TurboID-NES, and streptavidin-680 to visualize biotinylation. Secondary antibodies included goat-anti-rat 800, donkey-anti-goat 680, and donkey-anti-rabbit 800. All primary and secondary antibodies incubated for 1 hour at room temperature, and were probed serially to ensure the specificity of the antibodies for their target.

Sample preparation for Mass Spectrometry

From each sample, 1 mg of lysate was set aside for streptavidin AP, 50 μ g of protein were reserved as WC fractions, and the remaining protein was aliquoted and reserved for quality-control studies. Quality control studies were conducted prior to submitting samples for MS analysis to confirm the presence of biotinylated proteins via western blot, equal loading via

Coomassie, as well as ensure the specificity of streptavidin-purified preparations for biotinylated proteins via silver stain (Pierce, Thermo fisher #24612) and western blot.

Slightly modified from previous publications the AP samples were processed as follows: ^{331,348} 1 mg of protein derived from transduced and untransduced BV2 and N2A lysates were affinity-purified onto 83 μ L of magnetic streptavidin beads (Thermo #88817). Briefly, to each 1.5 mL Eppendorf LoBind tube, 1 mL of RIPA buffer (150 mM NaCl, 50mM Tris, 1% Triton X-100, 0.5% sodium deoxycholate, 0.1% SDS, pH 7.5) was added to the beads on rotation for 2 minutes at room temperature (RT). Using a magnetic stand (PureProteome, Millipore #LSKMAGS08), the buffer was removed from the beads. To each tube-containing-beads, 500 μ L of fresh RIPA lysis buffer was added before adding 1mg of protein. The samples incubated at 4°C overnight on a rotator. Samples were then briefly centrifuged, placed on the magnetic stand, and the supernatants were preserved and frozen at -20°C. After incubation, the beads containing the biotinylated proteins underwent series of washing procedures at RT. Beads were washed twice with 1 mL of RIPA lysis buffer for 8 minutes, 1 mL 1M KCL for 8 minutes, rapidly (~10 seconds) in 1 mL of 0.1 M sodium carbonate (Na₂CO₃), rapidly in 1 mL of 2M urea in 10mM Tris-HCl (pH 8.0), and twice with 1 mL RIPA lysis buffer for 8 minutes. 8-minute washing steps took place on a rotator, whereas rapid washing procedures took place on the magnetic stand using pipette rinsing to briefly mix the samples. Each buffer removal step was performed via manual pipetting, as aspirating the buffer with vacuum systems may deplete bead volume. The beads were resuspended in 1 mL of 1x PBS

before being transferred to a new Eppendorf Lo Bind tube where they were washed once more with 1 mL of 1x PBS. Finally, AP samples were resuspended into 83 μ L of PBS, wherein 8 μ L of beads-containing solution was transferred to a new tube and placed on a magnetic stand for >2 minutes. The remaining beads-containing solution was preserved. The PBS was removed and replaced with 30 μ L of 4x Laemmli protein buffer (Bio-Rad #1610747) supplemented with β -mercaptoethanol, 2mM biotin, 20mM dithiothreitol (DTT). Beads then incubated at 95°C for 15 minutes and 20 μ L were reserved for Western Blot verification of biotinylated proteins via Streptavidin 680 and 10 μ L were reserved for separate silver stain to verify minimal nonspecific binding between untransduced AP samples and transduced AP samples.

To confirm the quality, equal loading, and biotinylation of proteins in the WC samples, 10 μ g of protein from each sample resolved onto a 4-12% polyacrylamide gel for Coomassie Blue staining, and 20 μ g of protein was resolved on a separate gel to probe for actin and biotinylated proteins via immunoblotting. For Coomassie staining, gels were fixed in 50% methanol and 10% glacial acetic acid for 1 hour at RT in a sealed container on a rocking incubator. The gels were stained for 20 minutes (0.1% Coomassie Brilliant Blue R-250, 50% methanol, 10% glacial acetic acid). Finally, a destaining solution (40% methanol, 10% glacial acetic acid) was applied at room temperature while gels incubated with gentle rocking. Coomassie gels were imaged in the 700nm channel on the LiCor Odyssey imaging system. Confirmation of biotinylated proteins and equal

loading of WC samples took place by immunoblotting with streptavidin-conjugated fluorophore 680 (Strep680) and goat anti actin, respectively.

Peptide Digestion & Cleanup

Sample preparation for MS was performed according to our laboratory protocols modified from previous publications^{146,220,240,245,407-410}. Briefly, 50 µg of protein from each cell lysate sample was digested. Samples were reduced with 5 mM dithiothreitol (DTT) at room temperature for 30 minutes on a rotor, followed by alkylation with 10 mM iodoacetamide (IAA) at room temperature for 30 minutes on a rotor in dark. Samples were diluted with 50 mM of ammonium bicarbonate (ABC) to 4 M urea prior to undergoing overnight digestion with 2 µg of lysyl endopeptidase (Lys-C) (Wako #127-06621) at room temperature. Samples were then diluted to reduce the concentration of Urea to 1 M prior to trypsin digestion. Each sample received 2 µg of trypsin (Thermo, 90058) and were incubated overnight at room temperature. Acidifying buffer was added to the peptide solution for a final concentration of 1% formic acid (FA) and 0.1% trifluoroacetic acid (TFA) to stop the trypsin digestion. HLB columns were used to desalt samples (Waters #186003908). The samples were dried overnight using a centrifugal vacuum concentrator (SpeedVac Vacuum Concentrator).

AP samples underwent on-bead digestion. Beads were resuspended in 150 µL ABC. Application of DTT to a final concentration of 1 mM reduced the samples during a 30-minute

room-temperature incubation on a rotator. A 5 mM application of IAA alkylated the samples during a 30-minute incubation in the dark on a rotator. To each sample, 0.5 μg of LysC was added before incubating overnight at room temperature on a rotator. The digestion was completed overnight at room temperature on a rotator with the addition of 1 μg of trypsin to the samples. After overnight digestion, the samples were treated with acidifying buffer to stop the trypsin-mediated digestion. HLB columns were used to desalt samples. The samples were dried using the SpeedVac.

Liquid Chromatography and Mass Spectrometry

All samples were analyzed on the Evosep One system using an in-house packed 15 cm x 150 μm i.d. capillary column with 1.9 μm Reprosil-Pur C18 beads (Dr. Maisch, Ammerbuch, Germany) using the pre-programmed 44 min gradient (30 samples per day). Mass spectrometry was performed with a Q-Exactive Plus (Thermo) in positive ion mode using data-dependent acquisition with a top 20 method. Each cycle consisted of one full MS scan followed up to 20 MS/MS events. MS scans were collected at a resolution of 70,000, 400-1600 m/z range, 3×10^6 AGC, 100 ms maximum ion injection time. All higher energy collision-induced dissociation (HCD) MS/MS spectra were acquired at a resolution of 17,500 (1.6 m/z isolation width, 28% collision energy, 1×10^5 AGC target, 100 ms maximum ion time). Dynamic exclusion was set to exclude previously sequenced peaks for 30 seconds within a 10-ppm isolation window. MS raw files of WC and AP samples were searched together using the search engine Andromeda integrated into

MaxQuant (Ver 1.6.17.0). Raw files were searched against the August 2020 Uniprot *murine* database, wherein 91,442 entries were searched. Variable modifications include methionine oxidation, N-terminus acetylation, and deamidation of glutamine and asparagine residues. Fixed modifications include carbamidomethylation of cysteine residues. Only peptides with up to 2 missed cleavages were considered in the database search. Additional search parameters included a maximum peptide mass of 6000 Daltons (Da) and the minimum peptide length of 6 residues. The mass tolerance for precursor ions is 20 parts per million (ppm), and the mass tolerance for fragment ions is 0.05 Daltons. Peptide spectral match (PSM) false discovery rates (FDR), protein FDR, and site FDR were all set at 1 percent.

Annotated spectra of proteins identified on the basis of a single unique peptide can be found in **Supplemental data 1** for the 550 proteins identified in the WC samples and **Supplemental Data 2** for the 561 proteins identified in the AP samples. **Supplemental Datasheet 3** contains specifications for all proteins identified on the basis of a single unique peptide. We devised an R script that automates the MS/MS annotation of single peptide identifications' MaxQuant best-scored peptide spectral matches directly from Thermo RAW data files into pdf (**Supplemental Data 1** and **2**) and a data table (**Supplemental Datasheet 3**). This resource can be found at <https://github.com/edammer/MQ1pepAnnotate> and leverages the protViz and rawrr R packages.⁴¹¹

Data normalization and filtering, Principal Component Analyses, Differential

Expression Analyses, Clustering, Gene Set Enrichment Analysis

To analyze large datasets generated by MS, we used principal component analysis (PCA) as a dimension reduction strategy, differential expression analysis (DEA) was used to identify significant differences in protein intensities between samples, clustering analyses (k-means) identified discrete proteins with related abundance values within and across samples, and gene over-representation analysis functionally annotated enriched groups of proteins.

Filtering missingness, data normalization and log transformation.

Label-free quantification intensities and raw intensity values were uploaded onto Perseus (Ver 1.6.15) for analyses. Categorical variables were removed, intensity values were log-2 transformed, transduced AP intensity values were normalized to TurboID intensity to adjust for variability in TurboID expression, and data were in general filtered based on 50% missingness across group of samples that were selected for each analysis. Missing values were imputed from normal distribution.

PCA.

Principal component analyses of LFQ mass-spectrometry data were performed and visualized using SPSS (IBM Statistics, Version 28.0.1.0). The PCA on cytokine profiling with

Luminex were performed using the PCA function from the Monte Carlo Reference-based Consensus Clustering (M3C) library (Bioconductor, Version 3.15).⁴¹²

DEA.

Differential Expression analysis (DEA) were performed in Perseus using students two sample t-test comparisons (unadjusted p value ≤ 0.05). For comparisons within AP samples, including untransduced AP vs. transduced AP and transduced N2A AP vs. transduced BV2 AP, and transduced BV2+LPS AP vs. transduced BV2 AP, TurboID-NES-normalized intensity values were used. For within WC comparisons, including transduced BV2+LPS WC vs transduced BV2 WCs, LFQ intensity values were used. Differentially enriched proteins were visualized as volcano plots with Prism (GraphPad, Ver 9.3.1 for Windows, San Diego, California USA, <https://www.graphpad.com>). The DEA of cluster-level significant changes in response to LPS was performed using the average intensity values of all proteins within a specific cluster for each biological replicate within a group. Then, the average cluster-intensity across replicates within an experimental group was taken. The average cluster-level responses to LPS were compared between whole cell and transduced AP groups with Log2FC DEA using an unadjusted p value ≤ 0.05 , visualized as asterisks.

Clustering.

To identify discrete groups of differentially enriched proteins across samples or associated with LPS treatment, we performed K-means clustering. The elbow method was used to determine

the optimal number of clusters for K-means clustering by using Integrated Differential Expression and Pathway analysis (iDEP Ver .95 (<http://bioinformatics.sdstate.edu/idep>)). Clustering analyses were visualized as heatmaps generated using Morpheus.

Gene set enrichment analysis.

Gene set enrichment analysis (GSEA) of differentially expressed proteins was performed using over-representation analysis (ORA) with the software AltAnalyze (Ver 2.0). Fisher exact significance threshold of p value ≤ 0.05 (Z-score greater than 1.96) was used to identify significant gene ontologies. Functional annotation of proteins biotinylated by TurboID-NES which significantly differ by cell-type took place by using enriched N2A and BV2 proteins (404 and 936 proteins, respectively) as input lists and the list of proteins identified in the AP dataset as the background (2277 proteins). Over-represented terms and their corresponding Z-scores were visualized as bar graphs using Prism. SynGO was used to identify unique synaptic terms in N2A-enriched proteins⁴¹³. To functionally annotate K-means clusters, lists of gene symbols associated with each K-means cluster were input into AltAnalyze for ORA. The resulting z-scores underwent gene GO and KEGG hierarchical cosine-cosine clustering, and each cluster was functionally annotated and the associated z-scores were represented in heatmaps. Mapping gene-associated risk loci with Alzheimer's disease, Parkinson's disease and Amyotrophic Lateral Sclerosis relevant terms, MAGMA dataset sheets were directly obtained from a previous review publication from our lab.⁴⁰⁰

Mitochondrial oxygen consumption in living BV2 cells.

To determine if TurboID-NES expression, LPS treatment, or biotin supplementation impacts mitochondrial function in BV2 cells, we directly measured oxygen consumption rates (OCAR) and extracellular acidification (ECAR) parameters using a mitochondrial stress test in a Seahorse XFe96 extracellular flux analyzer (Agilent). In a 96-well cell microplate, 5,000 transduced or untransduced BV2 cells were seeded in 80 μL of complimented growth media and incubated at room temperature in sterile cell culture hood for 1 hour. After cells adhere to the bottom of the well, 120 μL of complimented growth media was added and cells incubated overnight at in the cell culture incubator at 37° C and 5% CO₂. After 24 hours incubation, cells underwent a complete media change and were exposed to 1000ng/mL LPS or PBS as a vehicle control for 48 hours. The sensor cartridge was hydrated overnight at 37° C and 0% CO₂ using 200 μL of sterile deionized water added to each well of the utility plate. After incubating overnight without CO₂, water was removed from the utility plate and 200 μL of calibrant pre-warmed to 37° C was added to each well. The sensor plate incubated in calibrant at 37° in a CO₂-free incubator for 1 hour prior to loading the cartridge. Prior to assay, cells were washed thrice with 180 μL of Seahorse Media (Phenol-free 5mM HEPES Seahorse XF media, 10mM glucose, 2mM L-glutamine, and 1 mM sodium pyruvate, pH 7.4). Cells incubated in a CO₂-free incubator for 1 hour at 37° C. Sensor cartridges were loaded with 20 μL of Oligomycin (1.5 μM / well), 22 μL of carbonyl cyanide-4 (trifluoromethoxy) phenylhydrazone (FCCP) (0.75 μM / well), and 25 μL of Rotenone and Antimycin (0.5 μM / well)

and calibrated. After calibration, the seahorse-assay plate containing BV2 cells was run using the mitochondrial stress test in Wave (Version 2.6). Cells were then stained with Hoechst 33342 dye for 20 minutes and imaged using ImageXpress™ Micro Confocal imaging, and cells were counted using the Find Blobs feature of MetaExpress Software's Count Nuclei Application. Oxygen Consumption Rates (OCR) and Extracellular Acidification Rates (ECAR) were normalized to cell counts.

Cytokine profiling of supernatants

Cytokine profiling was performed as previously published with modifications.³³¹ Luminex multiplexed immunoassays (Cat # MCYTMAG-70K-PX32) quantified cytokines from cultured supernatants of transduced and untransduced BV2 and N2A cells receiving LPS or PBS SHAM stimulus (n = 6 / group). The cytokine panel detected Eotaxin, GM-CSF, INF- γ , IL-1a, IL-1b, IL-2, IL-4, IL-3, IL-5, IL-6, IL-7, IL-9, IL-10, IL-12p40, IL12p70, LIF, IL-13, LIX, IL-15, IL-17, IP-10, KC, MCP-1, MIP-1a, MIP-1b, M-CSF, MIP-2, MIG, RANTES, VEGF, and TNF- α . The average background intensity reading from each cytokine panel was subtracted from the raw cytokine abundance values and negative values were imputed to zero. To find appropriate loading volume for samples, linear ranging was performed as previously published⁴¹⁴ and 24% of total sample volume was loaded. Assays were read on a MAGPIX instrument (Luminex).

Experimental Design and Statistical Rationale

The sample conditions were prepared as follows: cell type (microglia or neuroblastoma), inflammatory challenge (LPS or PBS), TurboID-NES expression status (transduced or untransduced), and biotin-enrichment status (AP or WC). For each individual sample condition, there were 4 biological replicates, except for the WC BV2+LPS condition, in which there were 3 biological replicates. Overall, a total of 63 samples analyzed and described in the results. The maximum number of biological replicates were chosen within budgeted allowance; an a-priori power analysis was not performed. Sample acquisition order was randomized by the random number generator function in Excel, maintaining the following conditions: (1) whole-cell samples were randomized and acquired before AP samples and (2) randomized untransduced AP samples ran before randomized transduced AP samples, to prevent contamination of biotin-labeled proteins by TurboID in untransduced AP samples.

vii. Chapter III. Figures

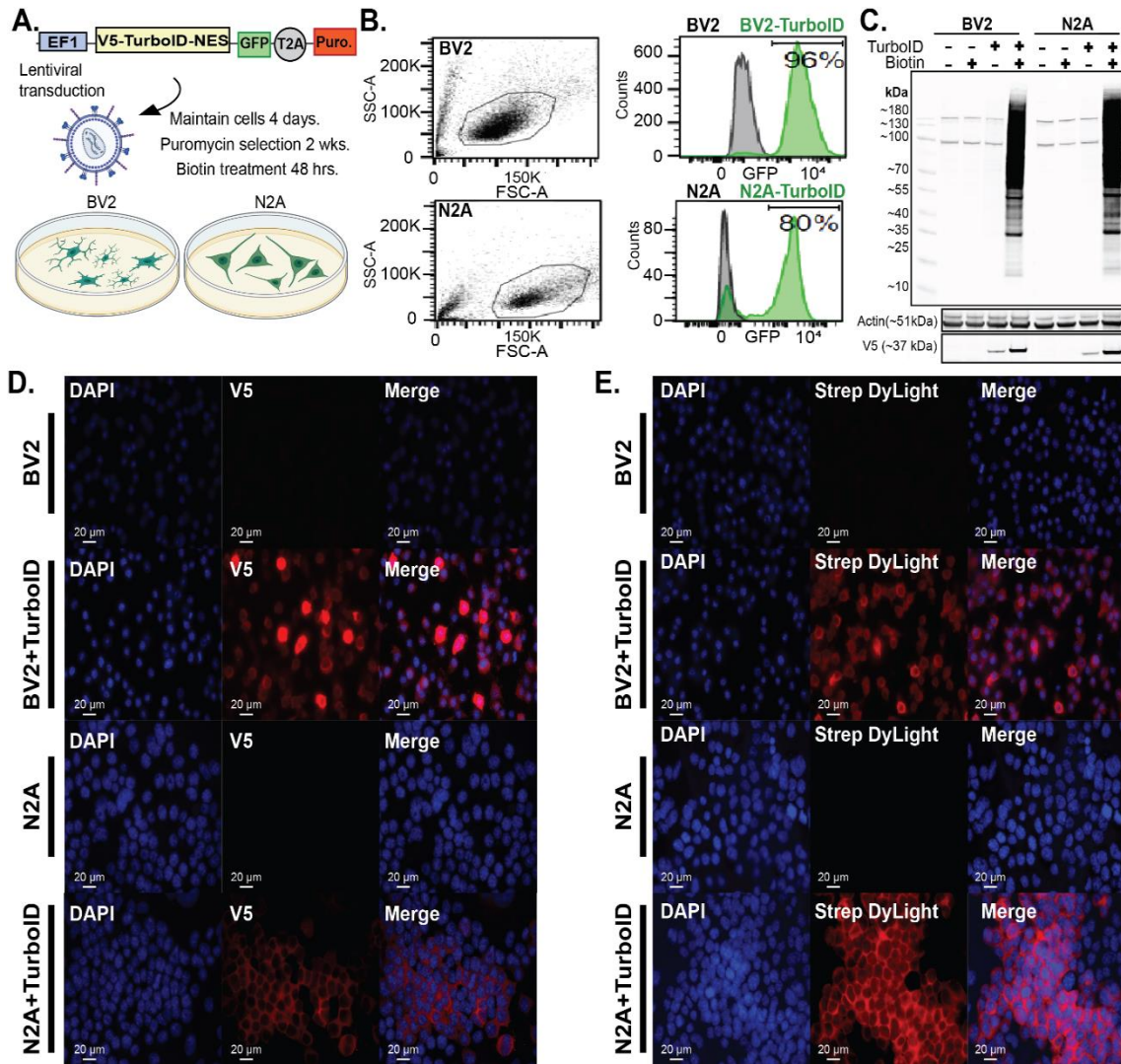


Figure 3.1. Creation of stably transduced BV2 microglia and N2A neuroblastoma cell lines that express cytosolic TurboID. **A.** Schematic of transduction. The genetic construct packaged into a lentivirus contains V5-tagged TurboID-NES driven under an EF1 promoter and a GFP sequence separated by a T2A linker. N2A and BV2 cells were transduced and maintained for 4 days prior to 2 weeks of puromycin selection and biotin supplementation in media. **B.** Following puromycin selection, FLOW cytometry confirms GFP positivity in a majority of BV2 (96%) and N2A (80%) cells. **C.** Western blot (WB) of transduced and untransduced cell lysates confirming presence of TurboID (V5) and biotin-dependent robust biotinylation of proteins. Actin was used as a loading control. **D.** Immunofluorescence (IF) confirming cytoplasmic localization of V5-

TurboID-NES in transduced cells. E. IF confirming cytosolic biotinylation of proteins in transduced BV2 and N2A cells.

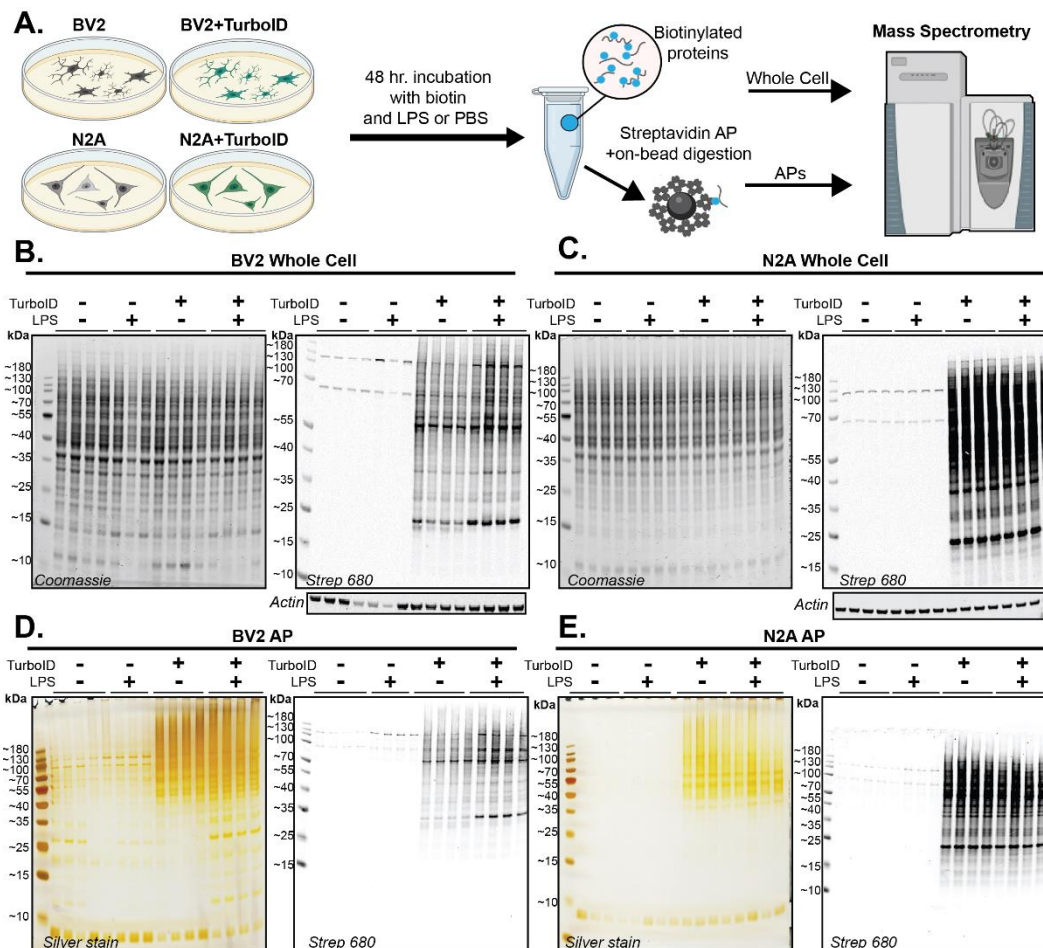


Figure 3.2. Experimental design and quality control of whole-cell and AP samples prior to MS. A. Schematic of experimental design. Transduced and untransduced BV2 and N2A cells were treated with biotin and LPS or PBS for 48 hrs. Whole-cell (WC) lysates and streptavidin- affinity purified (AP) samples were processed in parallel with Mass Spectrometry (MS) B. Western blot (WB) and Coomassie confirming biotinylation of proteins in transduced BV2 WC lysates. C. WB and Coomassie confirming biotinylation of proteins in transduced N2A WC lysates D. WB and silver stain confirming biotinylation of proteins bound to streptavidin beads and specificity of streptavidin beads for biotinylated species in BV2 AP preparations. LPS impacts banding patterns (10-40kDa) in transduced BV2 biotinylated proteins visualized with both Silver Stain and WB. E. WB and silver stain confirming biotinylation of proteins bound to streptavidin beads and specificity of streptavidin beads for biotinylated species in N2A AP preparations.

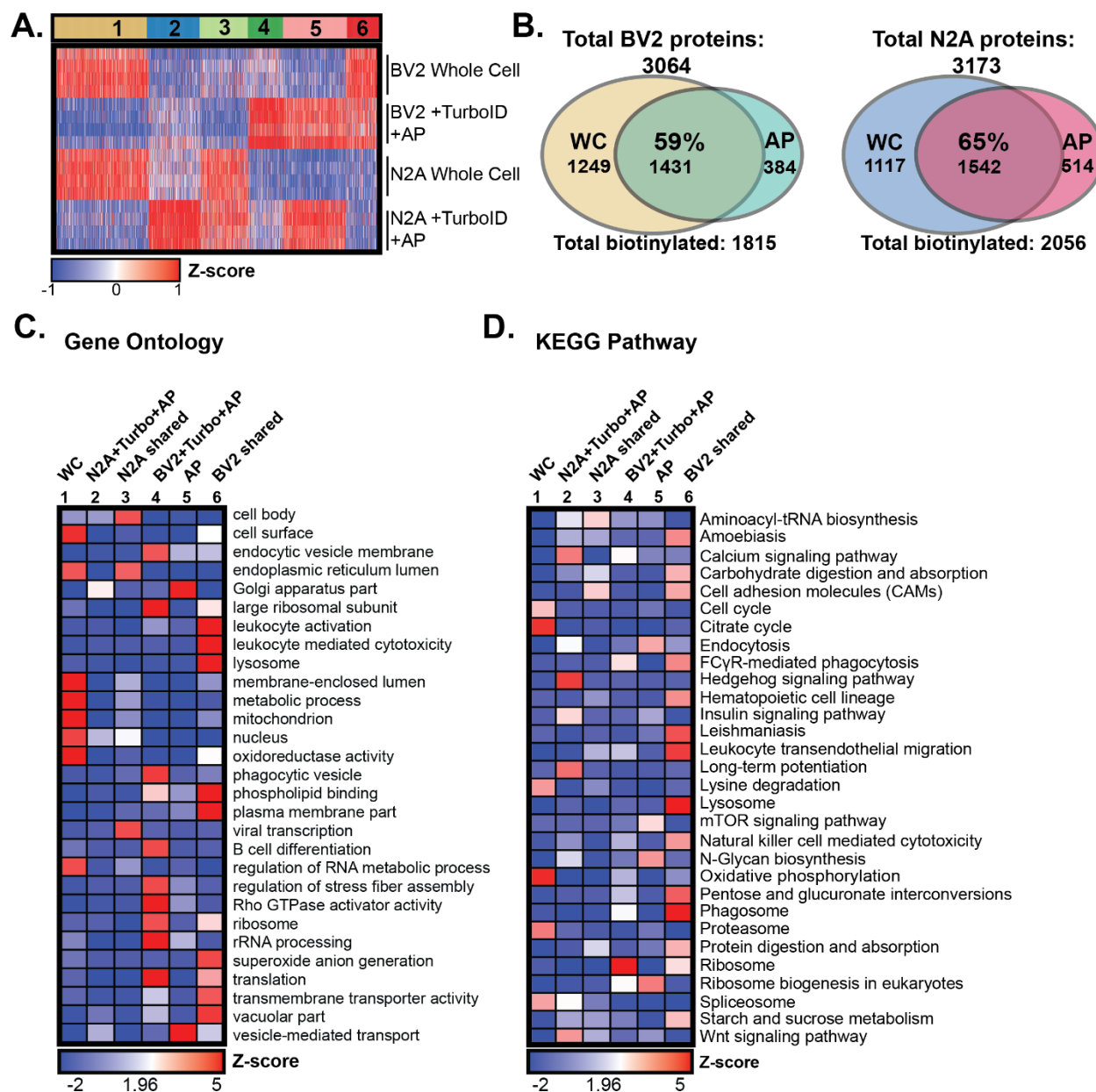


Figure 3.3 Global profiling of TurboID labeling in microglial and neuronal cell lines. **A.** K-means clustered heatmap representation of LFQ intensity data of proteins identified by MS in WC and biotinylated and AP proteomes ($n = 4$ per experimental group) in microglial and neuronal cell lines. 6 distinct clusters represent labeling profile of TurboID, including proteomes enriched in whole-cell preparations, AP preparations, and by cell type. **B.** Venn diagram of protein counts identified in BV2 WC samples and BV2+TurboID+AP samples and N2A WC and N2A+TurboID+AP samples. In BV2 cells, TurboID-NES labels ~59% of the total proteins captured by LFQ MS. In N2A cells, TurboID-NES captures ~65% of the total proteins identified by LFQ MS. **C.** Functional annotation of gene-set enrichment based on gene-ontology (GO) over-

representation analysis (ORA). Heatmap color intensity is based on Z-score enrichment across the 6 clusters. **D.** Heatmap representation and functional annotation of clusters derived from the KEGG pathways.

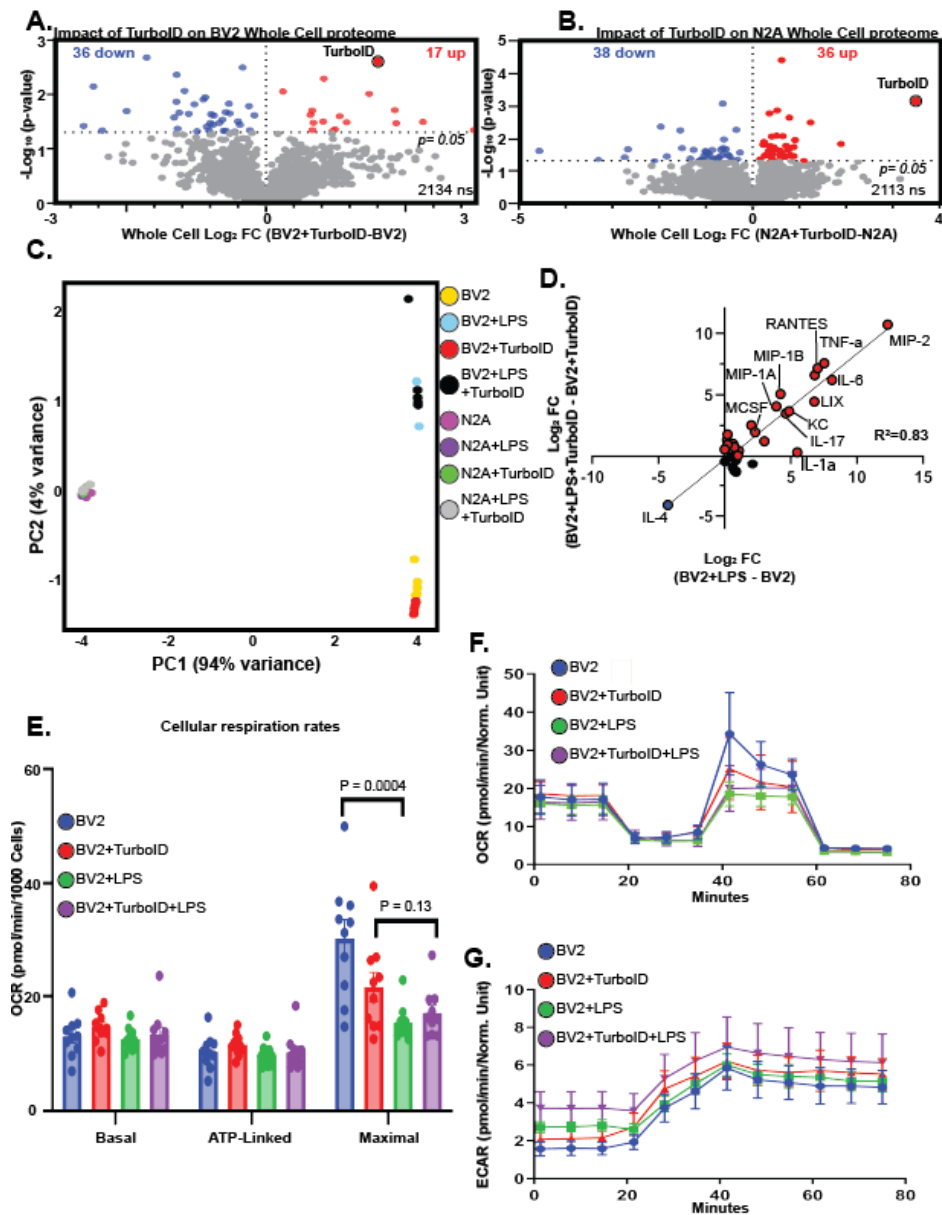


Figure 3.4. TurboID does not impact cellular phenotypes. **A.** Differential expression analysis (DEA) comparing WC transduced BV2 cell lysates with untransduced BV2 cell lysates identifies 53 Differentially expressed proteins (DEPs) in BV2 with TurboID expression. **B.** DEA comparing WC transduced and untransduced N2A Identifies 74 DEPs **C.** PCA of cytokine profiles derived from cultured supernatants indicates PC1 captures 94% of the variance across samples, accounting for differences in cell type. PC2 captures 4% of the variance, accounting for LPS impact on BV2 cytokines. **D.** Linear regression of LPS cytokine fold-change induction of untransduced (x-axis) and transduced (y-axis) BV2 cells demonstrates high correlation (R²=0.83). **E.** Bar graph depicting Basal, ATP-linked and Maximal cellular respiration rates of transduced and untransduced BV2 cells. LPS significantly decreases the maximal respiration of untransduced

BV2 cells ($p=0.0004$) and decreases maximal respiration in transduced BV2 cells, though this finding is statistically insignificant ($p=0.13$). F. Oxygen consumption rate (OCR) traces for transduced and LPS exposed BV2 cells highlight LPS response in maximal respiration. G. Extracellular acidification rate (ECAR) highlights the basal glycolytic rate as higher when cells are exposed to LPS but are not impacted by transduction status.

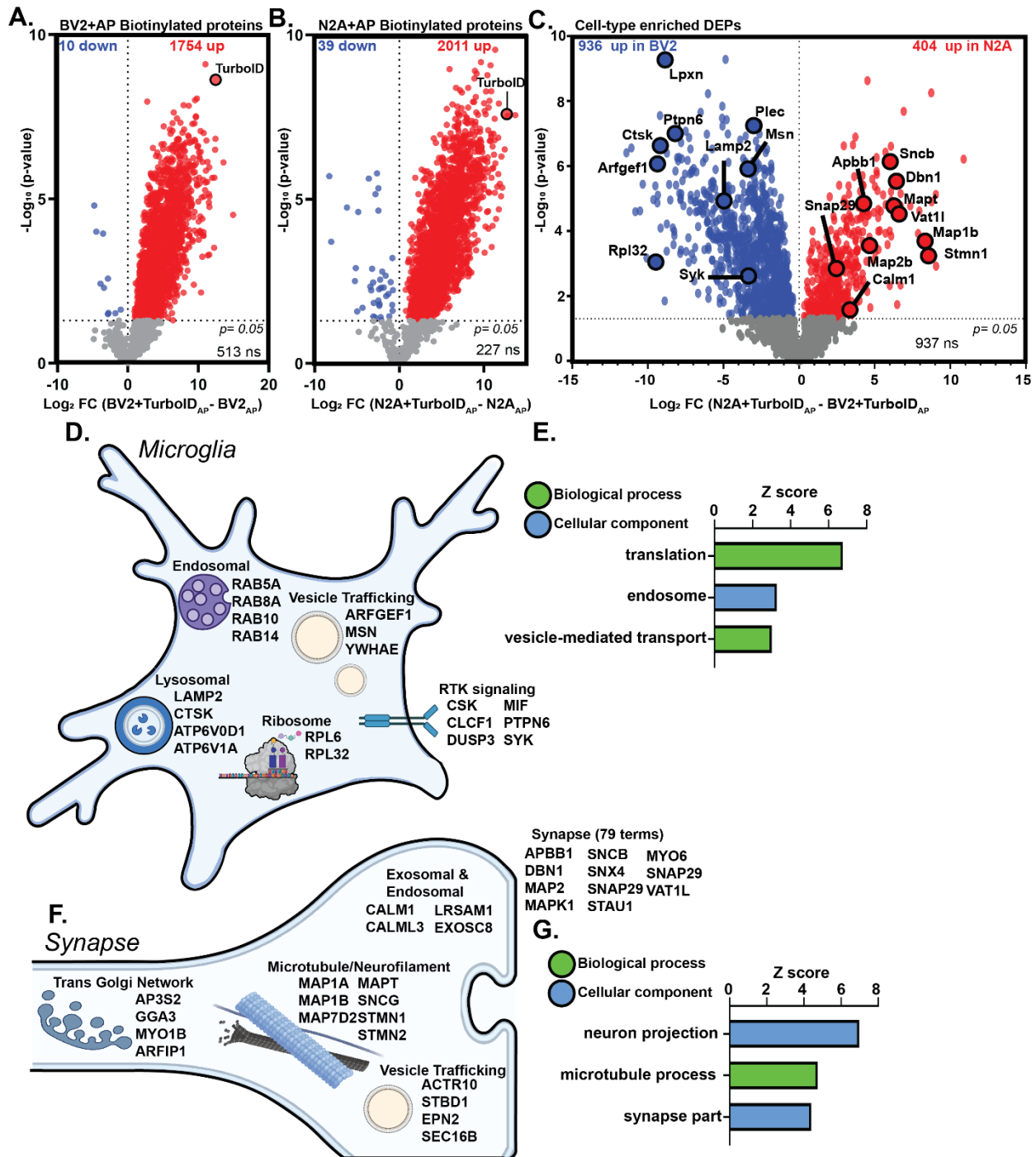


Figure 3.5. TurboID labeling and Streptavidin AP captures cellularly distinct proteomes. A. DEA of BV2 AP samples showing robust TurboID biotinylation of over >1700 proteins over endogenously biotinylated proteins derived from untransduced cell lines. **B.** DEA depicting biotin enrichment of N2A transduced AP proteome reveals >2000 proteins labeled by TurboID **C.** DEA comparing transduced AP proteomes of BV2 (left) and N2A (right) TurboID-biotinylated

proteomes. There are 936 proteins labeled by TurboID enriched in BV2 and 404 proteins enriched in N2A biotin-labeled proteomes. Proteins with disease-relevance to neurodegenerative disease are highlighted. **D.** Schematic of the variety of subcellular compartments labeled by TurboID in microglia (BV2). **E.** Gene Ontology (GO) of highly enriched cellular components and biological processes within the biotin-labeled BV2 proteome. TurboID biotinylates translational machinery, endosomal machinery, and vesicle-bound membranes in BV2 cells. **F.** Schematic of diversity of subcellular compartments labeled by TurboID in synaptic compartment (N2A). **G.** GO of significantly enriched cellular components and biological processes within the biotin-labeled N2A proteome confirms that TurboID biotinylates neuronal processes including synaptic machinery and neuron projection.

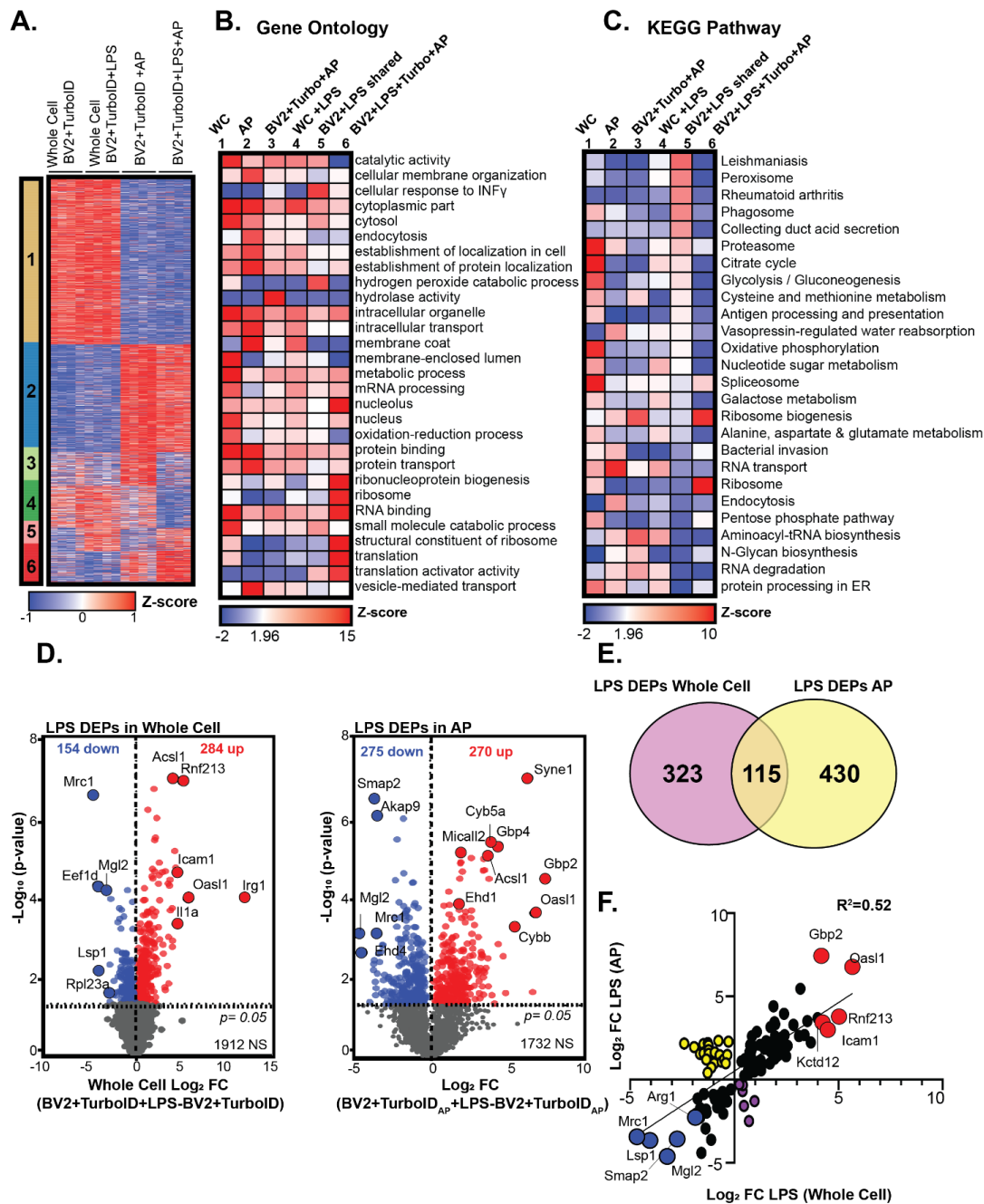


Figure 3.6. TurboID-mediated biotinylation partially captures LPS-driven proteomic changes. **A.** K-means clustered heatmap representation of LFK intensity data of proteins differentially expressed by TurboID in whole-cell and transduced AP BV2 proteomes ($n = 4$ per experimental group). **B.** Heatmap representation and functional annotation of gene ontology from *murine* GO database. Heatmap color intensity depicts Z-score values. **C.** Heatmap representation of z-scores associated with LPS DEPs derived from KEGG pathways database. **D.** DEA of LPS DEPs in WC (*left*) and AP (*right*) identifies 438 and 545 LPS DEPs, respectively. **E.** Venn diagram

depicting 323 LPS DEPs unique to whole-cell BV2 samples, 115 shared LPS DEPs and 430 unique LPS DEPs in BV2 AP samples. **F.** Linear regression of Log₂FC values of BV2 AP samples (y-axis) and BV2 whole-cell samples (x-axis) reveals a modest correlation ($r^2=0.52$) of log₂FC of the shared 115 LPS DEPs. Red points depict proteins the top 5 proteins significantly upregulated with LPS treatment in AP and whole-cell samples. Yellow points represent proteins significantly increased in AP samples and significantly decreased in whole-cell samples with LPS treatment. Blue points illustrate the top 5 proteins significantly decreased with LPS in both AP and whole-cell BV2 samples. Purple points depict proteins which are significantly increased in the whole-cell proteome and significantly decreased in the AP proteome with LPS treatment.

Chapter IV. Extension of TurboID into murine Camk2a

neurons.

*Chapter IV contains modified excerpts of findings and methodologies originally published in a coauthored publication in *Nature Communications* on May 25th, 2022 (2927) DOI: <https://doi.org/10.1038/s41467-022-30623-x>

i. Introduction

The brain is an immensely complex organ comprising many different cell types including neurons, glia, and vascular and endothelial tissue. The complexity inherent to brain homogenate poses technical challenges to purifying proteomes from distinct cells. Traditional challenges associated with cellular isolation (*see section 2.7*) with fluorescence activated cell sorting (FACS) and magnetic activated cell sorting (MACS) have spurred technological advancements in proximity labeling and affinity purification methods as procedures to purify cellularly-distinct proteomes from total brain homogenate. Of recent proximity-labeling methods advanced (*see section 2.7*), the biotin ligase TurboID is a remarkable tool capable of rapidly labeling proteins in a 9-10 nm radius in living cells and physiological contexts^{327,328}. Expressing the robustly catalytic and cytosolic-directed biotin ligase, TurboID-NES, under cell-type specific promoters can biotin-label native cell-type specific proteomes in living mice without the need for cellular isolation. Affinity purification methods incorporating streptavidin-conjugated magnetic beads effectively

leverage the strongest non-covalent interaction affinity between biotin and streptavidin, with a dissociation constant $K_d = 4 \times 10^{-14}$ ⁴¹⁵. Purified proteomes can then be prepared for down-stream MS-based proteomics. Our research worked to develop the approach called Cell type-specific In vivo Biotinylation Of Proteins (CIBOP) for the first-ever extension of TurboID into living mice. This was made possible in part through successive validation studies testing the functionality and cell-type specificity of the Cre-flox- TurboID targeting vector supporting both the Neuronal Adeno Associated Viral (AAV9) delivery (AAV-CIBOP) strategy and novel transgenic mouse line (Tg-CIBOP) strategy published in excitatory neurons and astrocytes³³¹. We successively validated the TurboID targeting-vector through a series of in vitro and in vivo validation studies described in Chapter IV of this thesis. The creation of the *Rosa26^{TurboID}* was made possible by combined efforts of many scientists working in collaboration. Studies generating mice stereotaxically injected with adeno-associated viruses were also a collaborative effort between affiliated scientists. The author of this thesis performed key in vitro experiments in this chapter (**Figures 4.2 and 4.3**), as well as the immunoblotting and immunofluorescence experiments validating adeno-associated viral direction of TurboID-dsRED to *Camk2a-Cre^{ERT2}* mice (**Figure 4.4**). The author of this thesis performed immunoblotting of affinity purified and whole-brain homogenate derived from mice injected with AAV9-hSyn-Cre to *Rosa26^{TurboID}* mice (**Figure 4.5**). The author of this thesis did not perform stereotaxic injections of key viral constructs. Immunofluorescence verification of neuronal biotinylated proteins in hSyn-Cre to *Rosa26^{TurboID}* mice was not performed

by the author of this thesis (**Figure 4.5B**), nor were the immunofluorescence of transgenic *Rosa26^{TurboID}/Camk2a* mouse brain studies included in **Figure 4.6** Immunofluorescence verification of neuron-specific biotinylated proteins in *Rosa26^{TurboID}/Camk2a* mice are necessary and foundational for experiments using these mice (*Chapter 5*), and have been included here for reference.

ii. Paving the way to in vivo extensions of TurboID

In vitro validation studies confirm the Cre-lox genetic strategy

To express TurboID-NES in specific cell populations, we designed a targeting vector using a Cre-Flox-STOP genetic strategy (**Figure 4.1**). With a promoter-stop sequence flanked by lox-p sites upstream of TurboID-NES, TurboID may only be expressed in the presence of Cre recombinase. If Cre recombinase is expressed under a cell-type specific promoter, then TurboID-NES will only be expressed in that cell type, and biotinylate cytosolic proteomes in a cell-type-specific manner. We obtained V5-TurboID-NES_pCDNA3 as a gift from Alice Ting (Addgene plasmid #107169) to generate the AsiS1-Kozak-V5-TurboID-NES-stop-Mlu1 construct. This was further cloned into the R26 CAG AsiSI/MluI targeting vector, a gift from Ralf Kuehn (Addgene plasmid # 74286), to generate the a *Rosa26* (chromosome 6) targeting vector containing the CAG promoter, a floxed STOP site (loxp-STOP-loxp), and V5-TurboID with a nuclear export signal (TurboID-NES). Prior to generating transgenic mice expressing construct, we validated its functionality via transfection of human embryonic kidney 293 (HEK293) cells in the presence or

absence of a CMV-Cre plasmid, a gift from Dr. Xinping Huang, Emory University. By transfecting HEK293 cells with the stop-floxed V5-TurboID-NES plasmid alone, or the CMV-Cre plasmid alone, or by co-transfecting HEK293 cells with the stop-floxed V5-TurboID-NES we could verify that HEK293 cells will V5-TurboID-NES is expressed and functional only in the presence of CMV-Cre and biotin via western blotting and immunohistochemistry techniques (**Figure 4.2**).

To optimize affinity purification of biotin-labeled proteins against the complex background of brain homogenate, we obtained cell lysates from N2A cells transduced with V5-TurboID-NES and brain homogenate from wildtype mouse brain. After performing BCA on these samples, we prepared 7 fractions of brain homogenate containing increasing amounts of proteins derived from transduced N2A cell lines ranging from 0%, 9%, 17%, 50%, 83%, 90% and 100% (**Figure 4.3A**). Protein compositions were performed by protein amount to a total protein amount of 20 μ g immobilized with gel electrophoresis and visualized by streptavidin-680 and ponceau staining via western blotting. By varying the composition of the biotin-labeled proteins in a graded fashion, we could establish the minimum compositional range of biotinylated species derived from cells expressing functional V5-TurboID-NES against a background of complex brain homogenate necessary to obtain sufficient signal to noise via Western Blotting and Ponceau Staining techniques (**Figure 4.3B**). We qualitatively determined that a complex mixture of brain homogenate containing 17% of proteins derived from N2A cells transduced with TurboID-V5 was sufficient to overcome noise introduced by brain homogenate associated endogenously

biotinylated species. This experiment established feasibility for extension of the CIBOP approach into murine models wherein V5-TurboID-NES may be expressed in minority cell types, such as microglia. This experiment also instrumental in optimizing the affinity purification procedures and establishing a minimal compositional range of biotinylated proteins able to be visualized with streptavidin-based western blotting techniques. Extending the CIBOP approach into murine models expressing TurboID under sub-populations of neuronal promoters, astrocytic promoters, or microglial promoters was established as feasible because of the qualitative confirmation of the ability to resolve biotinylated proteins from minority concentrations.

iii. In-vivo biotinylation of murine neuronal proteomes mediated by adeno associated viral delivery.

After these series of in vitro validation studies, we extended CIBOP into murine excitatory neurons or pan-neuronal CIBOP by means of AAV stereotaxic delivery into brain regions. Prior to the development of transgenic mice, we established feasibility through AAV-CIBOP by first packaging and targeting TurboID^{fl/fl}-dsRED into an AAV9 into *Camk2a-Cre^{ERT2}* mice in a foundational pilot study. After generating transgenic *TurboID^{fl/fl}* mice, we virally directed pan-neuronal synaptic Cre in an AAV9 vector under the hSyn promoter. These complementary in vivo AAV9 feasibility studies were instrumental in establishing the functionality of expressing floxed TurboID in a *Camk2a-Cre^{ERT2}* physiological context as well as the successful biotinylation of

proteins by the transgenic *TurboID^{fl/fl}* mice. Both of these strategic components were necessary to support the long-term goal of genetically crossing *TurboID^{fl/fl}* mice with *Camk2a-Cre^{ERT2}* mice to obtain excitatory neuronal proteomes.

AAV9-TurboID-dsRED into *Camk2a-Cre^{ERT2}* cortex and striatum.

Pilot feasibility studies began with stereotaxically injecting AAV9-TurboID^{fl/fl} - dsRED bilaterally into the cortex and striatum of 6-month-old *Camk2a-Cre^{ERT2}* mice (n=2; Female) (**Figure 4.4A**). After 3 weeks, mice received 5 days of tamoxifen injections to induce recombination and 2 weeks of biotin water (37.5 mg/L)⁴¹⁶ supplementation. Brain homogenates of uninjected *Camk2a-Cre^{ERT2}* mice as well as *Camk2a-Cre^{ERT2}* mice receiving TurboID-AAV9 injections were resolved using gel electrophoresis and streptavidin-680 visualized biotinylated proteins on corresponding western blots (**Figure 4.4B**). Histological verification of TurboID-dsRED cortical expression and biotinylated proteins with Streptavidin-488 provided preliminary verification of the first physiological extension of TurboID into mice (**Figure 4.4C**). Notably, there was no observable change in weight or locomotor activity with TurboID-mediated biotinylation in living mice.

AAV9-hSyn-Cre into hippocampi of TurboID floxed mice

We generated and validated TurboID^{fl/fl} mice by integrating a loxp-stop-loxp cassette with TurboID with a nuclear export sequence (NES) in the *Rosa26* locus (*Rosa26^{TurboID}*). We stereotaxically administered AAV9 containing hSyn-Cre to direct Cre-recombinase specifically

to neurons (**Figure 4.5A**), leading to excision of the stop codon and pan-neuronal expression of TurboID. Specifically, we stereotaxically injected AAV9-hSyn-Cre into bilateral hippocampi of 2-month-old *Rosa26^{TurboID}* mice (n=3; male) and wildtype (WT) littermate controls (n=3; male), and uninjected WT mice served as negative controls (n=3; male) After 4 weeks, mice received 2 weeks of biotin water (37.5 mg/L)⁴¹⁶ to drive biotinylation of cytosolic and synaptic proteins in vivo as confirmed by WB (probing streptavidin-pulldown (“IP”) proteins and total brain homogenate (“input”) for post-synaptic density 95 (PSD95) and actin (**Figure 4.5C & 4.5D**). Immunofluorescence (IF) verification of neuron-specific biotinylation of proteins was performed by using NeuN as a neuronal nuclear marker and Alexafluor 488 conjugated streptavidin colocalization (**Figure 4.5B**). These preliminary findings supported the feasibility of our approach in directing Cre-dependent neuronal expression of TurboID to label and capture cytosolic and synaptic proteins from adult mouse brain.

iv. Creation and validation of the novel Rosa26^{TurboID/wt} mice

Establishing the first known genetic cross between transgenic *Rosa26^{TurboID/wt}* mice with *Camk2a-Cre^{Ert2}* mice was a collaborative undertaking made successful by the combined effort of many scientists. The following section validating the neuronal-specific biotinylation of proteins via immunofluorescence and immunoblotting is an excerpt from our co-authored publication³³¹. All experimental studies shown in **Figure 4.6** were reported in a prior collaborative publication from our group and these data and their corresponding methodology have been included here as

they were instrumental in establishing feasibility for proceeding experiments in this thesis using *Rosa26^{TurboID/wt}/Camk2a* mice (See Chapter 5). We employed a transgenic approach to express TurboID within Camk2a neurons by breeding *Rosa26^{TurboID/wt}* mice with *Camk2a-Cre^{Ert2}* and inducing Cre recombinase expression by intraperitoneal tamoxifen. Camk2a (Ca²⁺/calmodulin-activated protein kinase 2A) is an abundant serine-threonine kinase highly expressed by excitatory neurons, particularly in the synapse, where it regulates synaptic transmission, excitability, and long-term potentiation. Camk2a was chosen based on extensive validation, specificity, and non-leakiness of available *Camk2a-Cre^{Ert2}* driver lines and the well-characterized expression patterns of Camk2a across brain regions^{417,418}. *Rosa26^{TurboID/wt}/Camk2a* and littermate controls received tamoxifen at 6 weeks of age, allowed 3 weeks for recombination, and followed by biotin supplementation for 2 weeks (**Figure 4.6A**). Western blot analysis of lysates from different brain regions (cortex, hippocampus, striatum/thalamus, pons/medulla, and cerebellum) confirmed robust biotinylation of proteins in the *Rosa26^{TurboID/wt}/Camk2a* mice as compared to minimal endogenous biotinylation observed in control mice (**Figure 4.6B**). Qualitatively, the highest level of labeling was observed in the cortex, hippocampus, and striatum/thalamus regions as compared to cerebellum and pons/medulla, consistent with known Camk2a expression patterns⁴¹⁹. We also confirmed TurboID protein expression via detection of V5 in *Rosa26^{TurboID/wt}/Camk2a* brain regions only, which followed a similar pattern to level of biotinylation (**Figure 4.6B**). Immunofluorescent imaging of the whole brain displayed wide-spread

biotinylation in *Rosa26^{TurboID/wt}/Camk2a* brains compared to control brains (**Figure 4.6C**). Map2 and streptavidin co-immunofluorescence confirmed neuronal labeling throughout the hippocampus (**Figure 4.6D**), as well as the cortex, striatum/thalamus, and cerebellum.

v. Methodology

Construct generation and cell culture studies

The V5-TurboID-NES_pCDNA3, a gift from Alice Ting (Addgene plasmid # 107169) was used to generate AsiS1-Kozak-V5-TurboID-NES-stop-Mlu1 construct. This was then cloned into the pR26 CAG AsiSI/MluI targeting vector, a gift from Ralf Kuehn68 (Addgene plasmid # 74286), to generate the a Rosa26 (chromosome 6) targeting vector containing the CAG promoter, a floxed STOP site (loxp-STOP-loxp), and V5-TurboID with a nuclear export signal (TurboID-NES). This Rosa26TurboID targeting vector was verified in vitro for Cre-mediated TurboID expression and biotinylation in HEK293 cells. Human embryonic kidney 293 (HEK293 from ATCC CRL-1573) cells were maintained in Dulbecco's modified Eagle's medium (DMEM) supplemented with 10% fetal bovine serum (FBS) and 1% penicillin/streptomycin at 37 °C in a 5% CO₂ atmosphere. For transient transfection, cells grown to 70–80% confluency in 6-well plates were transfected (Lipofectamine 3000, Thermo, L3000001) with 2.5 µg/well of Rosa26TurboID targeting vector and Cre plasmid (CMV-Cre, a gift from Dr. Xinping Huang, Emory University), Rosa26TurboID targeting vector alone, or Cre plasmid alone according to manufacturer's protocol. Untransfected cells also served as negative controls. Twenty-four hours post-transfection, cells were treated with

200 μ M biotin for another 24 h. Subsequently, cells were rinsed with cold 1X phosphate buffered saline (PBS) and harvested in urea lysis buffer (8 M urea, 10 mM Tris, 100 mM NaH₂PO₄, pH 8.5) containing 1X HALT protease inhibitor cocktail without EDTA (Thermo, 87786). The cells were sonicated for 3 rounds consisting of 5 s of active sonication at 25% amplitude with 10 s incubation periods on ice between sonication. Lysed cells were then centrifuged for 5 min at 15,000 \times g and the supernatants were transferred to a new tube. Protein concentration was determined by bicinchoninic acid (BCA) assay (Thermo, 23225). To confirm protein biotinylation, 10 μ g of cell lysates were resolved on a 4–12% Bis-Tris gel, transferred onto a nitrocellulose membrane, and probed with streptavidin-Alexa680 (Thermo, S32358) diluted 1:10 K in Start Block (Thermo, 37543) for 1 h at room temperature. Subsequently, the membrane was washed in 1X tris buffered saline containing 0.1% Tween20 (TBS-T) and incubated over-night with mouse anti-V5 (1:250; Thermo, R960-25) or anti-Gapdh (1:3000; Abcam, ab8245) diluted in Start Block. After washes in TBS-T, membranes were incubated with goat anti-mouse 700 (1:10 K) and imaged using Odyssey Infrared Imaging System (LI-COR Biosciences).

Generation of the Rosa26 TurboID mouse

The Rosa26TurboID targeting vector was electroporated into C57BL/6 N embryonic stem (ES) cells (from Taconic, ES Cell Line # JM8A3) at Texas A&M Institute for Genomic Medicine (TIGM). After confirming homologous recombination in ES clones, they were microinjected into albino goGermlineTM blastocysts (Ozgene) and implanted into pseudo pregnant CD-1 female mice²¹

(Emory Mouse Transgenic and Gene Targeting Core). The resulting chimeric mice were crossed to wild-type (WT) C57BL6/J69 mice to yield F1 Rosa26TurboID heterozygous mice (Rosa26TurboID/wt) and littermate controls. Genotyping was performed on DNA extracted from a tail biopsy from mice using the following primers: (TurboID_fwd) 5' ATCCCGCTGCTGAACGCTAAAC 3', (TurboID_rev) 5' ACCATTCCTCCCTCTGCTTCC 3', (ROSA26_fwd) 5' CTCTTCCCTCGTGATCTGCAACTCC 3', (ROSA_rev) 5' CATGTCTTTAATCTACCTCGATGG 3'. Mice were designated as heterozygous (Rosa26TurboID/wt) by the presence of a band approximately 181bp corresponding to the TurboID transgene and a 299bp band produced by the endogenous ROSA26 allele, while WT contained only the 299bp endogenous ROSA26 band.

Animal studies

Approval from the Emory University Institutional Animal Care and Use Committee was obtained prior to all animal-related studies (IACUC protocols # PROTO201800252 and PROTO201700821). All mice used in the present study were housed in the Department of Animal Resources at Emory University under a 12 h light/12 h dark cycle with ad libitum access to food and water. Animals were housed in the vivarium under standard conditions for mice (temperature 72F, humidity range 40–50%). All procedures were approved by the Institutional Animal Care and Use Committee of Emory University and were in strict accordance with the National Institute of Health's "Guide for the Care and Use of Laboratory Animals."

AAV9-mediated expression of TurboID in neurons

Individual mice were anesthetized with isoflurane, given sustained-release buprenorphine subcutaneously (0.5 mg/kg), and immobilized on a stereotaxic apparatus. The mice were maintained on 1–2.5% isoflurane and monitored closely for breathing abnormalities throughout the surgery. Bilateral intrahippocampal injections (coordinates from bregma: –2.1 mm posterior, ±2.0 mm lateral, and ±1.8 mm ventral) were performed over a 5 min period with 1 µL of AAV9-hSyn-Cre (Titer $\geq 1 \times 10^{13}$ vg/mL, Addgene, 105553-AAV9) or un-injected: un-injected WT mice (n=3, male), wild-type mice injected with AAV9-hSyn-Cre (n=3, male), and Rosa26TurboID/wt mice injected with AAV9-hSyn-Cre (n=3, male) (Fig. 1b). The incision was closed with tissue adhesive (Fisher, NC0304169), isoflurane was discontinued, and the animal was revived in a new, clean cage atop a heating pad. The mice were monitored every 15 min for 1 h after surgery and routinely for the 3-day post-surgery survival period under normal vivarium conditions. After 4 weeks, mice were given water supplemented with biotin (37.5 mg/L)⁴¹⁶ for 2 weeks until euthanasia at 3 months of age. The pilot experiment directing AAV9-TurboID^{fl/fl}-dsRED into *Camk2a-Cre^{ERT2}* mice (Titer $\geq 1 \times 10^{12}$ per mL) into the cortex and striatum were performed using co-ordinates from the Allen Institute for Brain Science (<https://mouse.brain-map.org/>). 6-month old *Camk2a-Cre^{ERT2}* were injected with AAV9-TurboID^{fl/fl}-dsRED (n=2), though only 1 showed labeling. Un-injected *Camk2a-Cre^{ERT2}* brain homogenate and brain sections were used as control for immunofluorescence and western blotting.

Immunocytochemistry

For immunocytochemistry (ICC), human embryonic kidney (HEK293) cells grown to 50% confluency on coverslips were transfected and treated with biotin as described above. Subsequently, cells were washed 3X with warm sterile PBS for 5 min each and fixed with 1X ICC fixation buffer (Invitrogen, 00-8222-49) for 30 min. After PBS washes, cells were permeabilized (Invitrogen, 00-8333-56) for 20 min and blocked in 10% normal horse serum (NHS) in PBS for 45 min at room temperature. The cells were then incubated with mouse anti-V5 diluted in 2% NHS in PBS overnight. After thorough washes with PBS, cells were incubated with anti-mouse Rhodamine Red (1:500, goat anti-mouse Rhodamine-red, Thermo, R6393) and streptavidin Alexa-fluor 488 (1:500, Thermo, S11223) diluted in 2% NHS in PBS for 1 h. Coverslips were mounted onto slides using mounting media containing DAPI (Sigma-Aldrich, F6057) and images were captured using an Olympus fluorescence microscope (Olympus BX51) and camera (Olympus DP70) and processed using Image J software (FIJI Version 1.51).

Immunofluorescent staining

Fixed brains were cut into 30 μ m thick sagittal sections using a cryostat. For immunofluorescence (IF) staining, 2-3 brain sections from each mouse were thoroughly washed to remove cryopreservative, blocked in 8% normal horse serum (NHS), diluted in TBS containing 0.1% Triton X-100 for 1 h, and incubated with primary antibodies diluted in PBS containing 2% NHS overnight (1:200 mouse anti-Map2, BD Pharmagen, 556320;). Following thorough washes

and incubation in the appropriate fluorophore-conjugated secondary antibody (1:500, goat anti-mouse Rhodamine-red, Thermo, R6393) and streptavidin Alexa-fluor 488 (1:500, Thermo, S11223) for 1 h at room temperature, sections were mounted on slides with mounting media containing DAPI (Sigma-Aldrich, F6057) for nuclear staining. Representative images of the same regions across all samples were taken using the Keyence BZ-X810 and all image processing was performed using Image J software (FIJI Version 1.51).

Transgenic approach for neuronal Cre recombinase expression in

Rosa26^{TurboID/wt} mice

Rosa26^{TurboID/wt} mice were crossed with *Camk2a-Cre^{Ert2}* mice (Jackson Labs, Stock No. 012362) to generate heterozygous *Camk2a-Cre^{Ert2}* (“*Camk2a*”, n=2; male) and *Rosa26^{TurboID/wt}/*Camk2a-Cre^{Ert2}** (“*Rosa26^{TurboID/wt}/*Camk2a**”, n=2; 1 male and 1 female) littermate mice. All mice were given tamoxifen (75 mg/kg) intraperitoneally for 5 days at 6 weeks of age. After 3 weeks, mice were given water supplemented with biotin (37.5 mg/L) for 2 weeks until euthanasia at 3 months of age. Consistent with previous publications⁴²⁰ we have previously validated the *Camk2a-Cre^{Ert2}* line for neuron-specific labeling and non-leaky Cre activity. After biotin supplementation (37.5 mg/L) for 2 weeks, mice were anesthetized with ketamine (ketamine 87.5 mg/kg, xylazine 12.5 mg/kg) followed by transcardial perfusion with 30 mL of ice-cold PBS. The brain was immediately removed and hemi-sectioned along the mid-sagittal line. The left hemisphere was fixed in 4% paraformaldehyde (PFA) for 24 h and then transferred to 30% sucrose after through washes in PBS.

vi. Chapter IV Figures.

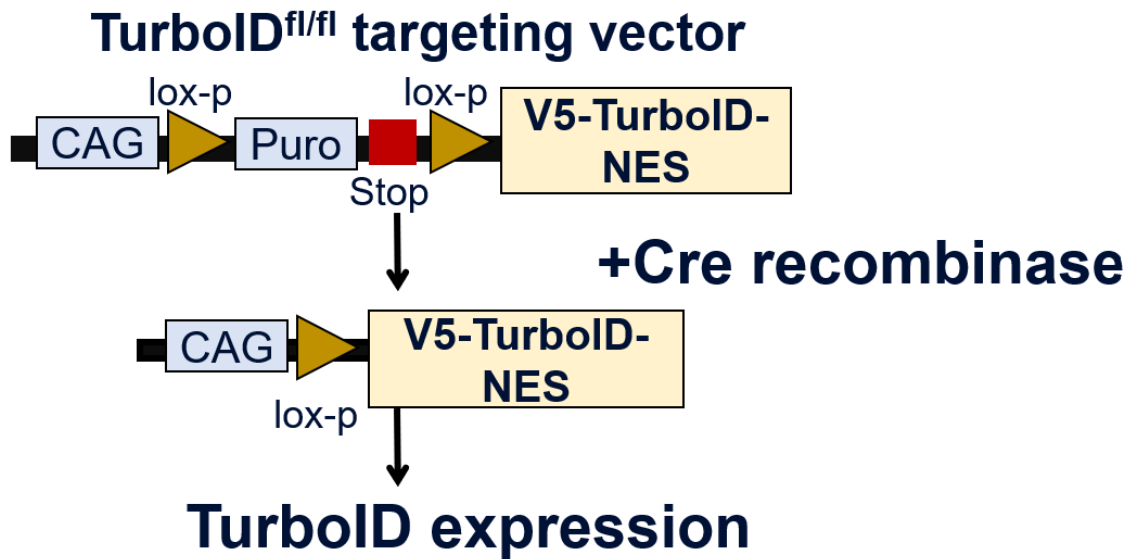


Figure 4.1 Schematic of the genetic strategy employing Cre-dependent TurboID expression. The genetic strategy underlying cre recombinase dependent TurboID expression includes a lox-p floxed stop sequence after the CAG promoter. In the presence of Cre recombinase enzyme, the stop sequence is excised and RNA polymerase transcribes mRNA encoding for V5-TurboID-NES. Cre may be expressed in specific cell types under cellularly-distinct promoters, ensuring that only cells expressing Cre recombinase will translate V5-TurboID-NES.

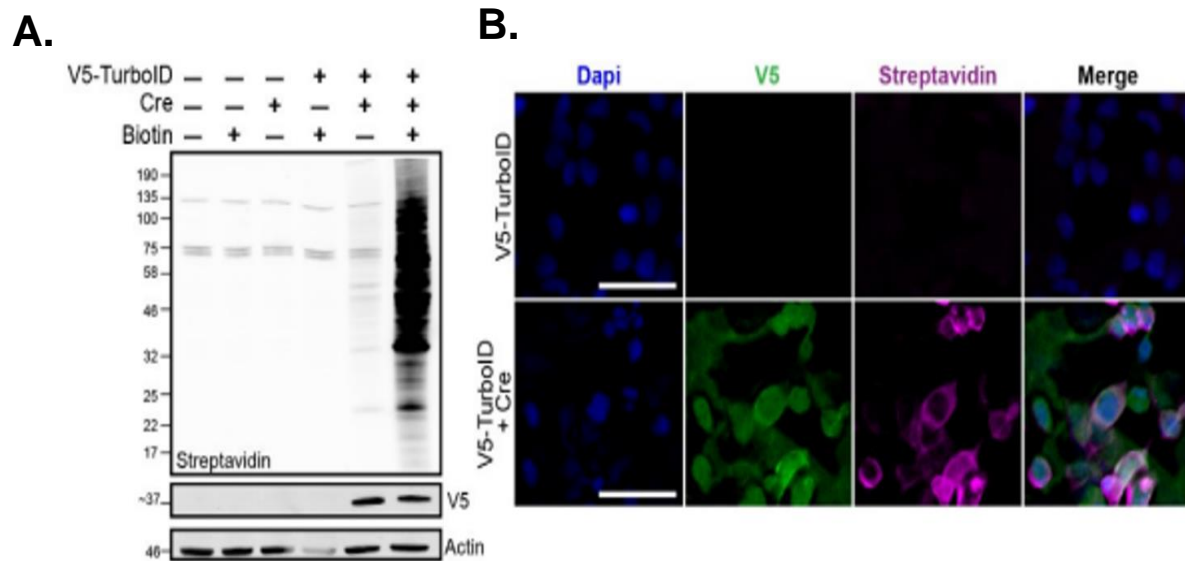


Figure 4.2 Cotransfection of HEK293 cells to validate cre-recombinase-dependent expression of TurboID. HEK293 cells were co-transfected with cre recombinase and stop-floxed V5-TurboID-NES and biotin was supplemented into the culture medium for biotinylation of proteins. Lysates of cotransfected HEK293 cells were prepared along with mono-transfected controls and non-biotin-treated cultures as controls. **A.** Western blot analyses probing for actin, V5, and biotinylated proteins (Streptavidin-680) confirmed cre-dependent expression of TurboID. **B.** Representative immunofluorescence images of cells ($n = 3$) independent experiments per condition adhered to coverslips, from experiments in confirming expression of V5-TurboID-NES (green) and biotinylation (magenta) in co-transfected HEK293 cells. Scale bar = 200 μm .

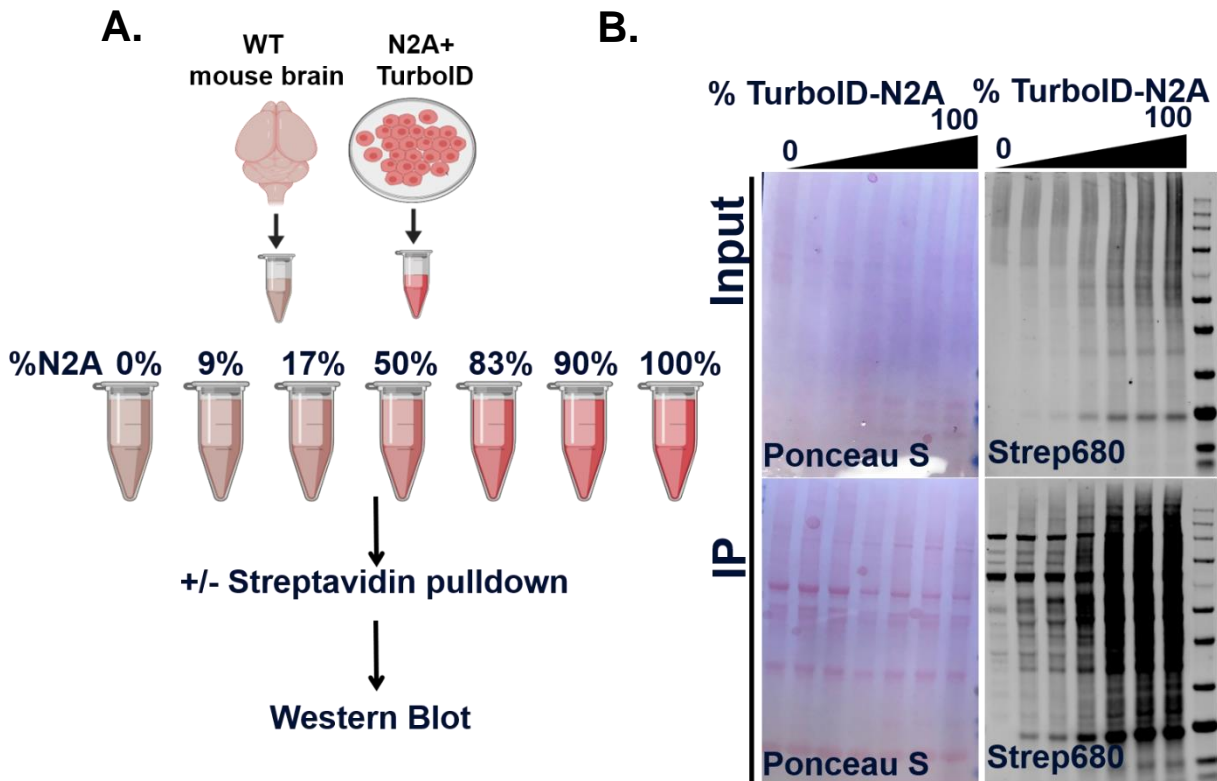


Figure 4.3 Establishing a minimal composition of biotinylated proteins in a background of brain homogenate necessary for detection by immunoblotting. **A.** Schematic of experiment. WT mouse brain homogenate was combined by protein amount percentage with protein derived from neuroblastoma cell lines expressing TurboID. Lysate-homogenate mixtures underwent streptavidin-based affinity purification. **B.** The total mixtures ('Input') were visualized in comparison with the proteins bound to the streptavidin beads ('IP'). Total protein intensity was qualitatively assessed with ponceau staining whereas biotinylation of proteins was assessed with streptavidin-680 western blots.

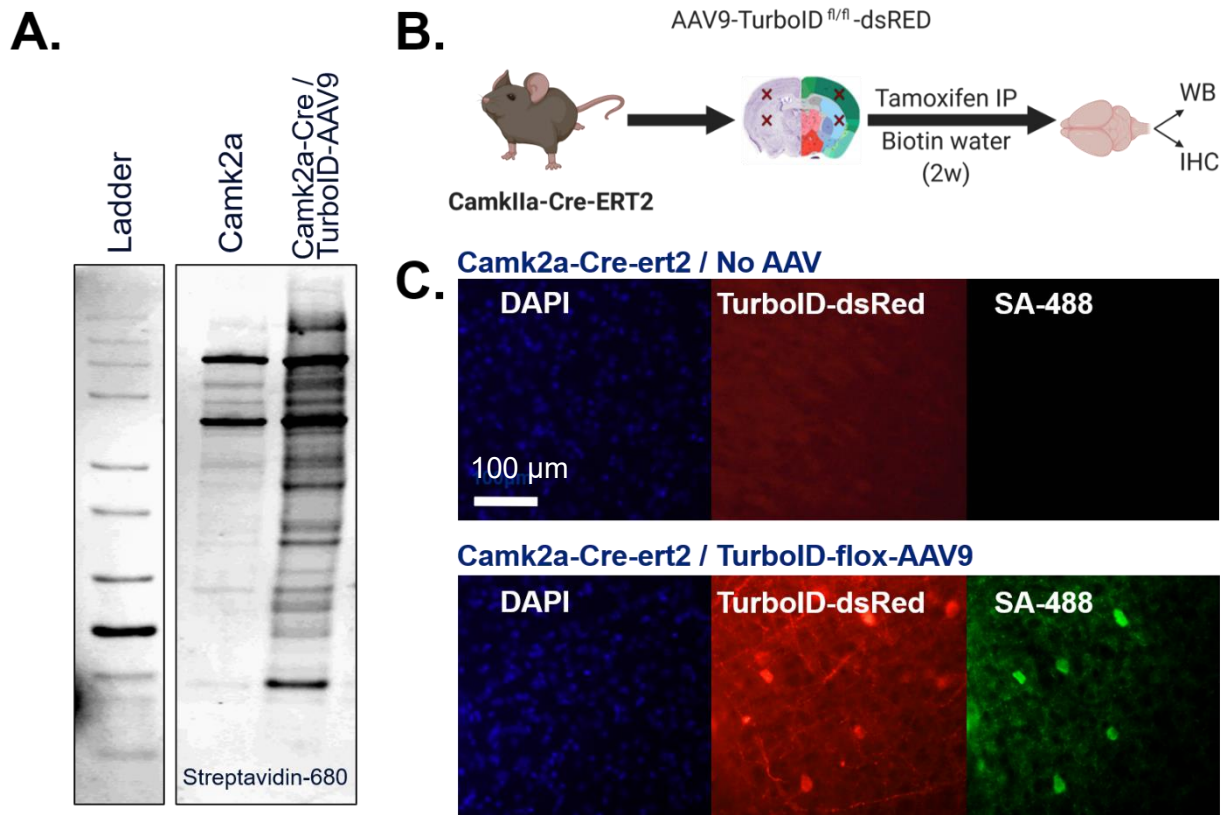


Figure 4.4 Pilot experiments establishing feasibility of TurboID-NES extension into living mice. **A.** Western blot of biotinylated proteins derived from brain homogenate of Camk2a-Cre^{ERT2} mice with and without AAV9-TurboID-dsRED. **B.** Experimental schematic of Camk2a-Cre^{ERT2} mice receiving transcranial cortical and striatum injections of AAV9-TurboID-dsRED before receiving intraperitoneal injections of tamoxifen and 2 weeks of biotin-water. Brain samples were prepared for immunohistochemistry and immunoblotting verification of TurboID-dsRED expression and biotinylated proteins. **C.** Immunohistochemistry experiments confirming functional expression of TurboID and biotinylated proteins in Camk2a-Cre mice receiving AAV9-TurboID.

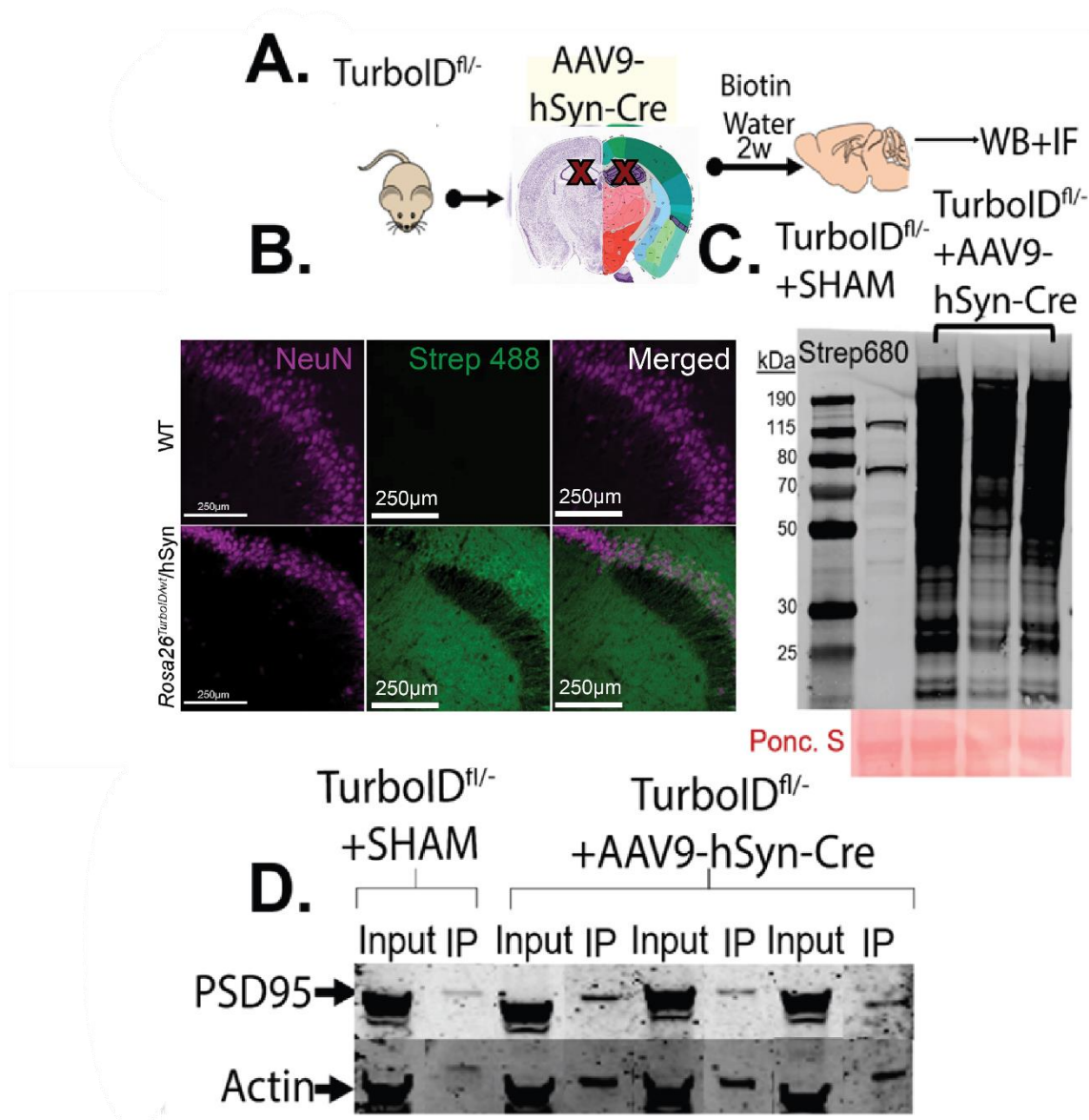


Figure 4.5 Validation of Neuronal-Cre dependent expression of TurboID in TurboID transgenic mice. **A. Schematic of experiment.** We generated transgenic TurboID mice without genetic expression of Cre recombinase. **A.** AAV9-hSyn-Cre (or sham) injected bilaterally into hippocampi of TurboID floxed mice and biotin supplementation. **B.** IF confirmation of TurboID expression and biotinylation (SA488) of neuronal proteins (NeuN). **C.** Western blot probing biotinylation in sham and TurboID brain homogenate. **D.** Brain homogenate of TurboID floxed mice before (input) and after streptavidin-IP (IP), probed for synaptic marker PSD-95 and Actin.

Chapter V. Impact of LPS on Rosa26^{TurboID}/Camk2a-Cre^{ERT2} proteomes

i. Introduction

In *Chapter 3*, we confirmed that TurboID-NES can capture main proteomic responses to lipopolysaccharide (LPS)-induced inflammation in cultured microglia including activation of an interferon-response and inflammasome associated proteins, a metabolic shift towards glycolysis, and generation and neutralization of reactive oxygen species and peroxide (See *Chapter 6* for an expanded summary of LPS proteomic changes captured by TurboID-NES in microglia). However, we wanted to understand how microglial activation by LPS challenge impacts neurons in living mice. Specifically, the hypothesis motivating the studies in this chapter posited that chronically-activated microglia may prune synapses via complement-mediated signaling; resulting in synaptic loss. As previously discussed in *Chapter 2*, chronically activated microglia can prune synapses via complement signaling, and an increase in complement proteins have been implicated at the bulk-brain proteomic level to correlate with the transition from MCI to advanced AD. Therefore, we wanted to use TurboID-NES as a discovery tool to profile neuron-specific proteomic changes correlated with chronic microglial activation in response to peripheral LPS challenge.

ii. Experimental design

Resolving the impact of LPS on excitatory neurons in vivo.

One exciting application of TurboID-NES includes resolving the impacts of inflammation on excitatory neuronal proteomes. We aim to use TurboID-NES as a discovery tool to understand the proteomic transformations which take place at the level of the neuronal and synaptic proteome in response to chronic inflammatory challenge. To this end, we generated $Rosa26^{TurboID/wt}/Camk2a-Cre^{ERT2}$ mice (N = 7; 2F, 5M) and 4 control mice (N = 2 negative for $Camk2a-Cre^{ERT2}$; 2M & N = 2 negative for TurboID-NES; 1F,1M). All mice were aged from 3.5 months – 6.7 months. All mice received tamoxifen (75 mg/kg) intraperitoneally for 4 days proceeded by 3.5 weeks to allow recombination prior to 11 days of biotin-water treatment (37.5 mg/L). 4 days prior to sacrifice, 10 µg of lipopolysaccharide ($Rosa26^{TurboID/wt}/Camk2a-Cre^{ERT2}$ +LPS; N = 3; WT+LPS; N=2) or phosphate buffer saline sham ($Rosa26^{TurboID/wt}/Camk2a-Cre^{ERT2}$ +SHAM; N=4; WT+SHAM; N = 2) were injected daily intraperitoneally. Following sacrifice, brain samples were cut in half along hemispheres. One half-hemisphere was preserved for sagittal sectioning and immunofluorescence according to previously published methodology³²⁹, and the cortex and striatum of the remaining hemisphere were preserved for immunoblotting and mass spectrometry studies (**Figure 5.1**). Iba-1 visualization confirmed morphological changes consistent with activation of microglia in brain regions derived from mice treated with LPS (**Figure 5.2**) (*antibodies listed in Table 5.1*). Neuronal biotinylation exclusive to $Rosa26^{TurboID/wt}$ mice was confirmed via immunofluorescence in previous

publications³³¹. Total brain homogenates were prepared in 8M urea and 1 mg of protein was affinity purified onto streptavidin beads and washed according to published protocols³²⁹. 20 µg of protein contents derived from total brain homogenate samples of cortical and striatal brain sections were visualized with Coomassie staining according to previous protocols³³⁰. In parallel immunoblotting of 20 µg of total cortical and striatal brain homogenate visualized biotinylated proteins with streptavidin-conjugated Alexa Fluor 680 (Streptavidin-680), and PSD-95 to visualize any impact of LPS on post-synaptic proteins, and alpha tubulin was used as a loading control (**Figure 5.3**). We did not observe qualitative differences in PSD-95 intensity via western blotting with LPS. Enrichment of biotinylated proteins was confirmed via silver stain and Streptavidin-680 (**Figure 5.3**). We prepared total brain (TB) homogenates and affinity-purified (AP) fractions which enrich for neuronal proteins biotin-labeled by TurboID, for label free quantitative mass spectrometry according to previously published methods^{329,330}. All samples were categorically annotated in Perseus, categorical variables were removed and 50% missingness filters were applied, and proteomes were log-2 transformed and imputed based on normalized distribution. Label free quantitative mass spectrometry identified 3,288 proteins in the TB proteomes. After implementing a 50% missingness filter, 2,959 proteins remained in the total brain dataset. Principal component analyses of the total brain proteome reveal that difference in brain region (i.e., cortex versus striatum proteome) drives 28.5% of the variance in this dataset (**Figure 5.4 A**). Interestingly, genotype differences drive 9.1% of the variance in the total brain homogenate

proteomes, with genotype driving most variance in the striatum proteomes (**Figure 5.4 A**). identified 2,469 proteins in the proteomes which underwent streptavidin-based affinity purification (AP). A 50% missingness filter based on genotype was implemented to preserve enrichment of proteins biotin-labeled by TurboID, according to previously published methods; 2,358 proteins remained in the AP dataset³³⁰. Imputed intensity values derived from AP datasets were grouped by genotype and normalized to sum intensity. Dimension reduction with principal component analyses demonstrate that principal component 1 separates samples based on genotype; driving the majority of the variance in AP proteomes (43.7%) (**Figure 5.4B**). Brain region distinguishes samples along principal component 2, accounting for 15.2% of the variance across AP proteomes (**Figure 5.4B**). Differential expression analysis of AP datasets by genotype identified 1,611 neuronal-enriched proteins, of which ~30% were identified using SynGO to be synapse-associated (**Figure 5.5**). After implementing a Log₂ fold-change filter of >1.5, we performed over-representation analysis on 476 of the 1,611 neuronal proteins using the total AP dataset (2,358 proteins) as the background set. The gene ontology confirmed an enrichment of glutamatergic and synaptic proteins in the affinity purified datasets (**Figure 5.6**). We used differential expression analysis to identify LPS-driven protein changes in Striatum TB proteomes, Striatum AP proteomes, Cortical TB proteomes, and Cortical AP proteomes. In the TB striatum and cortex proteomes, we identified 86 LPS differentially-expressed proteins (DEPs) in the striatum and 133 LPS-DEPs in the cortex. Importantly, complement proteins (C1qa, C1qc) were

significantly increased in the total brain proteomes and amyloid precursor protein was also significantly increased in the Striatum TB proteome with LPS. Over representation analyses revealed that LPS increased proteins associated with regulation of myeloid cell differentiation and virus host interaction in the TB striatum while decreasing axonogenesis and programmed cell death (**Figure 5.7A, 5.7B**). In the TB cortex, LPS increased proteins involved with regulation of T-cell activation, immune responses, and post synaptic density while decreasing caspase activation and apoptosis (**Figure 5.8A, 5.8B**). Of the neuronally enriched proteins in the AP dataset, we identified 78 LPS-DEPs in the Striatum AP and 86 LPS-DEPs in the neuronal enriched cortical AP proteomes. Over representation analysis revealed that striatal neuronal proteomes feature an increase in homeostatic regulation, cellular response to chemical stimulus, apoptosis, and synaptic components with LPS treatment and a decrease in DNA-dependent transcription and metabolic processes (**Figure 5.7C, 5.7D**). In the neuronal-enriched cortical proteome, LPS increased post-synaptic density proteins and decreased proteins involved with phospholipid biosynthesis (**Figure 5.8C, 5.8D**). Despite the relatively modest number of differentially expressed proteins with LPS, the over-representation analyses suggest a dual anti-inflammatory and pro-inflammatory impact on the total brain and neuronal-enriched proteomes. We were surprised to see an increase in synaptic proteins with LPS, in combination with terms associated with regulation of immune responses. In the cortical TB and AP proteomes, we selected complement C1Q chain (C1QC) and Glutamate receptor 1 (GRIA1), respectively as proteins significantly

increased following in correlation with LPS. We correlated the intensity values of GRIA1 from cortical AP proteomes of *Rosa26^{TurboID/wt}/Camk2a-Cre* mice with the LFQ intensity values of C1QC in cortical TB proteomes of *Rosa26^{TurboID/wt}/Camk2a-Cre* mice (Coefficient of determination, $R^2=0.85$) (**Figure 5.9**). Therefore, there is a strong correlation between C1QC in total cortical brain homogenate with GRIA1 derived from the cortical glutamatergic neuronal proteome. Though these findings are currently being developed and are preliminary at the time of this thesis publication, they suggest that low-levels of LPS given peripherally to mice are sufficient to activate microglia, as confirmed by morphological transformations using immunofluorescence, may induce early-stage mechanisms of synaptic preservation, or perhaps reflective of hyper-excitability which could potentially lead to excitotoxicity with progressive inflammatory stimulus (see section 4 ; Preliminary conclusions).

iii. Methodology

Immunofluorescence & Immunoblotting

Table 5.1. Antibodies

Antibody	Manufacturer	Catalogue #	Dilution
Rat anti α -tubulin	Millipore Sigma	MAB1864	1:1000
Goat anti Rat 800	LI-COR	926-32219	1:10,000
Rabbit anti PSD-95	Cell Signaling	25075	1:1000

Streptavidin, Alexa-Fluor 680 Conjugate	Invitrogen	S32358	1:10,000
DAPI	Roche	10236276001	1 µg/mL
Rabbit anti Iba-1	Abcam	ab178846	1:2,000
Donkey anti Rabbit 647	Thermofisher	A32795	1:1,000
Donkey anti Rabbit 800	Invitrogen	A11374	1:10,000

Brain hemispheres were fixed overnight at 4 °C in 4% paraformaldehyde and transferred to 30% sucrose prior to being cut into 40 µm thick sagittal sections with a cryostat. Free-floating sections were washed thrice for 10 minutes in 1x Tris buffer Saline (TBS). Brain sections were permeabilized by incubation with 0.3% Triton in PBS for 10 minutes. Brain sections were blocked in 5% normal horse serum in TBS with 0.3% Triton (TBST) for 1 hour at room temperature. Primary antibodies were incubated overnight at 4 °C. Brain sections were then washed thrice in 0.3% TBST for 10 minutes. Secondary antibodies incubated overnight at 4 °C. Brain sections were washed thrice in 0.3% TBST for 10 minutes prior to receiving DAPI for 2 minutes in PBS. Brain samples were finally washed twice with PBS and mounted using ProLong Diamond antifade medium (Invitrogen, #P36970).

In each well, 10-20 µg of protein from total brain homogenate in 8M urea resolved in a 4-12% polyacrylamide gel and transferred onto iBlot 2 Transfer Stack containing nitrocellulose membrane using the BOLT transfer system. The membranes incubated for 1 hour at room

temperature in StartingBlockT20 before receiving primary antibody (PSD-95 or alpha tubulin) overnight at 4 °C. After primary antibody incubation, the membranes underwent three rapid washes with 1x TBST followed by three 10-minute washes with 1xTBST. Membranes then underwent three rapid washes with 1x TBS and three 10-minute washes with 1xTBS. The membranes incubated for 1 hour at room temperature in a secondary antibody cocktail of streptavidin 680 to visualize biotinylated proteins and donkey anti rabbit 800 to visualize PSD-95 or rat anti Tubulin to visualize alpha tubulin as a loading control. The membranes were then washed again as previously described before undergoing imaging via the Odyssey infrared Imaging System (LI-COR Biosciences). Coomassie staining was performed according to previous publications, and silver staining was performed to manufacturer specifications (Pierce, Thermo fisher #24612).

Peptide Digestion & Cleanup for Liquid Chromatography and Mass Spectrometry

Sample preparation for MS was performed according to our laboratory protocols modified from previous publications^{146,220,240,245,407-410}. Briefly, 50 µg of protein from each total brain homogenate sample was digested. Samples were reduced with 5 mM dithiothreitol (DTT) at room temperature for 30 minutes on a rotor, followed by alkylation with 10 mM iodoacetamide (IAA) at room temperature for 30 minutes on a rotor in dark. Samples were diluted with 50 mM of ammonium bicarbonate (ABC) to 4 M urea prior to undergoing overnight digestion with 2 µg of

lysyl endopeptidase (Lys-C) (Wako #127-06621) at room temperature. Samples were then diluted to reduce the concentration of Urea to 1 M prior to trypsin digestion. Each sample received 2 μ g of trypsin (Thermo, #90058) and were incubated overnight at room temperature. Acidifying buffer was added to the peptide solution for a final concentration of 1% formic acid (FA) and 0.1% trifluoroacetic acid (TFA) to stop the trypsin digestion. HLB columns were used to desalt samples (Waters #186003908). The samples were dried overnight using a centrifugal vacuum concentrator (SpeedVac Vacuum Concentrator). AP samples underwent on-bead digestion. Beads were resuspended in 150 μ L ABC. Application of DTT to a final concentration of 1 mM reduced the samples during a 30-minute room-temperature incubation on a rotator. A 5 mM application of IAA alkylated the samples during a 30-minute incubation in the dark on a rotator. To each sample, 0.5 μ g of LysC was added before incubating overnight at room temperature on a rotator. The digestion was completed overnight at room temperature on a rotator with the addition of 1 μ g of trypsin to the samples. After overnight digestion, the samples were treated with acidifying buffer to stop the trypsin-mediated digestion. HLB columns were used to desalt samples. The samples were dried using the SpeedVac.

Filtering missingness, data normalization and log transformation.

Label-free quantification intensities and raw intensity values were uploaded onto Perseus (Ver 1.6.15) for analyses. Categorical variables were removed, intensity values were log-2 transformed, transduced AP intensity values were normalized to sum intensity between genotypes, and data

were in general filtered based on 50% missingness across group of samples that were selected for each analysis. Missing values were imputed from normal distribution. Dimension reduction and differential expression analyses were performed in Perseus (Ver 1.6.15) according to previous publications³³⁰.

iv. Preliminary conclusions

This study represents the first proteomic interrogation of the impact of LPS on neuronal proteomes in *Rosa26^{TurboID/wt}/Camk2a-Cre* mice. We used immunofluorescence to visualize robust morphological changes of microglia in response to LPS, and we validated robust biotinylation of proteins in total brain homogenates and affinity-purified preparations derived from *Rosa26^{TurboID/wt}/Camk2a* mice. We identified 2,959 proteins in the total brain (TB) homogenate proteomes of cortical and striatal samples and 2,358 proteins in the affinity-purified (AP) proteomes of cortical and striatal samples. Interestingly, principal component analyses (PCA) indicate that genotype drives significant variance in striatum total brain proteomes (PC1), and this confound must be investigated further. PCA of the affinity purified proteomes demonstrate that genotype groupwise differences separate samples on PC1, as is expected given that TurboID biotinylates proteins which are captured by streptavidin-based affinity purification. PC2 of the AP PCA separates samples based on regional difference, but given the unresolved impact of TurboID on the TB striatum proteomes, it is difficult to conclusively compare regional proteomic differences at the AP level. Overall, the affinity purification of 1,611 proteins are highly enriched

in neuronal and glutamatergic synaptic terms, confirming successful enrichment of excitatory neuronal proteomes by TurboID biotinylation and affinity capture. We observed modest proteomic impacts of LPS on the number of proteins significantly altered by LPS in the TB and AP proteomes, though complement proteins (C1QC & C1QA) and amyloid precursor protein (APP) are significantly increased in both the cortical and striatal TB proteomes and the striatal TB proteome, respectively. Other studies also show an increase in complement proteins and amyloid precursor protein in response to LPS treatment, the former providing evidence confirming LPS activation of microglia, concurring with histological verification^{126,421}. Fascinatingly, our preliminary over-representation analyses show an increase in terms associated with immune system regulation in response to LPS, as well as an increase in post-synaptic density which is captured at the AP level. At this time, it is unclear if the dose and duration of LPS used in this study (10 µg, 4 days, intraperitoneal injection) may correlate with mechanisms of immune suppression and regulation coinciding with neuronal mechanisms of synaptic resilience. Further studies beyond the scope of this doctorate and thesis will be instrumental in understanding the biological context of these initial findings.

Study limitations and future directions

An important limitation to consider includes the methodology underlying regional dissection of brain samples. Specifically, the striatum isolation includes other regions of the mouse brain,

including the thalamus and hypothalamus. It is currently unclear if the inclusion of thalamic brain regions into the striatum may contribute to genotype-driven variance at the level of the total-brain homogenate. Future studies beyond the scope of this thesis will be needed to confirm if genotype drives proteomic variance in purely isolated striatum specimens, and if this result may be reproducible across mice, experiments, and technical sample preparations. Another important limitation to keep in mind includes the limited number of WT mice receiving sham PBS injections (N=2), and the limited number of WT mice receiving LPS injections (N=2). These controls are necessary to isolate inflammatory changes resulting from intraperitoneal injection itself, as well as comparing the impact of LPS on proteomes in the presence and absence of TurboID. Our preliminary interpretations of these findings suggest that peripheral administration of 10 µg of LPS for 4 days activate microglia and may correlate with early mechanisms of synaptic resilience. At this time, it is unclear if the increases in go-terms associated with post-synaptic density for example, are reflective of synaptogenesis or an elevated expression of post-synaptic density proteins in existing synapses. Immunohistochemistry-based assays using compartment-specific antibodies (i.e. pre-synaptic and post-synaptic markers) may be considered to quantify changes in synapse number correlating with LPS administration used in this study⁴²². Furthermore, pairing quantitative immunohistochemistry experiments with *ex vivo* electrophysiology studies could determine if there are changes in action potential firing frequency or intrinsic excitability. It may be possible that an increase in glutamatergic post-synaptic proteins may correlate with an

increase in resting excitability, potentially reflective of a transition towards hyper-excitability. Future electrophysiology studies could test if the LPS administration used in this protocol correlates with an increase in resting excitability in glutamatergic neurons. If glutamatergic neurons become hyper-excitabile in response to early inflammatory changes (4 days), it could be possible that prolonged LPS administration may induce excitotoxicity. At the time of this thesis, these leading questions remain to be resolved experimentally. Together, quantitative immunohistochemistry studies and electrophysiology studies could provide meaningful biological validation to our preliminary findings of an increase in post-synaptic density proteins with LPS, and may reflect a transition of glutamatergic neurons towards hyper-excitability or even excitotoxicity in the long-term.

v. Chapter V Figures.

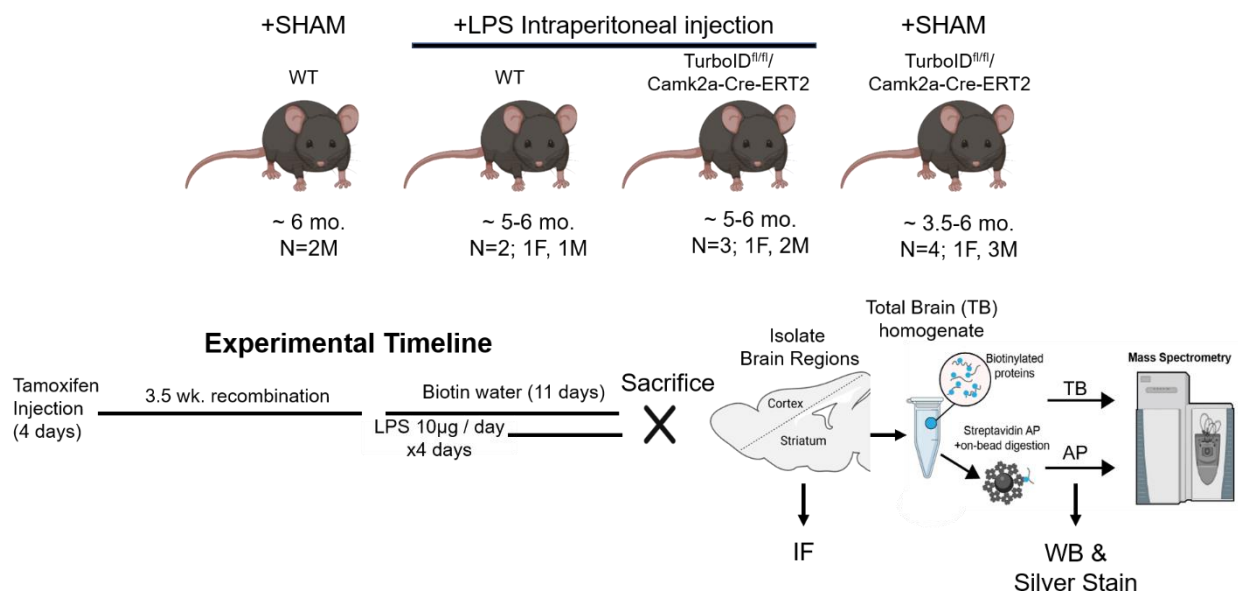


Figure 5.1 Experimental Schematic of *Rosa26*^{TurboID/wt}/*Camk2a-Cre* mice receiving inflammatory challenge. We prepared *Rosa26*^{TurboID/wt}/*Camk2a-Cre* ($n = 7$) mice and WT controls ($n = 4$) receiving either intraperitoneal injections of lipopolysaccharide or phosphate buffer saline sham. Intraperitoneal injections of tamoxifen were given for 4 days, and 3.5-week intermission provided time sufficient for Cre recombination. Biotin water was supplied 11 days prior to sacrifice and LPS was injected once a day for 4 days (10 µg /kg) prior to sacrifice. Hemispheres were separated; one hemisphere was prepared for immunofluorescence (IF) studies and the cortex and striatum of the other hemisphere was homogenized in 8M urea for downstream streptavidin affinity purification of proteins biotinylated by TurboID and mass spectrometry.

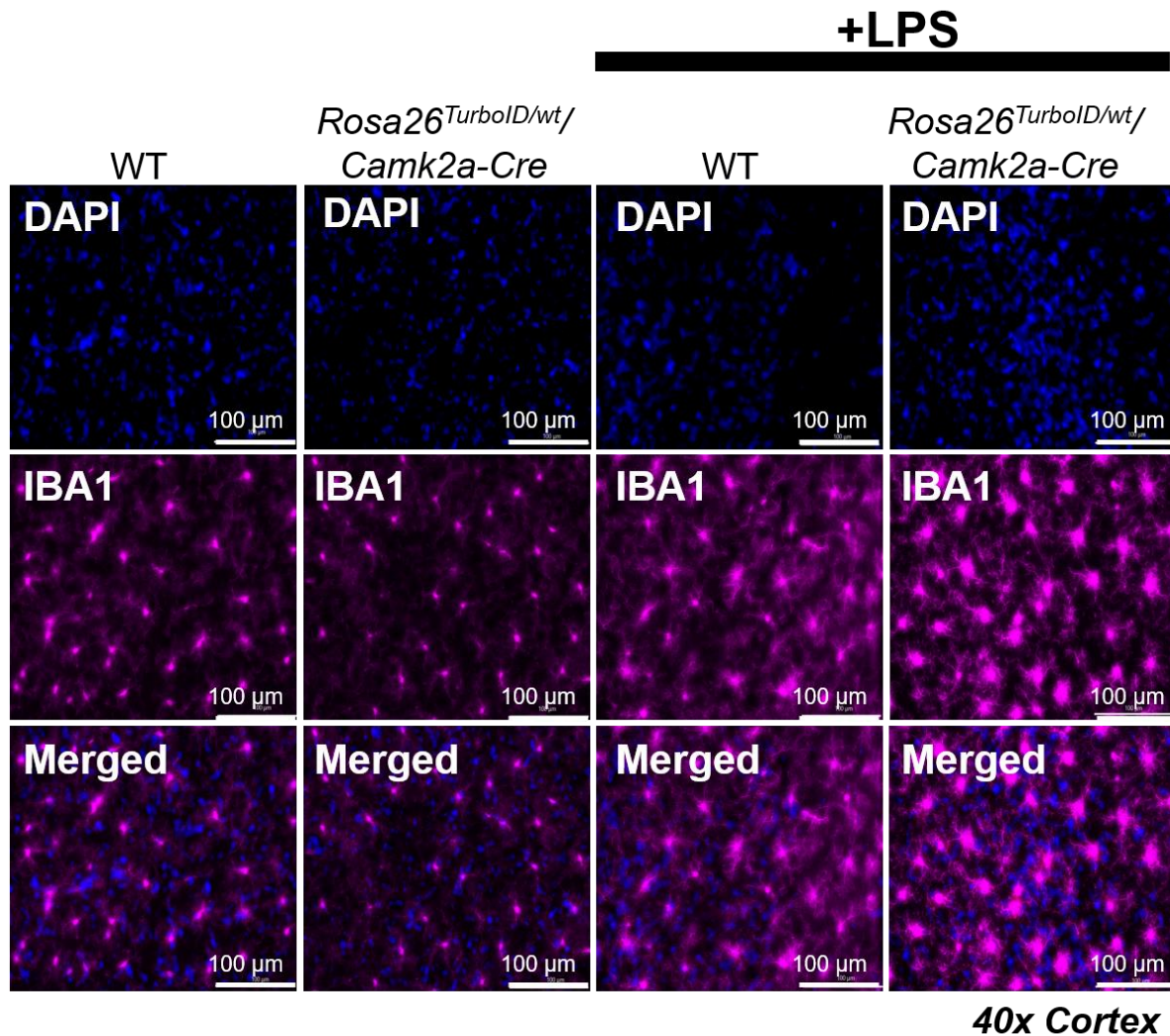


Figure 5.2 Immunofluorescence visualization of microglial morphological change with LPS. Representative image of cortical microglia morphological changes in mice receiving LPS intraperitoneal injections compared with phosphate buffer saline controls. Iba-1 staining visualized microglia, and in the presence of peripheral inflammatory challenge with LPS, microglia obtain amoeboid morphologies and increase in number. This morphological transformation is apparent in both *Rosa26^{TurboID/wt}/Camk2a-Cre* mouse brain as well as WT mouse brain. Staining performed by undergraduate mentee, Sneha Malepati.

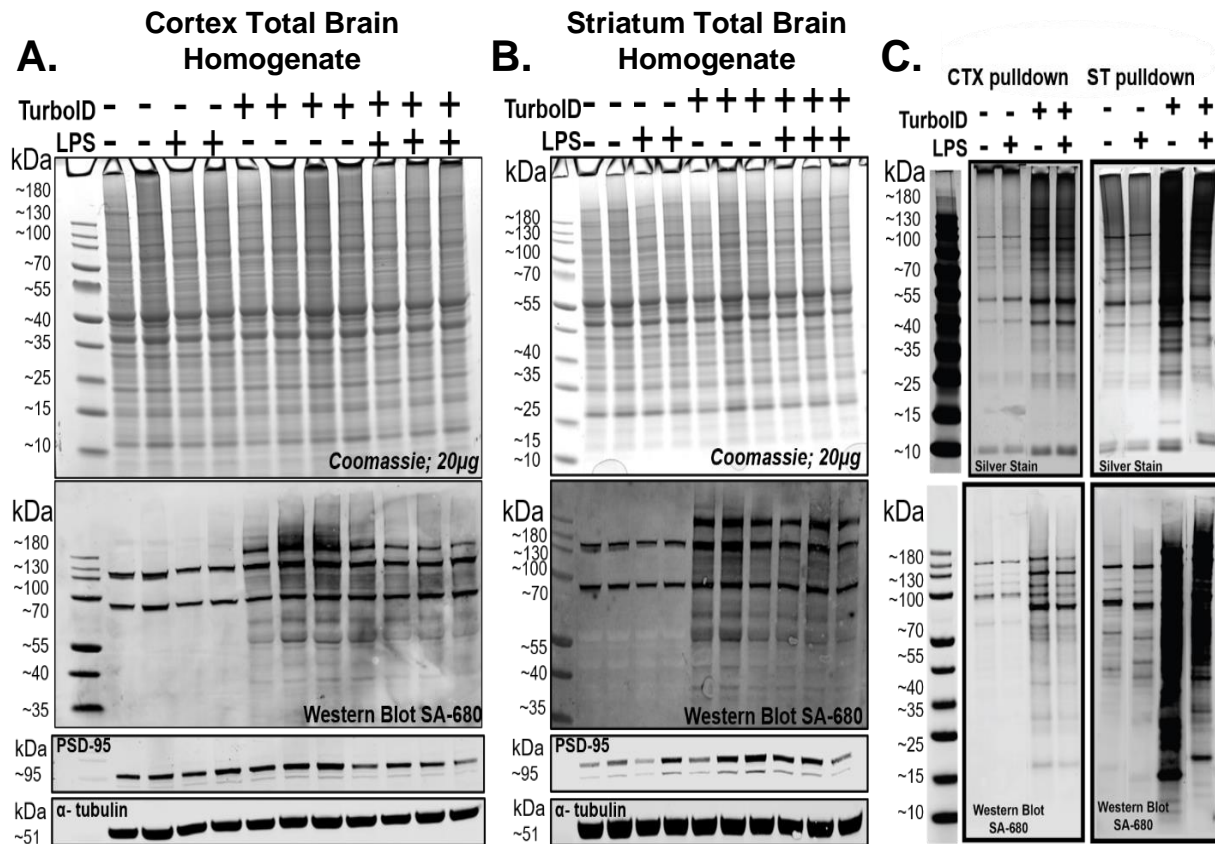


Figure 5.3 Quality control of total brain homogenates and affinity purified preparations prior to MS. **A.** Cortex total brain homogenate from *Rosa26^{TurboID/wt}/Camk2a-Cre* mice or WT controls receiving LPS or sham intraperitoneal injections underwent protein immobilization via SDS-page and the corresponding gel underwent Coomassie staining to visualize the total protein content per sample. In parallel, immunoblotting studies confirmed the presence of biotinylated proteins only in mice expressing TurboID. Cortical brain homogenate was probed for PSD-95 to visualize changes in postsynaptic density protein in response to LPS and alpha tubulin was used as a loading control. **B.** Striatum total brain homogenate from *Rosa26^{TurboID/wt}/Camk2a-Cre* mice or WT controls receiving LPS or sham intraperitoneal injections underwent protein immobilization via SDS-page and the corresponding gel underwent Coomassie staining to visualize the total protein content per sample. In parallel, immunoblotting studies confirmed the presence of biotinylated proteins only in mice expressing TurboID. Striatum brain homogenate was probed for PSD-95 to visualize changes in postsynaptic density protein in response to LPS and alpha tubulin was used as a loading control. Qualitatively, we did not observe apparent groupwise changes in post synaptic density in either cortical or striatum total brain homogenates. **C.** Representative affinity purified proteins derived from cortical and striatum samples. Silver stain confirmed minimal non-

specific binding to streptavidin beads and immunoblotting for biotinylated proteins with streptavidin 680 verified the robust enrichment of biotinylated proteins.

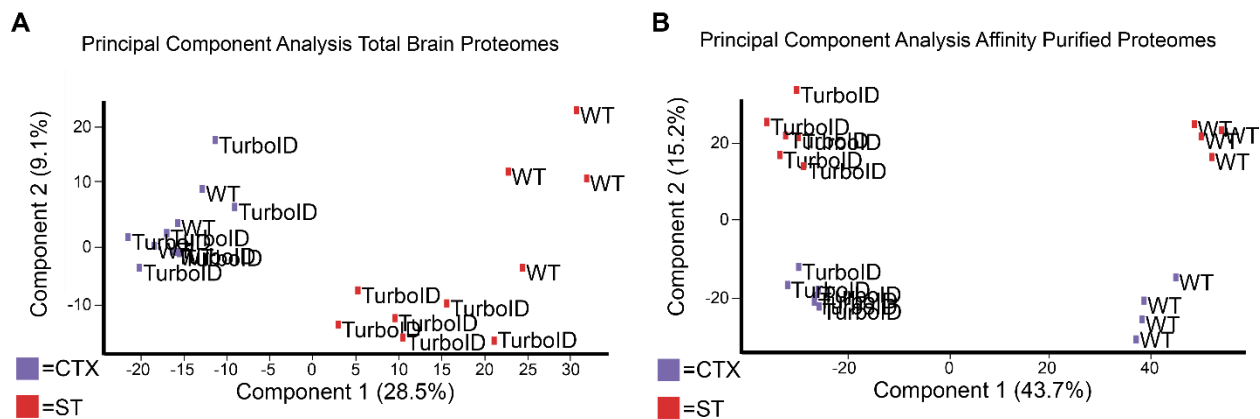


Figure 5.4. Principal Component Analysis of Total Brain and Affinity Purified Proteomes. A. Dimension reduction of total brain proteomes demonstrates that principal component 1 drives 28.5% of the variance across samples whereas principal component 2 accounts for 9.1% of the variance in total brain proteomes. Samples cluster across region on the PC1 axis whereas samples cluster along genotype only in the striatum samples along PC2. **B.** Dimension reduction of affinity purified proteomes demonstrates that principal component 1 accounts for 43.7% of the variance in the proteomic data wherein affinity-purified samples cluster apart based on TurboID expression- or genotype. Principal component 2 accounts for 15.2% of the variance in affinity purified datasets and samples cluster apart by regional variation.

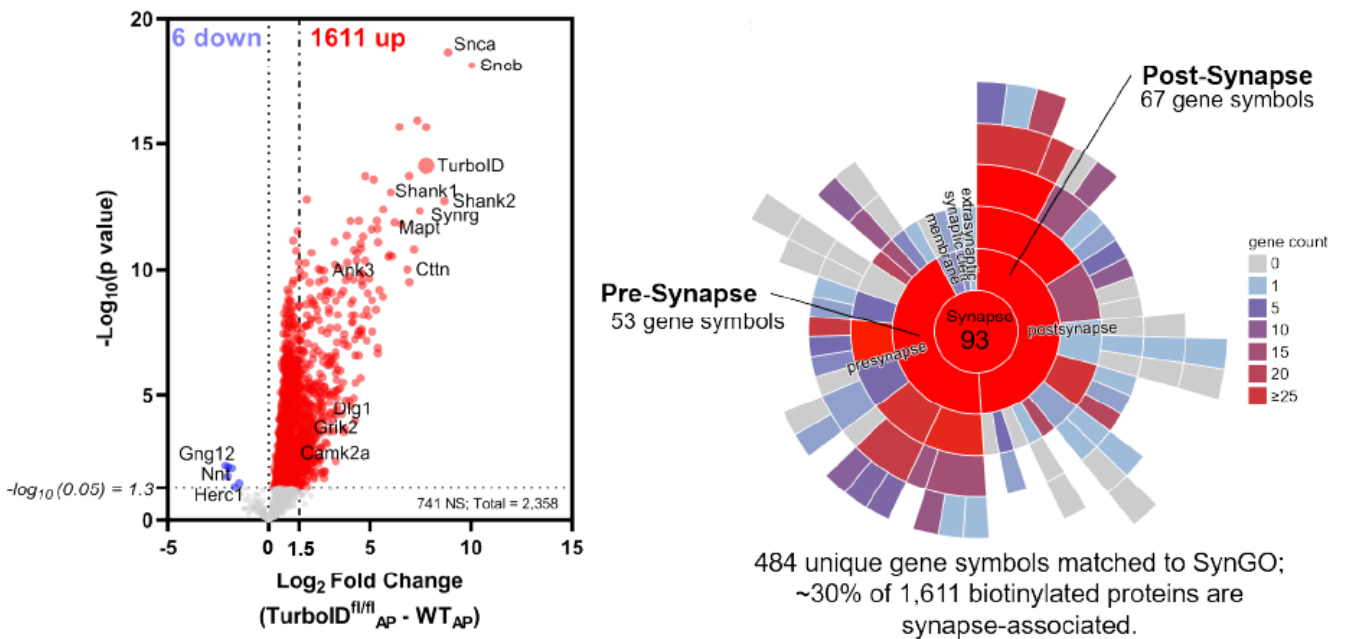


Figure 5.5 Differential expression analysis and over representation analysis with SynGO confirm robust enrichment of biotin-labeled synaptic proteins in the affinity purified dataset.

A. Differential expression analysis comparing affinity-purified proteomes of *Rosa26*^{TurboID/wt}/*Camk2a*-Cre and WT mice identify an enrichment of 1,611 proteins biotin-labeled by TurboID-NES. **B.** Sunburst plot representation of synaptic proteins biotin-labeled by TurboID-NES. Synaptic gene ontology (SynGO) over representation analysis ascribed to 484 unique gene symbols out of 1,611 proteins biotin-labeled by TurboID-NES; approximately 30% the proteins in the biotin enriched dataset were synaptic. TurboID-NES biotin-labeled a diversity of pre- and post-synaptic proteins.

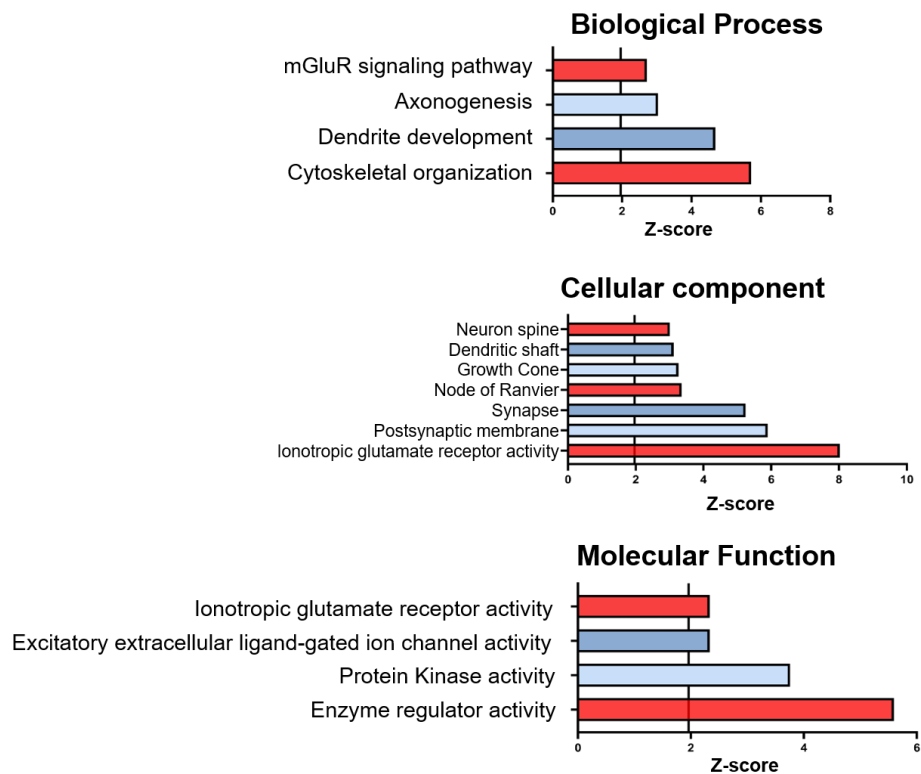


Figure 5.6 Over representation analysis confirms enrichment of glutamatergic synaptic proteins in TurboID-NES biotinylated proteomes. Over representation analysis of biotin-enriched proteins ($\text{Log}_2 \text{FC cutoff} \geq 1.5$; 476 proteins) compared with the background of 2,358 proteins identified in the affinity purified datasets. Gene ontology analysis confirms biotin-labeling by TurboID-NES and affinity-purification of glutamatergic synaptic proteins characteristic of excitatory neuronal proteomes.

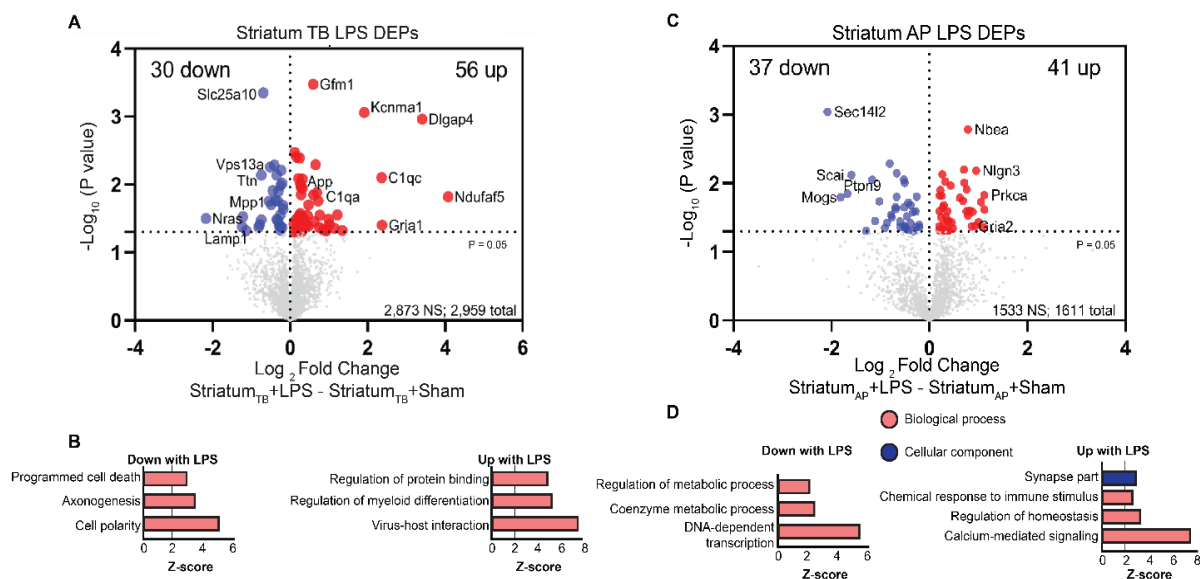


Figure 5.7 LPS impact on Striatum total brain and neuron enriched proteomes affinity purified. **A.** Differential expression analysis comparing LPS-treated striatum total brain proteomes with sham-injected striatum total brain proteomes. Differential expression analysis identified 56 proteins significantly increased with LPS treatment, including complement (C1QA, C1QC) and amyloid precursor protein (APP). There were 30 proteins significantly decreased in abundance with LPS. **B.** Over representation analysis of differentially abundant proteins (56 up with LPS and 30 down with LPS). LPS treatment correlates with biological process annotations associated with an increase in proteins associated with virus-host interactions as well as regulation of myeloid differentiation. LPS treatment correlates with a decrease in axonogenesis and cell polarity as well as a decrease in programmed cell death in the striatum total brain proteome. **C.** Differential expression analysis comparing LPS-treated striatum affinity purified (neuronal enriched) proteomes with sham-injected striatum neuronal-enriched proteomes. Differential expression analysis identified 41 proteins significantly increased with LPS treatment. There were 37 proteins significantly decreased in abundance with LPS. **D.** Over representation analysis of differentially abundant proteins (41 up with LPS and 37 down with LPS), using the 1,611 neuronal-enriched proteins as the background proteome. TurboID-NES captures an LPS-correlated increase in calcium signaling, immune response and synaptic components. TurboID-NES captures an LPS-correlated decrease in transcription and metabolic regulation in striatal neurons.

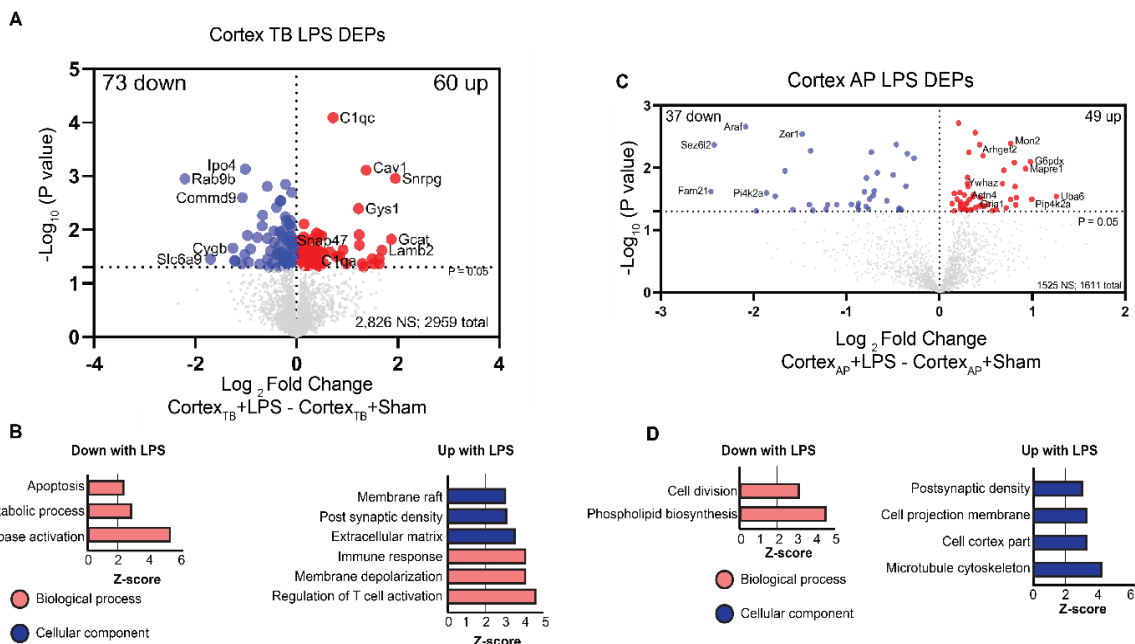


Figure 5.8 LPS impact on Cortex total brain proteome and neuron enriched affinity purified proteomes **A.** Differential expression analysis comparing LPS-treated cortical total brain proteomes with sham-injected cortical total brain proteomes. Differential expression analysis identified 60 proteins significantly increased with LPS treatment, including complement (C1QA, C1QC). There were 73 proteins significantly decreased in abundance with LPS. **B.** Overrepresentation analysis of differentially abundant proteins (60 up with LPS and 73 down with LPS). LPS treatment correlates with an increase in proteins associated with regulation T cell activation and in increase in post-synaptic density, and an increase in immune response. LPS treatment correlates with a decrease in axonogenesis and cell polarity as well as a decrease in programmed cell death in the striatum total brain proteome. **C.** Differential expression analysis comparing LPS-treated cortical neuronal enriched with sham-injected cortical neuronal enriched proteomes. Differential expression analysis identified 49 proteins significantly increased with LPS treatment. There were 37 proteins significantly decreased in abundance with LPS. **D.** Overrepresentation analysis of differentially abundant proteins correlating with LPS treatment. LPS treatment correlates with an increase in proteins associated with post-synaptic density and cell projection. LPS treatment correlates with a decrease in phospholipid synthesis and cell division in the cortical neuronal enriched proteome.

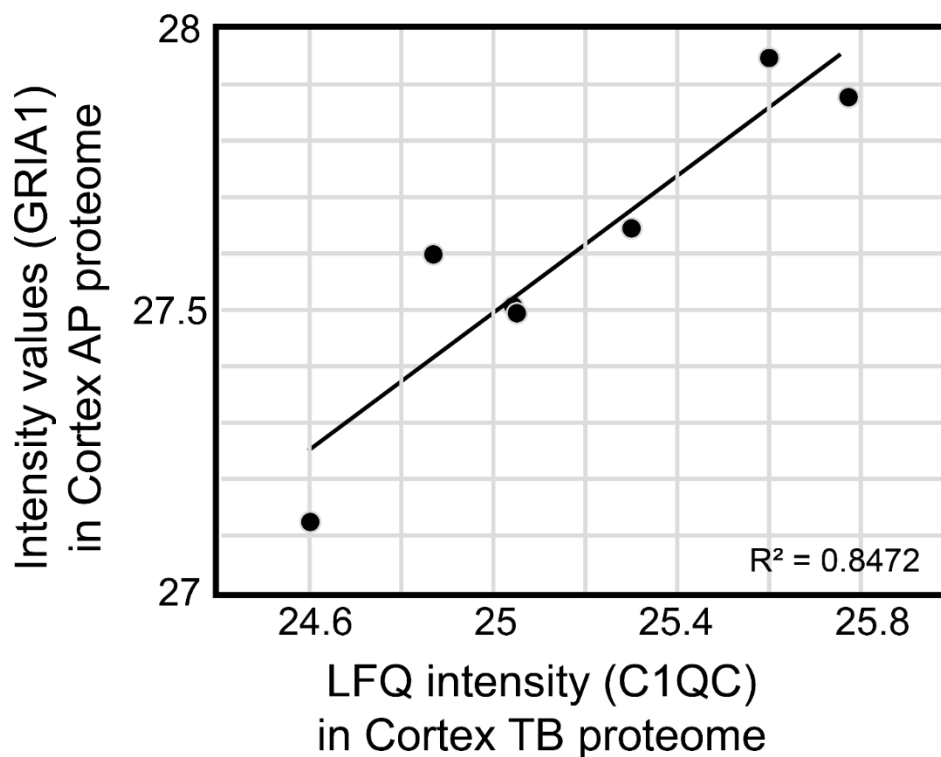


Figure 5.9. Positive correlation between complement protein and postsynaptic glutamate receptor in cortical total brain and affinity purified proteomes, respectively. Glutamate Receptor 1A (GRIA1) intensity values of *Rosa26^{TurboID/wt}/Camk2a-Cre* cortical AP proteomes strongly correlate with LFQ intensity of Complement C1 qC chain (C1QC) in *Rosa26^{TurboID/wt}/Camk2a-Cre* cortical total brain proteome (Coefficient of determination, $R^2=0.85$).

Chapter VI. Discussion

i. Integrated summary of findings & field implications

The cellular complexity inherent to the central nervous system poses challenges to systems-level analyses of neurodegeneration and neuroinflammation. Sub-populations of neurons are differentially vulnerable to specific pathological hallmarks of neurodegenerative disease and microglial phenotypic heterogeneity in disease states have made it historically difficult to interpret the relative impacts of the dual neuroprotective and neurotoxic roles of microglial disease associated phenotypes to disease progression. Cell-type specific protein-level interrogations are necessary to complement genomic and transcriptomic analyses because of the relatively poor concordance between RNA and protein²⁴³, the clinical precedence of proteins as drug targets and biomarkers of disease⁴²³⁻⁴²⁵, the orders of magnitude greater complexity of the unique protein products translated from the transcriptome⁴²⁶, and finally the relevance of post-translational modifications to neurodegenerative disease⁴²⁷⁻⁴²⁹. To this end, we developed and validated a novel approach to biotinylating cytosolic proteins with the biotin ligase TurboID, for the long-term application of purifying cellular proteomes from mouse brain homogenate (CIBOP). Specifically, if TurboID-NES can be expressed under a microglia-specific-promoter in a living mouse, then microglial proteins may be labeled *in vivo* without isolation-based artefacts, contamination from other cell-types, or reliance on well-validated surface-markers with dynamic

expression in disease states. Instead, broadly labeling cytosolic microglial proteomes with TurboID-NES for down-stream affinity purification and mass spectrometry would allow the field of neuroscience to resolve proteomic phenotypes from diverse microglia disease-associated states in murine models of neurodegeneration or in inflammatory contexts. If we can use proteomics to resolve the diverse phenotypic transformations of microglia which contribute to synaptic loss, or contribute to synaptic resilience, we could definitively isolate microglial contributions to cognitive decline or cognitive resilience, and potentially nominate therapeutic targets capable of shifting microglia towards neuroprotective states, or attenuate neurotoxic inflammatory states. Likewise, adult neurons do not survive cellular-isolation via FACS or MACS, making it exceptionally difficult to isolate neuron-specific proteomes from brain. Extending TurboID-NES into adult neurons for in vivo biotin-labeling could resolve the specific protein-level transformations neurons undertake upstream of synaptic loss in disease contexts. Furthermore, TurboID-NES could also be applied to specific sub-populations of inhibitory or excitatory neurons to distinguish proteomic phenotypes underlying differential vulnerability in neurodegenerative conditions. In the context of a peripheral inflammatory challenge, CIBOP could resolve bulk-proteomic inflammatory changes from neuron-specific inflammatory changes to understand the impact of inflammation on neurons and their synapses. Finally, by pharmacologically ablating microglia in mice using a colony-stimulating-factor-1 receptor antagonist (CSF1-R) in the context of inflammatory challenge and in homeostatic resting

conditions, neuronal CIBOP could resolve cell autonomous from non-cell autonomous proteome-level phenotypic changes with disease relevance. Given the abounding exciting possible applications of CIBOP to resolve cell-specific proteomic signatures and mechanisms of disease, it is critically important that we first test the basic parameters of this approach in well-controlled cell culture studies.

Establishing the proteomic breadth captured by TurboID-NES

Prior to applying TurboID-NES to in vivo contexts, we performed a series of rigorous in vitro studies to test, define, and publish the strengths and limitations with this approach. Our immunoblotting and immunofluorescent analyses demonstrate neuroblastoma and microglial cell lines stably expressing TurboID-NES do produce robustly biotinylated cytosolic proteomes, and silver stain analyses confirm purified enrichment of biotinylated proteins when compared to untransduced neuroblastoma and microglial cells. This publication, reproduced here in *Chapter 3*, represents the first published extension of TurboID-NES into microglia. Following validation of functional and cytosolic TurboID-NES, we used proteomics and bioinformatics to determine the proteomic breadth of proteins labeled by cytosolic TurboID compared to whole-cell proteomes of microglia and neurons. Our results show that cytosolic-TurboID captures 59-65% of the proteins identified in microglia and neuronal cells, respectively. This provides future investigators using TurboID-NES an approximate benchmark for the fraction of the proteome one could anticipate to recover from in vivo brain cells. Interrogating this fundamental proteomic

parameter lends itself best to in vitro cell culture conditions wherein TurboID-biotinylated proteomes purified from transduced microglia and neurons could be directly compared with their naïve whole cell proteomic counterparts derived from single cell culture systems.

TurboID-NES efficiently labels trafficking proteins and can be applied to capturing stress-induced changes in trafficking.

We identified clusters of proteins which were commonly enriched in TurboID-NES biotinylated proteomes between cell types. These proteins highlight those which TurboID-NES preferentially biotin-labels; Golgi apparatus, vesicle-mediated transport, and secretory compartments. Since publishing the publication in *Chapter 3*, we suspected that TurboID's ability to efficiently label trafficking proteins across both cell types may position this technology well as a discovery tool to capture proteins in transit, and potentially capture changes in protein trafficking under disease conditions. For example, TAR DNA binding protein 43 (TDP-43) is a nucleic-acid binding protein which must localize to the nucleus to regulate RNA processing⁴³⁰. In neurodegenerative conditions, TDP-43 is trafficked to the cytosol, where it can no longer regulate RNA processing⁴³¹⁻⁴³³. TurboID-NES can be applied to discover new protein-trafficking patterns the orchestrated cells under stress conditions. Indeed, a recent application of TurboID-NES, called TransitID, has been specifically applied to map trafficking of proteins between membraneless organelles in living cells⁴³⁴. This brilliant new application of proximity labeling enzymes features both TurboID, expressed in a source location, and APEX, expressed in a

destination location. Proteins tagged by both enzymes will be therefore trafficked from TurboID's destination to the destination of APEX. This ingenious study expresses cytosolic TurboID-NES which labels cytosolic proteins at the "source" destination, and expresses a mitochondrial-matrix-directed APEX2 (mito-APEX2) which labels proteins with alkyne-phenol⁴³⁴; resolving the spatial origin of nuclear encoded mitochondrial proteins, as only 13 mitochondrial proteins necessary for the respiratory transport chain are translated from mitochondrial DNA⁴³⁵. This study also used cytosolic TurboID-NES and nuclear APEX2 (APEX2-NLS) to label the proteome trafficked from the cytosol to the nucleus under conditions of sodium arsenite-induced oxidative stress. TransitID identified 127 mis-localized proteins enriched in protein folding and translation, and further imaging of these targets show several proteins relocalizing to stress-granules⁴³⁴. Importantly, our published biochemical fractionation studies indicate that TurboID-NES itself does not change its localization under inflammatory stress (**Figure 6.1**). Taken together, our initial findings demonstrated that cytosolic TurboID-NES efficiently labels trafficked proteins across distinct brain cell-types. Proceeding novel adaptations of TurboID-NES published this year built upon cytosolic TurboID's efficient labeling of trafficked proteins to capture changes in proteomic trafficking.

We also identified proteins which are not labeled robustly by TurboID-NES; including proteins on the cell-surface, proteins within the nucleus, and proteins within lumen-enclosed membranes. These results are critical in defining the preferential biotinylation of vesicle-

transporting proteins by TurboID-NES as well as defining limitations of TurboID-NES to labeling cell-surface proteins which are important for inter-cellular communication. Importantly, cell-surface receptors, proteins with nucleophilic residues internally folded within complex protein structures or within lipid membranes may not be readily accessible by TurboID-NES. Recently, a new methodology, iPEEL may be better positioned to label and capture cell-surface proteins specifically, as discussed in *Chapter 3*.

TurboID-NES has minimal impacts on cellular physiology

We defined the impact of broad cytosolic biotinylation of proteins on cellular physiology, to anticipate potential deleterious experimental confounds which may be introduced by TurboID-NES expression itself. Notably, TurboID biotinylates proteins at nucleophilic residues, most notably the primary amine inherent to the functional group of lysine amino acid side chains. Lysine residues are important sites of reversible post-translational modifications, and mass spectrometry has mapped more than 100,000 sites of Lysine modification in over 10,000 proteins^{436,437}. Critical to epigenetic regulation, Lysine residues in histone proteins are sites of methylation and acetylation^{438,439}. Because histones are translated in the cytoplasm during S-phase prior to nuclear transport, it is possible for cytosolic TurboID to biotin-label histones on lysine residues during translation. Additionally, lysines are important sites for ubiquitination, a post-translational modification crucial to protein turnover⁴⁴⁰. Therefore, we wanted to identify any possible protein-level changes relevant to lysine modification in the whole-cell proteome with

TurboID expression. Of 2,187 proteins identified by MS in the whole cell BV2 and N2A proteome, we identified 53 proteins significantly altered by TurboID expression, including TurboID itself, in the microglial proteome and 74 proteins, including TurboID itself, significantly impacted by TurboID expression in neuroblastoma proteomes, amounting to approximately 2% and 3%, respectively. Of these proteins, we did identify a modest yet significant increase in nuclear-associated proteins, including H1.0. Future studies using cell-lines expressing TurboID-NES may consider directly assessing transcriptomic changes with TurboID-transduction to capture any transcriptome-level alterations caused by TurboID biotinylation of histones during cytoplasmic translation. Additionally, it is possible that viral transduction and puromycin screening itself may account for changes in protein abundances. An important control to consider in future studies to isolate the specific impact of TurboID-NES on protein-level changes in the absence of lentiviral transduction, may be the incorporation of cell lines transduced with a lentiviral construct containing only a fluorescence reporter and a puromycin-resistance cassette. Comparing the differentially abundant proteins of cells transduced with TurboID with cells transduced with an identical vector without the TurboID sequence would isolate the direct impact of TurboID-NES on whole-cell proteomes. Furthermore, we did not identify any significant impacts of TurboID-NES transduction on cellular respiration or LPS-mediated cytokine release. Taken together, these analyses identified a limited impact on the abundance of various nuclear proteins with lentiviral transduction of TurboID-NES, with no significant changes to other measures of cellular

physiology. These findings themselves are critically important to the proteomic field and for future investigations using TurboID-NES as a discovery tool to broadly profile cytosolic proteins.

TurboID-NES captures cellularly distinct proteins of disease relevance

In addition to defining basic parameters of proteomic breadth and modest or non-significant impacts on protein abundance and cellular physiology, we confirmed a robust enrichment of biotinylated proteins derived from microglial and neuroblastoma proteomes, and we confirmed that TurboID-NES-based proteomics can effectively distinguish microglial proteomes from neuroblastoma proteomes, and capture proteins of relevance to neurodegenerative disease. We used risk loci published in AD, Parkinson's disease (PD), and Amyotrophic Lateral Sclerosis (ALS) datasets to identify 32-84 neurodegenerative risk loci in TurboID-NES biotinylated microglia-enriched proteomes and 17-46 neurodegenerative risk loci in TurboID-NES biotinylated neuroblastoma-enriched proteomes (**Figure 6.2**). Notable AD-hub proteins labeled by TurboID with cell-type valence include Moesin (MSN) in microglial cells and microtubule-associated protein tau (Mapt). These results demonstrate feasibility of using TurboID-NES to profile changes in known neurodegenerative-associated proteins.

Aspects of LPS-mediated inflammation captured by TurboID-NES labeling

Our clustering analyses identify a cluster of proteins, cluster 5 (131 proteins) which are upregulated with LPS in both transduced BV2 whole cell and transduced BV2 AP datasets. These proteins represent the aspect of LPS-driven up-regulated changes that TurboID-NES captures

well. These proteins are particularly enriched in terms associated with response to interferon gamma, oxidative stress, and peroxisomal functions. In this cluster, we identify proteins previously identified by our lab to be regulated by the voltage-gated potassium channel, KV 1.3, in response to LPS challenge, EHD1, TAP1, TAP2, ICAM1, IRG1, STAT1, and VASP⁴⁰¹. Other canonical LPS-associated proteins TurboID-NES captured include Nos2, Interleukin-1a, Complement Receptor 3, Toll-Like-Receptor-2, ABCF1 and SYK. As discussed in *Chapter 2*, SYK acts downstream of the surface receptor TREM2, an important risk locus for AD^{42 211,212}. This signaling pathway is critical for microglial binding of A β , and mice without SYK show exacerbated A β neuropathology and worse behavioral deficits^{209 213}. TurboID-NES also captured promoters of glycolytic genes, PKM and LDHA, as well as glucokinase, GYK⁴⁴¹. TurboID-NES captured many proteins involved with interferon-induction of inflammasomes, including caspases (CASP1, CASP2), guanylate binding proteins (GBP2, GBP4 and GBP7)^{442,443}, interferon stimulating gene 15 (ISG15)⁴⁴⁴, and oligoadenylate synthetases (OASL1, OAS3, OAS1A, OAS1G) which transcriptionally regulate type I interferons^{375,445}. TurboID-NES also captured many changes in both the production of and neutralization of reactive oxygen species and peroxides, including an increase in catalase enzymes (CAT) to neutralize hydrogen peroxide into O₂ and H₂O⁴⁴⁶, cytochrome B proteins (CYB5R3, CYBB) the latter encoding for a protein comprising a part of the enzyme NADPH oxidase and is a key producer of reactive oxygen species^{447 141,448}, peroxiredoxins (PRDX1 and PRDX4), which are antioxidants that control cytokine-induced

peroxide levels⁴⁴⁹, and mitochondrial fission protein preceding apoptosis⁴⁵⁰ (FIS1). TurboID-NES also captured markers of ferroptosis, including HMOX1 and GCLM^{451,452}. TurboID-NES successfully captured an increase in vacuolar-type ATPases (V-ATPase), including ATP6v1c1, and ATP6v1a, a highly conserved enzyme necessary for bacterial autophagy implicated in a genetic knockout study⁴⁵³. V-ATPases are localized to endosomes, lysosomes, Golgi-derived vesicles, and secretory vesicles and establish proton gradients and acidifying environments⁴⁵⁴. ATP6v1a is also upregulated in myeloid cells derived from transgenic models (APP_{SWE}/PS1 Δ E9) of AD⁴⁵⁵. V-ATPases are important initial mediators of host-immune defense to promote xenophagy. V-ATPases are massive protein complexes (640 kDa) which span organelle membranes⁴⁵⁴. Given the established preference of TurboID-NES to label proteins vesicular proteins, in combination with the large size of V-ATPases specifically, TurboID-NES may label a variety of cytoplasmic-facing nucleophilic residues. Overall, TurboID-NES captured major hallmarks of LPS-driven stress including metabolic reprogramming to increase glycolysis, interferon-induced inflammasome proteins, ferroptosis, and generation of and neutralization of reactive oxygen species. TurboID-NES also captured a decrease in anti-inflammatory proteins, notably MRC1, LSP1, and MGL2. Traditional classification of valanced-macrophage activation (M1 and M2) were informed in part by transcriptomic changes in response to interleukin-4 stimulation, including transcriptomic signatures for M2 Mannose receptor-1 (MRC1) and galactose-type C-Type Lectin 2 (MGL2)^{379,456,457}. Lymphocyte specific protein 1 (LSP1) is also implicated in immunosuppression⁴⁵⁸. These

canonical markers of immune-suppression were captured by TurboID-NES as being decreased with prolonged LPS. As discussed in *Chapter 1.3*, physiological impacts of LPS vary greatly by dose, duration, route of administration, and cell line/species assessed. In our studies, we aim to provide relatively lower doses of LPS for longer durations to best reflect chronic inflammation observed in human AD. BV2 cells are immortalized murine microglia characterized by their phagocytic capacities when activated by LPS⁴⁵⁹. When compared with primary microglia, LPS response is broadly shared (90% of genes altered in BV2 cells are also altered in primary microglia), though BV2 cells have a more modest magnitude in LPS induced gene up-regulation and nitric oxide production^{459,460}. Though BV2 cells replicate quickly, making them suitable for mass spectrometry studies requiring a high protein yield. While referencing precedent methodologies to inform the dose used in our in vitro studies (1 µg / mL; 48 hours), a few key references emerged. At a higher dose range, one study by Dai et al., 2014 compared different concentrations of LPS in cultured BV2 cells (10 µg / mL, 20 µg/mL, and 30 µg/mL) for 24 hours on TLR-4 and MyD88 expression⁴⁶¹, and nuclear NF-κB. Their findings demonstrate a significant and dose-dependent increase in TLR-4 by western blotting, and a peak increase in MyD88 at 20 µg/mL, and significant increases in nuclear NF-κB⁴⁶¹. When the media derived from BV2 cells treated with 10 µg / mL of LPS was applied to PC12 cells, there was significant immediate cell death in just 24 hours of treatment⁴⁶¹. These conditions may better reflect conditions associated with acute traumatic brain injury, rather than chronic neuroinflammation, and provided a useful upper-limit to LPS-dosage. In

contrast, another study authored by investigators in South Korea, Woo et al., 2017 performed quantitative mass spectrometry on cultured BV2 cells treated with LPS at 1 $\mu\text{g} / \text{mL}$ for 48 hours, and demonstrated proteomic changes in antigen processing and presentation, shifts in glycolysis and gluconeogenesis, natural killer cell mediated toxicity³⁷², several of these terms also appeared in our GO analyses. Overall, an important limitation may be that the dose and duration of LPS stimulation used in this study may capture long-term changes in response to LPS stimulation. Notably, ABCF1 and SYK are associated with a biphasic shift in immunity towards an endotoxin tolerance state toward the TRIF-IFN-I signaling axis. The signaling shift from MyD88 to TRIF signaling occurs during TLR4 endocytosis, associated with an anti-inflammatory response⁴⁶². Excitingly, TurboID-NES may have captured an LPS-induced shift in phenotype from mediated by ABCF1 signaling, though this conclusion would be supported by future experiments of transduced BV2 cells given different doses and durations of LPS to see if TurboID-NES can label different proteins reflective of chronic inflammatory conditions; or an anti-inflammatory stimulus like interleukin-4 to determine if TurboID-NES can capture distinct anti-inflammatory profiles. The study in this thesis assessed only if TurboID-NES can capture a proteomic-level shift in response to LPS, whereas future studies comparing biotinylated proteomes of different inflammatory challenges may reflect different microglia phenotypes relevant to disease.

Capturing LPS impacts on glutamatergic neuronal proteomes.

In *Chapter 5*, this thesis reports the novel use of TurboID-NES to capturing excitatory neuronal proteomic changes in response to peripheral LPS administration. Due to study limitations discussed in *Chapter 5.4*, this discussion section focuses only on the impact of LPS on cortical proteomes. Differential expression analysis of cortical TB and AP proteomes treated with LPS identify modest yet significant changes in disease associated proteins. In the TB proteome, there was notable increase in complement signaling proteins, including C1QA and C1QC and a decrease in several presynaptic SNARE associated proteins including Synaptotamin-12 (SYT12) and synaptosomal associated protein 47. There is also a decrease in Seizure 6-like protein 2 (SEZ6L2) in both the AP and TB proteomes, which has been reported to be a substrate of BACE-1⁴⁶³. In the AP cortical proteomes, LPS significantly increased cytosolic TDP-43, as TurboID-NES has a functional nuclear export sequence. TurboID captured an increase in 14-3-3 protein zeta/delta (YWHAZ), a gene which is consistently identified as a central and interconnected hub gene of Alzheimer's disease, and is regarded as a central regulator of disease progression with clinical value as a cerebral-spinal fluid biomarker⁴⁶⁴⁻⁴⁶⁸. Overall, the over-representation analysis of protein level changes at the cortical TB level reflect an increased regulation of immune activity, an increase in proteins associated with membrane depolarization and immune response as well as post-synaptic density. At the AP level, TurboID captured an increase in post-synaptic density, cytoskeletal proteins, and cell projection proteins. One study in adult mice demonstrated that

LPS-induced hyperexcitability correlated with a lowered seizure threshold by 34%, a doubled spontaneous EPSC frequency linked specifically to increased glutamate release probability from Schaffer collateral cells which correlated with a reduced presynaptic activity of GABA receptors⁴⁶⁹. It may be possible that inhibitory interneurons are uniquely vulnerable to inflammation, as LPS administration in mice correlates with a decreased expression of parvalbumin and a decreased number of perisomatic boutons in the hippocampus correlating with cognitive impairment¹²¹. Importantly, treatment of minocycline, a pharmacological compound which represses microglial activation, rescued hippocampal PV expression, restored perisomatic bouton number, and improved cognitive impairment¹²¹. Overall, Chapter 5 represents the first use of TurboID-NES to capture specific proteomic changes occurring in glutamatergic neurons with LPS treatment. Future immunohistochemistry and electrophysiology studies may be conducted to provide functional physiological context implicated by an increase in post-synaptic density proteins.

Conclusion

The broad objective of the studies performed in throughout this doctoral training were to apply TurboID-NES proximity labeling to resolve cell-type specific proteomic signatures of disease and neuroinflammation. The doctoral training corresponding to this thesis began the same year the invention of TurboID was first published³²⁸. In commencement, the use of TurboID to purify cell-type specific proteomes was regarded as a high-risk, high-reward undertaking,

given the novelty of the technology at that time. Over the course of this doctorate, we strategically planned step-wise incremental goals towards *in vivo* extensions of TurboID-NES; starting with nascent studies in transfected HEK293 cells (studies not included in this thesis), generating stably-transduced microglia and neuroblastoma cell lines expressing TurboID-NES, utilizing AAV9-based delivery of TurboID, and finally creating transgenic mice expressing TurboID in specific cell types. During the trajectory of this methodological development, *in vitro* studies were foundational for understanding the basic parameters and capabilities of using TurboID-proximity labeling to capture proteomes in homeostatic and inflammatory conditions. Extending this technology to murine models was a highly collaborative effort made possible by many talented scientists. Future applications of TurboID-NES will undoubtedly be transformative in our collective understanding of cell-type specific proteomic disease signatures in the brain.

ii. Future applications of TurboID

Resolving cell-autonomous and non-cell autonomous mechanisms of neuroinflammation.

CIBOP can also be applied to understand the mechanistic impact microglia have on neuronal proteomes in the context of neuroinflammation and disease. Pharmacological ablation of microglia in living mice is can be performed using rodent chow containing the small molecule PLX3397⁴⁷⁰. PLX3397 is an orally bioavailable antagonist of Colony Stimulating Factor Receptor 1 (CSF1R) which kills microglia in living animals without cognitive or behavioral impairment, or

blood brain barrier damage. Microglia depend on CSF1R signaling to survive PLX3397 can eliminate 99% of microglia within 7 days and repopulation of microglia can also be achieved within 7 days of drug cessation⁴⁷¹. Microglial ablation with PLX3397 correlates with reduced amyloid burden in amyloidogenic murine models⁴⁷²⁻⁴⁷⁴, and pharmacological ablation of microglia with another CSF1R inhibitor, PLX5622 correlates with improved cognition in aged (15 month old) 3xTg-AD mice⁴⁷⁵ and decreased tau propagation through exosomes⁴⁷⁶. Future studies will combine pharmacological depletion of microglia with neuronal CIBOP in disease and neuroinflammatory contexts to resolve the proteomic transformations taking place both with microglia ablation itself and as well as microglia role on synaptic proteins in challenges states. We began pilot experiments incorporating PLX3397 chow (229 ppm) for 5 weeks in wildtype (WT) C57BL/6 mice; 6 mice received PLX3397-chow and 4 mice received identical chow formula without PLX3397. After sacrifice, fixed mouse brain were cut into 40 μ m thick sagittal sections prior to IBA-1 based microglia counting (**Figure 6.3**). 5 weeks of pharmacological microglia ablation with PLX3397 chow reduced microglia counts significantly in the cortex and hippocampus (~50% reduction). This pilot analysis provides a proof-of-concept feasibility to administer in neuronal CIBOP mice in disease, inflammation, and homeostatic contexts.

Applications of TurboID-NES to systems level analyses in diverse brain cell types.

Collectively, our research is expanding applications to CIBOP into other cell types in the brain to resolve cellularly heterogeneous mechanisms of disease. Recent applications of TurboID-NES include extension into parvalbumin interneurons to understand proteomic signatures of disease vulnerability specific to fast-spiking interneurons in the 5xFAD model of AD⁴⁷⁷. TurboID-NES has also been successfully extended into astrocytes and Camk2a neurons for regional proteomic signature resolution in mice³²⁹. Ongoing methodological developments are also using TurboID to profile proteomes and transcriptomes simultaneously, specifically RNA-binding proteins, from brain cells in vitro and in vivo contexts⁴⁷⁸. If TurboID-NES can successfully be expressed in murine microglia in vivo, purified microglial-derived exosomes containing proteins biotinylated by TurboID may uncover microglial-exosome mediated mechanisms of neurodegeneration⁴⁷⁹. Additionally, split TurboID can be fused to specific proteins of interest, to label interactomes relevant to disease-associated transitions. For example, split-TurboID can be fused to the C and N termini of the voltage-gated potassium channel Kv1.3, to determine unique termini-level interactomes⁴⁸⁰. The use of TurboID as a discovery tool has an abundance of applications beyond wide profiling of cytosolic proteins, and will undoubtedly serve as a versatile discovery tool for many systems-level analyses.

iii. Chapter VI. Figures

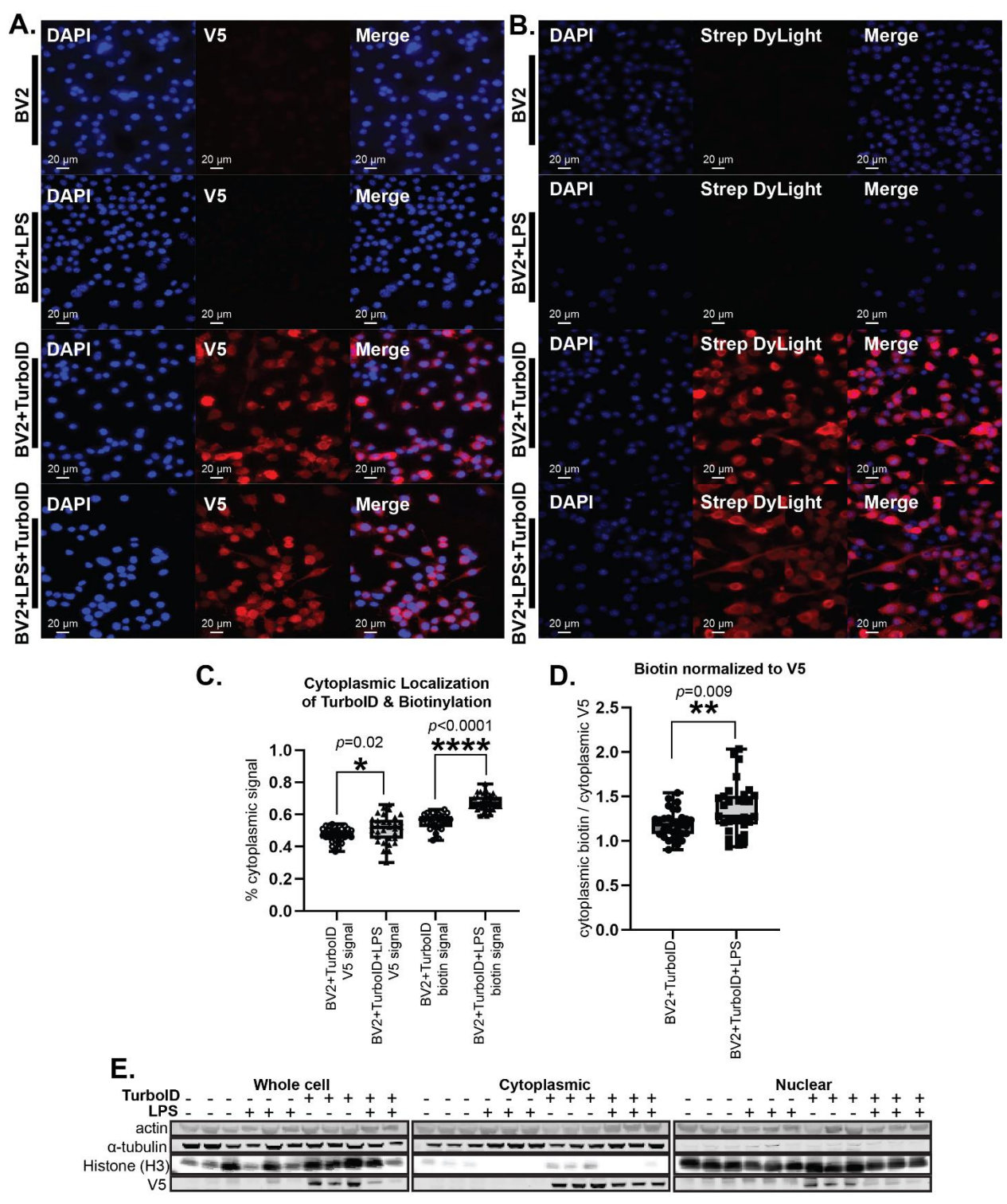


Figure 6.1 LPS challenge slightly increases cytosolic direction of TurboID and biotinylation of proteins. **A.** Immunofluorescence (IF) visualizing TurboID (V5, red) and nuclei (DAPI, blue) localization in transduced and untransduced BV2 cells with and without LPS challenge. Localization of V5-TurboID remains cytosolic under LPS challenge. **B.** IF visualizing biotinylation of proteins (StrepDylight, red) and nuclei (DAPI, blue) in contexts of LPS challenge in transduced and untransduced BV2 cells. Biotinylation of proteins remains cytosolic under LPS challenge. **C.** Colocalization analysis of the area of cytoplasmic V5 signal (left two box-plots) and cytoplasmic biotinylation signal (right two box-plots) indicates a significant increase in cytosolic V5 and biotinylated proteins with LPS challenge. Significant p values were determined using the two-tailed Mann-Whitney test. **D.** Biotinylation signals normalized to V5 signals within the cytoplasm. After normalizing the biotinylation intensity values to V5 intensity values, there is a significant increase in cytosolic biotinylation of proteins with LPS. Significant p values were determined using the two-tailed Mann-Whitney test. **E.** Western blot (WB) verification of subcellular-fractionation experiments of transduced and untransduced BV2 cells with and without LPS challenge (n=3/group). Using β -actin as a loading control, α -tubulin as a cytoplasmic marker, histone H3 as a nuclear marker, and V5 as a marker for TurboID, we can confirm purification of sub-cellular fractions with the decrease in α -tubulin signal in the nuclear fraction as compared with the whole cell and cytoplasmic fractions and a decrease in histone H3 in the cytoplasmic fraction as compared with the whole cell and cytoplasmic fractions. With actin signal intensity remaining constant as a loading control, there is no apparent difference in cytoplasmic V5 intensity with LPS challenge.

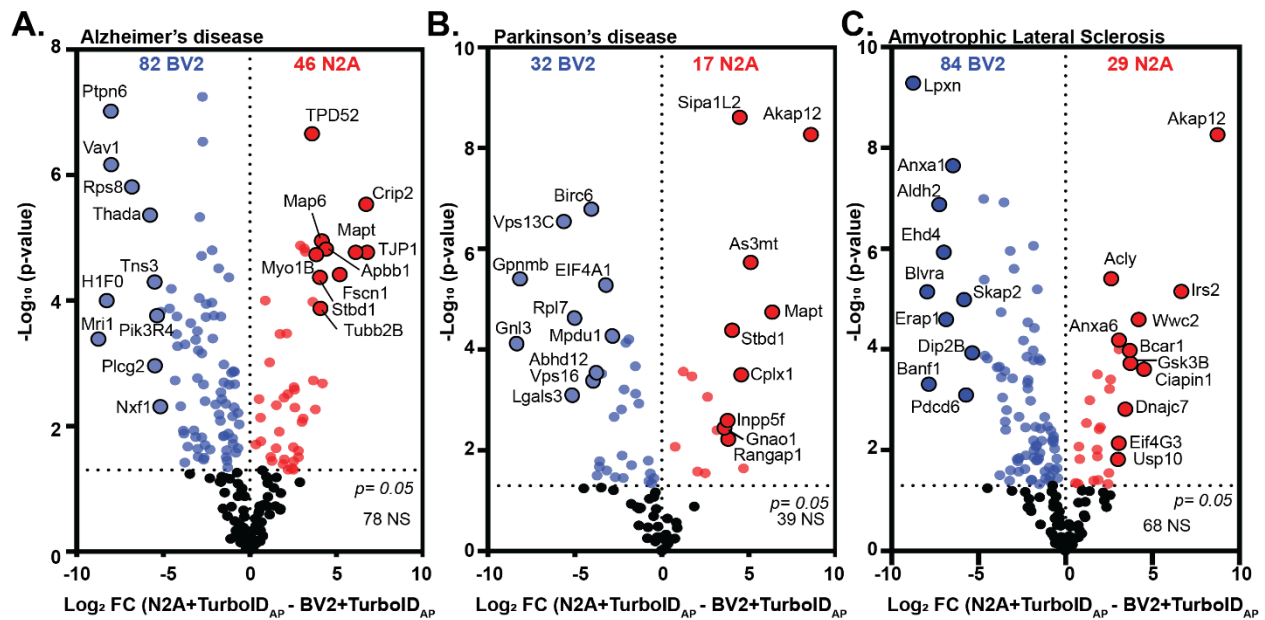


Figure 6.2 TurboID labels cellularly distinct proteins with relevance to neurodegenerative disease. Volcano plot representations of cellularly-distinct proteins labeled by TurboID (derived from significant DEP dataset in Fig 4A), and respective disease relevance. A. Mapping proteins onto the Alzheimer's disease (AD) AD MAGMA dataset, there are 82 AD-associated proteins enriched in biotin-labeled BV2 proteins and 46 AD-related proteins enriched in biotin-labeled N2A proteins. B. Mapping biotin-labeled and cellularly distinct proteins onto the Parkinson's disease (PD) MAGMA dataset, there are 32 PD-relevant proteins in the BV2 biotin-labeled proteome and 17 PD-relevant proteins in the N2A biotin-labeled proteome. C. Mapping proteins onto the Amyotrophic lateral Sclerosis (ALS) and Frontotemporal dementia (FTD) MAGMA dataset, there are 84 ALS/FTD-relevant BV2 proteins and 29 proteins in the N2A biotin-labeled proteins.

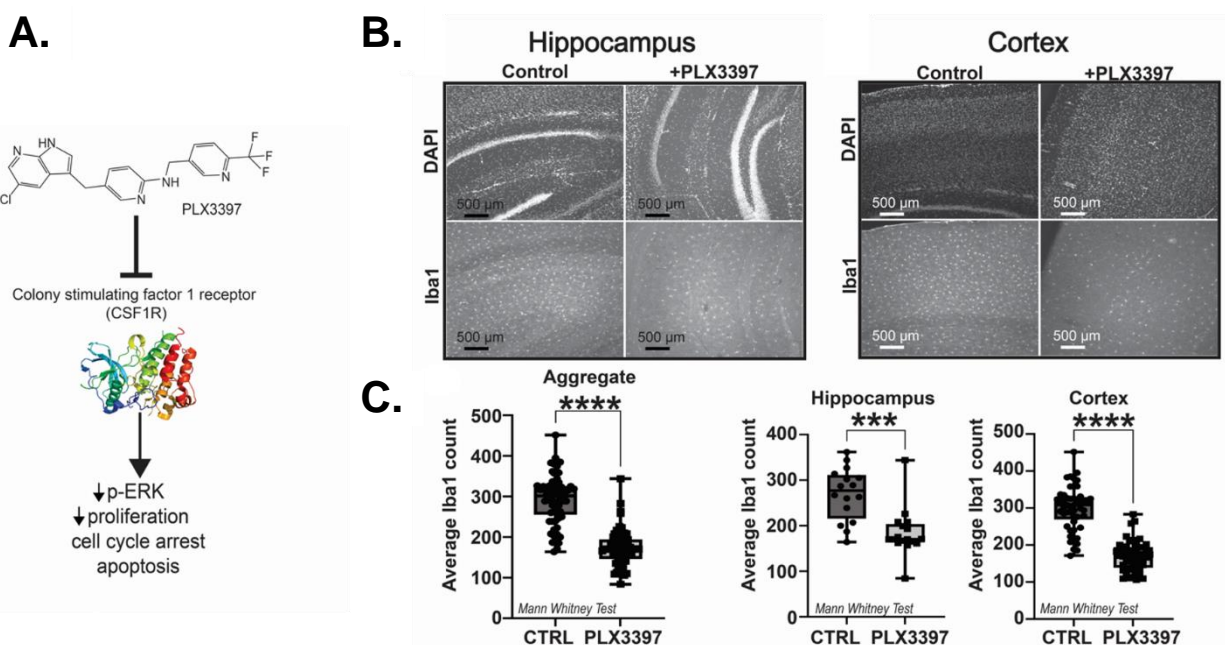


Figure 6.3 Pilot studies validating pharmacological ablation of microglia with CSF1R antagonism. **A.** Schematic of PLX3397 mechanism of action. PLX3397 is a small molecule which antagonizes Colony Stimulating Factor 1 Receptor (CSF1R). Downstream signaling lead to a decrease in phosphorylated ERK, decrease in microglia proliferation and apoptosis. **B.** Immunofluorescence of hippocampal sections of control mice (*left*) and mice receiving PLX3397-chow (*right*). Staining, counting, and analysis performed by undergraduate mentee, Hollis Zeng. **C.** Average counts of Iba1 puncta reveals significant decrease in Iba1 count with PLX3397 chow in total sections, hippocampal and cortical sections (Mann Whitney significance).

VII. Bibliography

- 1 Murphy, S. L., Xu, J., Kochanek, K. D. & Arias, E. Mortality in the United States, 2017. *NCHS Data Brief*, 1-8 (2018).
- 2 2023 Alzheimer's disease facts and figures. *Alzheimer's & Dementia* **19**, 1598-1695, doi:<https://doi.org/10.1002/alz.13016> (2023).
- 3 Serrano-Pozo, A., Frosch, M. P., Masliah, E. & Hyman, B. T. Neuropathological alterations in Alzheimer disease. *Cold Spring Harb Perspect Med* **1**, a006189, doi:10.1101/cshperspect.a006189 (2011).
- 4 Saunders, A. M. *et al.* Association of apolipoprotein E allele $\epsilon 4$ with late-onset familial and sporadic Alzheimer's disease. *Neurology* **43**, 1467-1467, doi:10.1212/wnl.43.8.1467 (1993).
- 5 Green, R. C. *et al.* Risk of Dementia Among White and African American Relatives of Patients With Alzheimer Disease. *JAMA* **287**, 329-336, doi:10.1001/jama.287.3.329 (2002).
- 6 Fratiglioni, L., Ahlbom, A., Viitanen, M. & Winblad, B. Risk factors for late-onset Alzheimer's disease: a population-based, case-control study. *Ann Neurol* **33**, 258-266, doi:10.1002/ana.410330306 (1993).
- 7 Mayeux, R., Sano, M., Chen, J., Tatemichi, T. & Stern, Y. Risk of dementia in first-degree relatives of patients with Alzheimer's disease and related disorders. *Arch Neurol* **48**, 269-273, doi:10.1001/archneur.1991.00530150037014 (1991).
- 8 Lautenschlager, N. T. *et al.* Risk of dementia among relatives of Alzheimer's disease patients in the MIRAGE study: What is in store for the oldest old? *Neurology* **46**, 641-650, doi:10.1212/wnl.46.3.641 (1996).
- 9 Farrer, L. A. *et al.* Effects of age, sex, and ethnicity on the association between apolipoprotein E genotype and Alzheimer disease. A meta-analysis. APOE and Alzheimer Disease Meta Analysis Consortium. *Jama* **278**, 1349-1356 (1997).
- 10 Wimo, A. *et al.* The worldwide costs of dementia in 2019. *Alzheimer's & Dementia n/a*, doi:<https://doi.org/10.1002/alz.12901>.
- 11 Hersi, M. *et al.* Risk factors associated with the onset and progression of Alzheimer's disease: A systematic review of the evidence. *NeuroToxicology* **61**, 143-187, doi:<https://doi.org/10.1016/j.neuro.2017.03.006> (2017).
- 12 Tynkkynen, L. K. *et al.* Health system reforms and the needs of the ageing population-an analysis of recent policy paths and reform trends in Finland and Sweden. *Eur J Ageing* **19**, 221-232, doi:10.1007/s10433-022-00699-x (2022).
- 13 Villemagne, V. L. *et al.* Amyloid β deposition, neurodegeneration, and cognitive decline in sporadic Alzheimer's disease: a prospective cohort study. *Lancet Neurol* **12**, 357-367, doi:10.1016/s1474-4422(13)70044-9 (2013).
- 14 Jack, C. R., Jr. *et al.* Hypothetical model of dynamic biomarkers of the Alzheimer's pathological cascade. *Lancet Neurol* **9**, 119-128, doi:10.1016/s1474-4422(09)70299-6 (2010).
- 15 Sperling, R. A. *et al.* Toward defining the preclinical stages of Alzheimer's disease: recommendations from the National Institute on Aging-Alzheimer's Association workgroups on diagnostic guidelines for Alzheimer's disease. *Alzheimers Dement* **7**, 280-292, doi:10.1016/j.jalz.2011.03.003 (2011).
- 16 Bertram, L. & Tanzi, R. E. The genetic epidemiology of neurodegenerative disease. *J Clin Invest* **115**, 1449-1457, doi:10.1172/jci24761 (2005).

- 17 Nelson, P. T. *et al.* Correlation of Alzheimer disease neuropathologic changes with cognitive status: a review of the literature. *J Neuropathol Exp Neurol* **71**, 362-381, doi:10.1097/NEN.0b013e31825018f7 (2012).
- 18 Jahn, H. Memory loss in Alzheimer's disease. *Dialogues Clin Neurosci* **15**, 445-454, doi:10.31887/DCNS.2013.15.4/hjahn (2013).
- 19 Botchway, B. O. A., Moore, M. K., Akinleye, F. O., Iyer, I. C. & Fang, M. Nutrition: Review on the Possible Treatment for Alzheimer's Disease. *J Alzheimers Dis* **61**, 867-883, doi:10.3233/jad-170874 (2018).
- 20 Scheltens, P. *et al.* Alzheimer's disease. *Lancet* **397**, 1577-1590, doi:10.1016/s0140-6736(20)32205-4 (2021).
- 21 Conti Filho, C. E. *et al.* Advances in Alzheimer's disease's pharmacological treatment. *Front Pharmacol* **14**, 1101452, doi:10.3389/fphar.2023.1101452 (2023).
- 22 Dhillon, S. Aducanumab: First Approval. *Drugs* **81**, 1437-1443, doi:10.1007/s40265-021-01569-z (2021).
- 23 Hoy, S. M. Lecanemab: First Approval. *Drugs* **83**, 359-365, doi:10.1007/s40265-023-01851-2 (2023).
- 24 Woloshin, S. & Kesselheim, A. S. What to Know About the Alzheimer Drug Aducanumab (Aduhelm). *JAMA Internal Medicine* **182**, 892-892, doi:10.1001/jamainternmed.2022.1039 (2022).
- 25 Marie-Eve Tremblay, A. S. *Microglia in Health and Disease*. 486 (Springer Science+Business Media, 2014).
- 26 Jones, E. G. Golgi, Cajal and the Neuron Doctrine. *J Hist Neurosci* **8**, 170-178, doi:10.1076/jhin.8.2.170.1838 (1999).
- 27 Ferrer, D. [Microglia (mesoglia or Rio Hortega cells) yesterday and today]. *Rev Med Univ Navarra* **17**, 145-161 (1973).
- 28 Daniele P. Theele, W. J. S. A Chronicle of Microglial Ontogeny. *Glia* **7**, 5-8 (1993).
- 29 Barron, K. D. The microglial cell. A historical review. *Journal of the Neurological Sciences* **134**, 57-68, doi:[https://doi.org/10.1016/0022-510X\(95\)00209-K](https://doi.org/10.1016/0022-510X(95)00209-K) (1995).
- 30 Rezaie, P. & Male, D. Mesoglia & microglia--a historical review of the concept of mononuclear phagocytes within the central nervous system. *J Hist Neurosci* **11**, 325-374, doi:10.1076/jhin.11.4.325.8531 (2002).
- 31 Tremblay, M., Lecours, C., Samson, L., Sánchez-Zafra, V. & Sierra, A. From the Cajal alumni Achúcarro and Río-Hortega to the rediscovery of never-resting microglia. *Front Neuroanat* **9**, 45, doi:10.3389/fnana.2015.00045 (2015).
- 32 García-Albea, E. & Pérez Trullen, J. M. The Spanish school of neurology and the first American cases of Alzheimer's disease. *J Hist Neurosci* **12**, 437-445, doi:10.1076/jhin.12.4.437.27919 (2003).
- 33 Hippus, H. & Neundörfer, G. The discovery of Alzheimer's disease. *Dialogues Clin Neurosci* **5**, 101-108, doi:10.31887/DCNS.2003.5.1/hhippius (2003).
- 34 Trejo-Lopez, J. A., Yachnis, A. T. & Prokop, S. Neuropathology of Alzheimer's Disease. *Neurotherapeutics* **19**, 173-185, doi:10.1007/s13311-021-01146-y (2022).
- 35 Giunta, B. *et al.* Inflammaging as a prodrome to Alzheimer's disease. *J Neuroinflammation* **5**, 51, doi:10.1186/1742-2094-5-51 (2008).
- 36 Hardy, J. A. & Higgins, G. A. Alzheimer's disease: the amyloid cascade hypothesis. *Science* **256**, 184-185, doi:10.1126/science.1566067 (1992).

- 37 Thal, D. R., Rüb, U., Orantes, M. & Braak, H. Phases of A β -deposition in the human brain and its relevance for the development of AD. *Neurology* **58**, 1791-1800, doi:10.1212/wnl.58.12.1791 (2002).
- 38 Fillenbaum, G. G. *et al.* Consortium to Establish a Registry for Alzheimer's Disease (CERAD): the first twenty years. *Alzheimers Dement* **4**, 96-109, doi:10.1016/j.jalz.2007.08.005 (2008).
- 39 Braak, H. & Braak, E. Neuropathological staging of Alzheimer-related changes. *Acta Neuropathol* **82**, 239-259, doi:10.1007/bf00308809 (1991).
- 40 O'Brien, R. J. *et al.* Neuropathologic studies of the Baltimore Longitudinal Study of Aging (BLSA). *J Alzheimers Dis* **18**, 665-675, doi:10.3233/jad-2009-1179 (2009).
- 41 Long, J. M. & Holtzman, D. M. Alzheimer Disease: An Update on Pathobiology and Treatment Strategies. *Cell* **179**, 312-339, doi:10.1016/j.cell.2019.09.001 (2019).
- 42 Andrade-Guerrero, J. *et al.* Alzheimer's Disease: An Updated Overview of Its Genetics. *Int J Mol Sci* **24**, doi:10.3390/ijms24043754 (2023).
- 43 Bateman, R. J. *et al.* Autosomal-dominant Alzheimer's disease: a review and proposal for the prevention of Alzheimer's disease. *Alzheimers Res Ther* **3**, 1, doi:10.1186/alzrt59 (2011).
- 44 Bekris, L. M., Yu, C. E., Bird, T. D. & Tsuang, D. W. Genetics of Alzheimer disease. *J Geriatr Psychiatry Neurol* **23**, 213-227, doi:10.1177/0891988710383571 (2010).
- 45 Bird, T. D. Genetic aspects of Alzheimer disease. *Genet Med* **10**, 231-239, doi:10.1097/GIM.0b013e31816b64dc (2008).
- 46 Suzuki, N. *et al.* An increased percentage of long amyloid β protein secreted by familial amyloid β protein precursor (β APP717) mutants. *Science* **264**, 1336-1340 (1994).
- 47 Raux, G. *et al.* Molecular diagnosis of autosomal dominant early onset Alzheimer's disease: an update. *Journal of medical genetics* **42**, 793-795 (2005).
- 48 Sherrington, R. *et al.* Alzheimer's disease associated with mutations in presenilin 2 is rare and variably penetrant. *Human molecular genetics* **5**, 985-988 (1996).
- 49 Kang, J. *et al.* The precursor of Alzheimer's disease amyloid A4 protein resembles a cell-surface receptor. *Nature* **325**, 733-736, doi:10.1038/325733a0 (1987).
- 50 Goate, A. *et al.* Segregation of a missense mutation in the amyloid precursor protein gene with familial Alzheimer's disease. *Nature* **349**, 704-706, doi:10.1038/349704a0 (1991).
- 51 Mullan, M. Familial Alzheimer's disease: second gene locus located. *BMJ: British Medical Journal* **305**, 1108 (1992).
- 52 De Strooper, B., Iwatsubo, T. & Wolfe, M. S. Presenilins and γ -secretase: structure, function, and role in Alzheimer Disease. *Cold Spring Harb Perspect Med* **2**, a006304, doi:10.1101/cshperspect.a006304 (2012).
- 53 Theuns, J. *et al.* Genetic variability in the regulatory region of presenilin 1 associated with risk for Alzheimer's disease and variable expression. *Human molecular genetics* **9**, 325-331 (2000).
- 54 Levy-Lahad, E. *et al.* Candidate gene for the chromosome 1 familial Alzheimer's disease locus. *Science* **269**, 973-977 (1995).
- 55 Tanzi, R. E. & Bertram, L. Twenty years of the Alzheimer's disease amyloid hypothesis: a genetic perspective. *Cell* **120**, 545-555 (2005).
- 56 Scheuner, D. *et al.* Secreted amyloid β -protein similar to that in the senile plaques of Alzheimer's disease is increased in vivo by the presenilin 1 and 2 and APP mutations linked to familial Alzheimer's disease. *Nature medicine* **2**, 864-870 (1996).
- 57 Kim, C. K. *et al.* Alzheimer's Disease: Key Insights from Two Decades of Clinical Trial Failures. *Journal of Alzheimer's Disease* **87**, 83-100, doi:10.3233/JAD-215699 (2022).

- 58 Blessed, G., Tomlinson, B. E. & Roth, M. The association between quantitative measures of dementia and of senile change in the cerebral grey matter of elderly subjects. *Br J Psychiatry* **114**, 797-811, doi:10.1192/bjp.114.512.797 (1968).
- 59 DeMarshall, C. *et al.* Detection of early-stage Alzheimer's pathology using blood-based autoantibody biomarkers in elderly hip fracture repair patients. *PLoS One* **14**, e0225178, doi:10.1371/journal.pone.0225178 (2019).
- 60 Benzing, W. C., Mufson, E. J. & Armstrong, D. M. Immunocytochemical distribution of peptidergic and cholinergic fibers in the human amygdala: their depletion in Alzheimer's disease and morphologic alteration in non-demented elderly with numerous senile plaques. *Brain Research* **625**, 125-138, doi:[https://doi.org/10.1016/0006-8993\(93\)90145-D](https://doi.org/10.1016/0006-8993(93)90145-D) (1993).
- 61 Oblak, A. L. *et al.* Comprehensive Evaluation of the 5XFAD Mouse Model for Preclinical Testing Applications: A MODEL-AD Study. *Frontiers in Aging Neuroscience* **13**, doi:10.3389/fnagi.2021.713726 (2021).
- 62 Oakley, H. *et al.* Intraneuronal β -amyloid aggregates, neurodegeneration, and neuron loss in transgenic mice with five familial Alzheimer's disease mutations: potential factors in amyloid plaque formation. *Journal of Neuroscience* **26**, 10129-10140 (2006).
- 63 Moechars, D., Lorent, K., De Strooper, B., Dewachter, I. & Van Leuven, F. Expression in brain of amyloid precursor protein mutated in the alpha-secretase site causes disturbed behavior, neuronal degeneration and premature death in transgenic mice. *The EMBO Journal* **15**, 1265-1274, doi:<https://doi.org/10.1002/j.1460-2075.1996.tb00468.x> (1996).
- 64 Kinney, J. W. *et al.* Inflammation as a central mechanism in Alzheimer's disease. *Alzheimers Dement (N Y)* **4**, 575-590, doi:10.1016/j.trci.2018.06.014 (2018).
- 65 Chen, L. *et al.* Inflammatory responses and inflammation-associated diseases in organs. *Oncotarget* **9**, 7204-7218, doi:10.18632/oncotarget.23208 (2018).
- 66 Chen, W. W., Zhang, X. & Huang, W. J. Role of neuroinflammation in neurodegenerative diseases (Review). *Mol Med Rep* **13**, 3391-3396, doi:10.3892/mmr.2016.4948 (2016).
- 67 Zhang, C., Wang, Y., Wang, D., Zhang, J. & Zhang, F. NSAID Exposure and Risk of Alzheimer's Disease: An Updated Meta-Analysis From Cohort Studies. *Front Aging Neurosci* **10**, 83, doi:10.3389/fnagi.2018.00083 (2018).
- 68 McGeer, P. L. & McGeer, E. G. NSAIDs and Alzheimer disease: epidemiological, animal model and clinical studies. *Neurobiol Aging* **28**, 639-647, doi:10.1016/j.neurobiolaging.2006.03.013 (2007).
- 69 in 't Veld, B. A. *et al.* NSAIDs and incident Alzheimer's disease. The Rotterdam Study. *Neurobiol Aging* **19**, 607-611, doi:10.1016/s0197-4580(98)00096-7 (1998).
- 70 Arvanitakis, Z. *et al.* Relation of NSAIDs to incident AD, change in cognitive function, and AD pathology. *Neurology* **70**, 2219-2225, doi:10.1212/01.wnl.0000313813.48505.86 (2008).
- 71 Rivers-Auty, J. *et al.* Anti-inflammatories in Alzheimer's disease—potential therapy or spurious correlate? *Brain Communications* **2**, doi:10.1093/braincomms/fcaa109 (2020).
- 72 Carson, M. J., Doose, J. M., Melchior, B., Schmid, C. D. & Ploix, C. C. CNS immune privilege: hiding in plain sight. *Immunol Rev* **213**, 48-65, doi:10.1111/j.1600-065X.2006.00441.x (2006).
- 73 Meizlish, M. L., Franklin, R. A., Zhou, X. & Medzhitov, R. Tissue Homeostasis and Inflammation. *Annu Rev Immunol* **39**, 557-581, doi:10.1146/annurev-immunol-061020-053734 (2021).
- 74 Rock, K. L. & Kono, H. The inflammatory response to cell death. *Annu Rev Pathol* **3**, 99-126, doi:10.1146/annurev.pathmechdis.3.121806.151456 (2008).
- 75 Sokol, C. L. & Luster, A. D. The chemokine system in innate immunity. *Cold Spring Harb Perspect Biol* **7**, doi:10.1101/cshperspect.a016303 (2015).

- 76 Chao, C. C., Hu, S. X., Ehrlich, L. & Peterson, P. K. Interleukin-1 and tumor necrosis factor- α synergistically mediate neurotoxicity: involvement of nitric oxide and of N-methyl-D-aspartate receptors. *Brain, behavior, and immunity* **9**, 355-365 (1995).
- 77 Chao, C. C. *et al.* Cytokine-stimulated astrocytes damage human neurons via a nitric oxide mechanism. *Glia* **16**, 276-284 (1996).
- 78 Gimsa, U., Peter, S. V., Lehmann, K., Bechmann, I. & Nitsch, R. Axonal damage induced by invading T cells in organotypic central nervous system tissue in vitro: involvement of microglial cells. *Brain Pathology* **10**, 365-377 (2000).
- 79 He, B. P., Wen, W. & Strong, M. J. Activated microglia (BV-2) facilitation of TNF- α -mediated motor neuron death in vitro. *Journal of Neuroimmunology* **128**, 31-38, doi:[https://doi.org/10.1016/S0165-5728\(02\)00141-8](https://doi.org/10.1016/S0165-5728(02)00141-8) (2002).
- 80 Jeohn, G.-H., Kong, L.-Y., Wilson, B., Hudson, P. & Hong, J.-S. Synergistic neurotoxic effects of combined treatments with cytokines in murine primary mixed neuron/glia cultures. *Journal of Neuroimmunology* **85**, 1-10, doi:[https://doi.org/10.1016/S0165-5728\(97\)00204-X](https://doi.org/10.1016/S0165-5728(97)00204-X) (1998).
- 81 Tan, J. *et al.* Activation of microglial cells by the CD40 pathway: relevance to multiple sclerosis. *Journal of neuroimmunology* **97**, 77-85 (1999).
- 82 Hendriks, J. J., Teunissen, C. E., de Vries, H. E. & Dijkstra, C. D. Macrophages and neurodegeneration. *Brain Res Brain Res Rev* **48**, 185-195, doi:10.1016/j.brainresrev.2004.12.008 (2005).
- 83 Cribbs, D. H. *et al.* Extensive innate immune gene activation accompanies brain aging, increasing vulnerability to cognitive decline and neurodegeneration: a microarray study. *Journal of neuroinflammation* **9**, 1-18 (2012).
- 84 Leulier, F. & Lemaitre, B. Toll-like receptors — taking an evolutionary approach. *Nature Reviews Genetics* **9**, 165-178, doi:10.1038/nrg2303 (2008).
- 85 Tang, S.-C. *et al.* Pivotal role for neuronal Toll-like receptors in ischemic brain injury and functional deficits. *Proceedings of the National Academy of Sciences* **104**, 13798-13803 (2007).
- 86 Olson, J. K. & Miller, S. D. Microglia initiate central nervous system innate and adaptive immune responses through multiple TLRs. *The Journal of Immunology* **173**, 3916-3924 (2004).
- 87 Bowman, C. C., Rasley, A., Tranguch, S. L. & Marriott, I. Cultured astrocytes express toll-like receptors for bacterial products. *Glia* **43**, 281-291 (2003).
- 88 Rehli, M. Of mice and men: species variations of Toll-like receptor expression. *Trends Immunol* **23**, 375-378, doi:10.1016/s1471-4906(02)02259-7 (2002).
- 89 Kawasaki, T. & Kawai, T. Toll-Like Receptor Signaling Pathways. *Frontiers in Immunology* **5**, doi:10.3389/fimmu.2014.00461 (2014).
- 90 Brown, G. C. The endotoxin hypothesis of neurodegeneration. *Journal of Neuroinflammation* **16**, 180, doi:10.1186/s12974-019-1564-7 (2019).
- 91 Bian, Z.-M. *et al.* Expression and functional roles of caspase-5 in inflammatory responses of human retinal pigment epithelial cells. *Investigative ophthalmology & visual science* **52**, 8646-8656 (2011).
- 92 Alkasir, R., Li, J., Li, X., Jin, M. & Zhu, B. Human gut microbiota: the links with dementia development. *Protein Cell* **8**, 90-102, doi:10.1007/s13238-016-0338-6 (2017).
- 93 Fathi, P. & Wu, S. Isolation, Detection, and Characterization of Enterotoxigenic Bacteroides fragilis in Clinical Samples. *Open Microbiol J* **10**, 57-63, doi:10.2174/1874285801610010057 (2016).
- 94 Foster, J. A., Lyte, M., Meyer, E. & Cryan, J. F. Gut Microbiota and Brain Function: An Evolving Field in Neuroscience. *Int J Neuropsychopharmacol* **19**, doi:10.1093/ijnp/pyv114 (2016).

- 95 Ghaisas, S., Maher, J. & Kanthasamy, A. Gut microbiome in health and disease: Linking the microbiome–gut–brain axis and environmental factors in the pathogenesis of systemic and neurodegenerative diseases. *Pharmacology & therapeutics* **158**, 52-62 (2016).
- 96 Hug, L. A. *et al.* A new view of the tree of life. *Nat Microbiol* **1**, 16048, doi:10.1038/nmicrobiol.2016.48 (2016).
- 97 Lukiw, W. J. Bacteroides fragilis Lipopolysaccharide and Inflammatory Signaling in Alzheimer's Disease. *Front Microbiol* **7**, 1544, doi:10.3389/fmicb.2016.01544 (2016).
- 98 Rogers, M. A. & Aronoff, D. M. The influence of non-steroidal anti-inflammatory drugs on the gut microbiome. *Clinical Microbiology and Infection* **22**, 178. e171-178. e179 (2016).
- 99 Sender, R., Fuchs, S. & Milo, R. Are we really vastly outnumbered? Revisiting the ratio of bacterial to host cells in humans. *Cell* **164**, 337-340 (2016).
- 100 Sharon, G., Sampson, T. R., Geschwind, D. H. & Mazmanian, S. K. The Central Nervous System and the Gut Microbiome. *Cell* **167**, 915-932, doi:10.1016/j.cell.2016.10.027 (2016).
- 101 d'Hennezel, E., Abubucker, S., Murphy, L. O. & Cullen, T. W. Total Lipopolysaccharide from the Human Gut Microbiome Silences Toll-Like Receptor Signaling. *mSystems* **2**, 10.1128/msystems.00046-00017, doi:doi:10.1128/msystems.00046-17 (2017).
- 102 Narayan, S., Liew, Z., Bronstein, J. M. & Ritz, B. Occupational pesticide use and Parkinson's disease in the Parkinson Environment Gene (PEG) study. *Environ Int* **107**, 266-273, doi:10.1016/j.envint.2017.04.010 (2017).
- 103 Zhao, Y., Jaber, V. & Lukiw, W. J. Secretory Products of the Human GI Tract Microbiome and Their Potential Impact on Alzheimer's Disease (AD): Detection of Lipopolysaccharide (LPS) in AD Hippocampus. *Front Cell Infect Microbiol* **7**, 318, doi:10.3389/fcimb.2017.00318 (2017).
- 104 Zhang, R. *et al.* Circulating endotoxin and systemic immune activation in sporadic amyotrophic lateral sclerosis (sALS). *Journal of Neuroimmunology* **206**, 121-124, doi:10.1016/j.jneuroim.2008.09.017 (2009).
- 105 Hajjar, A. M., Ernst, R. K., Tsai, J. H., Wilson, C. B. & Miller, S. I. Human Toll-like receptor 4 recognizes host-specific LPS modifications. *Nature immunology* **3**, 354-359 (2002).
- 106 Bryant, C. E., Spring, D. R., Gangloff, M. & Gay, N. J. The molecular basis of the host response to lipopolysaccharide. *Nature Reviews Microbiology* **8**, 8-14 (2010).
- 107 Morris, M. C., Gilliam, E. A. & Li, L. Innate immune programming by endotoxin and its pathological consequences. *Frontiers in immunology* **5**, 680 (2015).
- 108 Rivest, S. Regulation of innate immune responses in the brain. *Nature Reviews Immunology* **9**, 429-439, doi:10.1038/nri2565 (2009).
- 109 Bossù, P. *et al.* A single intraperitoneal injection of endotoxin in rats induces long-lasting modifications in behavior and brain protein levels of TNF- α and IL-18. *J Neuroinflammation* **9**, 101, doi:10.1186/1742-2094-9-101 (2012).
- 110 Sun, J. *et al.* IL-17A is implicated in lipopolysaccharide-induced neuroinflammation and cognitive impairment in aged rats via microglial activation. *J Neuroinflammation* **12**, 165, doi:10.1186/s12974-015-0394-5 (2015).
- 111 Pfalzgraff, A. & Weindl, G. Intracellular lipopolysaccharide sensing as a potential therapeutic target for sepsis. *Trends in Pharmacological Sciences* **40**, 187-197 (2019).
- 112 Yamamoto, Y. *et al.* Septic shock is associated with receptor for advanced glycation end products ligation of LPS. *The Journal of Immunology* **186**, 3248-3257 (2011).
- 113 Daws, M. R. *et al.* Pattern recognition by TREM-2: binding of anionic ligands. *The Journal of Immunology* **171**, 594-599 (2003).
- 114 Hampton, R. Y., Golenbock, D. T., Penman, M., Krieger, M. & Raetz, C. R. Recognition and plasma clearance of endotoxin by scavenger receptors. *Nature* **352**, 342-344 (1991).

- 115 Wright, S. D., Levin, S. M., Jong, M., Chad, Z. & Kabbash, L. CR3 (CD11b/CD18) expresses one binding site for Arg-Gly-Asp-containing peptides and a second site for bacterial lipopolysaccharide. *The Journal of experimental medicine* **169**, 175-183 (1989).
- 116 Wright, S. D. & Jong, M. Adhesion-promoting receptors on human macrophages recognize *Escherichia coli* by binding to lipopolysaccharide. *The Journal of experimental medicine* **164**, 1876-1888 (1986).
- 117 Jawhar, S., Trawicka, A., Jenneckens, C., Bayer, T. A. & Wirths, O. Motor deficits, neuron loss, and reduced anxiety coinciding with axonal degeneration and intraneuronal A β aggregation in the 5XFAD mouse model of Alzheimer's disease. *Neurobiol Aging* **33**, 196.e129-140, doi:10.1016/j.neurobiolaging.2010.05.027 (2012).
- 118 Eimer, W. A. & Vassar, R. Neuron loss in the 5XFAD mouse model of Alzheimer's disease correlates with intraneuronal A β 42 accumulation and Caspase-3 activation. *Molecular Neurodegeneration* **8**, 2, doi:10.1186/1750-1326-8-2 (2013).
- 119 Wirths, O. & Bayer, T. A. Neuron loss in transgenic mouse models of Alzheimer's disease. *Int J Alzheimers Dis* **2010**, doi:10.4061/2010/723782 (2010).
- 120 Zhao, J. *et al.* Neuroinflammation induced by lipopolysaccharide causes cognitive impairment in mice. *Scientific Reports* **9**, 5790, doi:10.1038/s41598-019-42286-8 (2019).
- 121 Mao, M., Zhou, Z., Sun, M., Wang, C. & Sun, J. The dysfunction of parvalbumin interneurons mediated by microglia contributes to cognitive impairment induced by lipopolysaccharide challenge. *Neurosci Lett* **762**, 136133, doi:10.1016/j.neulet.2021.136133 (2021).
- 122 Xin, Y. R. *et al.* The Immune System Drives Synapse Loss During Lipopolysaccharide-Induced Learning and Memory Impairment in Mice. *Front Aging Neurosci* **11**, 279, doi:10.3389/fnagi.2019.00279 (2019).
- 123 Griffin, W. S. *et al.* Brain interleukin 1 and S-100 immunoreactivity are elevated in Down syndrome and Alzheimer disease. *Proc Natl Acad Sci U S A* **86**, 7611-7615, doi:10.1073/pnas.86.19.7611 (1989).
- 124 Strauss, S. *et al.* Detection of interleukin-6 and alpha 2-macroglobulin immunoreactivity in cortex and hippocampus of Alzheimer's disease patients. *Lab Invest* **66**, 223-230 (1992).
- 125 Brosseron, F., Krauthausen, M., Kummer, M. & Heneka, M. T. Body fluid cytokine levels in mild cognitive impairment and Alzheimer's disease: a comparative overview. *Mol Neurobiol* **50**, 534-544, doi:10.1007/s12035-014-8657-1 (2014).
- 126 Lee, J. W. *et al.* Neuro-inflammation induced by lipopolysaccharide causes cognitive impairment through enhancement of beta-amyloid generation. *Journal of Neuroinflammation* **5**, 37, doi:10.1186/1742-2094-5-37 (2008).
- 127 Asti, A. & Gioglio, L. Can a bacterial endotoxin be a key factor in the kinetics of amyloid fibril formation? *Journal of Alzheimer's Disease* **39**, 169-179 (2014).
- 128 Gardner, L., White, J., Eimerbrink, M., Boehm, G. & Chumley, M. Imatinib methanesulfonate reduces hyperphosphorylation of tau following repeated peripheral exposure to lipopolysaccharide. *Neuroscience* **331**, 72-77 (2016).
- 129 Bhaskar, K. *et al.* Regulation of tau pathology by the microglial fractalkine receptor. *Neuron* **68**, 19-31 (2010).
- 130 Buxbaum, J. D. *et al.* Cholinergic agonists and interleukin 1 regulate processing and secretion of the Alzheimer beta/A4 amyloid protein precursor. *Proc Natl Acad Sci U S A* **89**, 10075-10078, doi:10.1073/pnas.89.21.10075 (1992).
- 131 Blasko, I., Marx, F., Steiner, E., Hartmann, T. & Grubeck-Loebenstien, B. TNFalpha plus IFNgamma induce the production of Alzheimer beta-amyloid peptides and decrease the secretion of APPs. *Faseb j* **13**, 63-68, doi:10.1096/fasebj.13.1.63 (1999).

- 132 Hirose, Y. *et al.* Glial conditioned medium alters the expression of amyloid precursor protein in SH-SY5Y neuroblastoma cells. *Biochem Biophys Res Commun* **198**, 504-509, doi:10.1006/bbrc.1994.1074 (1994).
- 133 Sastre, M. *et al.* Nonsteroidal anti-inflammatory drugs and peroxisome proliferator-activated receptor-gamma agonists modulate immunostimulated processing of amyloid precursor protein through regulation of beta-secretase. *J Neurosci* **23**, 9796-9804, doi:10.1523/jneurosci.23-30-09796.2003 (2003).
- 134 Yang, J., Wise, L. & Fukuchi, K. I. TLR4 Cross-Talk With NLRP3 Inflammasome and Complement Signaling Pathways in Alzheimer's Disease. *Front Immunol* **11**, 724, doi:10.3389/fimmu.2020.00724 (2020).
- 135 Gorecki, A. M., Anyaegbu, C. C. & Anderton, R. S. TLR2 and TLR4 in Parkinson's disease pathogenesis: the environment takes a toll on the gut. *Transl Neurodegener* **10**, 47, doi:10.1186/s40035-021-00271-0 (2021).
- 136 Paudel, Y. N. *et al.* Impact of HMGB1, RAGE, and TLR4 in Alzheimer's Disease (AD): From Risk Factors to Therapeutic Targeting. *Cells* **9**, doi:10.3390/cells9020383 (2020).
- 137 Gale, S. C. *et al.* APO ϵ 4 is associated with enhanced in vivo innate immune responses in human subjects. *J Allergy Clin Immunol* **134**, 127-134, doi:10.1016/j.jaci.2014.01.032 (2014).
- 138 Zakaria, R. *et al.* Lipopolysaccharide-induced memory impairment in rats: a model of Alzheimer's disease. *Physiol Res* **66**, 553-565, doi:10.33549/physiolres.933480 (2017).
- 139 Fink, M. P. Animal models of sepsis. *Virulence* **5**, 143-153, doi:10.4161/viru.26083 (2014).
- 140 Zhu, B. *et al.* Chronic lipopolysaccharide exposure induces cognitive dysfunction without affecting BDNF expression in the rat hippocampus. *Exp Ther Med* **7**, 750-754, doi:10.3892/etm.2014.1479 (2014).
- 141 Qin, L., Liu, Y., Hong, J. S. & Crews, F. T. NADPH oxidase and aging drive microglial activation, oxidative stress, and dopaminergic neurodegeneration following systemic LPS administration. *Glia* **61**, 855-868 (2013).
- 142 Qin, L. *et al.* Systemic LPS causes chronic neuroinflammation and progressive neurodegeneration. *Glia* **55**, 453-462 (2007).
- 143 Tufekci, K. U., Genc, S. & Genc, K. The endotoxin-induced neuroinflammation model of Parkinson's disease. *Parkinson's disease* **2011** (2011).
- 144 Zakaria, R. *et al.* Lipopolysaccharide-induced memory impairment in rats: a model of Alzheimer's disease. *Physiological research* **66** (2017).
- 145 Couch, Y., Alvarez-Erviti, L., Sibson, N. R., Wood, M. J. & Anthony, D. C. The acute inflammatory response to intranigral α -synuclein differs significantly from intranigral lipopolysaccharide and is exacerbated by peripheral inflammation. *Journal of neuroinflammation* **8**, 1-14 (2011).
- 146 Rangaraju, S. *et al.* Quantitative proteomics of acutely-isolated mouse microglia identifies novel immune Alzheimer's disease-related proteins. *Mol Neurodegener* **13**, 34, doi:10.1186/s13024-018-0266-4 (2018).
- 147 Rangaraju, S. *et al.* Identification and therapeutic modulation of a pro-inflammatory subset of disease-associated-microglia in Alzheimer's disease. *Molecular Neurodegeneration* **13**, 24, doi:10.1186/s13024-018-0254-8 (2018).
- 148 McGeer, P., Itagaki, S., Tago, H. & McGeer, E. Occurrence of HLA-DR reactive microglia in Alzheimer's disease. *Annals of the New York Academy of Sciences* **540**, 319-323 (1988).
- 149 Rogers, J., Lubert-Narod, J., Styren, S. D. & Civin, W. H. Expression of immune system-associated antigens by cells of the human central nervous system: relationship to the pathology of Alzheimer's disease. *Neurobiol Aging* **9**, 339-349, doi:10.1016/s0197-4580(88)80079-4 (1988).

- 150 Colonna, M. & Butovsky, O. Microglia function in the central nervous system during health and neurodegeneration. *Annual review of immunology* **35**, 441-468 (2017).
- 151 Stevens, B. *et al.* The classical complement cascade mediates CNS synapse elimination. *Cell* **131**, 1164-1178, doi:10.1016/j.cell.2007.10.036 (2007).
- 152 Crapser, J. D., Arreola, M. A., Tsourmas, K. I. & Green, K. N. Microglia as hackers of the matrix: sculpting synapses and the extracellular space. *Cell Mol Immunol* **18**, 2472-2488, doi:10.1038/s41423-021-00751-3 (2021).
- 153 Penfield, W. *Cytology & Cellular Pathology of the Nervous System*. Vol. 2 (PB Hoeber, Incorporated, 1932).
- 154 Ling, E. A., Ng, Y. K., Wu, C. H. & Kaur, C. Microglia: its development and role as a neuropathology sensor. *Prog Brain Res* **132**, 61-79, doi:10.1016/s0079-6123(01)32066-6 (2001).
- 155 Hanisch, U. K. Microglia as a source and target of cytokines. *Glia* **40**, 140-155, doi:10.1002/glia.10161 (2002).
- 156 Heppner, F. L., Prinz, M. & Aguzzi, A. in *Progress in Brain Research* Vol. 132 737-750 (Elsevier, 2001).
- 157 Keren-Shaul, H. *et al.* A Unique Microglia Type Associated with Restricting Development of Alzheimer's Disease. *Cell* **169**, 1276-1290.e1217, doi:10.1016/j.cell.2017.05.018 (2017).
- 158 Lawson, L. J., Perry, V. H. & Gordon, S. Turnover of resident microglia in the normal adult mouse brain. *Neuroscience* **48**, 405-415, doi:10.1016/0306-4522(92)90500-2 (1992).
- 159 Lawson, L. J., Perry, V. H., Dri, P. & Gordon, S. Heterogeneity in the distribution and morphology of microglia in the normal adult mouse brain. *Neuroscience* **39**, 151-170, doi:10.1016/0306-4522(90)90229-w (1990).
- 160 Ginhoux, F. *et al.* Fate mapping analysis reveals that adult microglia derive from primitive macrophages. *Science* **330**, 841-845, doi:10.1126/science.1194637 (2010).
- 161 Hickman, S., Izzy, S., Sen, P., Morsett, L. & El Khoury, J. Microglia in neurodegeneration. *Nat Neurosci* **21**, 1359-1369, doi:10.1038/s41593-018-0242-x (2018).
- 162 Luo, X. G., Ding, J. Q. & Chen, S. D. Microglia in the aging brain: relevance to neurodegeneration. *Mol Neurodegener* **5**, 12, doi:10.1186/1750-1326-5-12 (2010).
- 163 Lambert, J. C. *et al.* Meta-analysis of 74,046 individuals identifies 11 new susceptibility loci for Alzheimer's disease. *Nat Genet* **45**, 1452-1458, doi:10.1038/ng.2802 (2013).
- 164 Lambert, J. C. *et al.* Genome-wide association study identifies variants at CLU and CR1 associated with Alzheimer's disease. *Nat Genet* **41**, 1094-1099, doi:10.1038/ng.439 (2009).
- 165 Hollingworth, P. *et al.* Common variants at ABCA7, MS4A6A/MS4A4E, EPHA1, CD33 and CD2AP are associated with Alzheimer's disease. *Nat Genet* **43**, 429-435, doi:10.1038/ng.803 (2011).
- 166 Harold, D. *et al.* Genome-wide association study identifies variants at CLU and PICALM associated with Alzheimer's disease. *Nat Genet* **41**, 1088-1093, doi:10.1038/ng.440 (2009).
- 167 Jansen, I. E. *et al.* Genome-wide meta-analysis identifies new loci and functional pathways influencing Alzheimer's disease risk. *Nat Genet* **51**, 404-413, doi:10.1038/s41588-018-0311-9 (2019).
- 168 Naj, A. C. *et al.* Common variants at MS4A4/MS4A6E, CD2AP, CD33 and EPHA1 are associated with late-onset Alzheimer's disease. *Nat Genet* **43**, 436-441, doi:10.1038/ng.801 (2011).
- 169 Efthymiou, A. G. & Goate, A. M. Late onset Alzheimer's disease genetics implicates microglial pathways in disease risk. *Mol Neurodegener* **12**, 43, doi:10.1186/s13024-017-0184-x (2017).
- 170 Masuda, T., Sankowski, R., Staszewski, O. & Prinz, M. Microglia Heterogeneity in the Single-Cell Era. *Cell Rep* **30**, 1271-1281, doi:10.1016/j.celrep.2020.01.010 (2020).

- 171 Mittelbronn, M., Dietz, K., Schluesener, H. J. & Meyermann, R. Local distribution of microglia in the normal adult human central nervous system differs by up to one order of magnitude. *Acta Neuropathol* **101**, 249-255, doi:10.1007/s004010000284 (2001).
- 172 Kloske, C. M. & Wilcock, D. M. The Important Interface Between Apolipoprotein E and Neuroinflammation in Alzheimer's Disease. *Front Immunol* **11**, 754, doi:10.3389/fimmu.2020.00754 (2020).
- 173 Shi, Y. & Holtzman, D. M. Interplay between innate immunity and Alzheimer disease: APOE and TREM2 in the spotlight. *Nat Rev Immunol* **18**, 759-772, doi:10.1038/s41577-018-0051-1 (2018).
- 174 Bottcher, C. *et al.* Human microglia regional heterogeneity and phenotypes determined by multiplexed single-cell mass cytometry. *Nat Neurosci* **22**, 78-90, doi:10.1038/s41593-018-0290-2 (2019).
- 175 Corder, E. H. *et al.* Gene dose of apolipoprotein E type 4 allele and the risk of Alzheimer's disease in late onset families. *Science* **261**, 921-923, doi:10.1126/science.8346443 (1993).
- 176 Guerreiro, R. J., Gustafson, D. R. & Hardy, J. The genetic architecture of Alzheimer's disease: beyond APP, PSENs and APOE. *Neurobiol Aging* **33**, 437-456, doi:10.1016/j.neurobiolaging.2010.03.025 (2012).
- 177 Karch, C. M. & Goate, A. M. Alzheimer's disease risk genes and mechanisms of disease pathogenesis. *Biol Psychiatry* **77**, 43-51, doi:10.1016/j.biopsych.2014.05.006 (2015).
- 178 Gratuze, M., Leyns, C. E. G. & Holtzman, D. M. New insights into the role of TREM2 in Alzheimer's disease. *Mol Neurodegener* **13**, 66, doi:10.1186/s13024-018-0298-9 (2018).
- 179 Ulland, T. K. *et al.* TREM2 Maintains Microglial Metabolic Fitness in Alzheimer's Disease. *Cell* **170**, 649-663 e613, doi:10.1016/j.cell.2017.07.023 (2017).
- 180 Ulrich, J. D., Ulland, T. K., Colonna, M. & Holtzman, D. M. Elucidating the Role of TREM2 in Alzheimer's Disease. *Neuron* **94**, 237-248, doi:10.1016/j.neuron.2017.02.042 (2017).
- 181 Guerreiro, R. *et al.* TREM2 variants in Alzheimer's disease. *N Engl J Med* **368**, 117-127, doi:10.1056/NEJMoa1211851 (2013).
- 182 Jonsson, T. *et al.* Variant of TREM2 associated with the risk of Alzheimer's disease. *N Engl J Med* **368**, 107-116, doi:10.1056/NEJMoa1211103 (2013).
- 183 Krasemann, S. *et al.* The TREM2-APOE Pathway Drives the Transcriptional Phenotype of Dysfunctional Microglia in Neurodegenerative Diseases. *Immunity* **47**, 566-581.e569, doi:10.1016/j.immuni.2017.08.008 (2017).
- 184 Wang, Y. *et al.* TREM2-mediated early microglial response limits diffusion and toxicity of amyloid plaques. *J Exp Med* **213**, 667-675, doi:10.1084/jem.20151948 (2016).
- 185 Zhu, B. *et al.* Trem2 deletion enhances tau dispersion and pathology through microglia exosomes. *Mol Neurodegener* **17**, 58, doi:10.1186/s13024-022-00562-8 (2022).
- 186 Fitz, N. F. *et al.* Phospholipids of APOE lipoproteins activate microglia in an isoform-specific manner in preclinical models of Alzheimer's disease. *Nat Commun* **12**, 3416, doi:10.1038/s41467-021-23762-0 (2021).
- 187 Keren-Shaul, H. *et al.* A Unique Microglia Type Associated with Restricting Development of Alzheimer's Disease. *Cell* **169**, 1276-1290.e1217, doi:10.1016/j.cell.2017.05.018 (2017).
- 188 Paolicelli, R. C. *et al.* Microglia states and nomenclature: A field at its crossroads. *Neuron* **110**, 3458-3483, doi:10.1016/j.neuron.2022.10.020 (2022).
- 189 Chen, Y. & Colonna, M. Microglia in Alzheimer's disease at single-cell level. Are there common patterns in humans and mice? *J Exp Med* **218**, doi:10.1084/jem.20202717 (2021).
- 190 Deczkowska, A. *et al.* Disease-Associated Microglia: A Universal Immune Sensor of Neurodegeneration. *Cell* **173**, 1073-1081, doi:10.1016/j.cell.2018.05.003 (2018).

- 191 Spurgat, M. S. & Tang, S. J. Single-Cell RNA-Sequencing: Astrocyte and Microglial Heterogeneity
in Health and Disease. *Cells* **11**, doi:10.3390/cells11132021 (2022).
- 192 Mathys, H. *et al.* Single-cell transcriptomic analysis of Alzheimer's disease. *Nature* **570**, 332-337,
doi:10.1038/s41586-019-1195-2 (2019).
- 193 Zhou, Y. *et al.* Human and mouse single-nucleus transcriptomics reveal TREM2-dependent and
TREM2-independent cellular responses in Alzheimer's disease. *Nat Med* **26**, 131-142,
doi:10.1038/s41591-019-0695-9 (2020).
- 194 Del-Aguila, J. L. *et al.* A single-nuclei RNA sequencing study of Mendelian and sporadic AD in the
human brain. *Alzheimers Res Ther* **11**, 71, doi:10.1186/s13195-019-0524-x (2019).
- 195 Geirsdottir, L. *et al.* Cross-Species Single-Cell Analysis Reveals Divergence of the Primate
Microglia Program. *Cell* **181**, 746, doi:10.1016/j.cell.2020.04.002 (2020).
- 196 Olah, M. *et al.* Single cell RNA sequencing of human microglia uncovers a subset associated with
Alzheimer's disease. *Nat Commun* **11**, 6129, doi:10.1038/s41467-020-19737-2 (2020).
- 197 Srinivasan, K. *et al.* Alzheimer's Patient Microglia Exhibit Enhanced Aging and Unique
Transcriptional Activation. *Cell Rep* **31**, 107843, doi:10.1016/j.celrep.2020.107843 (2020).
- 198 Council, N. R. *Guide for the Care and Use of Laboratory Animals: Eighth Edition.* (The National
Academies Press, 2011).
- 199 Thrupp, N. *et al.* Single-Nucleus RNA-Seq Is Not Suitable for Detection of Microglial Activation
Genes in Humans. *Cell Rep* **32**, 108189, doi:10.1016/j.celrep.2020.108189 (2020).
- 200 Geirsdottir, L. *et al.* Cross-Species Single-Cell Analysis Reveals Divergence of the Primate
Microglia Program. *Cell* **179**, 1609-1622.e1616, doi:10.1016/j.cell.2019.11.010 (2019).
- 201 Graves, P. R. & Haystead, T. A. J. Molecular Biologist's Guide to Proteomics. *Microbiology and
Molecular Biology Reviews* **66**, 39-63, doi:doi:10.1128/MMBR.66.1.39-63.2002 (2002).
- 202 Hickman, S. E. *et al.* The microglial sensome revealed by direct RNA sequencing. *Nat Neurosci*
16, 1896-1905, doi:10.1038/nn.3554 (2013).
- 203 Chidambaram, H., Das, R. & Chinnathambi, S. Interaction of Tau with the chemokine receptor,
CX3CR1 and its effect on microglial activation, migration and proliferation. *Cell & Bioscience* **10**,
109, doi:10.1186/s13578-020-00474-4 (2020).
- 204 Bolós, M. *et al.* Absence of CX3CR1 impairs the internalization of Tau by microglia. *Mol
Neurodegener* **12**, 59, doi:10.1186/s13024-017-0200-1 (2017).
- 205 Zhang, Y. *et al.* Purification and Characterization of Progenitor and Mature Human Astrocytes
Reveals Transcriptional and Functional Differences with Mouse. *Neuron* **89**, 37-53,
doi:10.1016/j.neuron.2015.11.013 (2016).
- 206 Wang, Y. *et al.* TREM2 lipid sensing sustains the microglial response in an Alzheimer's disease
model. *Cell* **160**, 1061-1071, doi:10.1016/j.cell.2015.01.049 (2015).
- 207 Yeh, F. L., Wang, Y., Tom, I., Gonzalez, L. C. & Sheng, M. TREM2 Binds to Apolipoproteins,
Including APOE and CLU/APOJ, and Thereby Facilitates Uptake of Amyloid-Beta by Microglia.
Neuron **91**, 328-340, doi:10.1016/j.neuron.2016.06.015 (2016).
- 208 Atagi, Y. *et al.* Apolipoprotein E Is a Ligand for Triggering Receptor Expressed on Myeloid Cells 2
(TREM2). *J Biol Chem* **290**, 26043-26050, doi:10.1074/jbc.M115.679043 (2015).
- 209 Zhao, Y. *et al.* TREM2 Is a Receptor for beta-Amyloid that Mediates Microglial Function. *Neuron*
97, 1023-1031 e1027, doi:10.1016/j.neuron.2018.01.031 (2018).
- 210 Takahashi, K., Rochford, C. D. & Neumann, H. Clearance of apoptotic neurons without
inflammation by microglial triggering receptor expressed on myeloid cells-2. *J Exp Med* **201**, 647-
657, doi:10.1084/jem.20041611 (2005).
- 211 Konishi, H. & Kiyama, H. Microglial TREM2/DAP12 Signaling: A Double-Edged Sword in Neural
Diseases. *Front Cell Neurosci* **12**, 206, doi:10.3389/fncel.2018.00206 (2018).

- 212 Haure-Mirande, J. V., Audrain, M., Ehrlich, M. E. & Gandy, S. Microglial TYROBP/DAP12 in
Alzheimer's disease: Transduction of physiological and pathological signals across TREM2. *Mol*
Neurodegener **17**, 55, doi:10.1186/s13024-022-00552-w (2022).
- 213 Wang, S. *et al.* TREM2 drives microglia response to amyloid- β ; via SYK-dependent and -
independent pathways. *Cell* **185**, 4153-4169.e4119, doi:10.1016/j.cell.2022.09.033 (2022).
- 214 Peng, Q. *et al.* TREM2- and DAP12-dependent activation of PI3K requires DAP10 and is inhibited
by SHIP1. *Sci Signal* **3**, ra38, doi:10.1126/scisignal.2000500 (2010).
- 215 Zou, Z., Tao, T., Li, H. & Zhu, X. mTOR signaling pathway and mTOR inhibitors in cancer: progress
and challenges. *Cell & Bioscience* **10**, 31, doi:10.1186/s13578-020-00396-1 (2020).
- 216 Kim, E. K. & Choi, E. J. Pathological roles of MAPK signaling pathways in human diseases. *Biochim*
Biophys Acta **1802**, 396-405, doi:10.1016/j.bbadis.2009.12.009 (2010).
- 217 Chen, M. J. *et al.* Extracellular signal-regulated kinase regulates microglial immune responses in
Alzheimer's disease. *J Neurosci Res* **99**, 1704-1721, doi:10.1002/jnr.24829 (2021).
- 218 Johnson, E. C. B. *et al.* Large-scale deep multi-layer analysis of Alzheimer's disease brain reveals
strong proteomic disease-related changes not observed at the RNA level. *Nat Neurosci* **25**, 213-
225, doi:10.1038/s41593-021-00999-y (2022).
- 219 Seyfried, N. T. *et al.* A Multi-network Approach Identifies Protein-Specific Co-expression in
Asymptomatic and Symptomatic Alzheimer's Disease. *Cell Syst* **4**, 60-72 e64,
doi:10.1016/j.cels.2016.11.006 (2017).
- 220 Johnson, E. C. B. *et al.* Large-scale deep multi-layer analysis of Alzheimer's disease brain reveals
strong proteomic disease-related changes not observed at the RNA level. *Nature Neuroscience*
25, 213-225, doi:10.1038/s41593-021-00999-y (2022).
- 221 Mahdessian, D. *et al.* Spatiotemporal dissection of the cell cycle with single-cell proteogenomics.
Nature **590**, 649-654, doi:10.1038/s41586-021-03232-9 (2021).
- 222 Specht, H. *et al.* Single-cell proteomic and transcriptomic analysis of macrophage heterogeneity
using SCoPE2. *Genome Biology* **22**, 50, doi:10.1186/s13059-021-02267-5 (2021).
- 223 Buccitelli, C. & Selbach, M. mRNAs, proteins and the emerging principles of gene expression
control. *Nature Reviews Genetics* **21**, 630-644, doi:10.1038/s41576-020-0258-4 (2020).
- 224 Slavov, N. Scaling Up Single-Cell Proteomics. *Mol Cell Proteomics* **21**, 100179,
doi:10.1016/j.mcpro.2021.100179 (2022).
- 225 Matejuk, A. & Ransohoff, R. M. Crosstalk Between Astrocytes and Microglia: An Overview.
Frontiers in Immunology **11**, doi:10.3389/fimmu.2020.01416 (2020).
- 226 Vainchtein, I. D. & Molofsky, A. V. Astrocytes and Microglia: In Sickness and in Health. *Trends in*
Neurosciences **43**, 144-154, doi:10.1016/j.tins.2020.01.003 (2020).
- 227 Liddelow, S. A. *et al.* Neurotoxic reactive astrocytes are induced by activated microglia. *Nature*
541, 481-487, doi:10.1038/nature21029 (2017).
- 228 Barbierato, M. *et al.* Astrocyte-microglia cooperation in the expression of a pro-inflammatory
phenotype. *CNS Neurol Disord Drug Targets* **12**, 608-618, doi:10.2174/18715273113129990064
(2013).
- 229 Facci, L. *et al.* Toll-like receptors 2, -3 and -4 prime microglia but not astrocytes across central
nervous system regions for ATP-dependent interleukin-1 β release. *Sci Rep* **4**, 6824,
doi:10.1038/srep06824 (2014).
- 230 Schartz, N. D. & Tenner, A. J. The good, the bad, and the opportunities of the complement
system in neurodegenerative disease. *J Neuroinflammation* **17**, 354, doi:10.1186/s12974-020-
02024-8 (2020).
- 231 Schafer, D. P. *et al.* Microglia sculpt postnatal neural circuits in an activity and complement-
dependent manner. *Neuron* **74**, 691-705, doi:10.1016/j.neuron.2012.03.026 (2012).

- 232 Lehrman, E. K. *et al.* CD47 Protects Synapses from Excess Microglia-Mediated Pruning during
Development. *Neuron* **100**, 120-134.e126, doi:10.1016/j.neuron.2018.09.017 (2018).
- 233 Shi, Q. *et al.* Complement C3 deficiency protects against neurodegeneration in aged plaque-rich
APP/PS1 mice. *Sci Transl Med* **9**, doi:10.1126/scitranslmed.aaf6295 (2017).
- 234 Dejanovic, B. *et al.* Changes in the Synaptic Proteome in Tauopathy and Rescue of Tau-Induced
Synapse Loss by C1q Antibodies. *Neuron* **100**, 1322-1336 e1327,
doi:10.1016/j.neuron.2018.10.014 (2018).
- 235 Hong, S. *et al.* Complement and microglia mediate early synapse loss in Alzheimer mouse
models. *Science* **352**, 712-716, doi:10.1126/science.aad8373 (2016).
- 236 Wu, T. *et al.* Complement C3 Is Activated in Human AD Brain and Is Required for
Neurodegeneration in Mouse Models of Amyloidosis and Tauopathy. *Cell Rep* **28**, 2111-
2123.e2116, doi:10.1016/j.celrep.2019.07.060 (2019).
- 237 Bai, B. *et al.* Deep Multilayer Brain Proteomics Identifies Molecular Networks in Alzheimer's
Disease Progression. *Neuron* **105**, 975-991.e977, doi:10.1016/j.neuron.2019.12.015 (2020).
- 238 Doens, D. & Fernandez, P. L. Microglia receptors and their implications in the response to
amyloid beta for Alzheimer's disease pathogenesis. *J Neuroinflammation* **11**, 48,
doi:10.1186/1742-2094-11-48 (2014).
- 239 Rangaraju, S. *et al.* Identification and therapeutic modulation of a pro-inflammatory subset of
disease-associated-microglia in Alzheimer's disease. *Mol Neurodegener* **13**, 24,
doi:10.1186/s13024-018-0254-8 (2018).
- 240 Seyfried, N. T. *et al.* A Multi-network Approach Identifies Protein-Specific Co-expression in
Asymptomatic and Symptomatic Alzheimer's Disease. *Cell Systems* **4**, 60-72.e64,
doi:<https://doi.org/10.1016/j.cels.2016.11.006> (2017).
- 241 Higginbotham, L. *et al.* Integrated proteomics reveals brain-based cerebrospinal fluid
biomarkers in asymptomatic and symptomatic Alzheimer's disease. *Sci Adv* **6**,
doi:10.1126/sciadv.aaz9360 (2020).
- 242 Vogel, C. & Marcotte, E. M. Insights into the regulation of protein abundance from proteomic
and transcriptomic analyses. *Nat Rev Genet* **13**, 227-232, doi:10.1038/nrg3185 (2012).
- 243 Sharma, K. *et al.* Cell type- and brain region-resolved mouse brain proteome. *Nat Neurosci* **18**,
1819-1831, doi:10.1038/nn.4160 (2015).
- 244 Rayaprolu, S. *et al.* Systems-based proteomics to resolve the biology of Alzheimer's disease
beyond amyloid and tau. *Neuropsychopharmacology* **46**, 98-115, doi:10.1038/s41386-020-
00840-3 (2021).
- 245 Johnson, E. C. B. *et al.* Large-scale proteomic analysis of Alzheimer's disease brain and
cerebrospinal fluid reveals early changes in energy metabolism associated with microglia and
astrocyte activation. *Nat Med* **26**, 769-780, doi:10.1038/s41591-020-0815-6 (2020).
- 246 Warburg, O. On respiratory impairment in cancer cells. *Science* **124**, 269-270 (1956).
- 247 Vander Heiden, M. G., Cantley, L. C. & Thompson, C. B. Understanding the Warburg effect: the
metabolic requirements of cell proliferation. *Science* **324**, 1029-1033,
doi:10.1126/science.1160809 (2009).
- 248 Griffin, J. L. & Shockcor, J. P. Metabolic profiles of cancer cells. *Nature reviews cancer* **4**, 551-561
(2004).
- 249 Arnold, S. E. *et al.* Brain insulin resistance in type 2 diabetes and Alzheimer disease: concepts
and conundrums. *Nat Rev Neurol* **14**, 168-181, doi:10.1038/nrneurol.2017.185 (2018).
- 250 Lee, S., Tong, M., Hang, S., Deochand, C. & de la Monte, S. CSF and Brain Indices of Insulin
Resistance, Oxidative Stress and Neuro-Inflammation in Early versus Late Alzheimer's Disease. *J
Alzheimers Dis Parkinsonism* **3**, 128, doi:10.4172/2161-0460.1000128 (2013).

- 251 Moloudizargari, M. *et al.* NLRP inflammasome as a key role player in the pathogenesis of environmental toxicants. *Life Sciences* **231**, 116585, doi:<https://doi.org/10.1016/j.lfs.2019.116585> (2019).
- 252 Hanslik, K. L. & Ulland, T. K. The Role of Microglia and the Nlrp3 Inflammasome in Alzheimer's Disease. *Front Neurol* **11**, 570711, doi:10.3389/fneur.2020.570711 (2020).
- 253 Venegas, C. *et al.* Microglia-derived ASC specks cross-seed amyloid- β in Alzheimer's disease. *Nature* **552**, 355-361, doi:10.1038/nature25158 (2017).
- 254 Ising, C. *et al.* NLRP3 inflammasome activation drives tau pathology. *Nature* **575**, 669-673, doi:10.1038/s41586-019-1769-z (2019).
- 255 Stancu, I. C. *et al.* Aggregated Tau activates NLRP3-ASC inflammasome exacerbating exogenously seeded and non-exogenously seeded Tau pathology in vivo. *Acta Neuropathol* **137**, 599-617, doi:10.1007/s00401-018-01957-y (2019).
- 256 Tan, M. S. *et al.* Amyloid- β induces NLRP1-dependent neuronal pyroptosis in models of Alzheimer's disease. *Cell Death Dis* **5**, e1382, doi:10.1038/cddis.2014.348 (2014).
- 257 Denes, A. *et al.* AIM2 and NLRC4 inflammasomes contribute with ASC to acute brain injury independently of NLRP3. *Proc Natl Acad Sci U S A* **112**, 4050-4055, doi:10.1073/pnas.1419090112 (2015).
- 258 Johnson, E. C. B. *et al.* Large-scale proteomic analysis of Alzheimer's disease brain and cerebrospinal fluid reveals early changes in energy metabolism associated with microglia and astrocyte activation. *Nature Medicine* **26**, 769-780, doi:10.1038/s41591-020-0815-6 (2020).
- 259 Swanson, K. V., Deng, M. & Ting, J. P. Y. The NLRP3 inflammasome: molecular activation and regulation to therapeutics. *Nature Reviews Immunology* **19**, 477-489, doi:10.1038/s41577-019-0165-0 (2019).
- 260 Meissner, F., Molawi, K. & Zychlinsky, A. Superoxide dismutase 1 regulates caspase-1 and endotoxic shock. *Nat Immunol* **9**, 866-872, doi:10.1038/ni.1633 (2008).
- 261 Kuwar, R. *et al.* A Novel Inhibitor Targeting NLRP3 Inflammasome Reduces Neuropathology and Improves Cognitive Function in Alzheimer's Disease Transgenic Mice. *J Alzheimers Dis* **82**, 1769-1783, doi:10.3233/jad-210400 (2021).
- 262 Magdalon, J. *et al.* Complement System in Brain Architecture and Neurodevelopmental Disorders. *Frontiers in Neuroscience* **14**, doi:10.3389/fnins.2020.00023 (2020).
- 263 Andoh, M. & Koyama, R. Microglia regulate synaptic development and plasticity. *Developmental Neurobiology* **81**, 568-590, doi:<https://doi.org/10.1002/dneu.22814> (2021).
- 264 Litvinchuk, A. *et al.* Complement C3aR Inactivation Attenuates Tau Pathology and Reverses an Immune Network Deregulated in Tauopathy Models and Alzheimer's Disease. *Neuron* **100**, 1337-1353.e1335, doi:10.1016/j.neuron.2018.10.031 (2018).
- 265 Shi, Q. *et al.* Complement C3-Deficient Mice Fail to Display Age-Related Hippocampal Decline. *J Neurosci* **35**, 13029-13042, doi:10.1523/jneurosci.1698-15.2015 (2015).
- 266 Bai, B. *et al.* U1 small nuclear ribonucleoprotein complex and RNA splicing alterations in Alzheimer's disease. *Proceedings of the National Academy of Sciences* **110**, 16562-16567, doi:10.1073/pnas.1310249110 (2013).
- 267 Bai, B. *et al.* Deep Multilayer Brain Proteomics Identifies Molecular Networks in Alzheimer's Disease Progression. *Neuron* **106**, 700, doi:10.1016/j.neuron.2020.04.031 (2020).
- 268 Subramanian, J., Savage, J. C. & Tremblay, M.-È. Synaptic Loss in Alzheimer's Disease: Mechanistic Insights Provided by Two-Photon in vivo Imaging of Transgenic Mouse Models. *Frontiers in Cellular Neuroscience* **14**, doi:10.3389/fncel.2020.592607 (2020).

- 269 de Wilde, M. C., Overk, C. R., Sijben, J. W. & Masliah, E. Meta-analysis of synaptic pathology in Alzheimer's disease reveals selective molecular vesicular machinery vulnerability. *Alzheimer's & Dementia* **12**, 633-644, doi:<https://doi.org/10.1016/j.jalz.2015.12.005> (2016).
- 270 Oakley, H. *et al.* Intraneuronal beta-amyloid aggregates, neurodegeneration, and neuron loss in transgenic mice with five familial Alzheimer's disease mutations: potential factors in amyloid plaque formation. *J Neurosci* **26**, 10129-10140, doi:10.1523/jneurosci.1202-06.2006 (2006).
- 271 Neuman, K. M. *et al.* Evidence for Alzheimer's disease-linked synapse loss and compensation in mouse and human hippocampal CA1 pyramidal neurons. *Brain Struct Funct* **220**, 3143-3165, doi:10.1007/s00429-014-0848-z (2015).
- 272 Buskila, Y., Crowe, S. E. & Ellis-Davies, G. C. Synaptic deficits in layer 5 neurons precede overt structural decay in 5xFAD mice. *Neuroscience* **254**, 152-159, doi:10.1016/j.neuroscience.2013.09.016 (2013).
- 273 Seo, N. Y. *et al.* Selective Regional Loss of Cortical Synapses Lacking Presynaptic Mitochondria in the 5xFAD Mouse Model. *Front Neuroanat* **15**, 690168, doi:10.3389/fnana.2021.690168 (2021).
- 274 Ramesha, S., Rayaprolu, S. & Rangaraju, S. Flow Cytometry Approach to Characterize Phagocytic Properties of Acutely-Isolated Adult Microglia and Brain Macrophages In Vitro. *J Vis Exp*, doi:10.3791/61467 (2020).
- 275 Rangaraju, S. *et al.* Quantitative proteomics of acutely-isolated mouse microglia identifies novel immune Alzheimer's disease-related proteins. *Molecular Neurodegeneration* **13**, 34, doi:10.1186/s13024-018-0266-4 (2018).
- 276 Rayaprolu, S. *et al.* Flow-cytometric microglial sorting coupled with quantitative proteomics identifies moesin as a highly-abundant microglial protein with relevance to Alzheimer's disease. *Mol Neurodegener* **15**, 28, doi:10.1186/s13024-020-00377-5 (2020).
- 277 Bohlen, C. J., Bennett, F. C. & Bennett, M. L. Isolation and Culture of Microglia. *Curr Protoc Immunol* **125**, e70, doi:10.1002/cpim.70 (2019).
- 278 Nolle, A. *et al.* Enrichment of Glial Cells From Human Post-mortem Tissue for Transcriptome and Proteome Analysis Using Immunopanning. *Front Cell Neurosci* **15**, 772011, doi:10.3389/fncel.2021.772011 (2021).
- 279 Mizee, M. R. *et al.* Isolation of primary microglia from the human post-mortem brain: effects of ante- and post-mortem variables. *Acta Neuropathologica Communications* **5**, 16, doi:10.1186/s40478-017-0418-8 (2017).
- 280 Crotti, A. & Ransohoff, R. M. Microglial Physiology and Pathophysiology: Insights from Genome-wide Transcriptional Profiling. *Immunity* **44**, 505-515, doi:10.1016/j.immuni.2016.02.013 (2016).
- 281 Hickman, S. E. *et al.* The microglial sensome revealed by direct RNA sequencing. *Nature Neuroscience* **16**, 1896-1905, doi:10.1038/nn.3554 (2013).
- 282 Bennett, M. L. *et al.* New tools for studying microglia in the mouse and human CNS. *Proceedings of the National Academy of Sciences* **113**, E1738-E1746, doi:10.1073/pnas.1525528113 (2016).
- 283 El Khoury, J. *et al.* Ccr2 deficiency impairs microglial accumulation and accelerates progression of Alzheimer-like disease. *Nature Medicine* **13**, 432-438, doi:10.1038/nm1555 (2007).
- 284 Rangaraju, S. *et al.* Differential Phagocytic Properties of CD45low Microglia and CD45high Brain Mononuclear Phagocytes—Activation and Age-Related Effects. *Frontiers in Immunology* **9**, doi:10.3389/fimmu.2018.00405 (2018).
- 285 Pan, J. & Wan, J. Methodological comparison of FACS and MACS isolation of enriched microglia and astrocytes from mouse brain. *Journal of Immunological Methods* **486**, 112834, doi:<https://doi.org/10.1016/j.jim.2020.112834> (2020).
- 286 Kang, S. S. *et al.* Microglial translational profiling reveals a convergent APOE pathway from aging, amyloid, and tau. *J Exp Med* **215**, 2235-2245, doi:10.1084/jem.20180653 (2018).

- 287 Swartzlander, D. B. *et al.* Concurrent cell type-specific isolation and profiling of mouse brains in inflammation and Alzheimer's disease. *JCI Insight* **3**, doi:10.1172/jci.insight.121109 (2018).
- 288 Sutermeister, B. A. & Darling, E. M. Considerations for high-yield, high-throughput cell enrichment: fluorescence versus magnetic sorting. *Scientific Reports* **9**, 227, doi:10.1038/s41598-018-36698-1 (2019).
- 289 Guerreiro, R. & Bras, J. The age factor in Alzheimer's disease. *Genome Med* **7**, 106, doi:10.1186/s13073-015-0232-5 (2015).
- 290 Flowers, A., Bell-Temin, H., Jalloh, A., Stevens, S. M., Jr. & Bickford, P. C. Proteomic analysis of aged microglia: shifts in transcription, bioenergetics, and nutrient response. *J Neuroinflammation* **14**, 96, doi:10.1186/s12974-017-0840-7 (2017).
- 291 Byles, V. *et al.* The TSC-mTOR pathway regulates macrophage polarization. *Nature Communications* **4**, 2834, doi:10.1038/ncomms3834 (2013).
- 292 Bracho-Valdés, I. *et al.* mTORC1- and mTORC2-interacting proteins keep their multifunctional partners focused. *IUBMB Life* **63**, 896-914, doi:<https://doi.org/10.1002/iub.558> (2011).
- 293 Godbout, J. P. *et al.* Exaggerated neuroinflammation and sickness behavior in aged mice following activation of the peripheral innate immune system. *Faseb j* **19**, 1329-1331, doi:10.1096/fj.05-3776fje (2005).
- 294 Sierra, A., Gottfried-Blackmore, A. C., McEwen, B. S. & Bulloch, K. Microglia derived from aging mice exhibit an altered inflammatory profile. *Glia* **55**, 412-424, doi:10.1002/glia.20468 (2007).
- 295 Sheng, J. G., Mrak, R. E. & Griffin, W. Enlarged and phagocytic, but not primed, interleukin-1 α - immunoreactive microglia increase with age in normal human brain. *Acta neuropathologica* **95**, 229-234 (1998).
- 296 Damani, M. R. *et al.* Age-related alterations in the dynamic behavior of microglia. *Aging cell* **10**, 263-276 (2011).
- 297 Tremblay, M. È., Zettel, M. L., Ison, J. R., Allen, P. D. & Majewska, A. K. Effects of aging and sensory loss on glial cells in mouse visual and auditory cortices. *Glia* **60**, 541-558 (2012).
- 298 Gomez-Nicola, D. & Boche, D. Post-mortem analysis of neuroinflammatory changes in human Alzheimer's disease. *Alzheimer's research & therapy* **7**, 1-8 (2015).
- 299 Sudduth, T. L., Schmitt, F. A., Nelson, P. T. & Wilcock, D. M. Neuroinflammatory phenotype in early Alzheimer's disease. *Neurobiology of aging* **34**, 1051-1059 (2013).
- 300 Knezevic, D. & Mizrahi, R. Molecular imaging of neuroinflammation in Alzheimer's disease and mild cognitive impairment. *Progress in Neuro-Psychopharmacology and Biological Psychiatry* **80**, 123-131 (2018).
- 301 Lagarde, J., Sarazin, M. & Bottlaender, M. In vivo PET imaging of neuroinflammation in Alzheimer's disease. *Journal of Neural Transmission* **125**, 847-867 (2018).
- 302 Zimmer, E. R. *et al.* Tracking neuroinflammation in Alzheimer's disease: the role of positron emission tomography imaging. *Journal of neuroinflammation* **11**, 1-12 (2014).
- 303 Yu, Q. S., Feng, W. Q., Shi, L. L., Niu, R. Z. & Liu, J. Integrated Analysis of Cortex Single-Cell Transcriptome and Serum Proteome Reveals the Novel Biomarkers in Alzheimer's Disease. *Brain Sci* **12**, doi:10.3390/brainsci12081022 (2022).
- 304 Lambert, J. C. *et al.* Genome-wide association study identifies variants at CLU and CR1 associated with Alzheimer's disease. *Nat Genet* **41**, 1094-1099, doi:10.1038/ng.439 (2009).
- 305 Wang, L. M. *et al.* Lipopolysaccharide endotoxemia induces amyloid- β and p-tau formation in the rat brain. *Am J Nucl Med Mol Imaging* **8**, 86-99 (2018).
- 306 Kahn, M. S. *et al.* Prolonged elevation in hippocampal A β and cognitive deficits following repeated endotoxin exposure in the mouse. *Behavioural brain research* **229**, 176-184 (2012).

- 307 Tejera, D. *et al.* Systemic inflammation impairs microglial A β clearance through NLRP 3 inflammasome. *The EMBO journal* **38**, e101064 (2019).
- 308 Boza-Serrano, A., Yang, Y., Paulus, A. & Deierborg, T. Innate immune alterations are elicited in microglial cells before plaque deposition in the Alzheimer's disease mouse model 5xFAD. *Sci Rep* **8**, 1550, doi:10.1038/s41598-018-19699-y (2018).
- 309 Lloyd, A. F. *et al.* Deep proteomic analysis of human microglia and model systems reveal fundamental biological differences of in vitro and ex vivo cells. *bioRxiv*, 2022.2007.2007.498804, doi:10.1101/2022.07.07.498804 (2022).
- 310 Ocañas, S. R. *et al.* Minimizing the Ex Vivo Confounds of Cell-Isolation Techniques on Transcriptomic and Translatomic Profiles of Purified Microglia. *eneuro* **9**, ENEURO.0348-0321.2022, doi:10.1523/ENEURO.0348-21.2022 (2022).
- 311 Dieterich, D. C., Link, A. J., Graumann, J., Tirrell, D. A. & Schuman, E. M. Selective identification of newly synthesized proteins in mammalian cells using bioorthogonal noncanonical amino acid tagging (BONCAT). *Proc Natl Acad Sci U S A* **103**, 9482-9487, doi:10.1073/pnas.0601637103 (2006).
- 312 Alvarez-Castelao, B. *et al.* Cell-type-specific metabolic labeling of nascent proteomes in vivo. *Nature Biotechnology* **35**, 1196-1201, doi:10.1038/nbt.4016 (2017).
- 313 Prabhakar, P. *et al.* Monitoring regional astrocyte diversity by cell-type specific proteomic labeling in vivo. *bioRxiv*, 2022.2006.2007.495069, doi:10.1101/2022.06.07.495069 (2022).
- 314 Martell, J. D. *et al.* Engineered ascorbate peroxidase as a genetically encoded reporter for electron microscopy. *Nat Biotechnol* **30**, 1143-1148, doi:10.1038/nbt.2375 (2012).
- 315 Rhee, H. W. *et al.* Proteomic mapping of mitochondria in living cells via spatially restricted enzymatic tagging. *Science* **339**, 1328-1331, doi:10.1126/science.1230593 (2013).
- 316 Nguyen, T. M. T., Kim, J., Doan, T. T., Lee, M. W. & Lee, M. APEX Proximity Labeling as a Versatile Tool for Biological Research. *Biochemistry* **59**, 260-269, doi:10.1021/acs.biochem.9b00791 (2020).
- 317 Mannix, K. M., Starble, R. M., Kaufman, R. S. & Cooley, L. Proximity labeling reveals novel interactomes in live Drosophila tissue. *Development* **146**, doi:10.1242/dev.176644 (2019).
- 318 Bersuker, K. *et al.* A Proximity Labeling Strategy Provides Insights into the Composition and Dynamics of Lipid Droplet Proteomes. *Dev Cell* **44**, 97-112.e117, doi:10.1016/j.devcel.2017.11.020 (2018).
- 319 Kaewsapsak, P., Shechner, D. M., Mallard, W., Rinn, J. L. & Ting, A. Y. Live-cell mapping of organelle-associated RNAs via proximity biotinylation combined with protein-RNA crosslinking. *Elife* **6**, doi:10.7554/eLife.29224 (2017).
- 320 Fazal, F. M. *et al.* Atlas of Subcellular RNA Localization Revealed by APEX-Seq. *Cell* **178**, 473-490.e426, doi:10.1016/j.cell.2019.05.027 (2019).
- 321 Chen, C. L. *et al.* Proteomic mapping in live Drosophila tissues using an engineered ascorbate peroxidase. *Proc Natl Acad Sci U S A* **112**, 12093-12098, doi:10.1073/pnas.1515623112 (2015).
- 322 Dumrongprechachan, V. *et al.* Cell-type and subcellular compartment-specific APEX2 proximity labeling reveals activity-dependent nuclear proteome dynamics in the striatum. *Nat Commun* **12**, 4855, doi:10.1038/s41467-021-25144-y (2021).
- 323 Hobson, B. D. *et al.* Subcellular proteomics of dopamine neurons in the mouse brain. *eLife* **11**, e70921, doi:10.7554/eLife.70921 (2022).
- 324 Mathew, B., Bathla, S., Williams, K. R. & Nairn, A. C. Deciphering Spatial Protein-Protein Interactions in Brain Using Proximity Labeling. *Mol Cell Proteomics* **21**, 100422, doi:10.1016/j.mcpro.2022.100422 (2022).

- 325 Qin, W., Cho, K. F., Cavanagh, P. E. & Ting, A. Y. Deciphering molecular interactions by proximity labeling. *Nat Methods* **18**, 133-143, doi:10.1038/s41592-020-01010-5 (2021).
- 326 Roux, K. J., Kim, D. I., Raida, M. & Burke, B. A promiscuous biotin ligase fusion protein identifies proximal and interacting proteins in mammalian cells. *J Cell Biol* **196**, 801-810, doi:10.1083/jcb.201112098 (2012).
- 327 Cho, K. F. *et al.* Proximity labeling in mammalian cells with TurboID and split-TurboID. *Nat Protoc* **15**, 3971-3999, doi:10.1038/s41596-020-0399-0 (2020).
- 328 Branon, T. C. *et al.* Efficient proximity labeling in living cells and organisms with TurboID. *Nat Biotechnol* **36**, 880-887, doi:10.1038/nbt.4201 (2018).
- 329 Rayaprolu, S. *et al.* Cell type-specific biotin labeling in vivo resolves regional neuronal and astrocyte proteomic differences in mouse brain. *Nat Commun* **13**, 2927, doi:10.1038/s41467-022-30623-x (2022).
- 330 Sunna, S. *et al.* Cellular proteomic profiling using proximity labelling by TurboID-NES in microglial and neuronal cell lines. *bioRxiv*, 2022.2009.2027.509765, doi:10.1101/2022.09.27.509765 (2022).
- 331 Rayaprolu, S. *et al.* Cell type-specific biotin labeling in vivo resolves regional neuronal and astrocyte proteomic differences in mouse brain. *Nature Communications* **13**, 2927, doi:10.1038/s41467-022-30623-x (2022).
- 332 Sierksma, A. *et al.* Novel Alzheimer risk genes determine the microglia response to amyloid- β but not to TAU pathology. *EMBO Molecular Medicine* **12**, e10606, doi:<https://doi.org/10.15252/emmm.201910606> (2020).
- 333 Arnoux, I. & Audinat, E. Fractalkine Signaling and Microglia Functions in the Developing Brain. *Neural Plast* **2015**, 689404, doi:10.1155/2015/689404 (2015).
- 334 Konishi, H. & Kiyama, H. Microglial TREM2/DAP12 Signaling: A Double-Edged Sword in Neural Diseases. *Frontiers in Cellular Neuroscience* **12**, doi:10.3389/fncel.2018.00206 (2018).
- 335 Turnbull, I. R. & Colonna, M. Activating and inhibitory functions of DAP12. *Nature Reviews Immunology* **7**, 155-161, doi:10.1038/nri2014 (2007).
- 336 Sobue, A. *et al.* Microglial gene signature reveals loss of homeostatic microglia associated with neurodegeneration of Alzheimer's disease. *Acta Neuropathologica Communications* **9**, 1, doi:10.1186/s40478-020-01099-x (2021).
- 337 Hulett, H. R., Bonner, W. A., Barrett, J. & Herzenberg, L. A. Cell sorting: automated separation of mammalian cells as a function of intracellular fluorescence. *Science* **166**, 747-749 (1969).
- 338 Schmitz, B. *et al.* Magnetic activated cell sorting (MACS) — a new immunomagnetic method for megakaryocytic cell isolation: Comparison of different separation techniques. *European Journal of Haematology* **52**, 267-275, doi:<https://doi.org/10.1111/j.1600-0609.1994.tb00095.x> (1994).
- 339 Tanrikulu, I. C., Schmitt, E., Mechulam, Y., Goddard III, W. A. & Tirrell, D. A. Discovery of Escherichia coli methionyl-tRNA synthetase mutants for efficient labeling of proteins with azidonorleucine in vivo. *Proceedings of the National Academy of Sciences* **106**, 15285-15290 (2009).
- 340 Link, A. J. *et al.* Discovery of aminoacyl-tRNA synthetase activity through cell-surface display of noncanonical amino acids. *Proc Natl Acad Sci U S A* **103**, 10180-10185, doi:10.1073/pnas.0601167103 (2006).
- 341 Kunkle, B. W. *et al.* Genetic meta-analysis of diagnosed Alzheimer's disease identifies new risk loci and implicates A β , tau, immunity and lipid processing. *Nat Genet* **51**, 414-430, doi:10.1038/s41588-019-0358-2 (2019).
- 342 Alvarez-Castelao, B. *et al.* Cell-type-specific metabolic labeling of nascent proteomes in vivo. *Nat Biotechnol* **35**, 1196-1201, doi:10.1038/nbt.4016 (2017).

- 343 Hodas, J. J. *et al.* Dopaminergic modulation of the hippocampal neuropil proteome identified by bioorthogonal noncanonical amino acid tagging (BONCAT). *Proteomics* **12**, 2464-2476, doi:10.1002/pmic.201200112 (2012).
- 344 Di Paolo, A. *et al.* Rat Sciatic Nerve Axoplasm Proteome Is Enriched with Ribosomal Proteins during Regeneration Processes. *J Proteome Res* **20**, 2506-2520, doi:10.1021/acs.jproteome.0c00980 (2021).
- 345 Choi-Rhee, E., Schulman, H. & Cronan, J. E. Promiscuous protein biotinylation by Escherichia coli biotin protein ligase. *Protein Sci* **13**, 3043-3050, doi:10.1110/ps.04911804 (2004).
- 346 Uezu, A. *et al.* Identification of an elaborate complex mediating postsynaptic inhibition. *Science* **353**, 1123-1129, doi:10.1126/science.aag0821 (2016).
- 347 Branon, T. C. *et al.* Efficient proximity labeling in living cells and organisms with TurboID. *Nature Biotechnology* **36**, 880-887, doi:10.1038/nbt.4201 (2018).
- 348 Cho, K. F. *et al.* Proximity labeling in mammalian cells with TurboID and split-TurboID. *Nature Protocols* **15**, 3971-3999, doi:10.1038/s41596-020-0399-0 (2020).
- 349 Szczesniak, L. M., Bonzerato, C. G. & Wojcikiewicz, R. J. H. Identification of the Bok Interactome Using Proximity Labeling. *Front Cell Dev Biol* **9**, 689951, doi:10.3389/fcell.2021.689951 (2021).
- 350 Xiong, Z., Lo, H. P., McMahan, K. A., Parton, R. G. & Hall, T. E. Proximity Dependent Biotin Labelling in Zebrafish for Proteome and Interactome Profiling. *Bio Protoc* **11**, e4178, doi:10.21769/BioProtoc.4178 (2021).
- 351 Artan, M. *et al.* Interactome analysis of Caenorhabditis elegans synapses by TurboID-based proximity labeling. *J Biol Chem* **297**, 101094, doi:10.1016/j.jbc.2021.101094 (2021).
- 352 Mair, A., Xu, S. L., Branon, T. C., Ting, A. Y. & Bergmann, D. C. Proximity labeling of protein complexes and cell-type-specific organellar proteomes in Arabidopsis enabled by TurboID. *Elife* **8**, doi:10.7554/eLife.47864 (2019).
- 353 Takano, T. & Soderling, S. H. Tripartite synaptomics: Cell-surface proximity labeling in vivo. *Neuroscience Research* **173**, 14-21, doi:<https://doi.org/10.1016/j.neures.2021.05.002> (2021).
- 354 Li, H., Frankenfield, A. M., Houston, R., Sekine, S. & Hao, L. Thiol-Cleavable Biotin for Chemical and Enzymatic Biotinylation and Its Application to Mitochondrial TurboID Proteomics. *J Am Soc Mass Spectrom* **32**, 2358-2365, doi:10.1021/jasms.1c00079 (2021).
- 355 Cho, K. F. *et al.* Split-TurboID enables contact-dependent proximity labeling in cells. *Proceedings of the National Academy of Sciences* **117**, 12143, doi:10.1073/pnas.1919528117 (2020).
- 356 Takano, T. *et al.* Chemico-genetic discovery of astrocytic control of inhibition in vivo. *Nature* **588**, 296-302, doi:10.1038/s41586-020-2926-0 (2020).
- 357 Niers, J. M., Chen, J. W., Weissleder, R. & Tannous, B. A. Enhanced in vivo imaging of metabolically biotinylated cell surface reporters. *Analytical chemistry* **83**, 994-999, doi:10.1021/ac102758m (2011).
- 358 Kanehisa, M. Toward understanding the origin and evolution of cellular organisms. *Protein Sci* **28**, 1947-1951, doi:10.1002/pro.3715 (2019).
- 359 Kanehisa, M. & Goto, S. KEGG: kyoto encyclopedia of genes and genomes. *Nucleic Acids Res* **28**, 27-30, doi:10.1093/nar/28.1.27 (2000).
- 360 Kanehisa, M., Furumichi, M., Sato, Y., Ishiguro-Watanabe, M. & Tanabe, M. KEGG: integrating viruses and cellular organisms. *Nucleic Acids Res* **49**, D545-d551, doi:10.1093/nar/gkaa970 (2021).
- 361 Ashburner, M. *et al.* Gene ontology: tool for the unification of biology. The Gene Ontology Consortium. *Nat Genet* **25**, 25-29, doi:10.1038/75556 (2000).
- 362 The Gene Ontology resource: enriching a GOld mine. *Nucleic Acids Res* **49**, D325-d334, doi:10.1093/nar/gkaa1113 (2021).

- 363 Rayaprolu, S. *et al.* Flow-cytometric microglial sorting coupled with quantitative proteomics identifies moesin as a highly-abundant microglial protein with relevance to Alzheimer's disease. *Molecular Neurodegeneration* **15**, 28, doi:10.1186/s13024-020-00377-5 (2020).
- 364 Swarup, V. *et al.* Identification of Conserved Proteomic Networks in Neurodegenerative Dementia. *Cell Reports* **31**, 107807, doi:<https://doi.org/10.1016/j.celrep.2020.107807> (2020).
- 365 Darmellah, A. *et al.* Ezrin/Radixin/Moesin Are Required for the Purinergic P2X7 Receptor (P2X7R)-dependent Processing of the Amyloid Precursor Protein*. *Journal of Biological Chemistry* **287**, 34583-34595, doi:<https://doi.org/10.1074/jbc.M112.400010> (2012).
- 366 Kikuchi, M. *et al.* Disruption of a RAC1-centred network is associated with Alzheimer's disease pathology and causes age-dependent neurodegeneration. *Hum Mol Genet* **29**, 817-833, doi:10.1093/hmg/ddz320 (2020).
- 367 Wißfeld, J. *et al.* Deletion of Alzheimer's disease-associated CD33 results in an inflammatory human microglia phenotype. *Glia* **69**, 1393-1412, doi:<https://doi.org/10.1002/glia.23968> (2021).
- 368 Walter, R. B. *et al.* ITIM-dependent endocytosis of CD33-related Siglecs: role of intracellular domain, tyrosine phosphorylation, and the tyrosine phosphatases, Shp1 and Shp2. *J Leukoc Biol* **83**, 200-211, doi:10.1189/jlb.0607388 (2008).
- 369 Kamboh, M. I. *et al.* Genome-wide association study of Alzheimer's disease. *Translational Psychiatry* **2**, e117-e117, doi:10.1038/tp.2012.45 (2012).
- 370 Nalls, M. A. *et al.* Identification of novel risk loci, causal insights, and heritable risk for Parkinson's disease: a meta-analysis of genome-wide association studies. *Lancet Neurol* **18**, 1091-1102, doi:10.1016/s1474-4422(19)30320-5 (2019).
- 371 Al-Chalabi, A. *et al.* The genetics and neuropathology of amyotrophic lateral sclerosis. *Acta Neuropathol* **124**, 339-352, doi:10.1007/s00401-012-1022-4 (2012).
- 372 Woo, J. *et al.* Quantitative Proteomics Reveals Temporal Proteomic Changes in Signaling Pathways during BV2 Mouse Microglial Cell Activation. *Journal of Proteome Research* **16**, 3419-3432, doi:10.1021/acs.jproteome.7b00445 (2017).
- 373 Orihuela, R., McPherson, C. A. & Harry, G. J. Microglial M1/M2 polarization and metabolic states. *Br J Pharmacol* **173**, 649-665, doi:10.1111/bph.13139 (2016).
- 374 Michelucci, A. *et al.* Immune-responsive gene 1 protein links metabolism to immunity by catalyzing itaconic acid production. *Proceedings of the National Academy of Sciences* **110**, 7820-7825, doi:10.1073/pnas.1218599110 (2013).
- 375 Lee, M. S., Kim, B., Oh, G. T. & Kim, Y.-J. OASL1 inhibits translation of the type I interferon-regulating transcription factor IRF7. *Nature Immunology* **14**, 346-355, doi:10.1038/ni.2535 (2013).
- 376 Kristiansen, H., Gad, H. H., Eskildsen-Larsen, S., Despres, P. & Hartmann, R. The oligoadenylate synthetase family: an ancient protein family with multiple antiviral activities. *J Interferon Cytokine Res* **31**, 41-47, doi:10.1089/jir.2010.0107 (2011).
- 377 Carrillo-Jimenez, A. *et al.* TET2 Regulates the Neuroinflammatory Response in Microglia. *Cell Reports* **29**, 697-713.e698, doi:<https://doi.org/10.1016/j.celrep.2019.09.013> (2019).
- 378 Meunier, E. *et al.* Caspase-11 activation requires lysis of pathogen-containing vacuoles by IFN-induced GTPases. *Nature* **509**, 366-370, doi:10.1038/nature13157 (2014).
- 379 Orecchioni, M., Ghosheh, Y., Pramod, A. B. & Ley, K. Corrigendum: Macrophage Polarization: Different Gene Signatures in M1(LPS+) vs. Classically and M2(LPS-) vs. Alternatively Activated Macrophages. *Front Immunol* **11**, 234, doi:10.3389/fimmu.2020.00234 (2020).
- 380 Rath, M., Müller, I., Kropf, P., Closs, E. I. & Munder, M. Metabolism via arginase or nitric oxide synthase: two competing arginine pathways in macrophages. *Frontiers in immunology* **5**, 532 (2014).

- 381 Chan, K. L. *et al.* Palmitoleate Reverses High Fat-induced Proinflammatory Macrophage Polarization via AMP-activated Protein Kinase (AMPK). *J Biol Chem* **290**, 16979-16988, doi:10.1074/jbc.M115.646992 (2015).
- 382 Raes, G. *et al.* Macrophage galactose-type C-type lectins as novel markers for alternatively activated macrophages elicited by parasitic infections and allergic airway inflammation. *Journal of leukocyte biology* **77**, 321-327 (2005).
- 383 Teplova, A. D., Serebryakova, M. V., Galiullina, R. A., Chichkova, N. V. & Vartapetian, A. B. Identification of Phytaspase Interactors via the Proximity-Dependent Biotin-Based Identification Approach. *Int J Mol Sci* **22**, doi:10.3390/ijms222313123 (2021).
- 384 Zhang, Y. *et al.* TurboID-Based Proximity Labeling for In Planta Identification of Protein-Protein Interaction Networks. *J Vis Exp*, doi:10.3791/60728 (2020).
- 385 Zhang, Y. *et al.* TurboID-based proximity labeling reveals that UBR7 is a regulator of NLR immune receptor-mediated immunity. *Nat Commun* **10**, 3252, doi:10.1038/s41467-019-11202-z (2019).
- 386 Larochelle, M., Bergeron, D., Arcand, B. & Bachand, F. Proximity-dependent biotinylation mediated by TurboID to identify protein–protein interaction networks in yeast. *Journal of Cell Science* **132**, jcs232249, doi:10.1242/jcs.232249 (2019).
- 387 Rosenthal, S. M. *et al.* A Toolbox for Efficient Proximity-Dependent Biotinylation in Zebrafish Embryos. *Mol Cell Proteomics* **20**, 100128, doi:10.1016/j.mcpro.2021.100128 (2021).
- 388 Xiong, Z. *et al.* In vivo proteomic mapping through GFP-directed proximity-dependent biotin labelling in zebrafish. *eLife* **10**, e64631, doi:10.7554/eLife.64631 (2021).
- 389 Zhang, B., Zhang, Y. & Liu, J. L. Highly effective proximate labeling in Drosophila. *G3 (Bethesda)* **11**, doi:10.1093/g3journal/jkab077 (2021).
- 390 Uçkun, E. *et al.* In vivo Profiling of the Alk Proximitome in the Developing Drosophila Brain. *Journal of Molecular Biology* **433**, 167282, doi:<https://doi.org/10.1016/j.jmb.2021.167282> (2021).
- 391 Sanchez, A. D. & Feldman, J. L. A proximity labeling protocol to probe proximity interactions in *C. elegans*. *STAR Protoc* **2**, 100986, doi:10.1016/j.xpro.2021.100986 (2021).
- 392 Kim, K. E. *et al.* Dynamic tracking and identification of tissue-specific secretory proteins in the circulation of live mice. *Nat Commun* **12**, 5204, doi:10.1038/s41467-021-25546-y (2021).
- 393 Chua, X. Y., Aballo, T., Elnemer, W., Tran, M. & Salomon, A. Quantitative Interactomics of Lck-TurboID in Living Human T Cells Unveils T Cell Receptor Stimulation-Induced Proximal Lck Interactors. *J Proteome Res* **20**, 715-726, doi:10.1021/acs.jproteome.0c00616 (2021).
- 394 Kragness, S., Clark, Z., Mullin, A., Guidry, J. & Earls, L. R. An Rtn4/Nogo-A-interacting micropeptide modulates synaptic plasticity with age. *PLOS ONE* **17**, e0269404, doi:10.1371/journal.pone.0269404 (2022).
- 395 May, D. G. *et al.* A BioID-Derived Proximity Interactome for SARS-CoV-2 Proteins. *Viruses* **14**, doi:10.3390/v14030611 (2022).
- 396 Hu, S. *et al.* Identification of mutant p53-specific proteins interaction network using TurboID-based proximity labeling. *Biochem Biophys Res Commun* **615**, 163-171, doi:10.1016/j.bbrc.2022.05.046 (2022).
- 397 Boutej, H. *et al.* Diverging mRNA and Protein Networks in Activated Microglia Reveal SRSF3 Suppresses Translation of Highly Upregulated Innate Immune Transcripts. *Cell Rep* **21**, 3220-3233, doi:10.1016/j.celrep.2017.11.058 (2017).
- 398 Ilik, İ. A. & Aktaş, T. Nuclear speckles: dynamic hubs of gene expression regulation. *The FEBS Journal* **n/a**, doi:<https://doi.org/10.1111/febs.16117> (2021).

- 399 Cammas, A. *et al.* Cytoplasmic relocalization of heterogeneous nuclear ribonucleoprotein A1 controls translation initiation of specific mRNAs. *Mol Biol Cell* **18**, 5048-5059, doi:10.1091/mbc.e07-06-0603 (2007).
- 400 Nelson, R. S., Dammer, E. B., Santiago, J. V., Seyfried, N. T. & Rangaraju, S. Brain Cell Type-Specific Nuclear Proteomics Is Imperative to Resolve Neurodegenerative Disease Mechanisms. *Front Neurosci* **16**, 902146, doi:10.3389/fnins.2022.902146 (2022).
- 401 Rangaraju, S. *et al.* A systems pharmacology-based approach to identify novel Kv1.3 channel-dependent mechanisms in microglial activation. *J Neuroinflammation* **14**, 128, doi:10.1186/s12974-017-0906-6 (2017).
- 402 Rangaraju, S. *et al.* Differential Phagocytic Properties of CD45(low) Microglia and CD45(high) Brain Mononuclear Phagocytes-Activation and Age-Related Effects. *Front Immunol* **9**, 405, doi:10.3389/fimmu.2018.00405 (2018).
- 403 Shuster, S. A. *et al.* In situ cell-type-specific cell-surface proteomic profiling in mice. *Neuron* **110**, 3882-3896.e3889, doi:<https://doi.org/10.1016/j.neuron.2022.09.025> (2022).
- 404 Pellegatti, P. *et al.* Increased level of extracellular ATP at tumor sites: in vivo imaging with plasma membrane luciferase. *PLoS One* **3**, e2599, doi:10.1371/journal.pone.0002599 (2008).
- 405 Tamura, R., Uemoto, S. & Tabata, Y. Augmented liver targeting of exosomes by surface modification with cationized pullulan. *Acta Biomaterialia* **57**, 274-284, doi:<https://doi.org/10.1016/j.actbio.2017.05.013> (2017).
- 406 Yarandi, S. S. *et al.* Characterization of Nef expression in different brain regions of SIV-infected macaques. *PLOS ONE* **15**, e0241667, doi:10.1371/journal.pone.0241667 (2020).
- 407 Guo, Q. *et al.* Targeted Quantification of Detergent-Insoluble RNA-Binding Proteins in Human Brain Reveals Stage and Disease Specific Co-aggregation in Alzheimer's Disease. *Front Mol Neurosci* **14**, 623659, doi:10.3389/fnmol.2021.623659 (2021).
- 408 Umoh, M. E. *et al.* A proteomic network approach across the ALS-FTD disease spectrum resolves clinical phenotypes and genetic vulnerability in human brain. *EMBO Mol Med* **10**, 48-62, doi:10.15252/emmm.201708202 (2018).
- 409 Ping, L. *et al.* Global quantitative analysis of the human brain proteome in Alzheimer's and Parkinson's Disease. *Scientific Data* **5**, 180036, doi:10.1038/sdata.2018.36 (2018).
- 410 Seyfried, N. T. *et al.* Quantitative Analysis of the Detergent-Insoluble Brain Proteome in Frontotemporal Lobar Degeneration Using SILAC Internal Standards. *Journal of Proteome Research* **11**, 2721-2738, doi:10.1021/pr2010814 (2012).
- 411 Kockmann, T. & Panse, C. The rawrr R Package: Direct Access to Orbitrap Data and Beyond. *Journal of Proteome Research* **20**, 2028-2034, doi:10.1021/acs.jproteome.0c00866 (2021).
- 412 John, C. R. *et al.* M3C: Monte Carlo reference-based consensus clustering. *Scientific Reports* **10**, 1816, doi:10.1038/s41598-020-58766-1 (2020).
- 413 Koopmans, F. *et al.* SynGO: An Evidence-Based, Expert-Curated Knowledge Base for the Synapse. *Neuron* **103**, 217-234.e214, doi:<https://doi.org/10.1016/j.neuron.2019.05.002> (2019).
- 414 Au - Brothers, R. O., Au - Bitarafan, S., Au - Pybus, A. F., Au - Wood, L. B. & Au - Buckley, E. M. Systems Analysis of the Neuroinflammatory and Hemodynamic Response to Traumatic Brain Injury. *JoVE*, e61504, doi:doi:10.3791/61504 (2022).
- 415 Michael Green, N. in *Methods in Enzymology* Vol. 184 (eds Meir Wilchek & Edward A. Bayer) 51-67 (Academic Press, 1990).
- 416 Riveron-Negrete, L. & Fernandez-Mejia, C. Pharmacological effects of biotin in animals. *Mini reviews in medicinal chemistry* **17**, 529-540 (2017).
- 417 Harris, J. A. *et al.* Anatomical characterization of Cre driver mice for neural circuit mapping and manipulation. *Frontiers in neural circuits* **8**, 76 (2014).

- 418 Madisen, L. *et al.* A robust and high-throughput Cre reporting and characterization system for the whole mouse brain. *Nature neuroscience* **13**, 133-140 (2010).
- 419 Multiple sclerosis genomic map implicates peripheral immune cells and microglia in susceptibility. *Science* **365**, doi:10.1126/science.aav7188 (2019).
- 420 Madisen, L. *et al.* A robust and high-throughput Cre reporting and characterization system for the whole mouse brain. *Nat Neurosci* **13**, 133-140, doi:10.1038/nn.2467 (2010).
- 421 Li, S., Holers, V. M., Boackle, S. A. & Blatteis, C. M. Modulation of mouse endotoxic fever by complement. *Infect Immun* **70**, 2519-2525, doi:10.1128/iai.70.5.2519-2525.2002 (2002).
- 422 Ippolito, D. M. & Eroglu, C. Quantifying synapses: an immunocytochemistry-based assay to quantify synapse number. *J Vis Exp*, doi:10.3791/2270 (2010).
- 423 Knox, C. *et al.* DrugBank 3.0: a comprehensive resource for 'omics' research on drugs. *Nucleic Acids Res* **39**, D1035-1041, doi:10.1093/nar/gkq1126 (2011).
- 424 Bickerton, G. R., Paolini, G. V., Besnard, J., Muresan, S. & Hopkins, A. L. Quantifying the chemical beauty of drugs. *Nat Chem* **4**, 90-98, doi:10.1038/nchem.1243 (2012).
- 425 de Felice, A., Aureli, S. & Limongelli, V. Drug Repurposing on G Protein-Coupled Receptors Using a Computational Profiling Approach. *Front Mol Biosci* **8**, 673053, doi:10.3389/fmolb.2021.673053 (2021).
- 426 Virág, D. *et al.* Current Trends in the Analysis of Post-translational Modifications. *Chromatographia* **83**, 1-10, doi:10.1007/s10337-019-03796-9 (2020).
- 427 Ramesh, M., Gopinath, P. & Govindaraju, T. Role of Post-translational Modifications in Alzheimer's Disease. *Chembiochem* **21**, 1052-1079, doi:10.1002/cbic.201900573 (2020).
- 428 Trist, B. G. *et al.* Altered SOD1 maturation and post-translational modification in amyotrophic lateral sclerosis spinal cord. *Brain* **145**, 3108-3130, doi:10.1093/brain/awac165 (2022).
- 429 Junqueira, S. C., Centeno, E. G. Z., Wilkinson, K. A. & Cimarosti, H. Post-translational modifications of Parkinson's disease-related proteins: Phosphorylation, SUMOylation and Ubiquitination. *Biochim Biophys Acta Mol Basis Dis* **1865**, 2001-2007, doi:10.1016/j.bbadis.2018.10.025 (2019).
- 430 Jo, M. *et al.* The role of TDP-43 propagation in neurodegenerative diseases: integrating insights from clinical and experimental studies. *Experimental & Molecular Medicine* **52**, 1652-1662, doi:10.1038/s12276-020-00513-7 (2020).
- 431 Ma, X. R. *et al.* TDP-43 represses cryptic exon inclusion in the FTD-ALS gene UNC13A. *Nature* **603**, 124-130 (2022).
- 432 Neumann, M. *et al.* Ubiquitinated TDP-43 in frontotemporal lobar degeneration and amyotrophic lateral sclerosis. *Science* **314**, 130-133 (2006).
- 433 Meneses, A. *et al.* TDP-43 Pathology in Alzheimer's Disease. *Molecular Neurodegeneration* **16**, 84, doi:10.1186/s13024-021-00503-x (2021).
- 434 Qin, W. *et al.* Dynamic mapping of proteome trafficking within and between living cells by TransitID. *Cell*, doi:<https://doi.org/10.1016/j.cell.2023.05.044> (2023).
- 435 Wang, F., Zhang, D., Zhang, D., Li, P. & Gao, Y. Mitochondrial Protein Translation: Emerging Roles and Clinical Significance in Disease. *Front Cell Dev Biol* **9**, 675465, doi:10.3389/fcell.2021.675465 (2021).
- 436 Hornbeck, P. V. *et al.* PhosphoSitePlus: a comprehensive resource for investigating the structure and function of experimentally determined post-translational modifications in man and mouse. *Nucleic acids research* **40**, D261-D270 (2012).
- 437 Wang, Z. A. & Cole, P. A. The Chemical Biology of Reversible Lysine Post-translational Modifications. *Cell Chem Biol* **27**, 953-969, doi:10.1016/j.chembiol.2020.07.002 (2020).

- 438 Luo, M. Chemical and Biochemical Perspectives of Protein Lysine Methylation. *Chem Rev* **118**, 6656-6705, doi:10.1021/acs.chemrev.8b00008 (2018).
- 439 Ali, I., Conrad, R. J., Verdin, E. & Ott, M. Lysine Acetylation Goes Global: From Epigenetics to Metabolism and Therapeutics. *Chem Rev* **118**, 1216-1252, doi:10.1021/acs.chemrev.7b00181 (2018).
- 440 Brooks, C. L. & Gu, W. p53 Ubiquitination: Mdm2 and Beyond. *Molecular Cell* **21**, 307-315, doi:<https://doi.org/10.1016/j.molcel.2006.01.020> (2006).
- 441 Zhao, Y. & Xu, H. Microglial lactate metabolism as a potential therapeutic target for Alzheimer's disease. *Molecular Neurodegeneration* **17**, 36, doi:10.1186/s13024-022-00541-z (2022).
- 442 Dickinson, Mary S. *et al.* LPS-aggregating proteins GBP1 and GBP2 are each sufficient to enhance caspase-4 activation both in cellulo and in vitro. *Proceedings of the National Academy of Sciences* **120**, e2216028120, doi:doi:10.1073/pnas.2216028120 (2023).
- 443 Kim, B. H. *et al.* Interferon-induced guanylate-binding proteins in inflammasome activation and host defense. *Nat Immunol* **17**, 481-489, doi:10.1038/ni.3440 (2016).
- 444 Perng, Y.-C. & Lenschow, D. J. ISG15 in antiviral immunity and beyond. *Nature Reviews Microbiology* **16**, 423-439, doi:10.1038/s41579-018-0020-5 (2018).
- 445 Sadler, A. J. & Williams, B. R. Interferon-inducible antiviral effectors. *Nat Rev Immunol* **8**, 559-568, doi:10.1038/nri2314 (2008).
- 446 Paintlia, M. K., Paintlia, A. S., Contreras, M. A., Singh, I. & Singh, A. K. Lipopolysaccharide-induced peroxisomal dysfunction exacerbates cerebral white matter injury: attenuation by N-acetyl cysteine. *Exp Neurol* **210**, 560-576, doi:10.1016/j.expneurol.2007.12.011 (2008).
- 447 Panday, A., Sahoo, M. K., Osorio, D. & Batra, S. NADPH oxidases: an overview from structure to innate immunity-associated pathologies. *Cellular & Molecular Immunology* **12**, 5-23, doi:10.1038/cmi.2014.89 (2015).
- 448 Yuan, S. *et al.* Cooperation between CYB5R3 and NOX4 via coenzyme Q mitigates endothelial inflammation. *Redox Biol* **47**, 102166, doi:10.1016/j.redox.2021.102166 (2021).
- 449 Wood, Z. A., Schröder, E., Robin Harris, J. & Poole, L. B. Structure, mechanism and regulation of peroxiredoxins. *Trends Biochem Sci* **28**, 32-40, doi:10.1016/s0968-0004(02)00003-8 (2003).
- 450 Mo, Y. *et al.* SS-31 reduces inflammation and oxidative stress through the inhibition of Fis1 expression in lipopolysaccharide-stimulated microglia. *Biochem Biophys Res Commun* **520**, 171-178, doi:10.1016/j.bbrc.2019.09.077 (2019).
- 451 Wang, S., Wang, H., Zhu, S. & Li, F. Systematical analysis of ferroptosis regulators and identification of GCLM as a tumor promotor and immunological biomarker in bladder cancer. *Front Oncol* **12**, 1040892, doi:10.3389/fonc.2022.1040892 (2022).
- 452 Wu, D. *et al.* Identification of HMOX1 as a Critical Ferroptosis-Related Gene in Atherosclerosis. *Front Cardiovasc Med* **9**, 833642, doi:10.3389/fcvm.2022.833642 (2022).
- 453 Xu, Y. *et al.* A Bacterial Effector Reveals the V-ATPase-ATG16L1 Axis that Initiates Xenophagy. *Cell* **178**, 552-566.e520, doi:10.1016/j.cell.2019.06.007 (2019).
- 454 Forgac, M. in *Encyclopedia of Biological Chemistry* (eds William J. Lennarz & M. Daniel Lane) 349-353 (Elsevier, 2004).
- 455 Thygesen, C. *et al.* Diverse Protein Profiles in CNS Myeloid Cells and CNS Tissue From Lipopolysaccharide- and Vehicle-Injected APP(SWE)/PS1(ΔE9) Transgenic Mice Implicate Cathepsin Z in Alzheimer's Disease. *Front Cell Neurosci* **12**, 397, doi:10.3389/fncel.2018.00397 (2018).
- 456 Martinez, F. O. & Gordon, S. The M1 and M2 paradigm of macrophage activation: time for reassessment. *F1000Prime Rep* **6**, 13, doi:10.12703/p6-13 (2014).

- 457 Rószler, T. Understanding the Mysterious M2 Macrophage through Activation Markers and Effector Mechanisms. *Mediators of Inflammation* **2015**, 816460, doi:10.1155/2015/816460 (2015).
- 458 Cao, J. *et al.* Elevated lymphocyte specific protein 1 expression is involved in the regulation of leukocyte migration and immunosuppressive microenvironment in glioblastoma. *Aging (Albany NY)* **12**, 1656 - 1684 (2020).
- 459 Stansley, B., Post, J. & Hensley, K. A comparative review of cell culture systems for the study of microglial biology in Alzheimer's disease. *Journal of Neuroinflammation* **9**, 115, doi:10.1186/1742-2094-9-115 (2012).
- 460 Horvath, R. J., Nutile-McMenemy, N., Alkaitis, M. S. & DeLeo, J. A. Differential migration, LPS-induced cytokine, chemokine, and NO expression in immortalized BV-2 and HAPI cell lines and primary microglial cultures. *Journal of neurochemistry* **107**, 557-569 (2008).
- 461 Dai, X. J. *et al.* Activation of BV2 microglia by lipopolysaccharide triggers an inflammatory reaction in PC12 cell apoptosis through a toll-like receptor 4-dependent pathway. *Cell Stress Chaperones* **20**, 321-331, doi:10.1007/s12192-014-0552-1 (2015).
- 462 Arora, H. *et al.* The ATP-Binding Cassette Gene ABCF1 Functions as an E2 Ubiquitin-Conjugating Enzyme Controlling Macrophage Polarization to Dampen Lethal Septic Shock. *Immunity* **50**, 418-431.e416, doi:10.1016/j.immuni.2019.01.014 (2019).
- 463 Pignoni, M. *et al.* Seizure protein 6 and its homolog seizure 6-like protein are physiological substrates of BACE1 in neurons. *Mol Neurodegener* **11**, 67, doi:10.1186/s13024-016-0134-z (2016).
- 464 Hill, M. A. & Gammie, S. C. Alzheimer's disease large-scale gene expression portrait identifies exercise as the top theoretical treatment. *Scientific Reports* **12**, 17189, doi:10.1038/s41598-022-22179-z (2022).
- 465 Kelly, J., Moyeed, R., Carroll, C., Albani, D. & Li, X. Gene expression meta-analysis of Parkinson's disease and its relationship with Alzheimer's disease. *Mol Brain* **12**, 16, doi:10.1186/s13041-019-0436-5 (2019).
- 466 Zhao, Y., Xie, Y. Z. & Liu, Y. S. Accelerated aging-related transcriptome alterations in neurovascular unit cells in the brain of Alzheimer's disease. *Front Aging Neurosci* **14**, 949074, doi:10.3389/fnagi.2022.949074 (2022).
- 467 Li, Y. *et al.* Identification of hub proteins in cerebrospinal fluid as potential biomarkers of Alzheimer's disease by integrated bioinformatics. *J Neurol* **270**, 1487-1500, doi:10.1007/s00415-022-11476-2 (2023).
- 468 Zhou, M. *et al.* Targeted mass spectrometry to quantify brain-derived cerebrospinal fluid biomarkers in Alzheimer's disease. *Clin Proteomics* **17**, 19, doi:10.1186/s12014-020-09285-8 (2020).
- 469 Carlos, D. G., Shaona, A., Megan, L. L., Justin, R. & Quentin, J. P. Increased Excitatory Synaptic Transmission Associated with Adult Seizure Vulnerability Induced by Early-Life Inflammation in Mice. *The Journal of Neuroscience* **41**, 4367, doi:10.1523/JNEUROSCI.2667-20.2021 (2021).
- 470 Elmore, M. R. P. *et al.* Colony-stimulating factor 1 receptor signaling is necessary for microglia viability, unmasking a microglia progenitor cell in the adult brain. *Neuron* **82**, 380-397, doi:10.1016/j.neuron.2014.02.040 (2014).
- 471 Najafi, A. R. *et al.* A limited capacity for microglial repopulation in the adult brain. *Glia* **66**, 2385-2396, doi:10.1002/glia.23477 (2018).
- 472 Sosna, J. *et al.* Early long-term administration of the CSF1R inhibitor PLX3397 ablates microglia and reduces accumulation of intraneuronal amyloid, neuritic plaque deposition and pre-fibrillar

- oligomers in 5XFAD mouse model of Alzheimer's disease. *Molecular Neurodegeneration* **13**, 11, doi:10.1186/s13024-018-0244-x (2018).
- 473 Spangenberg, E. *et al.* Sustained microglial depletion with CSF1R inhibitor impairs parenchymal plaque development in an Alzheimer's disease model. *Nature Communications* **10**, 3758, doi:10.1038/s41467-019-11674-z (2019).
- 474 Olmos-Alonso, A. *et al.* Pharmacological targeting of CSF1R inhibits microglial proliferation and prevents the progression of Alzheimer's-like pathology. *Brain* **139**, 891-907, doi:10.1093/brain/awv379 (2016).
- 475 Dagher, N. N. *et al.* Colony-stimulating factor 1 receptor inhibition prevents microglial plaque association and improves cognition in 3xTg-AD mice. *J Neuroinflammation* **12**, 139, doi:10.1186/s12974-015-0366-9 (2015).
- 476 Asai, H. *et al.* Depletion of microglia and inhibition of exosome synthesis halt tau propagation. *Nat Neurosci* **18**, 1584-1593, doi:10.1038/nn.4132 (2015).
- 477 Prateek, K. *et al.* Native-state proteomics of Parvalbumin interneurons identifies novel molecular signatures and metabolic vulnerabilities to early Alzheimer's disease pathology. *bioRxiv*, 2023.2005.2017.541038, doi:10.1101/2023.05.17.541038 (2023).
- 478 Ramelow, C. C. *et al.* Simultaneous RNA and protein profiling using a TurboID proximity-labeling strategy. *Alzheimer's & Dementia* **17**, e058706, doi:<https://doi.org/10.1002/alz.058706> (2021).
- 479 Santiago, J. V., Rayaprolu, S., Xiao, H., Seyfried, N. T. & Rangaraju, S. Identification of state-specific proteomic characteristics of microglia-derived exosomes. *Alzheimer's & Dementia* **17**, e058665, doi:<https://doi.org/10.1002/alz.058665> (2021).
- 480 Bowen, C. A. *et al.* Identification of Kv1.3 potassium channel interacting proteins in mammalian cells. *Alzheimer's & Dementia* **17**, e058672, doi:<https://doi.org/10.1002/alz.058672> (2021).